



HAL
open science

Design and synthesis of plasmonic meta-atoms from patchy particles

Cyril Chomette

► **To cite this version:**

Cyril Chomette. Design and synthesis of plasmonic meta-atoms from patchy particles. Material chemistry. Université de Bordeaux, 2015. English. NNT : 2015BORD0232 . tel-01635288

HAL Id: tel-01635288

<https://theses.hal.science/tel-01635288>

Submitted on 15 Nov 2017

HAL is a multi-disciplinary open access archive for the deposit and dissemination of scientific research documents, whether they are published or not. The documents may come from teaching and research institutions in France or abroad, or from public or private research centers.

L'archive ouverte pluridisciplinaire **HAL**, est destinée au dépôt et à la diffusion de documents scientifiques de niveau recherche, publiés ou non, émanant des établissements d'enseignement et de recherche français ou étrangers, des laboratoires publics ou privés.

THÈSE PRÉSENTÉE
POUR OBTENIR LE GRADE DE

DOCTEUR DE
L'UNIVERSITÉ DE BORDEAUX
ÉCOLE DOCTORALE DES SCIENCES CHIMIQUES
SPÉCIALITÉ : Physico-Chimie de la Matière Condensée

Par Cyril CHOMETTE

**Design and synthesis of plasmonic meta-atoms
from patchy particles**

Soutenue le : 13 novembre 2015

Membres du jury :

Mme ROUGIER, Aline
Mme SAVE, Maud
M. DUJARDIN, Erik
M. LIZ-MARZAN, Luis
M. SPALLA, Olivier

Directeur de recherche CNRS, ICMCB Bordeaux
Chargée de Recherche CNRS, IPREM Pau
Directeur de recherche CNRS, CEMES Toulouse
Professeur, Université Ikerbasque, Espagne
Chercheur CEA, LIONS Saclay

Président
Rapporteur
Rapporteur
Examineur
Examineur

M. DUGUET, Etienne
Mme TREGUER-DELAPIERRE, Mona
M. MANOHARAN, Vinothan N.

Professeur, Université de Bordeaux
Maître de conférences HDR, Université de Bordeaux
Professeur, Université d'Harvard, USA

Directeur de thèse
Co-directrice de thèse
Co-directeur de thèse

Remerciements

Les travaux de thèse décrits dans ce manuscrit ont été réalisés à l'Institut de Chimie de la Matière Condensée de Bordeaux, sous la direction d'Etienne Duguet et de Mona Tréguer-Delapierre, ainsi que sous la direction de Vinothan N. Manoharan à la *School of Engineering and Applied Science* de l'Université de Harvard, Cambridge, MA, USA.

Je souhaiterais remercier, en premier lieu, Monsieur Mario Maglione pour m'avoir accueilli au sein de son laboratoire, l'ICMCB, pendant ces trois années.

J'exprime toute ma gratitude à Maud Save et Erik Dujardin d'avoir accepté de rapporter cette thèse, ainsi qu'à Luis Liz-Marzan, Olivier Spalla et Aline Rougier pour avoir participé au jury de thèse. Je tiens à remercier mes directeurs de thèse : Etienne Duguet, Mona Tréguer-Delapierre et Vinothan N. Manoharan pour la liberté d'action qu'ils m'ont laissée durant ce projet ainsi que la confiance qu'ils m'ont accordée. Je tiens également à les remercier pour le temps qu'ils m'ont consacré, plus particulièrement lors de la rédaction de ce manuscrit, et pour l'ambiance de travail fort agréable qu'ils ont su créer et entretenir.

Cette thèse, financée par l'IdEx de Bordeaux, s'inscrit dans le cadre d'une étude sur les métamatériaux réalisée au sein du projet LabEx AMADEus. Un grand merci à tous ceux qui m'ont aidé durant ce projet : Serge Ravaine, Stéphane Mornet, Adeline Perro-Marre, Jérôme Majimel, mais également Philippe Barois, Virginie Ponsinet et Philippe Richetti qui ont su m'éclairer et partager leurs savoirs. *I would also like to acknowledge my colleagues from the Manoharan's group. First of all, I would like to thank the whole group that was very friendly to me. Then, I would like to thank, more especially, my two colleagues: Nabila Tanjeem and Nicholas Schade that taught me a bit of physics and who share a lot of their patience on the dark field single object characterization project.*

Je remercie les nombreux stagiaires que j'ai eu le plaisir d'encadrer et avec qui j'ai pu apprendre : Céline, Marthe, Alexandra, Kévin, Elham et Nicolas. Je voudrais les remercier pour s'être tant investi durant leur stage et pour avoir eu cet esprit constructif qui m'a fait apprécier de travailler au quotidien à leurs côtés. Je souhaiterais également remercier Ming Sun avec qui j'ai eu beaucoup de plaisir à travailler pendant un an et demi ainsi que Carmen Vasquez Vasquez qui est venue travailler dans l'équipe durant quelques mois.

J'ai eu la chance d'évoluer au sein de l'ICMCB, un institut qui présente de nombreux services nous facilitant le travail au quotidien... merci à eux!

Je remercie l'ensemble des membres du Groupe 5 et ceux qui sont passés par le groupe et que j'ai pu côtoyer pendant ces années. Les permanents qui participaient activement à l'ambiance du groupe: MHD, Graziella et Lydia. Les non permanents : Laurent, Stéphanie, Sergio, Noélia, Anthony, Aurélie, Arnaud, Magalie, Quentin, Thomas, Brice, Nora à qui je souhaite beaucoup de réussite pour la suite. Je souhaite bon courage aux nouveaux : Weiya, Véro et PE qui débutent leur thèse et qui vont amener plus loin les systèmes colloïdaux développés dans l'équipe.

Enfin, cette dernière phrase de remerciement va à mes amis et surtout à Mathilde.

Résumé de la thèse en Français

Les métamatériaux sont une classe de matériaux émergents. Il s'agit typiquement de composites artificiels possédant des propriétés électromagnétiques extraordinaires. Ces matériaux sont formés de sous unités élémentaires, considérées comme des blocs de construction, constituant le matériau 3D. L'objectif de cette thèse est de fabriquer par auto-assemblage des métamatériaux tridimensionnels possédant une réponse magnétique aux fréquences optiques dans le visible ou le proche infrarouge. Cette réponse s'exprime par une perméabilité relative μ_r différente de la valeur 1 du vide. De tels matériaux, inconnus dans la nature, contreviennent à l'argument classique de Landau et Lifshitz selon lequel la magnétisation et la perméabilité magnétique n'ont pas de sens aux fréquences optiques. L'existence de modes magnétiques optiques associés à des résonances de plasmons localisés et couplés a néanmoins été démontrée sur des surfaces métalliques nanostructurées de type « fishnets » élaborées par lithographie [1]. Cette technique permet de structurer la matière de façon remarquable à de très petites échelles, mais elle ne permet pas d'élaborer des structures volumiques avec des valeurs de perméabilité μ_r différentes de 1 en grande quantité. Ce sont de telles structures que nous proposons de fabriquer : (i) élaboration par voie "bottom-up" de nanorésonateurs magnétiques, (ii) modélisation de la réponse magnétique et sa mesure expérimentale et (iii) assemblage en matériaux tridimensionnels. Les nanorésonateurs tridimensionnels les plus prometteurs (en théorie) sont basés sur l'utilisation de nanoparticules d'or ou d'argent disposées autour d'un noyau central diélectrique. De tels nanoclusters sont supposés posséder une résonance magnétique, pour laquelle les plasmons de chaque nanoparticule métallique satellite se couplent à travers le cœur central. Cela devrait créer une perméabilité négative dans une certaine plage de fréquences dans le spectre optique. Puisque cette structure a également une résonance de permittivité proche, il a été montré que, dans un domaine de fréquences donné, un arrangement optiquement dense de ces nanorésonateurs conduirait à un milieu à indice optique négatif opérant dans le visible [2,3]. Les principaux enjeux pour la synthèse de ces clusters concernent le contrôle des dimensions, du nombre de satellites et de leur monodispersité en taille et en forme. Pour contrôler l'agencement relatif des nanoparticules plasmoniques, nous avons exploré le concept de particules à « patch », définies comme des sphères présentant une surface structurée (topologiquement et/ou chimiquement) capables d'induire des interactions selon des directions pré-déterminées (Figure 1). Nous avons utilisé ces particules à patch comme substrat pour assembler des particules d'or et obtenir des systèmes hybrides silice/or.

Les particules à « patch » en silice ont été élaborées à partir de clusters colloïdaux de géométries tétraédrique, octaédrique et icosaédrique (trois des cinq solides de Platon). Ces objets constitués d'une particule centrale de silice autour de laquelle s'agencent précisément 4, 6 ou 12 nodules de polystyrène ont été élaborés par une approche de polymérisation ensemencée en émulsion [4] (Figure 1). Les nodules de PS pouvant être éliminés ultérieurement par dissolution dans le THF, cette approche offre la possibilité de préparer des particules de silice à patchs ou à fossettes

identiques. Les cavités des particules à fossettes ont été modifiées en surface, avec succès, pour les rendre collantes pour des germes d'or de 2-3 nm de diamètre.

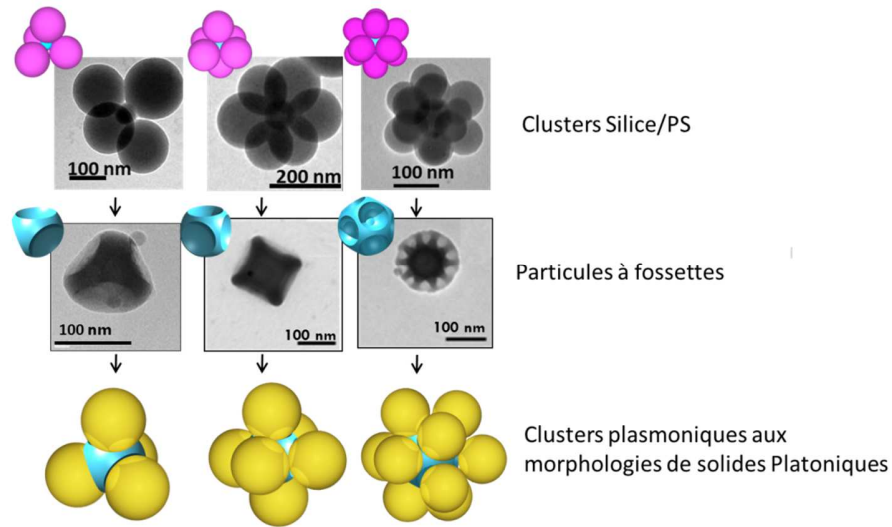


Figure 1 : Schéma des clusters hybrides silice-polystyrène ; Schéma des particules à patches qui en dérivent et des clusters plasmoniques ciblés présentant des morphologies de types solide de platon.

En initiant la croissance des germes d'or à partir des cavités fonctionnalisées du cœur de silice, des édifices hybrides proches des architectures recherchées ont été élaborés (Figure 2). Cependant, la forme de leurs satellites d'or est plutôt aplatie aux pôles et leur surface très rugueuse en fin de croissance. Afin d'améliorer leur sphéricité, plusieurs traitements post-croissance ont été envisagés. Ces traitements ont permis de "lisser" la morphologie des particules d'or, mais leur inter-distance s'est avérée trop importante pour générer des couplages intenses autour du cœur diélectrique.

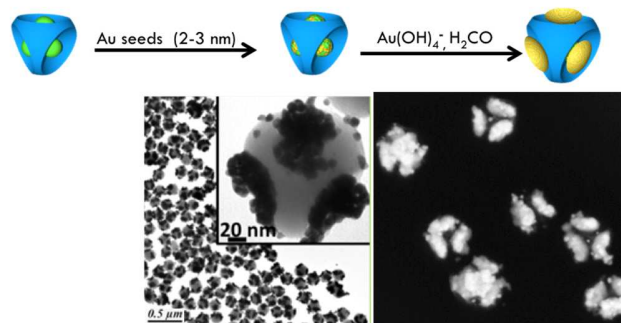


Figure 2: Synthèse des clusters plasmoniques par croissance de germes d'or ancrés en surface des fossettes.

Une approche différente, basée sur l'accostage de satellites de silice sur lesquels nous avons ensuite fait croître une coquille d'or, a également été développée. Cette seconde voie s'est avérée la plus efficace pour contrôler la morphologie des clusters et notamment la distance entre les

satellites d'or (quelques nanomètres).

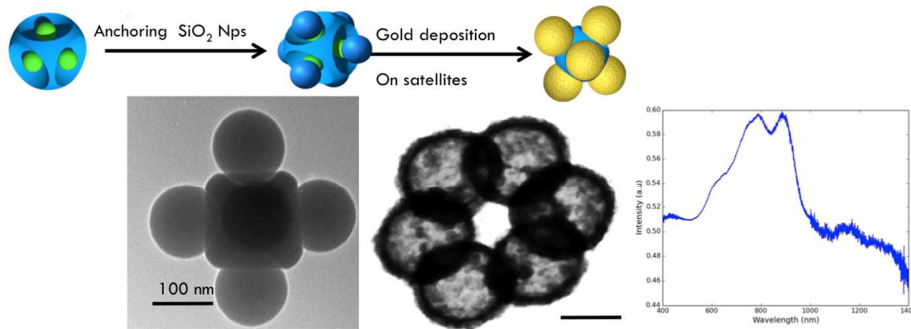


Figure 3: Synthèse et propriétés optiques de clusters plasmoniques formés par auto-assemblage de nanoparticules pré-formées.

Les propriétés optiques de ces édifices plasmoniques ont été modélisées et mesurées. Un mode magnétique a été mis en évidence dans le proche infra-rouge. L'enjeu est désormais d'étudier les propriétés spécifiques et collectives des assemblages supra-particulaires.

[1] S. Linden, C. Enkrich, M. Wegener, J. Zhou, T. Koschny, and C. M. Soukoulis, "Magnetic response of metamaterials at 100 terahertz.," *Science*, vol. 306, pp. 1351–1353, 2004.

[2] Y. A. Urzhumov, G. Shvets, J. Fan, F. Capasso, D. Brandl, and P. Nordlander, "Plasmonic nanoclusters: a path towards negative-index metafluids.," *Opt. Express*, vol. 15, pp. 14129–14145, 2007.

[3] A. Alù and N. Engheta, "The quest for magnetic plasmons at optical frequencies.," *Opt. Express*, vol. 17, pp. 5723–5730, 2009.

[4] A. Désert, I. Chaduc, S. Fouilloux, J.-C. Taveau, O. Lambert, M. Lansalot, E. Bourgeat-Lami, A. Thill, O. Spalla, S. Ravaine, and E. Duguet, "High-yield preparation of polystyrene/silica clusters of controlled morphology," *Polym. Chem.*, vol. 3, pp. 1130–1132, 2012.

[5] Y.J. Lee, N. B. Schade, L. Sun, J. A. Fan, D. R. Bae, M. M. Mariscal, G. Lee, F. Capasso, S. Sacanna, V. N. Manoharan, G. R. Yi. "Ultrasmooth Highly Spherical Monocrystalline Gold Particles for Precision Plasmonics" *ACS nano*, vol. 7, pp. 11064-11070, 2013.

Outline

<i>List of abbreviations</i>	<i>1</i>
<i>Introduction</i>	<i>3</i>
1 Concept of metamaterial	5
2 Electromagnetic metamaterials	5
3 The quest for a negative refractive index...	6
4 ...at optical frequencies	9
5 Our objectives	12
6 References	13
<i>Chapter 1: Synthesis of patchy silica particles</i>	<i>17</i>
1 Synthesis of patchy particles: state of the art	19
1.1 Technique exploiting the confinement on a substrate with neighboring particles: the glancing angle deposition (GLAD) technique	20
1.2 Techniques exploiting the confinement within emulsion droplets	21
1.3 Techniques exploiting the confinement around sticky protrusions	22
1.4 Techniques exploiting the confinement on a seed by emulsion polymerization	23
1.5 State-of-the-art conclusion and strategy to be implemented	24
2 Preparation of silica particles bearing 4, 6 or 12 dimples	26
2.1 Synthesis of size-monodisperse silica seeds	26
2.1.1 Synthesis of silica nanospheres	26
2.1.2 Surface activation of the silica nanospheres by grafting of organoalkoxysilanes	28
2.2 Synthesis of the multipod-like silica/PS clusters by seeded-growth emulsion polymerization	29
2.3 Derivatization of the multipod-like silica/PS clusters into dimpled silica particles	32
2.3.1 Template regrowth of the silica cores	32
2.3.2 Dimple development by dissolution of the PS nodules	34
2.3.3 Morphology and chemical composition of the dimpled silica particles	35
2.3.4 Towards the control of the dimple depth	37
2.4 Making the dimples sticky by chemical modification of the residual PS	41
2.4.1 First stage: chloromethylation of PS macromolecules	42
2.4.2 Second stage: amination of the chloromethylated PS macromolecules	45
2.4.3 Alternative second stage: thiolation of the chloromethylated PS macromolecules	46
2.4.4 Indirect proof of the PS modification success	46
3 Conclusion	49
4 References	50
<i>Chapter 2: Structured plasmonic nanoclusters through the site-specific and seed-mediated growth of the satellites</i>	<i>55</i>
1 Seeded-growth of gold satellites on thiolated patchy particles	57
1.1 Growth of the anchored gold seeds	58
1.1.1 Seed-mediated growth derived from the Rodriguez-Fernandez's work	59
1.1.2 Seed-mediated growth derived from the Puentes' work	60

1.1.3	Seed-mediated growth derived from the Eychmüller's work	61
1.2	Closing remarks on this strategy involving thiolated patchy particles	63
2	Seeded-growth of gold satellites on aminated patchy particles	64
2.1	Impact of the seed size	65
2.2	Optimization of the growth reaction conditions of the tiny gold seeds anchored onto the aminated silica surface	67
2.2.1	A conventional method applied on atypical colloids	67
2.2.2	Optimization of the pH value of the seed dispersion	70
2.2.3	Optimization of the pH value of the growth medium	71
2.2.4	Optimization of the reduction procedure: iterative regrowth	72
2.3	Growth of the tiny gold seeds anchored to the aminated PS bumps at the bottom of the patchy particles	73
3	Spheroidization of the gold satellites	77
4	Extension to patchy particles bearing 6 and 12 dimples	81
5	Conclusion	83
6	References	83

Chapter 3: Structured plasmonic nanoclusters through the assembly of preformed dimpled particles and satellites _____ **87**

1	Assembly of (nano)particles: state-of-the-art	89
1.1	Forces involved in the assembly of particles	89
1.1.1	Van der Waals forces	90
1.1.2	Electrostatic forces	90
1.1.3	Depletion forces	91
1.1.4	Hydrophobic effect	92
1.1.5	Chemical coupling between particle surface through reactive species	92
1.2	Assembly in 2-D or 3-D arrays	93
1.3	Assembly into discrete clusters	93
1.3.1	Assembly route exploiting electrostatic interactions	94
1.3.2	Assembly route exploiting hydrophobic effect	94
1.3.3	Assembly route exploiting depletion forces	95
1.3.4	Assembly routes exploiting supramolecular or covalent coupling	96
1.4	Conclusion and assembly strategy taken on for this study	98
2	Synthesis of silica/silica multipod-like clusters by assembly	99
2.1	Synthesis of silica particles bearing carboxylic acid groups	100
2.1.1	First stage: synthesis of amino-modified silica particles	101
2.1.2	2 nd stage: derivatization of the amino groups into carboxylic acid ones	102
2.2	Assembly of carboxylic-modified silica particles with aminated patchy particles	104
2.2.1	Effect of the concentration on the assembly	106
2.2.2	Effect of reaction time on the assembly	107
3	Derivatization of the silica/silica clusters into silica/silica@gold clusters	108
3.1	Strategy (I): assembly with silica satellites previously decorated by gold nuclei	109
3.2	Strategy (II): post-assembly decoration of the silica satellites by gold nuclei	111
3.2.1	Amination of the silica satellites attached to the patchy silica core and their subsequent decoration with gold nuclei	111
3.2.2	Growth of the gold nuclei to get silica@gold satellites	113
3.2.3	Toward the control of the inter-satellites distance	114
4	Conclusion	119

5	References	119
<i>Chapter 4: Measurement of the optical response of an unique plasmonic nanocluster using dark-field spectroscopy</i>		
		125
1	The dark field set-up used for the optical measurement	128
2	Modeling of the optical properties of a plasmonic nanocluster	129
3	Optical response of a single nanocluster	133
4	Optical signature of a nanocluster in the near infra-red region	136
5	Conclusion and perspectives	137
6	References	138
<i>Conclusion and future work</i>		
		141
1	Main achievements	143
2	References	146
<i>Appendices</i>		
		147
1	Appendix: characterization techniques	149
1.1	UV-Visible spectroscopy	149
1.2	Diffuse Reflectance Infrared Fourier Transform Spectroscopy (DRIFT)	149
1.3	Energy-dispersive X-ray Spectroscopy (EDX)	149
1.4	Implementation of the TEM, HRTEM, STEM, EDX	149
1.5	Scanning Electron Microscopy (SEM)	150
1.6	Zetametry	150
2	Appendix: calculations used for protocol	151
2.1	Calculation of the TEOS volume required for silica regrowth	151
2.2	Calculation of the inter-patch surface areas and the amount of coupling agent required for a given surface modification	153
2.3	Calculation of the amount of gold precursor required to grow a shell of a given thickness.	154
3	Appendix: synthesis of the chloromethylating agent	155
4	Appendix: from gold nanoshells to nanocages	156
5	Appendix: dark-field spectroscopy	157
5.1	Geometrical construction used for the simulation	157
5.2	Series of TEM images used for the cluster targeting	158
6	Appendix list of chemical	159
7	Appendix list of protocols	160
8	References	168

List of abbreviations

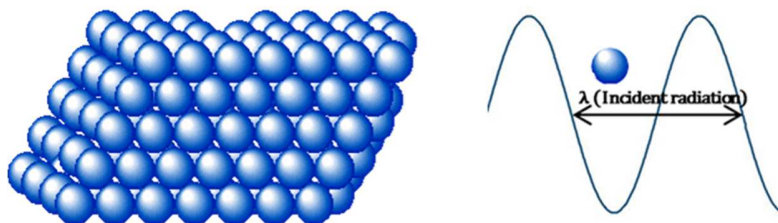
AMS	Acetoxypropyltrimethoxysilane
APTES	Aminopropyltriethoxysilane
CAs	Colloidal atoms
CCs	Colloidal crystals
CMC	Critical micellar concentration
CTAB	Cetyl trimethylammonium bromide
DLVO	Derjaguin-Landau-Vervey-Overbeek
DMF	Dimethylformamide
DMSO	Dimethylsulfoxide
DRIFT	Diffuse reflectance infrared Fourier transform
ECF	Ethyl chloroformate
EELS	Electron energy losses spectroscopy
EDX	Energy-dispersive X-ray spectroscopy
fcc	Face-centered cubic
GLAD	Glancing angle deposition
GPS	Gold plating solution
hcp	Hexagonal-close packed
IEP	Isoelectric point
IR	Infrared
MMS	Methacryloxymethyltriethoxysilane
NBP	Nitrobenzyl pyridine
PDI	Polydispersity index
PEG	Polyethylene glycol
PS	Polystyrene
PVP	Polyvinylpyrrolidone

SDS	Sodium dodecyl sulfate
SEC	Size exclusion chromatography
SEM	Scanning Electron Microscopy
STED	Stimulated Emission Depletion Microscopy
NP 30	Polyethylene glycol nonylphenyl ether
TEA	Triethylamine
TEM	Transmission Electron Microscopy
TEOS	Tetraethoxysilane
TGA	Thermogravimetric analysis
THF	Tetrahydrofuran
TPM	Trimethoxysilyl-propylmethacrylate
TT	Thermal treatment
VdW	Van der Waals

Introduction

1 Concept of metamaterial

Metamaterials are a class of artificial composite materials whose physical properties are unknown in natural materials. The most spectacular optical property of metamaterials is the negative value of the optical refractive index. They could be produced by self-assembly of engineered meta-atoms. These meta-atoms are designed to interact with a given kind of waves depending on the range of the desired properties. Indeed, the wave-matter interaction depends on the shape, the orientation, the geometry and especially on the size of the subunit constituting the metamaterial (the meta-atom). Typically, the dimension of the subunit has to be small compared to the wavelength of the incident radiation since a metamaterial should be considered like a continuous medium (**Scheme 1**).



Scheme 1: Representation of a metamaterial subdivided into meta-atoms (blue spheres); the size of each subunit is small compared to the wavelength of the incident radiation.

Such properties are extremely useful for applications across many different fields, such as antenna technology,[1],[2] solar cell one,[3] superlens [4],[5] cloaking devices [6], among others. Mechanical metamaterials are also in development. They offer promising perspectives to improve the seismic protection, [7] sound filtering [8],[9] and more generally to tune the mechanical materials properties by playing with the appropriate design.

2 Electromagnetic metamaterials

In the framework of this Ph.D project, we focused our work on the conception of meta-atoms that confer to the overall material the capability to interact with an electromagnetic beam within the visible-IR range by exploiting the phenomenon of surface plasmon resonance (SPR) (**Figure 1**). Our objective is to fabricate meta-atoms with a size much smaller than the wavelength of the visible light, *i.e.* a few tens to one hundred nanometers.

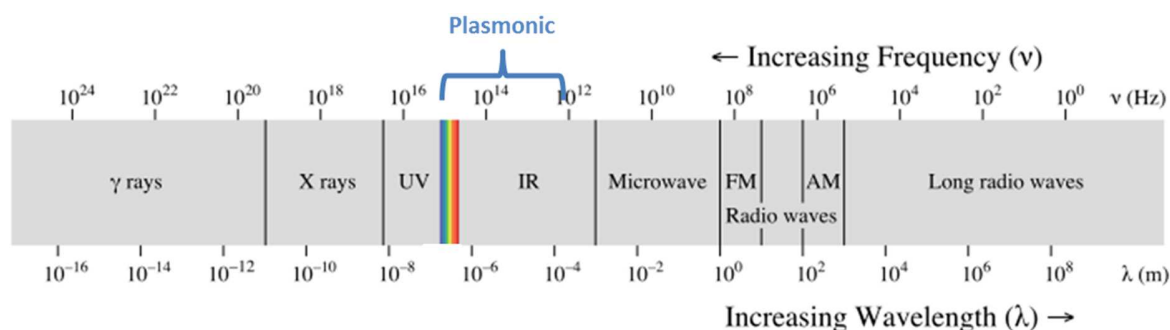


Figure 1: Electromagnetic spectrum. The plasmonic meta-atoms are typically interesting for applications in the visible and the infra-red region.

3 The quest for a negative refractive index...

From a historical point of view, Veselago was the first in 1967 to describe theoretically a material with reversed physical characteristics expected in the visible range.[10] He evidenced that a material exhibiting a negative refractive index could transmit light with a phase velocity (\mathbf{k}) wave vector antiparallel to the direction of the Poynting vector (\mathbf{S}). In this case, the wave propagation is oppositely oriented compared to natural materials. This kind of materials, also called left-handed material, exhibits a specific behavior. Indeed, the right hand rule is no more followed; this is why the electromagnetic wave can convey energy against the phase velocity (\mathbf{k}). To get such a negative refractive index n , the requirement for the material is to present both a negative dielectric permittivity ($\epsilon < 0$) and magnetic permeability ($\mu < 0$) (**Figure 2**).

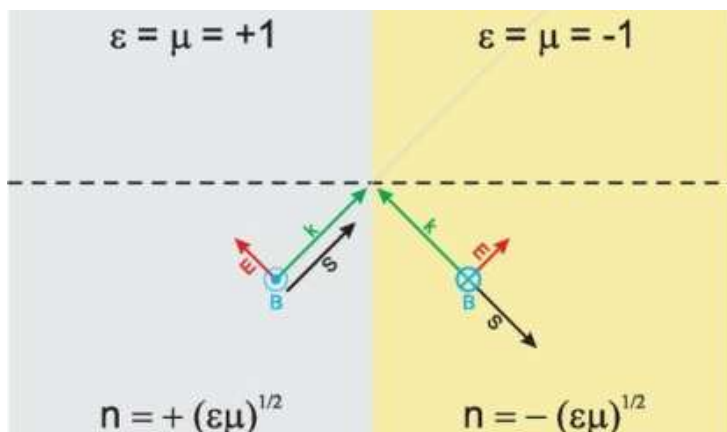


Figure 2: Illustration of the behavior expected for both ϵ and μ positive material on left and for both ϵ and μ negative also called left-handed material on right.

Indeed, n can be expressed from an electromagnetic point of view as $n = \pm \sqrt{\epsilon \cdot \mu}$, where ϵ is the dielectric permittivity of a material, measuring the capability of a material to transmit an electric field; μ is the magnetic permeability of a material, measuring the ability of the material to support the formation of a magnetic field within itself and corresponding to the magnetization obtained by a material in response to an applied magnetic field. Negative permittivity is achieved in metals

at least far enough below their plasma frequency. Reaching negative permeability is more challenging. In 1999, Pendry was the first to propose a way to obtain a composite material which exhibits both negative permittivity and permeability.[11] Indeed, the idea starts with the analogy in between “atoms” and “meta-atoms”. At first glance, atoms can be considered like dipoles which affect the light velocity by the factor n , *i.e.* the refractive index, where $n = C/v$ with C corresponding to the speed of the light in the vacuum and v the speed of the light in the considered medium (**Figure 3**).

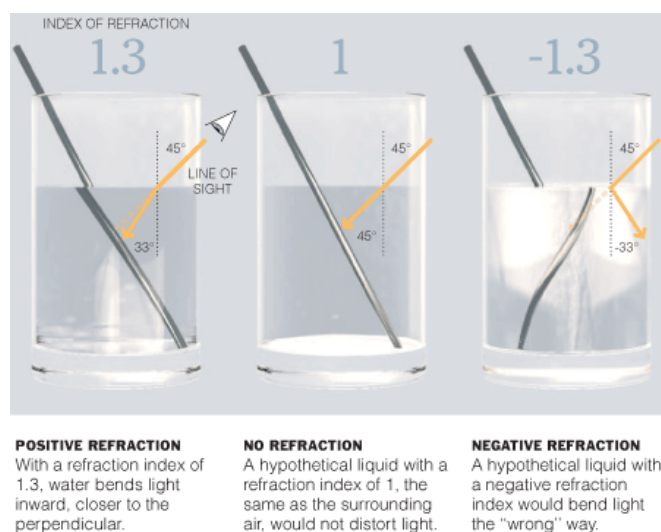


Figure 3: Representation of the expected effect of several refraction index values for the liquid contained in the recipient, reproduced from reference [12].

In the case of meta-atoms, Pendry and coworkers propose to use split ring resonators (SRR) to tune the μ_{eff} for values not accessible in the natural material. For convenience, the dimensions of this kind of structures were about few millimeters and consequently they were supposed to be active in the micro-wave range.

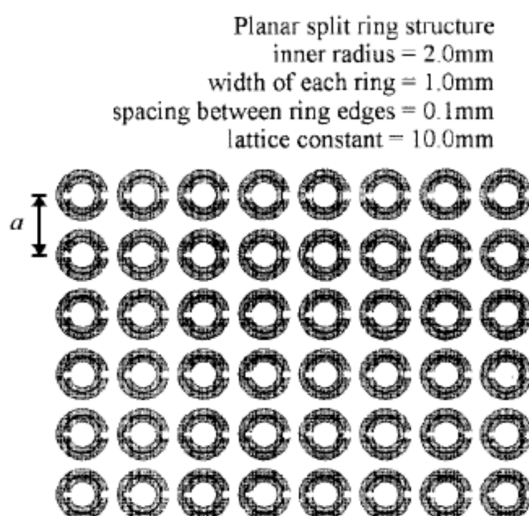


Figure 4: Illustration of a square array of SRR extracted from reference [11].

In 2000, Smith *et al* showed that the creation of a structure corresponding to the concept proposed by Pendry *et al*. He built a structure combining a periodic arrangement of parallel metallic wires, aligned along the propagation direction of the wave, and a periodic array of SRR. In that case, the ring and wire unit played the role of the meta-atomic dipole, according to the theory, the aligned wires acted like ferroelectric atoms, *i.e.* exhibiting a spontaneous electric polarization, and giving a negative permittivity ϵ for the considered frequency. On the other hand, the SRR acted as inductors (L) and the open parts as capacitors (C). The whole SRR served as an LC circuit exhibiting a resonance frequency and so a narrow range of wavelengths, near the high frequency side of the resonance, where the magnetic permeability is negative. By using this particular architecture, the proposed composite material is able to exhibit, for a range of wavelengths, both a negative ϵ and μ , and so forming a propagating band exhibiting a negative group velocity which is the main feature of a left-handed medium. Later in 2001, the same authors published a paper entitled “Experimental verification of a negative refractive index”, where they reported the measure and calculation of the refractive index of a material made of an arrangement of wires and SRR (**Figure 5a**).[13] The results showed a negative refractive index for a band comprised in between 10 and 11 GHz (**Figure 5b**).

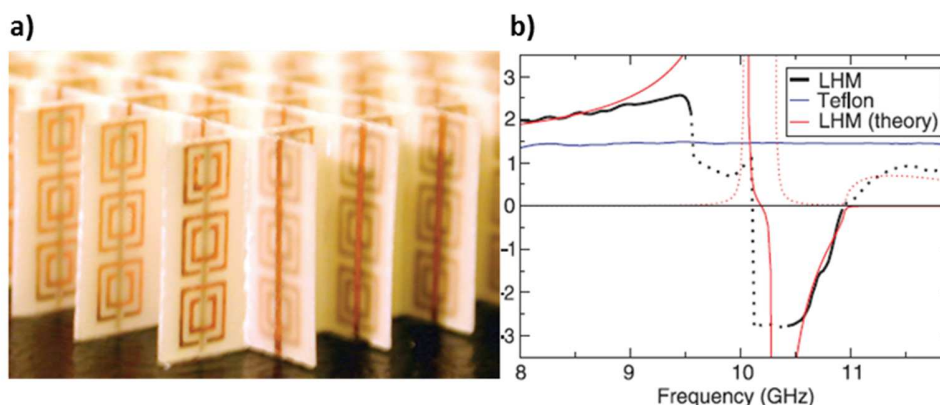


Figure 5: a) Picture of the material exhibiting a left-handed behavior. The sample is composed of square copper SRR on fiber glass circuit board material. The rings and wires are on opposite sides of the boards, and the boards have been cut and assembled into an interlocking lattice.[13] b) Graph representing n versus frequency, the blue curve corresponds to the Teflon sample. The black curve corresponds to the measured material. The dotted portions indicate the region where the index is expected to be out of the experimental limitation. The continuous red curve corresponds to the real component and the dotted one is the imaginary part of the theoretical expression.[13]

The first result of a negative refractive index was hence demonstrated for the microwave frequency range. Then it was used for smaller wavelengths, *i.e.* closer to optical frequencies, by decreasing the size of the device. In 2004, Linden *et al* published an article entitled “Magnetic response of Metamaterials at 100 Terahertz”. [14] In this report, they demonstrated that it was possible to obtain a negative value of μ at 85 THz (mid infrared) by using a SRR of a size below one micrometer (**Figure 6**). The analogy existing in between a LC circuit and a SRR is also illustrated on this figure. Later in 2005, the same team published their work on similar lithographed structures but made to be efficient at near infrared frequency, *e.g.* 200 THz.[15]

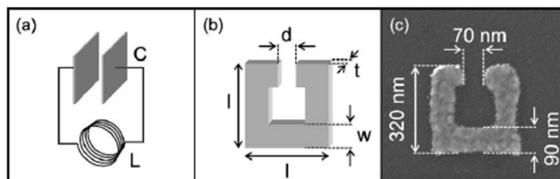


Figure 6: (a) Illustration of the analogy between a LC circuit and a single SRR, (b) scheme of the SRR geometry and (c) SEM image of a SRR fabricated by electron beam lithography extracted from [14].

The reported results evidenced that's it's possible to combine, for microwave frequencies, a composite material exhibiting $\epsilon < 0$ by using an array of wires and $\mu < 0$ by generating a resonance condition thanks to the SRR geometry.

4 ...at optical frequencies

For optical frequencies, on one hand the use of SRR prepared by lithography becomes trickier, due to the size reduction required for such high frequency. On the other hand, the need for a material bringing $\epsilon < 0$ in the composite material is also an issue especially because arrays of aligned wires are no more active at the optical range frequency. Moreover, the main drawback of this system is its anisotropy. Indeed, the incident wavelength needs to be in a particular direction to interact efficiently with the material and to exhibit meta-properties.

Aware of those limitations, Urzhumov *et al* proposed in 2007 a new concept to solve the anisotropy problem and at the same time to obtain a negative refractive index for visible frequencies.[16] They introduced the concept of metafluids which are liquid metamaterials typically made of a dispersion of plasmonic nanoclusters smaller than the wavelength of a visible beam.

A particular kind of plasmonic nanoclusters, called raspberry-like nanoclusters, has known a particular interest in the metamaterial community. They are typically made of a dielectric core surrounded by numerous plasmonic satellites randomly distributed. These structures were studied from both computational and experimental points of view. In 2009, Simovski and Tretyakov published a theoretical article focused on the use of such a structure considered as promising isotropic nano-resonator for optical magnetism purpose.[17] Later on, measurement and simulation were performed considering raspberries obtained by various methods, such as seeded-growth [18](**Figure 7**), electrostatic assemblies [19],[20], or bioinspired coupling.[21]

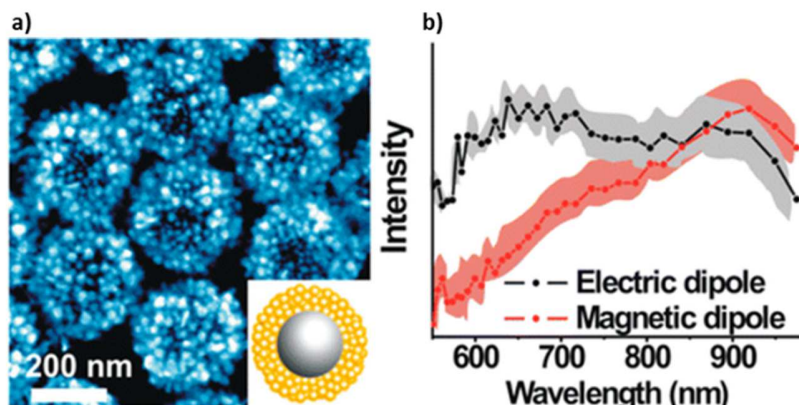


Figure 7: a) TEM image of the raspberry-like structure made of a central dielectric core surrounded by gold satellites obtained by a seeded-growth method; b) experimental spectra of the corresponding dispersion of nanoclusters showing the presence of both electric and magnetic dipoles.[18]

Meanwhile, Urzhumov *et al* theoretically investigated the case of a cluster made of four spherical plasmonic particles whose center were located along the vertices of a tetrahedron, called “tetramer”.[16] This structure presents a great interest because of its orientation-independent polarizabilities. Indeed, according to the group theory, several other structures can exhibit a similar feature: octahedron, icosahedron and dodecahedron. Among these geometrical arrangements, the tetrahedron is the simplest one and therefore chosen for the study. They numerically simulated the assembly of four gold nanoparticles spaced by a gap of few nanometers, in such condition the strong coupling coming from the closely-packed structure yielded into a magnetic resonance at optical frequencies. This magnetic resonance was strongly affected by the gap between particles as shown on **Figure 8**.

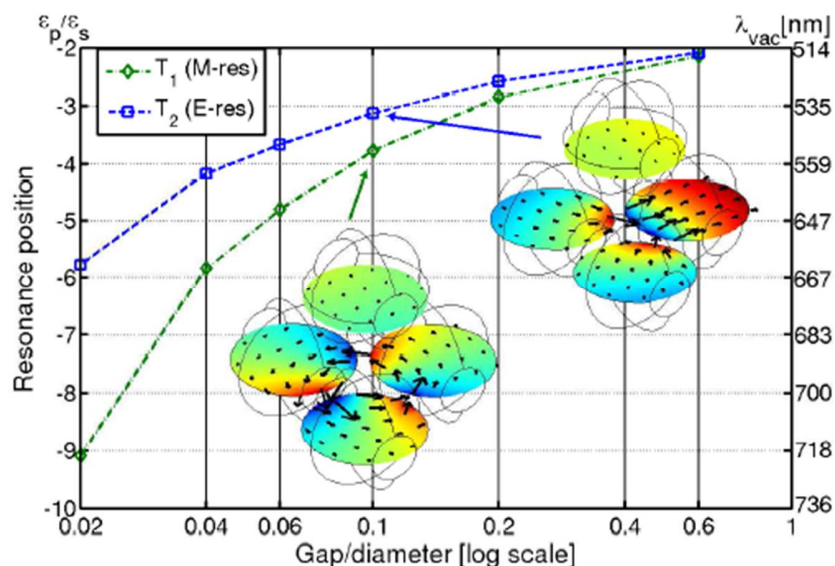


Figure 8: Simulated results presenting the location of the magnetic and electric resonances as a function of the gap-to-diameter ratio. The left axis corresponds to the resonant permittivity of a cluster over the solvent permittivity; the right axis corresponds to the resonant wavelength for a gold silica tetramer in the index matching solvent. Reported from reference [16]

The authors also presented numerical simulations performed in the case of an extremely small gap of 1 nm between each 90-nm gold spheres. A tight gap (nanometer range scale), was used to maximize the separation in between the electric and the magnetic resonances. **Figure 9** exhibits the dielectric permittivity and the magnetic permeability as a function of the wavelength for such structures.

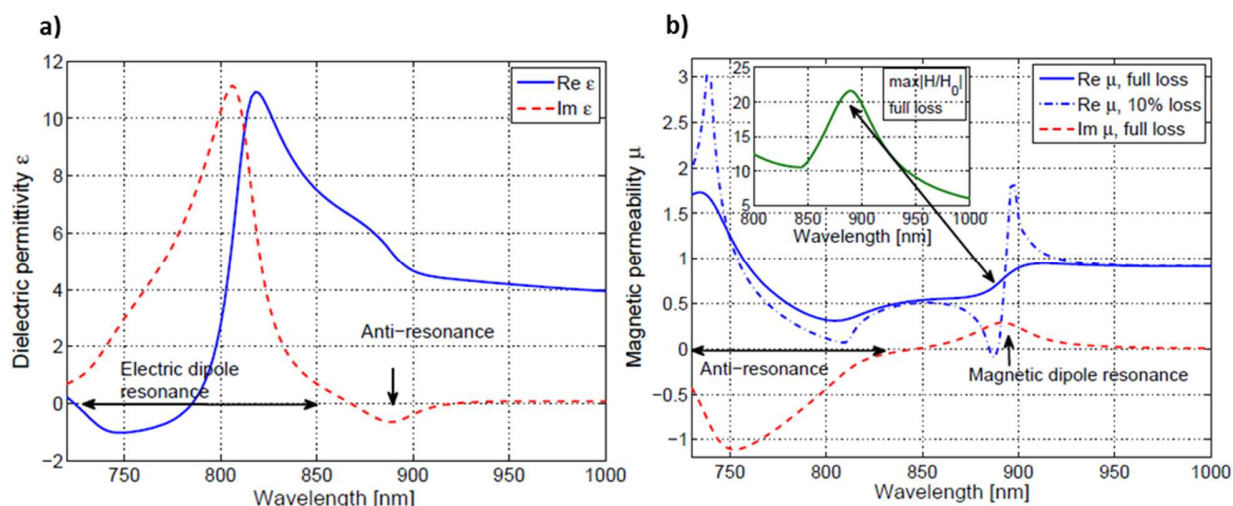


Figure 9: a) Simulated evolution of the dielectric permittivity as a function of the wavelength for a tetramer with a gap of 1 nm. The positions of the electric dipole resonance (810 nm) and magnetic dipole anti-resonance (890 nm) are identified by the two peaks of the red dotted curve ($\text{Im } \epsilon$). b) Simulated evolution of the magnetic permeability as a function of the wavelength. Reported from reference [16].

In the case of the calculation performed with only 10 % of the gold ohmic losses, it became possible to obtain $\mu_{\text{real}} < 0$ with a volume fraction of clusters in dispersion of 13 %. However to overcome the ohmic losses of gold a condensed material made of tetramers meta-atoms was an alternative to the fluid. According to the authors, achieving $\epsilon_{\text{eff}} < 0$ and $\mu_{\text{eff}} < 0$ required a specific design in term of gap. The idea is to be capable to position the magnetic dipole resonance frequency higher than the electric dipole frequency: $\omega_{MD} > \omega_{ED}$ in order to have a MD resonance within the narrow $\epsilon_{\text{eff}} < 0$.

Later, in 2009 Alu and Engheta proposed the use of plasmonic nanoclusters with an octahedral geometry and their numerical simulations allowed to predict a magnetic dipole resonance.[22] In 2011, Capolino and coworkers reported their simulation investigations on the optical properties of highly isotropic plasmonic nanoclusters considering the tetrahedral, icosahedral and raspberry-like morphologies.[23] They highlighted the efficiency of such structures to tune the optical properties. Moreover, they presented the effect of three kinds of morphological defects regarding the satellites which have effect on the properties. From the most to the less dramatical effect there is: lack of satellites > size inhomogeneity > position irregularities.

For the purpose of this work, we focused on the design of plasmonic nanoclusters for a magnetic dipole resonance in the visible range and negative refractive index, and especially on clusters

exhibiting an isotropic polarizability such as platonic solids, *e.g.* tetrahedral, octahedra and icosahedra.

From the experimental viewpoint, the synthesis and the measurements of regular plasmonic nanoclusters similar to these platonic solid were rarely reported. The synthesis was mainly performed by clusterization induced method [24] or by using DNA strand to guide the formation of the structure.[25]–[27] However, their main drawbacks were the lack of morphology control over the morphology and robustness, respectively. Indeed, the isotropy was lost while nanoclusters were flattened upon the drying step done prior to the optical measurements.

Furthermore, beyond the control over both geometry and robustness which is challenging in itself, the measurement of the optical properties of such structures is also not trivial and required specific conditions and equipment.

5 Our objectives

We intend to develop a novel route to fabricate isotropic meta-atoms by using patchy particles.[28] Those particles exhibit a highly structured surface and are defined by their site-specific modification. Moreover, there was a growing interest regarding the development of such particles especially because of their capability to self-assembled or to direct assembly along specific directions.[29],[30]

As far as we know, the use of patchy particles to form discrete and isotropic clusters of plasmonic particles has never been reported, making this approach original, innovative and challenging. Thanks to the high degree of control over the surface of such particles, we planned to build nanostructured isotropic resonators, made of a dielectric structuring patchy core surrounded by plasmonic satellites whose number and positions could be controlled.

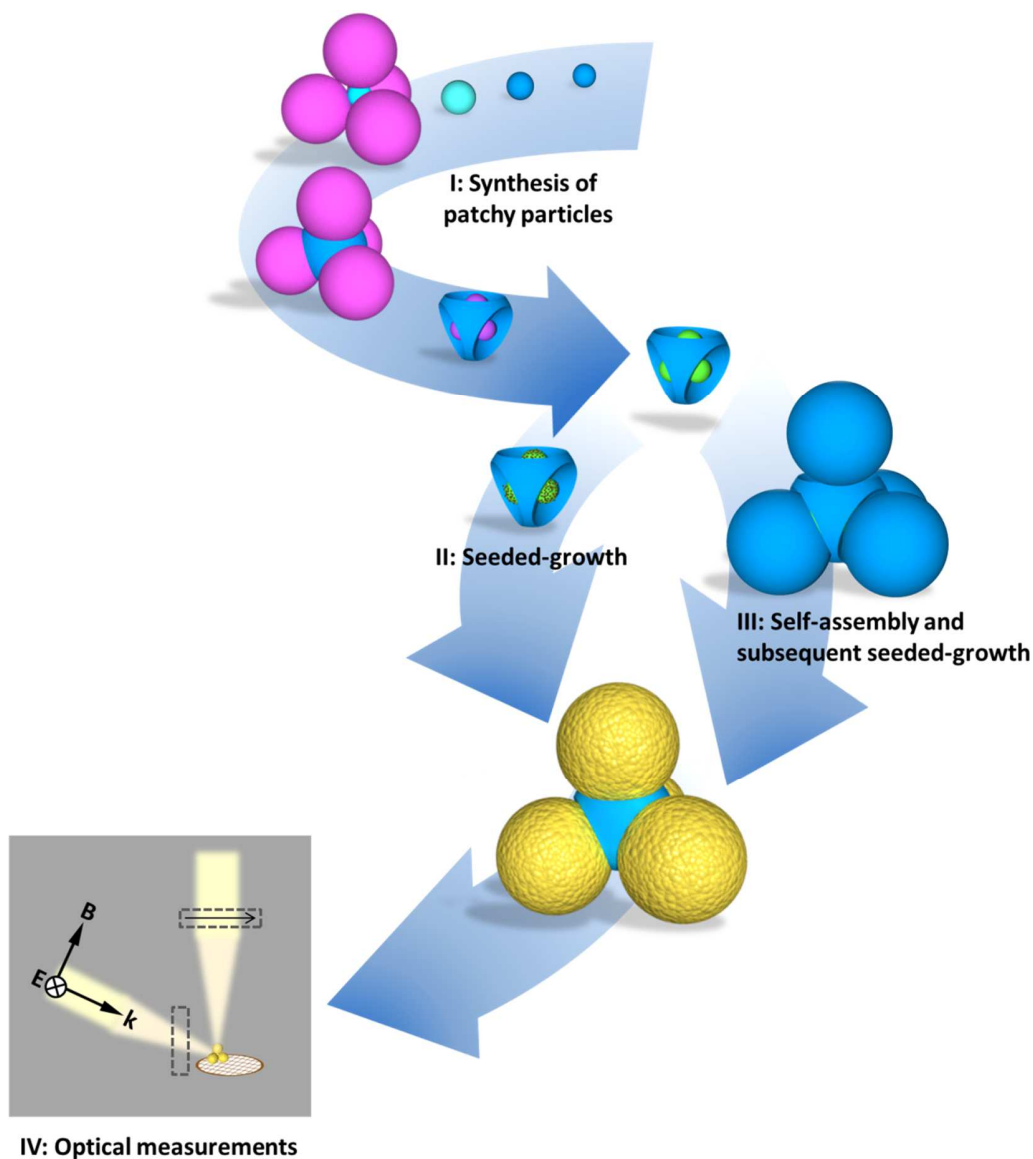
Our objectives were to produce discrete plasmonic nanoclusters in high yield exhibiting several requirements:

- Robustness,
- Control of the sphericity and orientation of the satellites and the inter-satellite gap
- Synthesis of the nanoclusters in large amounts for their subsequent assembling process.

An overview of the overall strategy is presented on **Scheme 2** and segmented as following:

- the first chapter describes the preparation of dielectric patchy particles with a size in the range of few tens of nanometers. The patchy particles are derived from silica/polystyrene multipod-like clusters, highly regular from a geometrical point of view;
- the second and third chapters present the elaboration of plasmonic nanoclusters by a seed-mediated growth approach or by assembly of preformed particles, respectively;

- the fourth chapter describes the characterizations of their optical properties.



Scheme 2: The overall strategy guiding this study: the chapter I describes the fabrication of the patchy particles; the chapters II and III report the formation of plasmonic nanoclusters through seeded-growth and self-assembly approaches, respectively; the chapter IV describes the preliminary optical measurements performed on single objects.

6 References

- [1] Y. Rahmat-Samii, "Metamaterials in Antenna Applications: Classifications, Designs and applications," *2006 IEEE international workshop*, vol. 2, pp.: 1–4, 2006.
- [2] B. Wu, W. Wang, J. Pacheco, X. Chen, T. Grzegorzczuk, J. A. Kong, and P. Art, "A study of using metamaterials as antenna substrate to enhance gain," *Prog. Electromagn. Res.*, pp. 295–328, 2005.

-
- [3] A. Vora, J. Gwamuri, N. Pala, A. Kulkarni, J. M. Pearce, and D. Ö. Güney, “Exchanging Ohmic losses in metamaterial absorbers with useful optical absorption for photovoltaics,” *Nature*, vol. 4, pp. 4901–4914, 2014.
- [4] J. B. Pendry, “Negative refraction makes a perfect lens,” *Phys. Rev. Lett.*, vol. 85, pp. 3966–3969, 2000.
- [5] X. Zhang and Z. Liu, “Superlenses to overcome the diffraction limit,” *Nat. Mater.*, vol. 7, pp. 435–441, 2008.
- [6] X. Ni, Z. J. Wong, M. Mrejen, Y. Wang, and X. Zhang, “An ultrathin invisibility skin cloak for visible light,” *Science*, vol. 349, pp. 1310–1313, 2015.
- [7] M. Brun, S. Guenneau, and A. B. Movchan, “Achieving control of in-plane elastic waves,” *Appl. Phys. Lett.*, vol. 94, pp. 061903–061906, 2009.
- [8] S. A. Cummer and D. Schurig, “One path to acoustic cloaking,” *New J. Phys.*, vol. 9, pp. 1–8, 2007.
- [9] D. Torrent and J. Sánchez-Dehesa, “Sound scattering by anisotropic metafluids based on two-dimensional sonic crystals,” *Phys. Rev. B*, vol. 79, pp. 174104–174113, 2009.
- [10] V. G. Veselago, “The electrodynamics of substances with simultaneously negative values of epsilon and mu,” *Sov. Phys. USPEKHI*, vol. 10, pp. 509–514, 1968.
- [11] J. B. Pendry, A. J. Holden, D. J. Robbins, and W. J. Stewart, “Magnetism from conductors and enhanced nonlinear phenomena,” *IEEE Trans. Microw. Theory Tech.*, vol. 47, pp. 2075–2084, 1999.
- [12] K. Chang, “Light Fantastic: Flirting With Invisibility,” *NY Times*, vol. June, 2007.
- [13] R. A. Shelby, D. R. Smith, and S. Schultz, “Experimental verification of a negative index of refraction,” *Science*, vol. 292, pp. 77–79, 2001.
- [14] S. Linden, C. Enkrich, M. Wegener, J. Zhou, T. Koschny, and C. M. Soukoulis, “Magnetic response of metamaterials at 100 terahertz,” *Science*, vol. 306, pp. 1351–1353, 2004.
- [15] C. Enkrich, M. Wegener, S. Linden, S. Burger, L. Zschiedrich, F. Schmidt, J. Zhou, T. Koschny, and C. Soukoulis, “Magnetic Metamaterials at Telecommunication and Visible Frequencies,” *Phys. Rev. Lett.*, vol. 95, pp. 203901–203905, 2005.
- [16] Y. A. Urzhumov, G. Shvets, J. Fan, F. Capasso, D. Brandl, and P. Nordlander, “Plasmonic nanoclusters: a path towards negative-index metafluids,” *Opt. Express*, vol. 15, pp. 14129–14145, 2007.
- [17] C. R. Simovski and S. A. Tretyakov, “Model of isotropic resonant magnetism in the visible range based on core-shell clusters,” *Phys. Rev. B*, vol. 79, pp. 045111–045120, 2009.
- [18] Z. Qian, S. P. Hastings, C. Li, B. Edward, C. K. McGinn, N. Engheta, Z. Fakhraai, and S. Park, “Raspberry-like Metamolecules Resonances,” *ACS Nano*, vol. 9, pp. 1263–1270, 2015.

-
- [19] A. Le Beulze, “Dissertation from Bordeaux 1 University: Synthesis and characterization of nanoresonators for metamaterials application in the visible range,” 2013.
- [20] S. Mühlig, A. Cunningham, J. Dintinger, M. Farhat, S. Bin Hasan, T. Scharf, T. Bürgi, F. Lederer, and C. Rockstuhl, “A self-assembled three-dimensional cloak in the visible.,” *Nature*, vol. 3, pp. 1–7, 2013.
- [21] S. N. Sheikholeslami, H. Alaeian, A. L. Koh, and J. A. Dionne, “A Metafluid Exhibiting Strong Optical Magnetism,” *Nano Lett.*, vol. 13, pp. 4137–4141, 2013.
- [22] A. Alù and N. Engheta, “The quest for magnetic plasmons at optical frequencies.,” *Opt. Express*, vol. 17, pp. 5723–5730, 2009.
- [23] A. Vallecchi, M. Albani, and F. Capolino, “Collective electric and magnetic plasmonic resonances in spherical nanoclusters.,” *Opt. Express*, vol. 19, pp. 2754–2772, 2011.
- [24] A. S. Urban, X. Shen, Y. Wang, N. Large, H. Wang, M. W. Knight, P. Nordlander, H. Chen, and N. J. Halas, “Three-dimensional plasmonic nanoclusters.,” *Nano Lett.*, vol. 13, pp. 4399–4403, 2013.
- [25] F. Li, D. P. Josephson, and A. Stein, “Colloidal assembly: the road from particles to colloidal molecules and crystals.,” *Angew. Chem. Int. Ed. Engl.*, vol. 50, pp. 360–388, 2011.
- [26] S. J. Barrow, X. Wei, J. S. Baldauf, A. M. Funston, and P. Mulvaney, “The surface plasmon modes of self-assembled gold nanocrystals.,” *Nat. Commun.*, vol. 3, pp. 1–9, 2012.
- [27] X. Shen, A. Asenjo-Garcia, Q. Liu, Q. Jiang, F. Javier García de Abajo, N. Liu and B. Ding, “Three-Dimensional Plasmonic Chiral Tetramers Assembled by DNA Origami,” *Nano Lett.*, vol. 13, pp. 2128–2133, 2013.
- [28] S. C. Glotzer and Z. Zhang, “Self-Assembly of Patchy Particles,” *Nano Lett.*, vol. 4, pp. 1407–1413, Aug. 2004.
- [29] G.R. Yi, D. J. Pine, and S. Sacanna, “Recent progress on patchy colloids and their self-assembly.,” *J. Phys. Condens. Matter*, vol. 25, pp. 193101–193113, May 2013.
- [30] G. Van Anders, N. K. Ahmed, R. Smith, M. Engel, and S.C. Glotzer, “Entropically Patchy Particles: Engineering Valence through Shape Entropy,” *ACS Nano*, vol. 8, pp. 931–940, 2014.

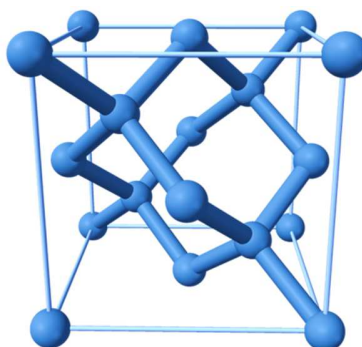
Chapter 1: Synthesis of patchy silica particles

In order to control the number and position of the plasmonic satellite particles, we intended to program their assembly or growth by decorating the surface of the central dielectric particle with sticky patches, *i.e.* chemical and/or topological discontinuities, the latter being generally called “dimples” when they are concave areas on a spherical (convex) particle.

This chapter is dedicated to the fabrication of dimpled particles bearing moreover a sticky patch at their bottom. It is firstly composed of the description of the state of the art about the fabrication of patchy particles. We reviewed the most promising techniques and then highlighted the relevance of our approach among all the other routes. The second part of this chapter is dedicated to the description of the fabrication of dimpled particles according to the seeded-growth emulsion polymerization process and subsequent surface modification reactions previously developed by Désert and coworkers. Nevertheless, some extra efforts were done for a better understanding of the involved processes. The last section presents original works to derive dimpled silica particles into patchy ones.

1 Synthesis of patchy particles: state of the art

At the origin, the concept of patchy particles has been introduced through computer simulations for trying to answer the question: “How to obtain non-compact three dimensional arrays of particles?”. Several teams have developed simulations to understand how giving valence to colloids is an efficient way to limit their interactions, such as those of Glotzer [1]–[4], Sciortino [5]–[7] or Bianchi.[8],[9] For instance, if a diamond-like structure is envisioned, the valence of the colloids shall be restricted to four by the creation of patches at their surface in order to limit and orient their interactions towards the four vertices of a tetrahedron.[6] Recent simulations showed that the patch-to-particle ratio is also a critical parameter (**Scheme 3**).[10]



Scheme 3: Diamond-like lattice evidencing its low compactness due to the four-fold valence of the constitutive carbon atoms.

Later, chemists and physical-chemists have started to work on that concept and tried to produce colloidal assemblies. Today, a few examples of patchy particles have been reported but none of them has yielded to a 3-dimensional array. Sometimes, the achieved assemblies have been a small number of discrete clusters. Several review articles have already been focused on patchy

particles.[11]–[16] Recently, Glotzer and coworkers introduced the complementary concept of enthalpic and entropic patches.[4] The first one refers to patches made of sticky chemical functions able to promote an assembly while the second one refers to the topological surface specificities capable of mechanically blocking directional interaction with other colloids. Here, for the sake of succinctness, the state of the art is restricted to the cases of particles with four patches or more. Generally, the robust fabrication techniques use temporary masks for the regioselective modification of the surface. Those masks are often other colloids which have to be previously positioned with the right number and at the right places. This positioning is generally managed by playing with steric repulsions in confinement situations, *e.g.* within colloidal crystals or droplets, or around a sticky protrusion or a seed.

1.1 Technique exploiting the confinement on a substrate with neighboring particles: the glancing angle deposition (GLAD) technique

The GLAD technique consists in using a given orientation of a particle monolayer packed on a substrate on which a metal vapor is deposited. In this configuration, any particle within the monolayer acts as a shadowing mask for their neighbors. This method was used by Pawar and Kretzschmar to produce patchy particles. Various particle sizes were used to create the monolayer. The shape of the gold patches was controlled by playing on both the orientation of substrate and beam, [17] allowing the elaboration of multifunctional patchy particles.[18] Moreover, stepwise GLAD was used to produce chiral nanostructures by varying the angle or the thickness of the deposition (**Figure 10**).[19] Later, a method combining GLAD with the use of a grooves carved into wafer substrate was reported.[20],[21] This progress allowed to increase the control over the patches formation because of the shadowing effect provided both by the groove and the neighbor particles yielding into new patch shapes such as crescent moon. Such patchy particles can be recovered by disassembly from the substrate.

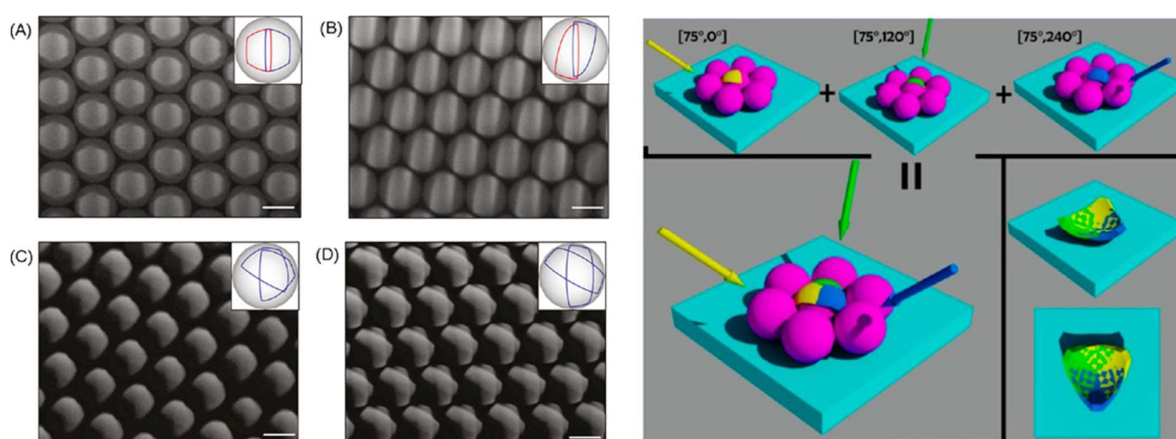


Figure 10: Left: Four SEM images showing monolayers of particles packed on a substrate after modification by GLAD for various angles of deposition and the corresponding picture in insert schematizing the areas affected by the beam.[18] Scale bar: 2 μm . Right: Scheme of the principle used during stepwise GLAD where three beams of deposited materials were iteratively sent on the particle monolayer at specific angles.[19]

1.2 Techniques exploiting the confinement within emulsion droplets

The technique was derived from the pioneering work of Manoharan *et al.* which consisted in using toluene-in-water emulsions to confine cross-linked polystyrene (PS) particles and get colloidal clusters.[22] In practice, the particles initially stabilized at the oil-water interface are forced to be closer and closer as far as the oil phase is evaporated. The number of particles making the clusters wasn't perfectly controlled and the complex mixtures of clusters were necessarily purified by centrifugation in density gradient solutions. Those colloidal clusters were later used to produce patchy particles as published by Wang *et al.*(**Figure 11**).[23] DNA was efficiently grafted on the surface of colloidal clusters previously prepared by clusterization of amidinated PS microspheres.[23] The clusters were swollen by styrene until the particles forming the clusters protrude from the swollen part; then the styrene was polymerized and the protruding particles became patches bearing amidine groups on their surface. Biotin was subsequently grafted specifically on the site marked with amidine forming biotin patches finally used to attach DNA via a biotin-streptavidin-biotin linkage for converting them into DNA patches.

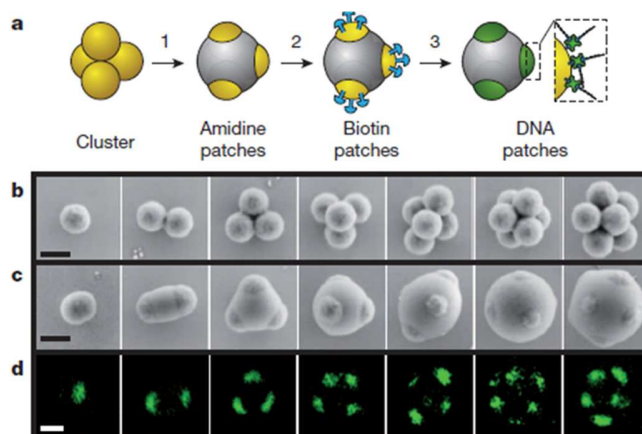


Figure 11: Fabrication of DNA-based patchy particles. a) Synthesis route: 1. a cluster of 4 amidinated PS microspheres is swollen with styrene which is then polymerized; 2. biotin is site-specifically functionalized on the patches; 3. biotin-DNA oligomers are bind to the particle patches via a biotin–streptavidin–biotin linkage. SEM images of the as-obtained amidinated b) clusters;c) patchy particles. d) Confocal fluorescent images of the latter. Scale bars: 500 nm.[23]

Furthermore, thanks to the recent work of Wang *et al.*[24], the concept used to produce patchy particles thanks to clusterization from one side [23],[25]–[27] and the lock-and-keys colloids on the other side [28] were combined in order to produce particles with several cavities, *i.e.* dimples (**Figure 12**).

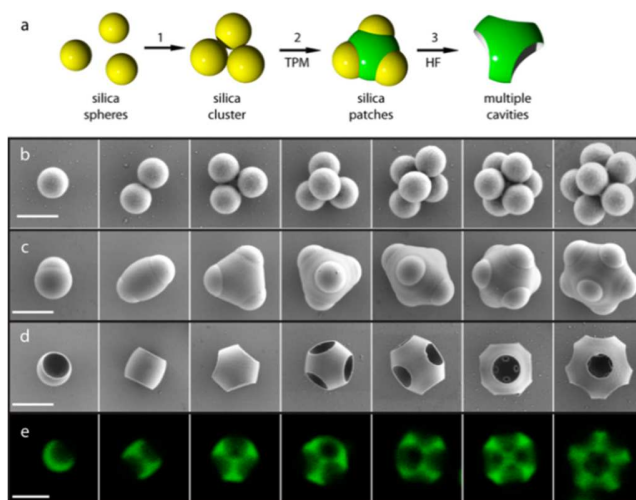


Figure 12: Multidimpled particle fabrication. a) Synthesis route: 1. a cluster of three silica spheres is prepared via an emulsion-encapsulation process; 2. partial encapsulation of the cluster with 3-(trimethoxysilyl)propylmethacrylate (TPM); 3. The silica cluster is etched out via treatment with hydrofluoric acid. SEM images of b) silica clusters, c) silica-TPM patchy particles, and d) multidimpled particles. e) Confocal fluorescent images of the fluorescently-labeled multidimpled particles. Scale bars: 500 nm.[24]

1.3 Techniques exploiting the confinement around sticky protrusions

The coalescence of polymer particles through liquid protrusions was used according to two main strategies. The first one consisted in connecting particles bearing liquid protrusions through their merging giving particles exhibiting protruding spheres considered as patches. As shown by Kraft *et al.*, cross-linked-PS colloids swollen with monomer, *e.g.* styrene, can be warmed in order to release protruding monomer drops through phase separation. During a subsequent step, monomer drops coalesced, linking the cross-linked-PS sphere into colloidal clusters [29] (**Figure 13 left**). Here, the protruding precursor cross-linked PS spheres may be considered as potential patches.

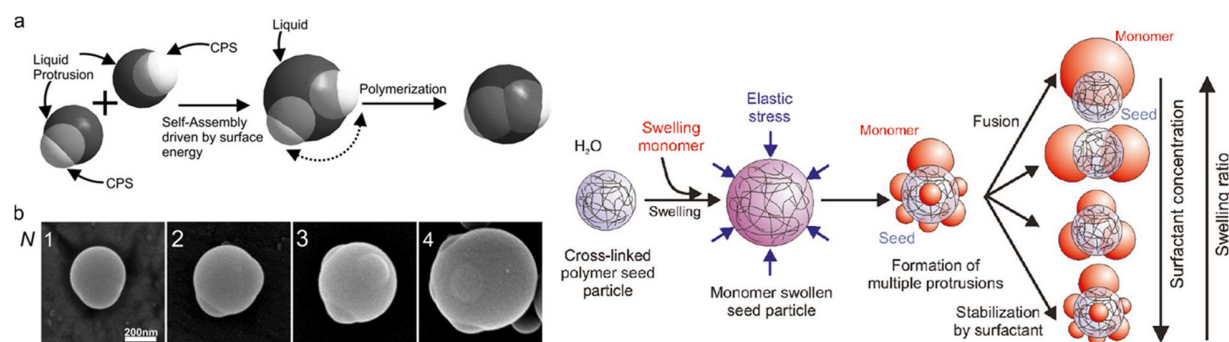


Figure 13: Left: a) The strategy used to produce submicronic patchy particles: Particles bearing a liquid protrusion are basically self-assembled together through the protrusion merging; b) SEM images for 1, 2, 3 and 4 patches on particles resulting from the previously-described process.[29] Right: Scheme of the strategy used to produce particles with various numbers of protrusions at the surface of the cross-linked seeds.[30]

The second strategy to generate patchy particles by playing with sticky protrusions was the controlled phase separation of cross-linked polymer spheres swollen by monomer. Indeed, a balance exists between the interfacial forces exerted at the surface of the particles and the elastic

stress.[30] The first one is directly related to the concentration of sodium dodecyl sulfate (SDS) in the medium while the second is inherent to the cross-linking degree of the particles. In such condition, by playing with the surfactant concentration and the cross-linking degree of the particles, the interfacial surface tension existing on the monomer drop was tuned and the drops merging controlled in such a way that the protruding monomer can be considered as patches (**Figure 13 right**).

1.4 Techniques exploiting the confinement on a seed by emulsion polymerization

Silica particles with a well-controlled number of dimples (from four to twelve) [31] were synthesized starting from silica/PS clusters prepared by a seeded-growth emulsion polymerization technique (**Figure 14** and **Figure 15**).[32]–[35]

Typically, silica/PS clusters made of 4, 6 or 12 PS satellites were prepared in high morphology yield (up to 80 %) and at the gram scale.[35],[36] The first step was the production of highly size-monodisperse silica particles through a seeded-growth approach [35],[37] immediately followed by a surface modification by using a hydrophobizing and copolymerizing silane molecule, *e.g.* methacryloxymethyltriethoxysilane (MMS), to enhance the affinity of the silica surface for styrene and growing PS macromolecules. The MMS surface density shall be low and controlled, because it conditions the wetting angle of the PS satellites onto the silica seed: The higher the surface density, the more wetting the PS satellites, *i.e.* leading to core-shell morphologies. It was demonstrated that the optimal nominal surface density was 0.5 function/nm². It may be noted that the adjective “nominal” means that this value corresponds to the amount of MMS introduced in the reactor and probably not exactly to the true value as it could be measured through time-consuming spectroscopic, gravimetric or dosage surface techniques. The second step is the seeded-growth emulsion polymerization of styrene performed in the presence of a surfactant mixture made of Synperonic[®] NP 30 and SDS and initiated by the thermal decomposition of sodium persulfate (**Figure 14**). Playing with experimental parameters, *e.g.* the size of the silica seeds, the SDS fraction in the surfactant mixture and the styrene concentration, the number of PS satellites per silica core were quite easily varied, getting batches with morphology purity as high as 80 %. In particular tetrapods, hexapods and dodecapods were got from silica seeds with diameters of 55, 85 and 85 nm, respectively.

Afterwards, the silica cores were regrown through a hydrolysis/condensation reaction of tetraethoxysilane (TEOS) and then the PS nodules were dissolved in tetrahydrofuran (THF). Those dimpled silica particles present PS bumps remaining at the bottom of the dimples and corresponding to the PS macromolecules covalently bonded to the silica surface thanks to the copolymerization of styrene and MMS-derived grafts.[23]

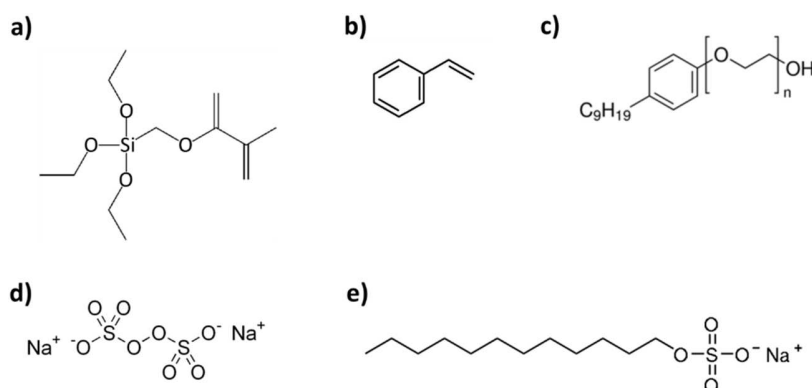


Figure 14: Chemical formulae of the main reagents used for getting silica PS/clusters through a seeded-growth emulsion polymerization: a) methacryloxymethyltriethoxysilane (MMS); b) styrene; c) Synperonic[®] NP 30; d) sodium persulfate and e) SDS.[35],[36]

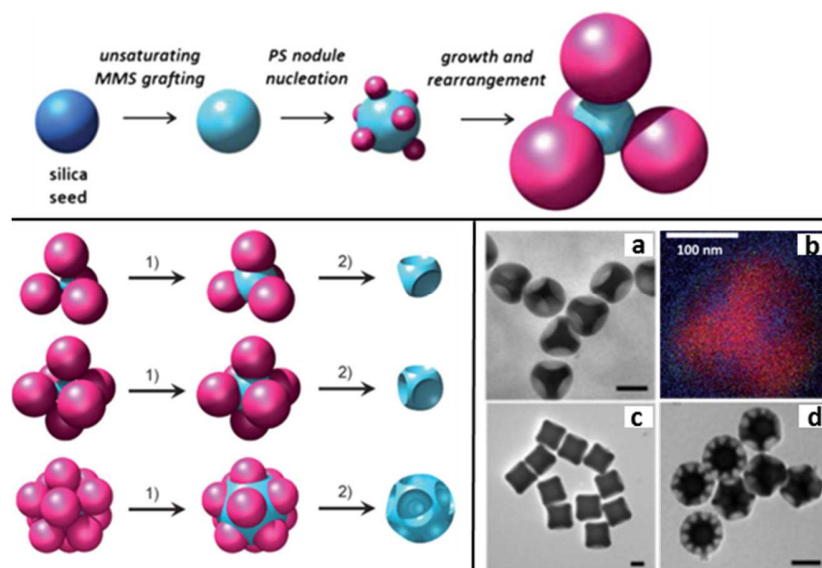


Figure 15: Top: Strategy of fabrication of silica-PS hybrid clusters from surface-modified silica seeds introduced in the reactive medium of an emulsion polymerization of styrene;[35] Bottom Right: Strategy used to synthesize dimpled silica particles of various controlled morphologies by 1) regrowth of the silica core in the presence of TEOS and 2) dissolution of the PS satellite nodules. On the right (Bottom): TEM images and EDX (Energy-dispersive X-ray spectroscopy) cartography of a four-dimpled silica particle a) and b), respectively. The EDX mapping highlight the presence of carbon (blue) within each dimpled area of the silica particle (silicon element in red) corresponding to the remaining PS chains.[31] The TEM images c) and d) correspond to six- and twelve-dimpled silica particles, respectively.

1.5 State-of-the-art conclusion and strategy to be implemented

Along this state-of-the art, we have listed various fabrication techniques of patchy particles. **Table 1** summarizes the main features of those techniques. We intentionally highlighted the critical aspects regarding our own objectives. We were indeed interested in a fabrication technique of patchy particles with a diameter of 50-200 nm. The patchy particles shall be homogeneous in term of size, morphology, patchiness and have to exhibit a strong stickiness potentiality to provide robustness to the future assembly. Moreover, they shall be produced at the

gram scale in order to develop ultimately metamaterials. The versatility was our last criterion by preferring synthesis routes capable to vary the number of patches, typically from four to twelve.

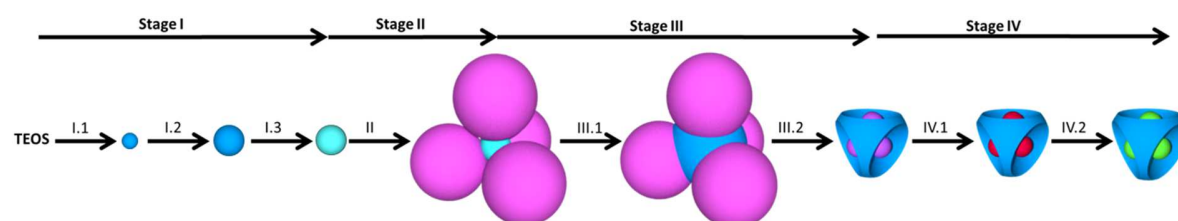
Table 1: Comparative summary of the features of the patchy particle fabrication techniques.

Fabrication techniques		On a substrate with neighboring particles	Within emulsion droplets	Around sticky protrusions	On a seed by emulsion polymerization
References		[17]–[21]	[22]–[24],[26]–[28]	[29],[30]	[31]–[36],[38]
Size domain	1–9 μm	⊙	⊙	⊙	
	100–999 nm	●		●	⊙
Accurate control over	Chemical composition	⊙	⊙	⊙	⊙
	Relative size		⊙		⊙
	Robustness	⊙	⊙	⊙	⊙
	Morphology yield	⊙			⊙
	Patch number	⊙	⊙		⊙
	Patch orientation	⊙	⊙		⊙
	Patch stickiness	●	⊙	●	⊙
Up-scalability up to the gram scale			●	●	⊙

⊙ already demonstrated; ● not yet demonstrated, but reasonably conceivable in terms of time and money

For these reasons, the technique exploiting the confinement on a central seed by emulsion polymerization was doubtlessly chosen. The main development to implement and fulfill our objectives was to make the dimples sticky. Therefore, we decided to take advantage of the presence of the residual PS macromolecules at the bottom of the dimples [31] for performing chemical modification reactions in order to create reactive groups along the chains.

Scheme 4 summarizes the overall strategy described in this chapter for synthesizing patchy particles made of a controlled number (4, 6 or 12) of sticky dimples. The next section describes the preparation of the dimpled particles (stages I to III).



Scheme 4: Four-stage synthetic strategy to fabricate silica dimpled particles with reactive PS chains at the bottom of the dimples. Stage I: synthesis of size-monodisperse silica seeds: I.1 synthesis of silica pre-seeds by the Hartlen’s method; [37] I.2 growth of the silica pre-seeds and I.3 silica surface modification using MMS. Stage II: synthesis of the multipod-like silica/PS clusters by seeded-growth emulsion polymerization. Stage III: derivatization of the multipod-like silica/PS clusters into dimpled silica particles: III.1 silica core regrowth and III.2 PS dissolution. Stage IV: making the dimples sticky for assembly purpose: IV.1 chloromethylation of the PS residue; IV.2 amination or thiolation of the chloromethylated PS residue.

Beyond the protocols previously developed by Désert and coworkers, we made some efforts for a better understanding and control of the final particle morphology. The last section concerns the

strategy that we implemented for making the dimples sticky with regard to gold, *i.e.* decorated with amino or thiol groups (stage IV).

2 Preparation of silica particles bearing 4, 6 or 12 dimples

The purpose of this section is to report the fabrication and characterization of dimpled particles through the multistep strategy developed by Désert and coworkers (**Scheme 4 stages I to III**).[31],[35],[36] For reasons previously mentioned, we focused on the particles with 4, 6 or 12 dimples, deriving from silica/PS clusters exhibiting tetrahedral, octahedral and icosahedral morphology, respectively. The stage I consisted in the synthesis of MMS-modified silica seeds with diameters of 55 and 85 nm for tetrapods and hexapods, respectively, while the dodecapods used in this study came from already-existing batches made from 85 nm silica particles.

2.1 Synthesis of size-monodisperse silica seeds

2.1.1 Synthesis of silica nanospheres

The production of highly monodisperse silica particles was based on a seeded-growth strategy, as initially reported by Hartlen *et al.* [37] and later improved by Désert *et al.*[36] The first step involved the production of silica nanoparticles, called “pre-seeds”. The “pre-seeds” are synthesized by the slow diffusion and then reaction of TEOS through the interface of a biphasic medium maintained at 60°C under controlled stirring in the soft alkaline conditions generated by an aqueous solution of arginine (**Figure 16a/b**).

The as-obtained “pre-seeds” are then regrown into seeds in an ethanol/ammonia mixture, *i.e.* in the more conventional conditions early described by Stöber and coworkers.[39] The final size of the silica seeds is controlled by the amount of added TEOS. The size-monodispersity is preserved by using a low TEOS concentration in order to avoid the occurrence of a secondary silica nucleation.

Protocol 1: Synthesis of the silica “pre-seeds”.

*One hundred mL of 6 mM L-Arginine (99 %, Sigma- Aldrich) aqueous solution are poured in a 150-mL double-walled vial and equipped with a reflux condenser (**Figure 16b**). When the temperature is stabilized at 60°C, 10 mL of TEOS (99 %, Sigma-Aldrich) are added. The magnetic stirring is set to 150 rpm for a 3-cm cylindrical magnetic stirrer to generate a small and stable vortex and an interface between both phases of constant surface area. The reaction goes on until the TEOS (upper phase) fully disappears. Typically, two days are required to convert 10 mL of TEOS into pre-seeds.[36]*

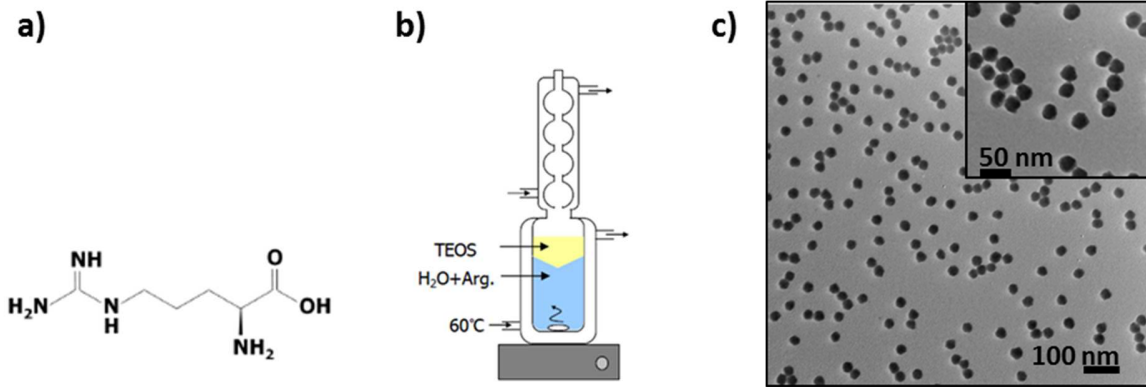


Figure 16: Synthesis of the silica “pre-seeds”: a) chemical formula of L-arginine; b) scheme of the setup and c) typical TEM images of the as-obtained particles.

The pre-seeds were characterized by transmission electron microscopy (TEM) (**Figure 16c**). A dispersion of silica “pre-seeds”, exhibiting an average diameter of 29.2 nm [determined by statistical analysis of TEM images performed over 100 particles] with a polydispersity index (PDI) of 1.01, as calculated thanks to the **Eq. 1**, was obtained. The dry extract method allowed to determine the silica concentration (25.2 g/L) and then to calculate the concentration of particles ($8.8 \cdot 10^{17}$ part/L) using **Eq. 2**.

$$PDI = \frac{D_w}{D_n} = \frac{\sum n_i \sum n_i \cdot d_i^4}{\sum n_i \cdot d_i \sum n_i \cdot d_i^3} \quad \text{Eq. 1}$$

$$C_{NP \text{ Silica}} = \frac{6 \cdot C_m(\text{Silica})}{\pi \cdot d_{\text{Silica}}^3 \cdot \rho_{\text{Silica}} \cdot 10^{-21}} \quad \text{Eq. 2}$$

$C_m(\text{Silica})$ = mass concentration of silica pre-seeds dispersion; ρ_{Silica} = silica density (2.2 g/cm^3); d_{Silica} = diameter of the silica “pre-seeds” as measured by TEM; D_w = weight-average diameter; D_n = number-average diameter.

The amount of TEOS added during the regrowth of the “pre-seeds” is critical to control the final size of the silica particles (**Eq. 3**) and depends on the targeted diameter of the silica particles D_f , the diameter of the silica pre-seeds D_i and the number of silica particles N_{Silica} contained in a given volume of pre-seeds dispersion. M_{TEOS} is the molecular weight of TEOS (208.32 g/mol); ρ_{TEOS} is the TEOS density (0.94 g/cm^3) and M_{Silica} is the molecular weight of silica (60.08 g/mol).

$$V_{\text{TEOS}} = \frac{M_{\text{TEOS}} \cdot \rho_{\text{Silica}}}{M_{\text{Silica}} \cdot \rho_{\text{TEOS}}} N_{\text{Silica}} \cdot \frac{\pi}{6} \cdot (D_f^3 - D_i^3) \quad \text{Eq. 3}$$

Protocol 2: Regrowth of the silica “pre-seeds”.

In a 1-L flask surmounted by a bubbler, 455 mL of ethanol (99 %), 35 mL of ammonia (28-30 %, J.T. Baker) corresponding to $[\text{NH}_3] = 1 \text{ M}$ and 10 mL of pre-seed aqueous

dispersion [H₂O] = 3.6 M are mixed by magnetic stirring. The proper volume of TEOS as calculated from Eq. 3 is added dropwise using a syringe pump at the rate of 0.5 mL/h.

These experiments were performed several times in order to get batches of silica seeds of three different sizes (**Figure 17, Table 2**). The average sizes and PDI values were calculated thanks to the results given by the Image J freeware [40] by counting over one to two hundreds of particles.

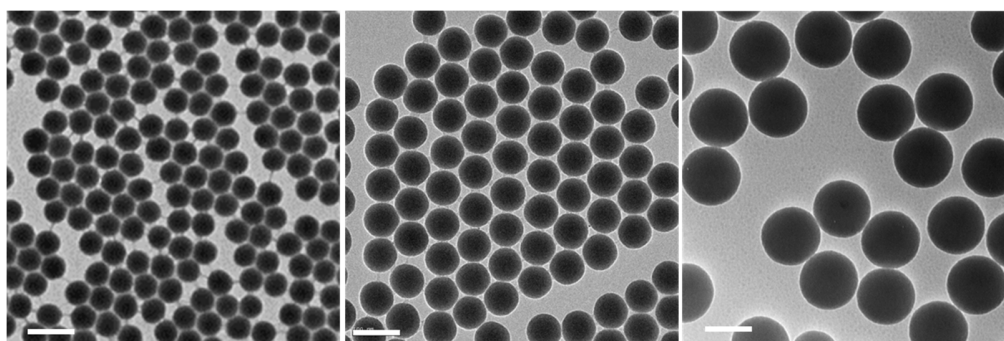


Figure 17: From left to right, typical TEM images of 52 nm, 86 nm and 137 nm silica spheres as-obtained through the controlled regrowth of 29.2 nm pre-seeds. Scale bars: 100 nm.

Table 2: Experimental conditions of the silica synthesis and regrowth stages and size measurement results of the silica seeds obtained as extracted from statistical analysis of TEM images.

Silica pre-seeds synthesis ⁽¹⁾			1 st regrowth stage ⁽²⁾					2 nd regrowth stage (optional) ⁽²⁾				
V _{TEOS} (mL)	D _{silica} (nm)	PDI ⁽³⁾	TEOS/silica wt. ratio	D _{silica} targeted (nm)	D _{silica} obtained (nm)	PDI ⁽³⁾	Conc. (part/L)	TEOS/silica wt. ratio	D _{silica} targeted (nm)	D _{silica} obtained (nm)	PDI ⁽³⁾	Conc. (part/L)
10	29.2	1.01	13	55	52	1.005	1.98x10 ¹⁶	-	-	-	-	-
-	-	-	83	85	86	1.002	1.47x10 ¹⁶	20	135	137	1.001	1.47x10 ¹⁶

(1) Reacting medium: 100 mL of L-arginine aqueous solution (6 mM) at 60°C

(2) Reacting medium: 455 mL of ethanol, 35 mL of ammonia and 10 mL of the aqueous dispersion of silica at room temp.

(3) See **Eq. 1**

The as-obtained silica particles exhibited a size in good agreement with the targeted one. That confirmed the robustness of both regrowth protocol and precursor amount calculations. Moreover, the calculated PDI values were comparable to those reported by Désert and coworkers.[36]

2.1.2 Surface activation of the silica nanospheres by grafting of organoalkoxysilanes

The process used to compatibilize the silica surface with styrene and then PS is a conventional surface modification using a hydrophobizing organoalkoxysilane to be covalently bonded to the seed surface. Basically, by playing with the nature and/or surface density of the hydrophobic grafts, it's possible to tune the contact angle existing in between the silica surface and the PS growing nodule. It was shown by Désert and coworkers that, using MMS, a nominal surface density of 0.5 graft per nm² of silica surface is the optimal value for getting multipod-like

particles.³³ Lower values make the clusters unstable, *e.g.* falling down on TEM grids, and higher values lead to silica cores more or less perfectly embedded in a continuous PS shell. The amount of MMS required was therefore calculated by using **Eq. 4** and it was added to the silica seeds dispersion directly to their regrowth medium.

$$V_{MMS} = \frac{6 \cdot d_{MMS} \cdot M_{MMS} \cdot V_{Silica\ sol} \cdot C_{Silica\ sol}}{N_A \cdot \rho_{MMS} \cdot \rho_{Silica} \cdot D_{Silica}} \quad \text{Eq. 4}$$

d_{MMS} = density of MMS function grafted by nm^2 ; M_{MMS} = molecular weight of MMS (262.37 g/mol) ; ρ_{MMS} = MMS density 0.998 g/cm^3 ; $V_{Silica\ sol}$ = volume of silica seeds suspension ; $C_{Silica\ sol}$ = concentration of silica seeds solution ; D_{Silica} = diameter of the silica seeds ; N_A = Avogadro's number.

Protocol 3: Functionalization of the silica seeds by MMS.

A known volume of the hydro-alcoholic dispersion of the silica seeds – as directly obtained from Protocol 2 is introduced in a flask over a magnetic stirrer and surmounted by a condenser. The MMS amount calculated using Eq. 4 is directly added to the reactor and let to react under stirring for 3 h at ambient temperature. The dispersion is then heated to 90°C for 1 h under reflux of ethanol. The dispersion is subsequently concentrated with a rotavap, let to cool down at room temperature and dialyzed against ultrapure water to remove ethanol and ammonia and replace them with water.

Table 3 summarizes the experimental conditions used to produce batches of MMS-modified silica particles.

Table 3: Experimental conditions used during the MMS surface modification of silica particles and their final concentrations after purification.

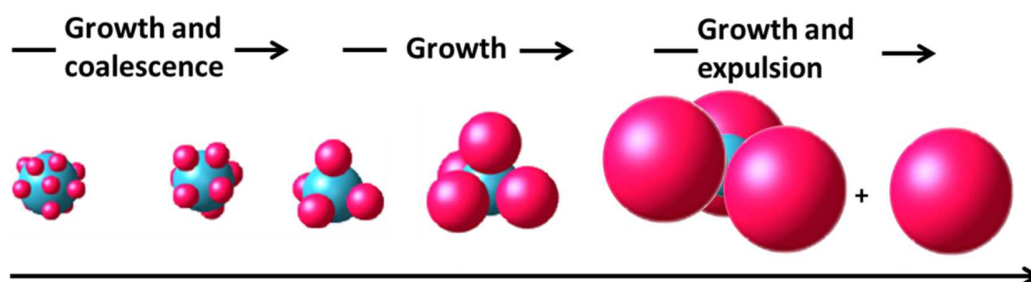
D_{Silica} (nm)	d_{MMS} function/ nm^2	$V_{Silica\ sol}$ (mL)	V_{MMS} (μL)	$C_{Silica\ MMS\ sol}$ (g/L)
52	0.5	100	2.87	34.5
86	0.5	100	5.80	28.0

2.2 Synthesis of the multipod-like silica/PS clusters by seeded-growth emulsion polymerization

The multipod-like silica/PS clusters were synthesized by seeded-growth emulsion polymerization. Briefly, the emulsion polymerization can be defined as a free-radical polymerization in a direct emulsion made of water, monomer and surfactants. When introduced above the critical micellar concentration (CMC) the surfactant molecules form micelles (small spherical assemblies minimizing their energy by sharing the hydrophobic tails of their constitutive surfactant molecules). From a chemical viewpoint, the monomer is mainly contained in the droplets, but a fraction of the monomer molecules diffuses through the water phase and swells the surfactant micelles. The polymerization starts with the addition of the water-soluble initiator and its thermal decomposition into free-radical. By meeting the monomer molecules,

active centers are generated, become more and more hydrophobic as the monomer addition and are finally captured by the micelles where the stocked monomer is polymerized according to the conventional propagation and termination stages. The micelles are permanently fed in monomer by diffusion from the reservoir droplets. From a colloidal viewpoint, the micelles grow and become polymer particles stabilized by the surfactant molecules and are generally called “latex” particles. It may be mentioned that (i) the air oxygen is an inhibitor for the polymerization and shall be removed from the reactor and (ii) when the monomer-to-polymer ratio increases from 20 to 50 %, the growing polymer particles are stickier and some coalescence phenomena are generally observed during this period.

Using seeds, *i.e.* MMS-modified silica particles, in the emulsion polymerization of styrene is the opportunity for the latex particles to nucleate at the surface of the silica seeds. For getting regular multipod-like silica/PS clusters, it was shown that the nature of the surfactant molecules is critical and that optimal results are obtained by using a mixture of Synperonic[®] NP 30 (non-ionic) and SDS (anionic). The latter boosts the polymerization reaction because it promotes the nucleation stage and therefore leads to more numerous but smaller PS particles. But used solely, it isn't capable to control the cluster morphology.[41] Lastly, it was demonstrated by electron tomography experiments performed at short polymerization times that the number of PS nodules growing onto the silica seeds decreases with time, evidencing coalescence and/or expulsion phenomena. Computer simulations allowed to confirm the high probability of such events: coalescence at low monomer-to-polymer conversion values and expulsion more readily at the end of the polymerization when the PS satellites are too bulky for continuing to grow simultaneously on the same seed (**Scheme 5**).



Scheme 5: Evolution of the PS satellite number and arrangement when growing during the emulsion polymerization process.

To control the morphology of the multipod-like silica/PS clusters, three main parameters may be varied: the size of the seeds (with a surface area kept constant); the proportion of SDS in the surfactant mixture and the styrene concentration. The best ever-reported yields in tetrapods or hexapods (more than 80 % with regard to the silica seeds) were obtained by using seeds with a diameter of 55 and 85 nm, respectively. During the present study, we typically performed several syntheses of clusters respecting these optimized conditions for tetrapods and hexapods. In the case of the dodecapods, we used a previously-fabricated batche obtained from 85 nm silica seeds and run with a lower monomer concentration. This batch was added to the results table even if it had been fabricated in a previous work.

Protocol 4: Synthesis of multipod-like silica/PS clusters.

In a 250-mL three-neck flask, equipped with a stirring anchor and a condenser itself surmounted by a bubbler, are introduced 50 mL of an aqueous solution made of the proper amounts of MMS-functionalized silica seeds, NP30 and SDS. The third neck is closed with a septum, and a long needle is used to ensure nitrogen bubbling into the dispersion for 1 h, the stirring speed being set to 170 rpm. Then, 5 g of styrene (99 % Sigma-Aldrich) are added and the stirring speed is momentarily increased to 250 rpm for 15 min. The nitrogen flux is reduced in order to keep a low over-pressure. The temperature is raised to 70°C with a thermostated oil bath. Then, 1 mL of an aqueous solution previously degassed and containing 25 mg of sodium persulfate (99 %, Sigma-Aldrich) is added. The polymerization is performed for 6 h. Then, the monomer-to-polymer conversion is gravimetrically measured from two 1-mL extracts dried in an oven.

By using these optimized conditions, we produced tetrapods and hexapods from the 52-nm and 86-nm silica seeds as-prepared and functionalized in the previous section (**Table 4**). In the following section and chapters, the original batches will be mentioned in brackets. The morphology composition of every batch was determined by statistical analysis from TEM images over one to two hundreds of clusters (**Figure 18**).

Table 4: Experimental conditions and final compositions of the multipod-like silica/PS clusters synthesized.

Batch name		T-52	H-86	D-85	T-86
Experimental conditions	Targeted clusters	Tetrapods	Hexapods	Dodecapods	Tetrapods
	D _{silica} (nm)	52	86	85	86
	N _{silica} (10 ¹⁵ L ⁻¹)	18	7.3	7.3	8.8
	S _{silica} (m ² .L ⁻¹)	153	166	166	170
	[styrene] ₀ (g.L ⁻¹)	100	100	45	100
	wt.% of SDS	5	5	5	1
	S-to-PS conversion (%)	78	80	89	71
Final batch composition in clusters	% mono/bipods	4	-	-	7
	% tripods	16	7	-	21
	% tetrapods	73	13	-	64
	% pentapods	1	18	} 4	6
	% hexapods	6	62		2
	% heptapods	-	-	-	-
	% octopods	-	-	5	-
	% nonapods	-	-	5	-
	% decapods	-	-	6	-
	% hendecapods	-	-	5	-
	% dodecapods	-	-	74	-
	% "multi-silica"	-	-	1	-
Typical TEM image on	Figure 18a	Figure 18b	Figure 18c	Figure 23a left	

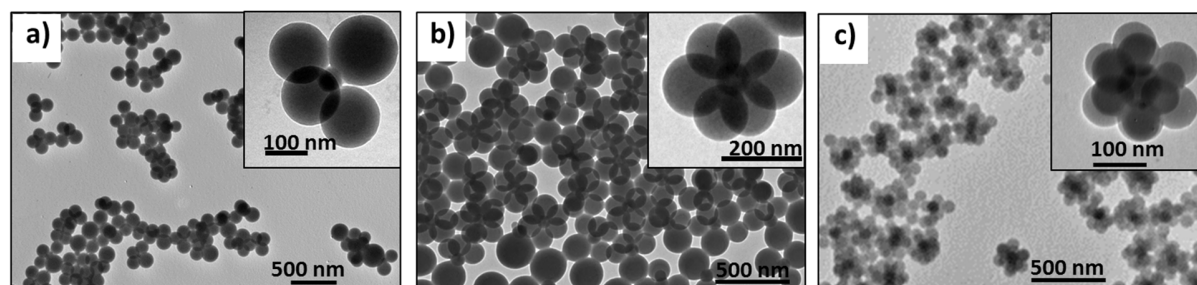


Figure 18: Typical large-field TEM images of a) tetrapods (T-52), b) hexapods (H-86) and c) dodecapods (D-85) and enlarged views in the respective inserts.

We obtained yields as high as 73 % and 62 % for tetrapods and hexapods, respectively. It may be mentioned that these values were lower than those obtained by Désert and coworkers, but we didn't spend time to optimize them because the main bottlenecks of this study concerned the further stages. The side-products were generally clusters with a smaller number of PS satellites than the targeted value, even if pentapods and hexapods were also observed in the tetrapod batches. It may be also observed the general prevalence of the platonic solid morphologies (tetrahedron, octahedron and icosahedron) because of their higher symmetry, satellite compactness and therefore stability. The small fraction of “multi-silica” clusters in the dodecapod batch are complex clusters made of two or three silica cores probably resulting from pre-aggregated silica seeds. They weren't observed in the other batches.

2.3 Derivatization of the multipod-like silica/PS clusters into dimpled silica particles

The first stage consisted into the regrowth of the silica core using the PS satellites as shaping masks and the second one was the removal of those masks by selective dissolution of the PS nodules.[42]

2.3.1 Template regrowth of the silica cores

It was performed in Stöber's conditions, *i.e.* in an ethanol/ammonia mixture through the addition of a controlled quantity of TEOS. It may be seen as an extra regrowth stage of the initial silica “pre-seeds” (*cf.* § 2.1.1) with the same requirement of avoiding a secondary nucleation of silica particles (managed by using a low TEOS concentration). On the other hand, two main extra difficulties linked to the presence of the PS masks should be managed: (i) the calculation of the exact amount of TEOS to be added for tuning the thickness of the newly-deposited silica, *i.e.* the depth of the forthcoming dimples, and (ii) the discriminatory growth of the silica cores for avoiding that silica was simultaneously deposited on the PS satellites. The 1st issue was overcome by developing the proper mathematical equation based on geometrical considerations including the initial size of the silica seeds, the size of the PS nodules, their average number per silica core and the desired dimple depth (see 2.1 in the appendix). The 2nd one was circumvented by taking advantage of the ethanolic nature of the silica growth dispersion supposed to inhibit the quite

hydrophilic character of the PS surface due to the probable presence of residual surfactant molecules.

Protocol 5: Regrowth of the silica cores of the silica/PS clusters.

450 mL of ethanol (99 %) and 35 mL of ammonia (28-30 %, J.T. Baker) corresponding to $[NH_3] = 1 M$ are introduced in a 1 L flask equipped with a magnetic stirrer. A volume of 10 mL of the aqueous dispersion of silica/PS clusters as obtained at the end of the polymerization stage is added leading to a total water concentration of 3.6 M. The flask is closed with a septum and the proper amount of ethanol solution of TEOS (10 vol.% concentrated) is dropwise added at a rate of 1 mL/h. The average size of the regrown silica cores is determined from the statistical analysis of the TEM images.

The experiments were successfully run on each batch of tetrapods, hexapods and dodecapods (**Table 5, Figure 19**). It appeared that the diameter of the silica was systematically increased of a value which was in good agreement with the expected ones, calculated by taking into account the morphology polydispersity of the cluster batches as described in **Table 4**. Some silica nanoparticles were sometimes observed on the TEM grid or attached to the PS satellites (**Figure 19b**), meaning that the mechanism of homogeneous nucleation or nucleation on the PS surface wouldn't be fully avoided, respectively. These silica nanoparticles attached to the PS nodules weren't an issue, because they were not supposed to resist to the forthcoming stages of PS dissolution and washing.

Table 5: Experimental conditions of the silica regrowth stage and final compositions of the batches of the as-obtained dimpled silica particles (after dissolution of the PS satellites).

Experimental conditions		Precursor cluster batch	Tetrapods (T-52)	Hexapods (H-86)	Dodecapods (D-85)
		Concentration part/L	3.6×10^{14}	1.5×10^{14}	6.25×10^{13}
		Initial D_{silica} (nm)	52	86	85
		Added VTEOS 10 % in ethanol (mL)	4.8	4.3	5.2
		Expected final D_{silica} (nm) *	111	145	180
		Measured final D_{silica} (nm)	110	145	178
Final composition dimpled particles	batch in silica	% mono/bidimpled	2	-	-
		% tridimpled	18	1	-
		% tetradimpled	74	12	-
		% pentadimpled	1	27	} 9
		% hexadimpled	5	60	
		% heptadimpled	-	-	
		% octodimpled	-	-	} 16
		% nonadimpled	-	-	
		% decadimpled	-	-	} 75
		% hendecadimpled	-	-	
	% dodecadimpled	-	-		
Typical TEM image on			Figure 19a	Figure 19b	Figure 19c

*The calculations were performed, as described in section 2.1 of the appendix, taking into account the exact cluster composition of each batch as described in **Table 4**.

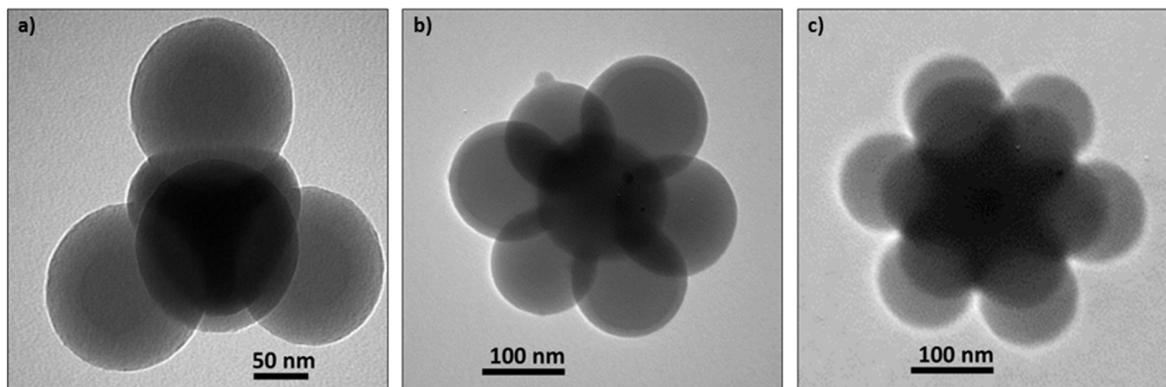


Figure 19: TEM images of a) tetrapod (T-52), b) hexapod (H-86) and c) dodecapod (D-85) after the regrowth stage of the silica core.

2.3.2 Dimple development by dissolution of the PS nodules

We took benefit of the solubility of the PS chains in common solvents such as dimethylformamide (DMF) and THF supposed to be inert with regard to the silica cores. Our efforts to optimize this stage showed that the colloidal stability of the dispersion in DMF may be preserved by using a rotary evaporator for removing slowly and fully the ethanol and water fractions. Typically, the initially white dispersion shall turn to a stable, colorless and very slightly diffusive one corresponding to the complete transfer of the silica particles from ethanol to DMF, because of the index matching phenomenon ($n_{\text{DMF}} = 1.4305$ and $n_{\text{amorphous Silica}} = 1.4585$ at 20°C for $\lambda = 589$ nm (Na D-line)).[43] In such conditions, the silica particles may be easily collected as a pellet after centrifugation.

Protocol 6: Dissolution of the PS nodules.

Typically, the dispersion of PS-silica clusters into the ethanol/ammonia mixture as obtained after the regrowth stage (Protocol 5) is transferred into a flask. A volume of DMF corresponding to 10 % of the total volume is added. Subsequently the dispersion is heated at 70°C and partially evaporated under vacuum using a rotavap. Then, the temperature is increased to 90°C and the evaporation continued until the dispersion turns from white to almost transparent. The removal of the dissolved PS is performed by 3 cycles of centrifugation at 10 000 g during 20 min and redispersion in THF.

The respect of the previously mentioned details allowed an efficient removal of the PS nodules resulting in the development of the expected concave areas at the places previously occupied by the PS nodules (**Figure 20**). Furthermore, this protocol is efficient to remove the PS forming the nodule but is also helpful to get rid of the silica nanoparticles appearing sometimes on the PS surface during the silica regrowth step. It makes sense when considering the difference of sedimentation rates existing in between the large dimpled silica particles and the silica nanoparticles.

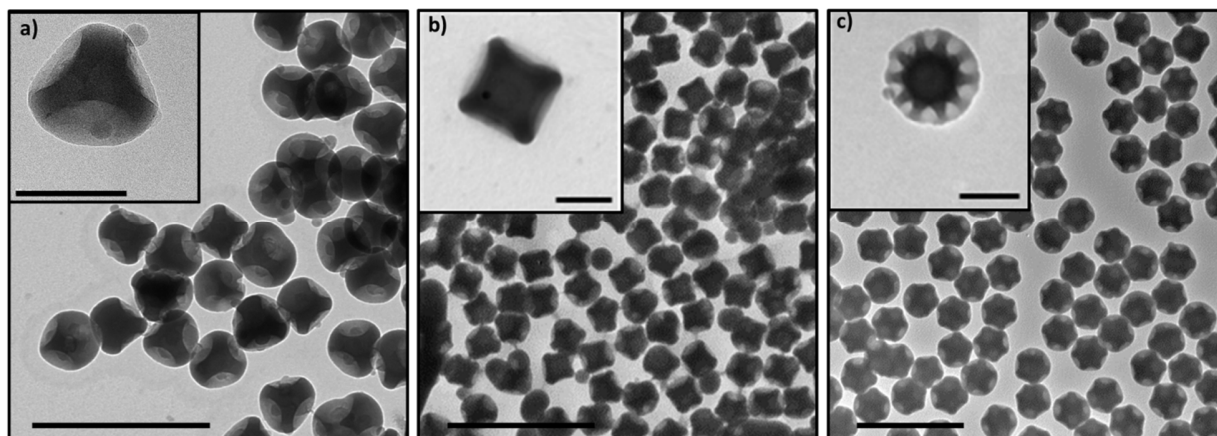


Figure 20: TEM images of the dimpled silica particles produced by regrowth of the silica core followed by dissolution of the PS nodules. a), b) and c) images correspond to batches of silica particles with 4 (T-52), 6 (H-86) and 12 (D-85) dimples, respectively (Scale bars: 500 nm and 100 nm specifically for inserts).

The statistical analysis of the TEM images (performed on 100-200 particles) showed that the morphology of the dimpled particles was dictated by the morphological composition of the batch of multipod-like silica/PS clusters used (**Table 5**). This means that, with regard to the control of the batch purity, the limiting step is the polymerization one. This means also that the silica regrowth stage doesn't modify the morphology and allows to preserve the number of PS satellites. Nevertheless, a thorough examination of the TEM images coupled to tomography experiments would be necessary for checking that these nodules keep truly their position and shape all along this stage. Interestingly, the concave shape of the dimples is easily evidenced on TEM images. It was expected that the bottom of the dimples was convex because made of the original silica seed surface previously protected by the PS nodules. But it seemed that the curvature is exaggerated showing that these bumps could be made of extra matter.

2.3.3 Morphology and chemical composition of the dimpled silica particles

EDX mapping was performed on the silica particles bearing four dimples in order to determine the chemical composition of the bumps observed by TEM at the bottom of the dimples (**Figure 21**). If the presence of silicon was confirmed in the whole body of the particles, it was observed that the bottom of the dimples was specifically rich in carbon atoms evidencing the remanence of some PS chains in these areas and more probably those which would be covalently bonded to the surface thanks to the copolymerization of the methacrylate groups of the MMS grafts with styrene (**Scheme 6**).^[44] In such a situation, the dissolution of the PS nodules by THF or DMF molecules consisted in the disentanglement of the chains and especially from those which remained covalently bonded to the silica surface. Therefore, the structure of the dimpled silica particles was more complex than initially expected: to their complex shapes shall be added their biphasic nature. Herein, the silica dimples can be considered as entropic patches as well as potential enthalpic ones due to the discrepancy in term of chemical reactivity exhibited by the silica from one side and the residual PS chains on the other side.

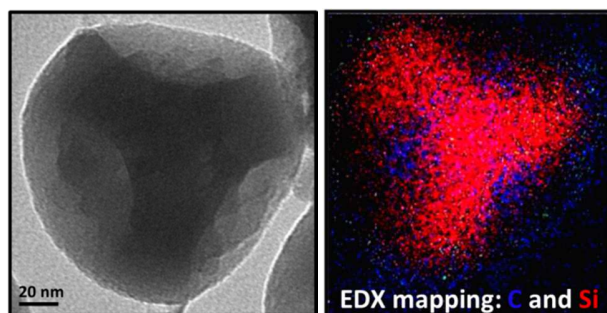
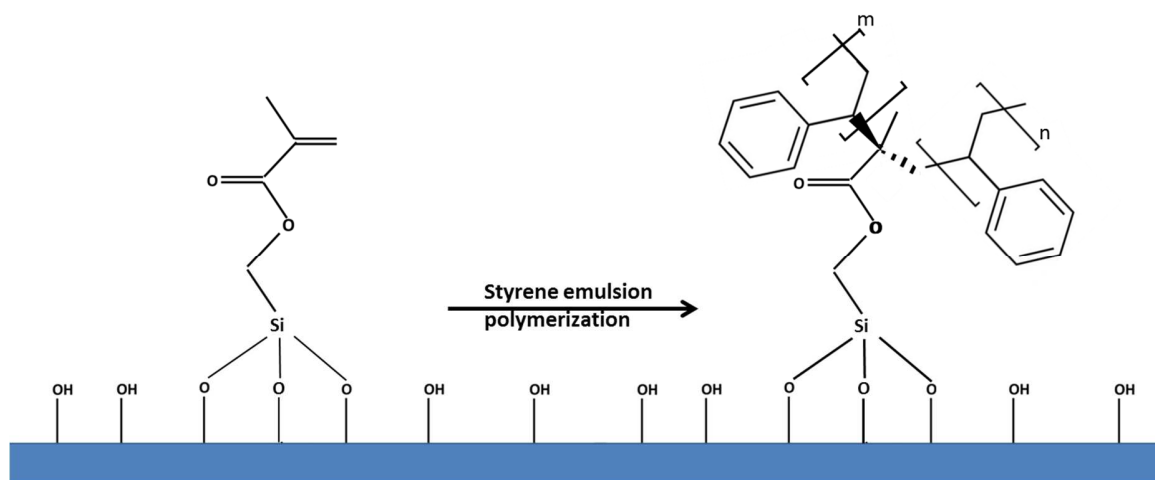


Figure 21: TEM image (left) and EDX mapping (right) of a dimpled silica particle made of four dimples (T-52); the traces of the silicon and carbon elements are plotted in red and blue, respectively.



Scheme 6: How MMS grafts may become the covalent anchors of some PS macromolecules, if the copolymerization of their methacrylate group with styrene has occurred (here the PS macromolecule is grafted through one MMS graft, but the insertion of several neighboring grafts in the same macromolecule and leading to a multi-anchoring of the macromolecule may be also readily envisioned).

In order to highlight the role of the MMS grafts in the formation of PS remaining bumps, we performed a styrene emulsion polymerization in the presence of 55-nm silica seeds surface-modified with acetoxypolytrimethoxysilane (AMS) instead of MMS, other parameters being equal and as described in *Protocol 3* to *Protocol 6*. The main difference between AMS and MMS is the absence of unsaturation and therefore the inability to (co)polymerize. TEM images of the as-obtained silica/PS clusters and derived dimpled particles are displayed on **Figure 22**. The morphology of the silica/PS clusters appeared not only less controlled (no major population) but also more fragile because all of them were found fallen down on the TEM grid (**Figure 22a**). This phenomenon was previously reported in the situations where there existed no covalent bonding between the silica seed and the PS satellites [45] or when the surface density of the MMS-derived grafts was too low.[36] On **Figure 22b**, no specific bump may be observed at the bottom of the dimples showing that no PS chain was covalently linked to the silica surface. Even if this result should be confirmed by extra EDX experiments, it is a proof that (i) the bumps previously observed were made of covalently bounded PS chains and (ii) the anchoring points are

the MMS grafts. Interestingly, these dimpled particles without PS bump may be considered as pure entropic patches.

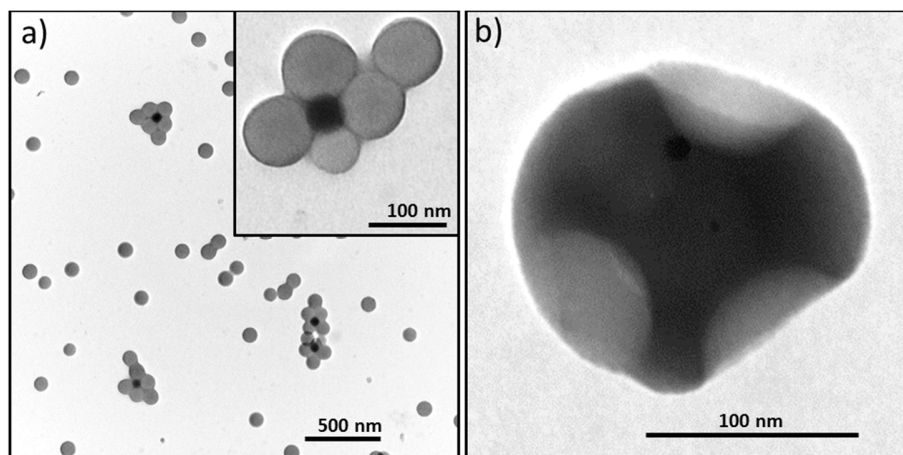


Figure 22: TEM images of a) the multipod-like silica/PS clusters obtained from 52-nm AMS-modified silica seeds and b) the dimpled silica particles obtained from the as-obtained clusters after silica regrowth and PS dissolution.

2.3.4 Towards the control of the dimple depth

In order to check that the thickness of the regrown silica layer on the silica cores was controlled, a series of regrowth stages was performed on the cluster batch containing a mixture of tetrapods and hexapods (T-86) by varying the added amount of TEOS according to *Protocol 5* and *Protocol 6* (Table 4 and Figure 23).

Table 6: Experimental conditions used for varying the thickness of the silica layer deposited on the cluster cores and final size of the dimpled particles obtained after PS dissolution.

Targeted thickness of the layer (nm)	Expected final D_{silica} (nm)	Added $V_{\text{TEOS 10 \%}}$ in ethanol (mL)	Measured final D_{silica} (nm)	Typical TEM image on Figure 23
0	86	0	86	a
1	88	0.1	86.5	b
5	96	0.8	92.3	c
10	106	1.7	107	d
15	116	2.7	115	e
17.5	121	3.2	121	f

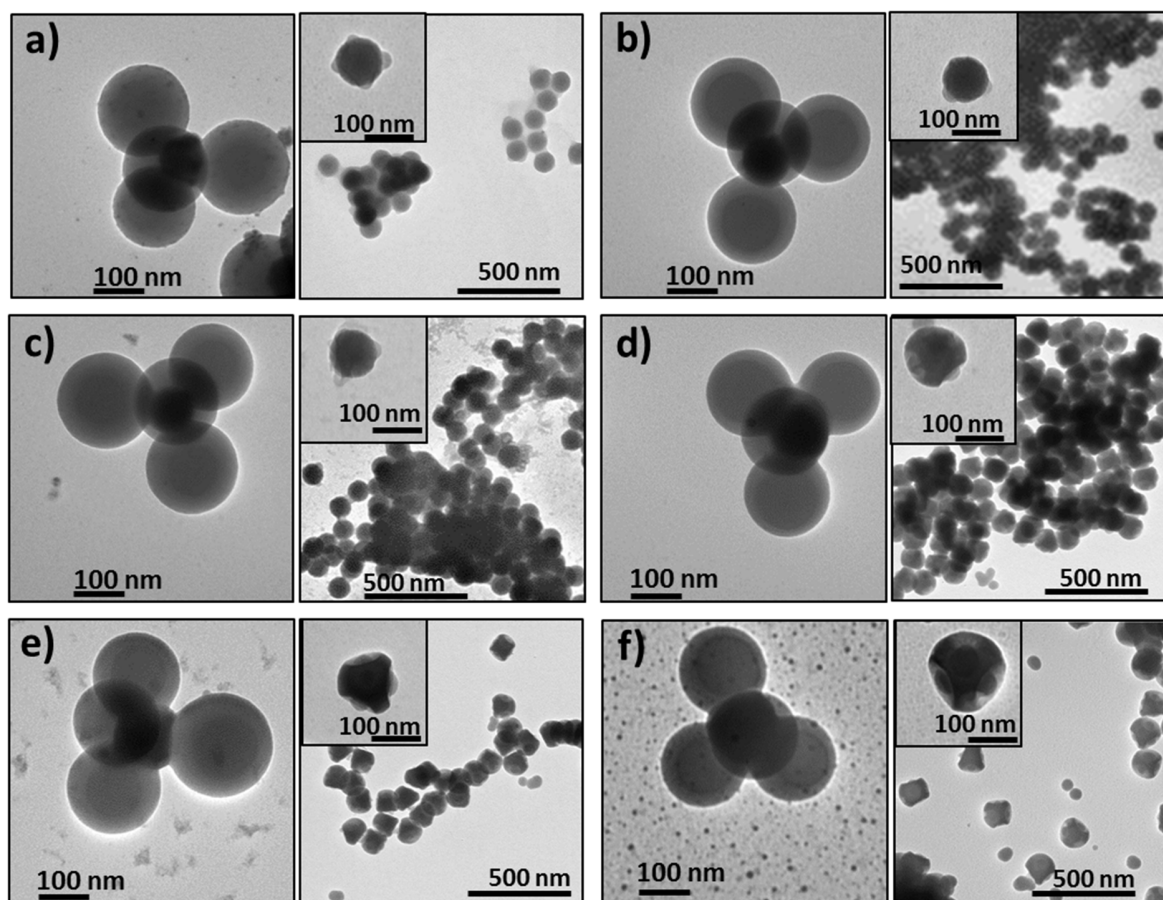


Figure 23: Left part of each pair: TEM images of multipod-like silica/PS clusters varying the thickness of the silica deposited; Right part of each pair: TEM images of the corresponding dimpled silica particles obtained by PS dissolution with a focused view on only one particle in the insert. Experimental conditions are described in Table 6.

The first consequence of the silica regrowth was the formation of a fresh silica coating between the PS nodules assuming that possible remaining MMS grafts were buried on this occasion. After the PS dissolution stage, the residual bumps made of anchored PS chains are clearly visible on TEM images insert whatever the thickness of the silica coating. Nevertheless, the thicker this coating (> 10 nm), the more stable the colloidal aqueous dispersions (when transferring from THF to water) and the less aggregated the silica particles on the TEM grids. This phenomenon could result from the following simple geometrical consideration: the deeper the dimples, the higher the silica walls protecting the PS bumps and therefore the longer the minimal distance between PS bumps of two different particles and the lower the hydrophobic interactions between them.

In order to go deeper in the characterization of the as-obtained patchy particles, we attempted to measure the average molar masses and amounts of the chains constituting the PS residue at the bottom of the dimples. Preliminary experiments for dissolving the silica component in fluorhydric acid and then recovering the grafted PS chains were unsuccessful, probably because of the very low amount of PS chains to be extracted from the complex and very reactive

dissolution medium. That is why the size exclusion chromatography (SEC) experiments were performed on the PS macromolecules recovered at the time of the dissolution of the PS satellites in THF and therefore concerned essentially the non-grafted chains.

Protocol 7: Preparation of the PS sample for SEC characterization.

The first THF supernatant containing the dissolved PS chains is collected from the Protocol 6. Afterward, this organic dispersion is dried and the solid is weighted and dissolved in THF at a mass concentration of 1 mg/mL. Typically, 5 mL of this PS solution in THF are employed for a SEC experiment after addition of 0.2 vol.% of trichlorobenzene as standard. The UV-detector is tuned at 260 nm which is the maximal absorption for the phenyl groups of the PS chains.

The measurement was performed twice from the PS chains extracted from a tetrapod batch (T-86) and gave similar results: $\overline{M}_n = 540\,000$ g/mol and $\overline{M}_w = 980\,000$ g/mol. These values are huge (out of the calibration range of the SEC setup which was restricted to molar masses less than 400 000 g/mol), but not surprising for macromolecules obtained according to an emulsion polymerization process. The questionable aspect of this experiment was to decide if the grafted PS chains were supposed to have the same average molar masses than the free ones. Similar attempts were reported in the literature for alumina or silica/PS or poly(ethyl)acrylate core-shell particles.[46]–[48] When the authors succeeded in the grafted chains extraction, they often observed that their average molar masses and molar mass distribution were higher than those of the free macromolecules. Sometimes, they incriminate siloxane bonding between the grafted molecules meaning that the MMS grafts serve as cross-linking groups and therefore assume formally or not that the average molar masses of grafted and non-grafted chains should be the same. Therefore, knowing the molecular weight of styrene (104 g/mol), the number-average degree of polymerization \overline{X}_n as well as the mass-average degree of polymerization \overline{X}_w of the grafted chains were considered equal to 5200 and 9400, respectively.

The determination of the average amount of PS residue per dimpled particle or per dimple was performed by comparing by thermogravimetric analysis (TGA) the relative weight losses of dimpled particles and control particles made of 86-nm silica spheres not MMS-modified that have experienced the same story: from the emulsion polymerization of styrene to the silica regrowth and dissolution of the hypothetical PS satellites.

Protocol 8: Preparation of control silica particles for TGA experiments.

Silica particles with a mean diameter of 86 nm used directly from their growth media (Protocol 2) and transferred into ultrapure water using the rotavap and centrifugation. Subsequently they are transferred into an emulsion polymerization of styrene and 5 g of styrene are polymerized according to the experimental conditions described in the Protocol 4. After completion of the polymerization, 10 mL of the mixture are added into a

*growth media and a silica regrowth is performed using 5 mL of TEOS in conditions similar to the **Protocol 5**. Those particles are treated according to the **Protocol 6** to wash out all the PS particles. Finally, the suspension is dried; the powder obtained is collected, then weighted for TGA experiments.*

The dimpled silica particles analyzed by TGA are similar to those presented on **Figure 23f**. The TGA curves were recorded under He atmosphere from ambient temperature to 600°C with a temperature ramp of 5°C/min (**Figure 24**). From ambient temperature to 120°C, the conventional weight loss due to the release of adsorbed water was observed. Between 120 and 600°C, the weight loss is known to result from water entrapped within the structure, degradation of organic compounds and condensation of the surface silanol groups.[49] Those losses were observed for both control and dimpled silica particles. However, the dimpled silica particles exhibit a significantly higher loss in the range 300-500°C, attributed to the thermal degradation of the PS chains.[46] This extra weight loss was equal to 5.5 wt.% of the sample.

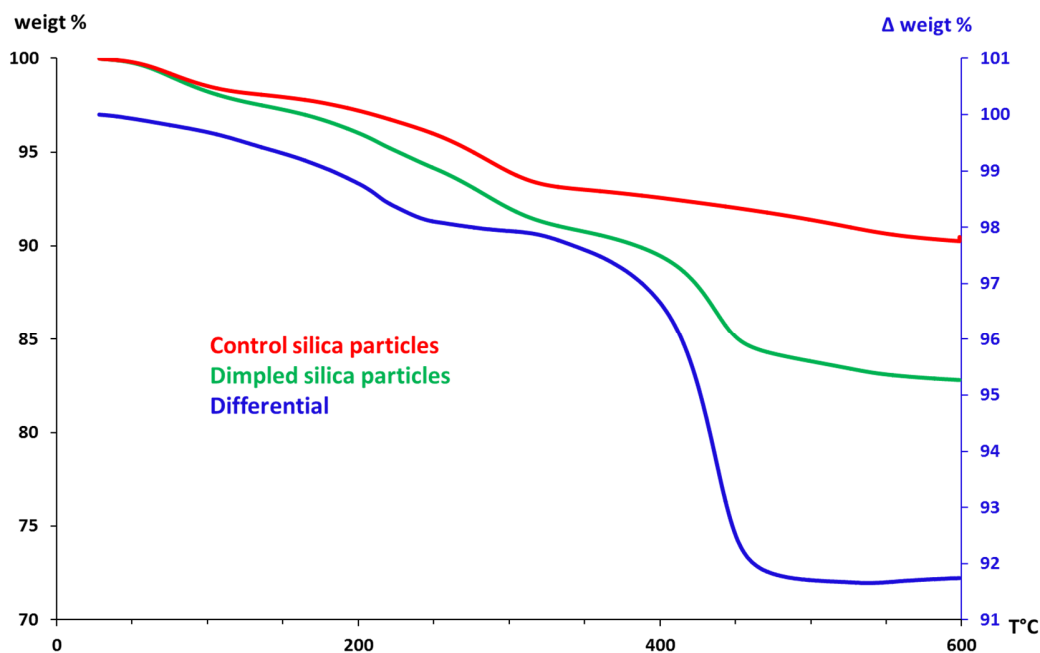


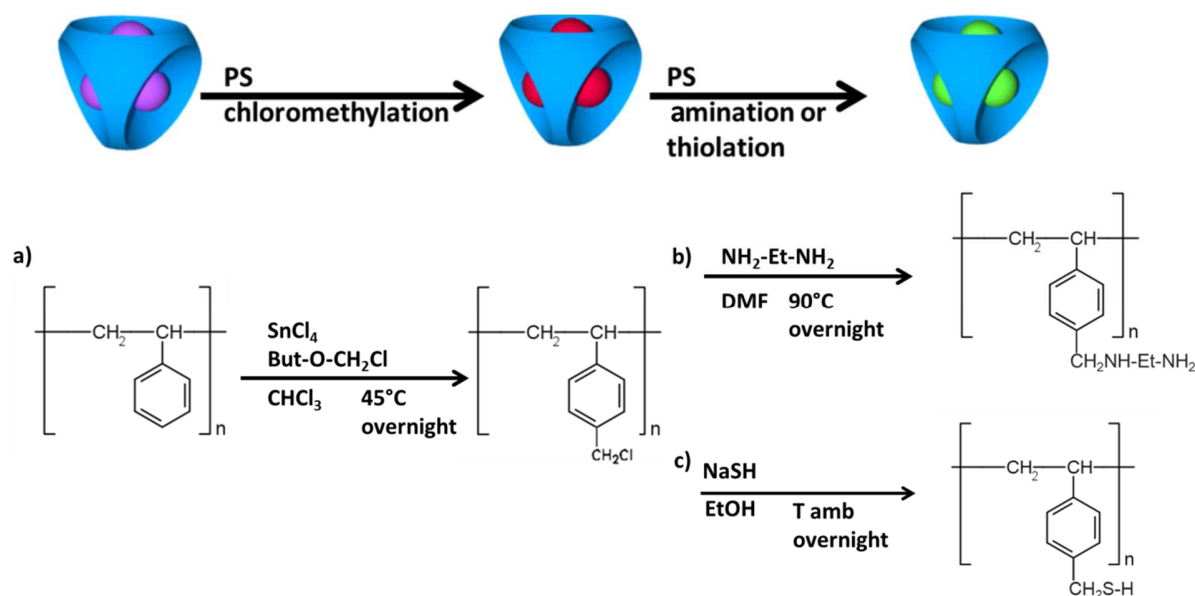
Figure 24: TGA curves of control silica particles, dimpled silica particles (T-86) and the differential between both.

Knowing the geometrical parameters of the precursor multipod-like clusters ($D_{\text{silica seed}} = 86 \pm 2$ nm; $D_{\text{PS}} = 180 \pm 2$ nm and average number of pods = 3.75 pods/seed) and the patchy particles ($D_{\text{dimpled silica}} = 121 \pm 2$ nm), we calculated their average weight by knowing their average geometrical parameter as described in the section 2.1 of the (appendix). Considering that 5.5 ± 0.1 wt.% of the particle was made of PS, we estimated that the average weight of PS was 9.53×10^{-17} g/dimpled particle and then 9.53×10^{-17} g / 3.75 = 2.54×10^{-17} g/dimple. Assuming the molar mass equivalence between the grafted and non-grafted chains ($\overline{M}_n = 540\,000$ g/mol with $\overline{M}_w/\overline{M}_n = 1.8$), we estimated that the bumps were made of 28 ± 12 PS chains. Considering the

density of PS (1.05 g/cm^3) and that the PS bumps exhibited a hemispherical shape (it means that the convex surface of the silica seed was considered as a plane at this scale length), we calculated that the average diameter of the PS bumps should be $45 \pm 4 \text{ nm}$. TEM thorough imaging on 20 particles showed that the average diameter of the PS bumps was of $32 \pm 4 \text{ nm}$, which may be considered of the same order, knowing the geometrical approximations on one side and the accuracy of the SEC, TGA and TEM measurements on the other side.

2.4 Making the dimples sticky by chemical modification of the residual PS

The PS bumps at the bottom of the dimples may be considered like sticky patches (enthalpic patches) if hydrophobic interactions are intended to be exploited. Nevertheless, because we decided to develop covalent coupling with metal satellites, PS bumps couldn't be used in their pristine state. It was mandatory to derivatize the PS macromolecules for making them capable to develop covalent bonds or electrostatic interactions. Fortunately, PS can be post treated using various methods. The most conventional ones are the sulfonation and the chloromethylation reactions. They are very used from an industrial point of view, in particular for the production of ion-exchange resins. The chemical functions accessible from the sulfonated PS are quite limited in term of potential subsequent coupling reactions. On the other hand, the chloromethylated PS can be converted into other kinds of functional PS by simple nucleophilic substitution reactions.[50] In the frame of this study, we focused onto aminated or thiolated PS, because of the affinity for gold colloids of amino and thiol groups, respectively (**Scheme 7**).



Scheme 7: The envisaged modification steps of the PS bumps; a) chloromethylation and b) amination or c) thiolation reactions.

2.4.1 First stage: chloromethylation of PS macromolecules

The chloromethylation reaction consists in a Friedel-Crafts reaction, *i.e.* an electrophilic substitution on the aromatic cycles where a hydrogen atom is replaced by a chloromethyl group. The reaction is typically performed in a good solvent of PS and catalyzed by a Lewis acid. It was therefore mandatory to use reagents/solvents that are inert with regard to the silica counterpart: butyl chloromethyl ether, SnCl₄ and chloroform appeared to be a suitable system. The chloromethylating agent is not commercial and was preliminarily prepared according to a specific protocol using butyl alcohol, paraformaldehyde and gaseous HCl at low temperature (5°C) the process is described in the section 3 of the appendix.[51],[52]

Protocol 9: Chloromethylation of the PS macromolecules on the silica patchy particles.

The dimpled silica particles obtained after the PS dissolution step (Protocol 6) are transferred into 40 mL of chloroform by using three cycles of centrifugation. 20 mL of this dispersion are introduced in a flask with 5 mL of butyl chloromethyl ether 3 M in chloroform (large excess) and 0.3 mL of SnCl₄. The temperature is set to 45°C and the mixture is aged overnight. Finally the solution is washed by three cycle of centrifugation/redispersion in HCl solution (4 wt.% in water) and three cycles of centrifugation/redispersion in water/EtOH (50/50 wt.%). Finally, the dimpled silica particles were redispersed in 20 mL of DMF. During each washing step, the particles are centrifuged at 12 000 g during 10 min.

It was very tricky to evidence the presence of the PS macromolecules by Diffuse Reflectance Infrared Fourier Transform (DRIFT), because of their very low amount. As a consequence, this technique wasn't directly used for checking the success of the PS modification stages. In practice, we performed in parallel the same experiments in similar conditions on free PS chains (coming from PS latex dried and dissolved in chloroform) and monitored the evolution of their infrared (IR) spectrum (**Figure 25**). The main differences between both spectra (before and after the chloromethylation reaction) are absorption bands easily assigned to the chloromethyl groups consistently with results from the literature.[52]

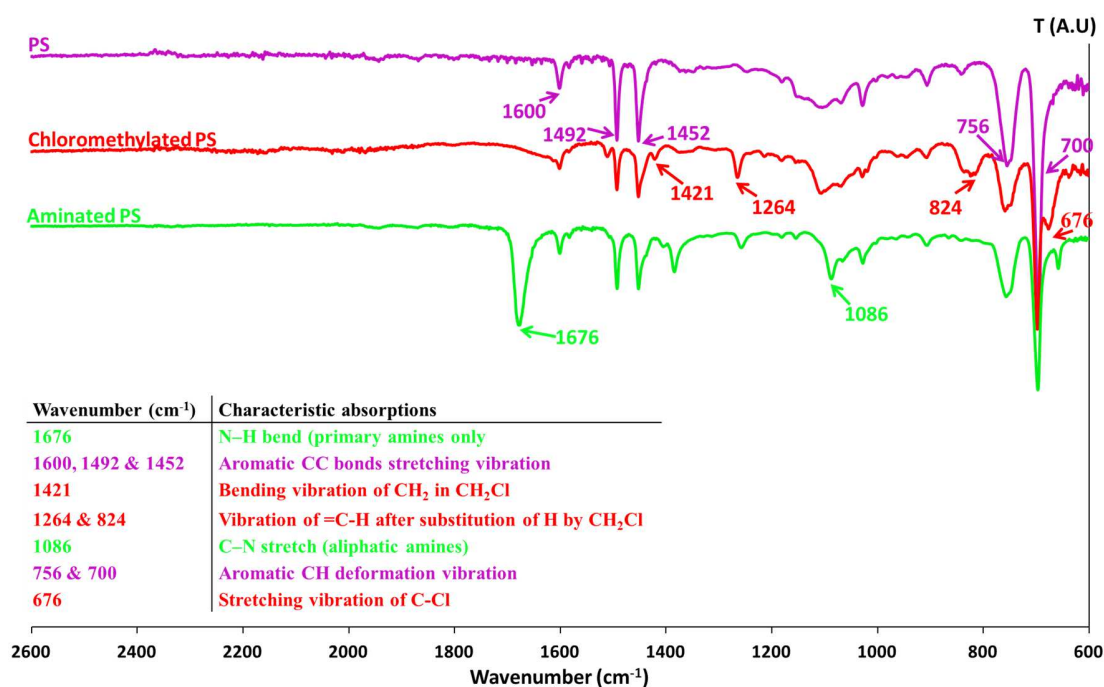


Figure 25: IR spectra of pristine PS, chloromethylated PS, aminated PS and thiolated PS macromolecules with the characteristic absorption bands pointed out and attributed to the corresponding chemical groups.

To go deeper in the characterization of those particles, and especially evidencing the regioselective character of the reaction, EELS (electron energy losses spectroscopy) mapping was performed (**Figure 26**). Here, EELS was preferred to EDX because of its higher sensitivity for heavy elements such as chlorine. It showed that the dimples were enriched in chlorine atoms whereas the rest of the particles appeared only made of silicon atoms. The combination of this result with that obtained by IR spectroscopy on free PS macromolecules confirmed that (i) the bumps at the bottom of the dimples were indeed made of grafted PS macromolecules and (ii) the chloromethylation stage was successful.

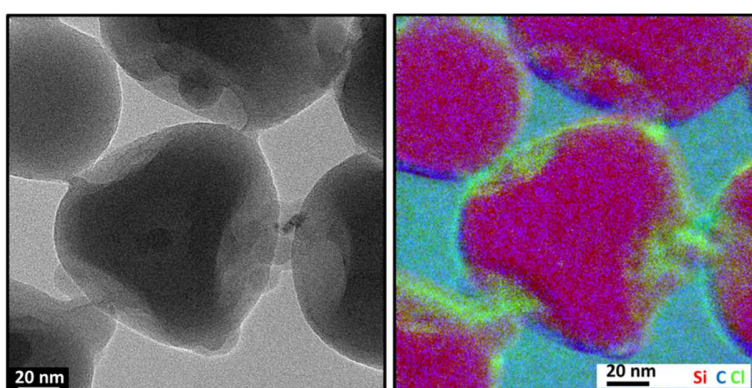
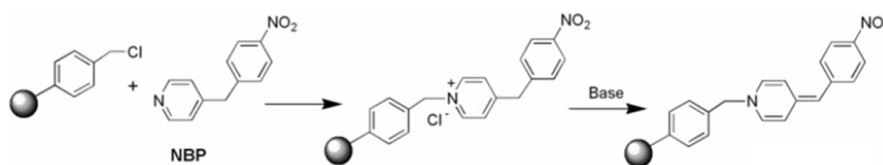


Figure 26: TEM image and EELS mapping of the patchy particles (T-52) bearing chloromethylated PS chains; the traces of the silicon, carbon and chlorine elements are plotted in red, blue and green, respectively.

Chlorine assay could have been performed on chloromethylated patchy particles, first to evaluate the efficiency of the method and then to reach a better control over the subsequent steps. Typically, the titration of the chloromethylated group was reported by performing quarternization of a tertiary amine followed by titration of the chloride ions using silver nitrate.[53] In this case, the end point was typically monitored by potentiometric method. Microanalysis can also be performed, but its accuracy is very limited for low chlorine concentrations.[54] Alternatively, a straight-forward approach consisting in a colorimetric method also exists.[55] In this case, the method - based on the reaction between nitrobenzyl pyridine (NBP) and chloromethyl groups - is typically qualitative (**Scheme 8**).



Scheme 8: Reaction of the nitrobenzyl pyridine (NBP) molecule with a chloromethylated phenyl group.

Protocol 10: Colorimetric test highlighting the presence of chloromethyl groups.

1 mL of dimpled silica particles dispersion in DMF (corresponding to 10^{12} particles) is introduced in a 10-mL flask. 2 mL of 0.05 M NBP (Sigma Aldrich) and 15 μ L of TEA (Aldrich) are added. The temperature is increased to 90°C and the mixture is kept at that temperature under stirring for 30 min. Finally the dispersion is transferred into a falcon tube and centrifuged at 12 000 g for 10 min and observed with the eye.

The colorimetric test was performed on the dimpled silica particles before and after chloromethylation (**Figure 27**). While before chloromethylation the silica particle dispersion remained colorless, the chloromethylated particles exhibited a noticeable pink/purple color which is in very good agreement with the results obtained for Merrifield-resin with NBP reported by Galindo *et al.*[55] This test was essentially qualitative, and we didn't find time enough for developing a quantitative method. Nevertheless, it may be easily assumed that the chloromethylation reaction of anchored PS chains is very probably partial because the monomer units, which are the closest to the silica surface, are less accessible to the reagents for steric hindrance reasons.

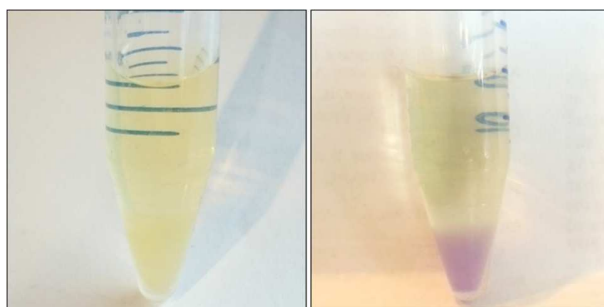


Figure 27: Picture of the NBP assay on dimpled silica particles (T-52) before (left) and after the chloromethylation reaction (right). The yellow color of the supernatant resulted from the presence on an excess of NBP.

2.4.2 Second stage: amination of the chloromethylated PS macromolecules

The chloromethylated styrene units of the PS chains were derived into aminated ones by reaction with a molecule bearing a reactive amino group through a nucleophilic substitution. Moreover, a substitution performed with a molecule such as ethylene diamine allowed to obtain a terminal primary amine (**Scheme 7**). In such a strategy, it was mandatory to use a large excess of ethylene diamine to prevent the cross linking of the PS through the reaction of both primary amino groups of ethylene diamine with chloromethyl groups. Indeed, if the diamine species are introduced in too low amounts with regard to the chloromethylated ones, the diamine could act like a bridging molecule inducing a lower number of primary amines and the cross-linking of the macromolecules making them less capable to be extended in good solvents.

Protocol 11: Amination of the chloromethylated PS macromolecules on the silica patchy particles.

Typically an amount of chloromethylated dimpled silica particles corresponding to 10^{13} particles dispersed in DMF is introduced in a flask equipped with a condenser and a magnetic stirrer. A volume of 3 mL of ethylene diamine which is assumed to be a large excess is introduced then the temperature is set to 90°C overnight. Then, the particles are washed by two cycles of centrifugation/redispersion in ethanol and then washed 2 times in water, finally the solution is acidified using few drops of HCl then the particles are centrifuged and dispersed in milliQ water.

Similarly to the 1st stage, the reaction success was checked in parallel on free PS macromolecules by IR spectroscopy (**Figure 25**). Typically, the IR spectrum obtained with the aminated PS presented several bands typically attributed to the primary amino groups such as the N-H bend at 1676 cm^{-1} , which only appears in the case of the primary amine, and the band at 1086 cm^{-1} attributed to the C-N stretch of the aliphatic amine.

To go deeper in the characterization, some EELS mapping experiments were attempted without success: the collected signal-to-noise ratio was indeed too low and too long counting times resulted in drifting issues. That is why we attempted to use optical fluorescence microscopy at the condition to substitute the ethylene diamine by fluorescein-amine at the time of the amination reaction. The conditions used to perform the nucleophilic substitution of the chlorine by the fluorescein-amine were inspired by the work of van Ravensteijn.[56] The strategy was to use a new kind of optical fluorescence microscope capable to go below the resolution limitations imposed by optics by taking benefit of an optical depletion technique called STED for stimulated emission depletion microscopy. However, the diffusion induced by the silica particles was really detrimental for the measurements; in addition the photo-bleaching of the dye due to the strong incident beam rapidly killed the signal.

The development of amino assay could be of great interest regarding the patchy particles. Ideally, two assays, one in water and one in a good solvent could be particularly relevant. Indeed, the

water titration of the amino group could be useful to determine the amount of accessible amino groups (essentially at the bump surface), when the particles are dispersed into water. Whereas, the assay performed into good solvents for PS could be relevant to determine the total amount of amino groups along the PS chains. Typically, the primary amine group could be titrated in water by using ninhydrin.[57] Such titration is well known in the field of the peptide synthesis in order to determine the amount of free amine remaining after reaction. The accurate assay in a good solvent for PS appears trickier for reagent solubility reasons. However, a titration method performed in acetone was reported.[58]

2.4.3 Alternative second stage: thiolation of the chloromethylated PS macromolecules

Alternatively, the nucleophilic substitution of the chloromethyl groups was performed with sodium hydrogen sulfide in ethanol in order to get thiol end-groups. Because ethanol is not a solvent for PS and for chloromethylated PS, we wondered to use, DMF or DMSO (dimethylsulfoxide) as solvent, even if the thiol group could be easily oxidized into aprotic and polar solvents. A compromise could have been to perform the reaction in toluene in presence of a phase transfer agent such as 18-crown-6. Unfortunately, the dimpled silica particles are not colloidally stable in toluene. That is why we finally carried out the reaction in ethanol, being aware that very probably only the low fraction of the styrene monomer units present at or close to the surface would be chemically modified.

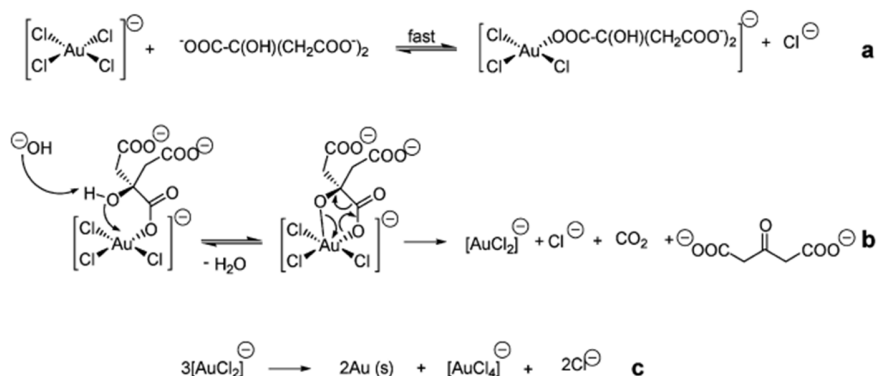
Protocol 12: Thiolation of the chloromethylated PS macromolecules on the silica patchy particles.

Typically, 10^{13} chloromethylated patchy particles are transferred into ethanol by centrifugation. Ten mL of ethanol containing 2-g of dissolved NaSH was added and let to react overnight under stirring. Finally, the particles are washed 5 times by centrifugation at 10 000 g during 15 min in ultrapure ethanol. The sample can be stored in ethanol. Before use, the particles are typically transferred into water then the potential disulfide bonding is reduced by the use of few drops of a dilute aqueous solution (1 M) of NaBH_4 . Finally the solution is washed by centrifugation and stored in degassed water.

2.4.4 Indirect proof of the PS modification success

A batch of 4-dimples chloromethylated patchy particles (T-52) was used and converted in aminated and thiolated ones. In order to obtain an indirect proof of the reactions success we intend to perform the site specific anchorage of gold seeds known to develop specific interactions with amino or thiol groups.[59] Citrate-stabilized gold nanoparticles were prepared according to the *Protocol 13*. [60]

Scheme 9, extracted from the work of Puntès and coworkers,[61] summarizes the growth mechanism of the gold nanospheres. In brief, the chloride ions are first exchanged with citrate ions a); this step is followed by the reduction from Au³⁺ in Au⁺ b) then finally the reduction of Au⁺ in Au⁰ c). In this approach, sodium citrate serves as both reducing agent and capping agent that stabilizes the nanoparticles.



Scheme 9: a) Ligand exchange occurring for the gold ion b) Decarboxylation and reduction of Au (III) into Au (I) and c) Dismutation of Au (I).

Protocol 13: Synthesis of citrate stabilized 12-nm gold nanoparticles.

A 1-L round bottom flask containing 700 mL of milliQ water was heated to 100°C under reflux and moderate agitation. Meanwhile, 314 mg of KAuCl₄ were diluted in 50 mL of milliQ water and then introduced in the round bottom flask. 1.53 g of trisodium citrate was diluted in 75 mL of milliQ water. When the solution temperature has reached 100°C, the citrate solution was added in one shot. The solution turned from yellow to colorless, black and then red. The dispersion was let to react during 15-20 min at 100°C.

A typical TEM image obtained from the colloidal dispersion is shown on **Figure 28**. Their average diameter was 12 ± 1 nm. They were stable in aqueous media and didn't show any sign of decomposition, even after several-months storage in air at room temperature. The UV-visible spectroscopic measurement showed a strong localized SPR band centered at approximately 520 nm. This was consistent with numerous studies reported for citrate-capped gold nanoparticles of this size.[62]–[64]

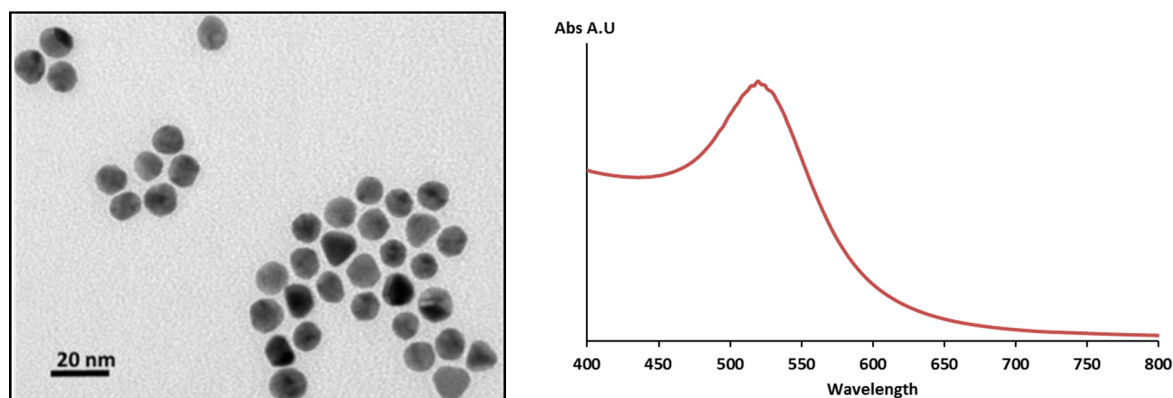


Figure 28: Typical TEM image and UV-vis absorption spectrum of colloidal gold seeds prepared according to *Protocol 13*.

The citrate-capped gold nanoparticles were subsequently used to decorate the chemically-modified PS bumps of the patchy silica particles. Self-assembly experiments with aminated and thiolated dimpled particles were performed according to the *Protocol 14* and *Protocol 15* respectively.

Protocol 14: Decoration of aminated dimpled silica particles by citrate stabilized gold nanoparticles.

5 mL of the aminated patchy particles dispersion as obtained after Protocol 11 are introduced into a 50-mL falcon tube. Few μL of HCl are added in order to adjust the pH to \square 4. After homogenization using vortex device, 40 mL of citrate-stabilized gold nanoparticles as obtained after Protocol 13 are added. The suspension is homogenized using vortex device and let overnight over the roller mixer. Afterward, the suspension is washed by 3 cycles of centrifugation/redispersion (4000 g; 15 min) with milliQ water.

Protocol 15: Decoration of thiolated dimpled silica particles by citrate stabilized gold nanoparticles.

In a 50-mL falcon tube, 45 mL of the citrate-stabilized gold nanoparticles in aqueous dispersion as prepared according to Protocol 13 are centrifuged at 8 000 g during 30 min. The particles are re-dispersed into 1 mL of ultrapure water and 1 mL of the dispersion of thiolated patchy particles prepared according to Protocol 12 is added in a gold-to-silica particle ratio of 400/1. After overnight incubation over stirring, the dispersion is washed by centrifugation using ultrapure water at 5 000 g for 10 min.

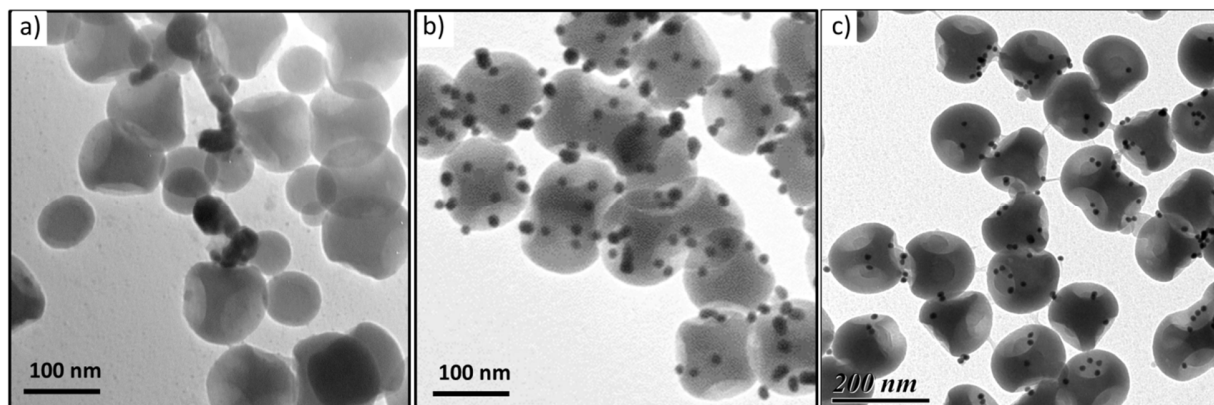


Figure 29: TEM images of the dimpled silica particles (T-52) after incubation with citrate-stabilized gold nanoparticles before a) and after amination b) or after thiolation c) of the PS chains at the bottom of the dimples.

Figure 29 compares TEM images of dimpled silica particles chemically modified, before and after, incubation with citrate stabilized gold nanoparticles according to the *Protocol 14* and *Protocol 15*.

This figure clearly evidences that gold nanoparticles labelled essentially the aminated and thiolated dimpled area while the chloromethylated dimples as well as the interpatches areas remain unlabeled. This result clearly highlights the successful chemical functionalization of the residual PS chains of the patches.

3 Conclusion

In this chapter, we have first presented a brief state-of-the-art regarding the synthesis of patchy particles, evidencing that the route proposed by Désert and coworkers is one of the most suitable for fabricating dimpled particles at the gram scale with a good control of the patch number.

Then, we described how we revisited again this route through the successive stages of: (i) synthesis of highly size-monodisperse batches of silica seeds, (ii) seeded-growth emulsion polymerization of styrene for getting several batches of multipod-like silica/PS clusters with average values of 4, 6 and 12 pods and (iii) regrowth of the silica cores and subsequent development of the dimples by dissolution of the PS satellites. We contributed to increase the knowledge of the involved mechanisms and the as-obtained morphology by showing:

- the control to the nm of the regrowth of the silica cores;
- the high efficacy of the conversion of multipod-like clusters into dimpled particles making only the emulsion polymerization stage limiting for controlling the number of dimples per particle;
- the mandatory role of the copolymerizable methacrylate group of the MMS grafts for getting residual PS bumps at the bottom of the dimples;
- the estimation of the average molar masses and average amount of PS constituting the bumps.

Lastly, we have reported original chemical pathways for grafting amino groups along the anchored PS macromolecules of each dimples 'surface. Similar chemical functionalization for getting thiol groups on dimples was trickier and only few PS chains were thiolated. Both the amino- and thio- group allows to anchor gold nanoparticles making hopeful the strategy for getting large gold satellites by nucleation and growth (*cf.* Chapter 2) or self-assembly (*cf.* Chapter 3).

4 References

- [1] I. C. Pons-Siepermann and S. C. Glotzer, "Design of Patchy Particles Using Quaternary Self-Assembled Monolayers," *ACS Nano*, vol. 6, pp. 3919–3924, 2012.
- [2] E. Jankowski and S. C. Glotzer, "Calculation of partition functions for the self-assembly of patchy particles.," *J. Phys. Chem. B*, vol. 115, pp. 14321–14326, 2011.
- [3] S. C. Glotzer, M. J. Solomon, and N. A. Kotov, "Self-assembly: From nanoscale to microscale colloids," *AIChE J.*, vol. 50, pp. 2978–2985, 2004.
- [4] G. Van Anders, N. K. Ahmed, R. Smith, M. Engel, and S. C. Glotzer, "Entropically Patchy Particles: Engineering Valence through Shape Entropy," *ACS Nano*, vol. 8, pp. 931–940, 2014.
- [5] F. Sciortino, E. Bianchi, J. F. Douglas, and P. Tartaglia, "Self-assembly of patchy particles into polymer chains: a parameter-free comparison between Wertheim theory and Monte Carlo simulation.," *J. Chem. Phys.*, vol. 126, pp. 194903–194310, 2007.
- [6] F. Romano, E. Sanz, and F. Sciortino, "Crystallization of tetrahedral patchy particles in silico.," *J. Chem. Phys.*, vol. 134, pp. 174502–174508, 2011.
- [7] F. Romano, E. Sanz, P. Tartaglia, and F. Sciortino, "Phase diagram of trivalent and pentavalent patchy particles.," *J. Phys. Condens. Matter*, vol. 24, pp. 064113–064121, 2012.
- [8] E. G. Noya, E. Bianchi, G. Kahl, and G. Doppelbauer, "Self-assembly scenarios of patchy colloidal particles," *Soft Matter*, vol. 8, pp. 7768–7772, 2012.
- [9] E. Bianchi, G. Doppelbauer, L. Fillion, M. Dijkstra, and G. Kahl, "Predicting patchy particle crystals: variable box shape simulations and evolutionary algorithms.," *J. Chem. Phys.*, vol. 136, pp. 214102–214111, 2012.
- [10] F. Smalenburg and F. Sciortino, "Liquids more stable than crystals in particles with limited valence and flexible bonds," *Nat. Phys.*, vol. 9, pp. 554–558, 2013.
- [11] A. B. Pawar and I. Kretzschmar, "Fabrication, Assembly, and Application of Patchy Particles," *Macromol. Rapid Commun.*, vol. 31, pp. 150–168, 2010.

-
- [12] J. Du and R. K. O'Reilly, "Anisotropic particles with patchy, multicompartement and Janus architectures: preparation and application.," *Chem. Soc. Rev.*, vol. 40, pp. 2402–2416, 2011.
- [13] E. Bianchi, R. Blaak, and C. N. Likos, "Patchy colloids: state of the art and perspectives.," *Phys. Chem. Chem. Phys.*, vol. 13, pp. 6397–6410, 2011.
- [14] D. Rodríguez-Fernández and L. M. Liz-Marzán, "Metallic Janus and Patchy Particles," *Part. Part. Syst. Charact.*, vol. 30, pp. 46–60, 2013.
- [15] G.-R. Yi, D. J. Pine, and S. Sacanna, "Recent progress on patchy colloids and their self-assembly.," *J. Phys. Condens. Matter*, vol. 25, pp. 193101–193113, 2013.
- [16] S. Sacanna and D. J. Pine, "Shape-anisotropic colloids: Building blocks for complex assemblies," *Curr. Opin. Colloid Interface Sci.*, vol. 16, pp. 96–105, 2011.
- [17] A. B. Pawar and I. Kretzschmar, "Patchy particles by glancing angle deposition.," *Langmuir*, vol. 24, pp. 355–358, 2008.
- [18] A. B. Pawar and I. Kretzschmar, "Multifunctional patchy particles by glancing angle deposition.," *Langmuir*, vol. 25, pp. 9057–9063, 2009.
- [19] Y. Hou, S. Li, Y. Su, X. Huang, Y. Liu, L. Huang, Y. Yu, F. Gao, Z. Zhang, and J. Du, "Design and fabrication of three-dimensional chiral nanostructures based on stepwise glancing angle deposition technology.," *Langmuir*, vol. 29, pp. 867–872, 2013.
- [20] Z. He and I. Kretzschmar, "Template-assisted fabrication of patchy particles with uniform patches.," *Langmuir*, vol. 28, pp. 9915–9919, 2012.
- [21] Z. He and I. Kretzschmar, "Template-assisted GLAD: approach to single and multipatch patchy particles with controlled patch shape.," *Langmuir*, vol. 29, pp. 15755–15761, 2013.
- [22] V. N. Manoharan, T. E. Mark, and D. J. Pine, "Dense packing and Symmetry in Small clusters of microspheres," *Science*, vol. 301, pp. 483–487, 2003.
- [23] Y. Wang, Y. Wang, D. R. Breed, V. N. Manoharan, L. Feng, A. D. Hollingsworth, M. Weck, and D. J. Pine, "Colloids with valence and specific directional bonding.," *Nature*, vol. 491, pp. 51–55, 2012.
- [24] Y. Wang, Y. Wang, X. Zheng, G.-R. Yi, S. Sacanna, D. J. Pine, and M. Weck, "Three-dimensional lock and key colloids.," *J. Am. Chem. Soc.*, vol. 136, pp. 6866–6869, 2014.
- [25] D. Zerrouki, B. Rotenberg, S. Abramson, J. Baudry, C. Goubault, F. Leal-Calderon, D. J. Pine, and J. Bibette, "Preparation of doublet, triangular, and tetrahedral colloidal clusters by controlled emulsification.," *Langmuir*, vol. 22, pp. 57–62, 2006.
- [26] G.-R. Yi, V. N. Manoharan, E. Michel, M. T. Elsesser, S.-M. Yang, and D. J. Pine, "Colloidal Clusters of Silica or Polymer Microspheres," *Adv. Mater.*, vol. 16, pp. 1204–1208, 2004.

-
- [27] Y.-S. Cho, G.-R. Yi, J.-M. Lim, S.-H. Kim, V. N. Manoharan, D. J. Pine, and S.-M. Yang, "Self-organization of bidisperse colloids in water droplets.," *J. Am. Chem. Soc.*, vol. 127, pp. 15968–15975, 2005.
- [28] S. Sacanna, W. T. M. Irvine, P. M. Chaikin, and D. J. Pine, "Lock and key colloids.," *Nature*, vol. 464, pp. 575–578, 2010.
- [29] D. J. Kraft, J. Groenewold, and W. K. Kegel, "Colloidal molecules with well-controlled bond angles," *Soft Matter*, vol. 5, p. 3823, 2009.
- [30] D. J. Kraft, J. Hilhorst, M. A. P. Heinen, M. J. Hoogenraad, B. Luigjes, and W. K. Kegel, "Patchy polymer colloids with tunable anisotropy dimensions.," *J. Phys. Chem. B*, vol. 115, pp. 7175–7181, 2011.
- [31] A. Désert, C. Hubert, Z. Fu, L. Moulet, J. Majimel, P. Barboteau, A. Thill, M. Lansalot, E. Bourgeat-Lami, E. Duguet, and S. Ravaine, "Synthesis and Site-Specific Functionalization of Tetravalent, Hexavalent, and Dodecavalent Silica Particles.," *Angew. Chem. Int. Ed. Engl.*, vol. 52, pp. 11068–11072, 2013.
- [32] S. Reculosa, C. Mingotaud, E. Bourgeat-Lami, E. Duguet, and S. Ravaine, "Synthesis of Daisy-Shaped and Multipod-like Silica / Polystyrene," *Nano Lett.*, vol. 4, pp. 1677–1682, 2004.
- [33] A. Perro, S. Reculosa, E. Bourgeat-Lami, E. Duguet, and S. Ravaine, "Synthesis of hybrid colloidal particles: From snowman-like to raspberry-like morphologies," *Colloids Surfaces A Physicochem. Eng. Asp.*, vol. 284–285, pp. 78–83, 2006.
- [34] A. Perro, E. Duguet, O. Lambert, J.-C. Taveau, E. Bourgeat-Lami, and S. Ravaine, "A Chemical Synthetic Route towards 'Colloidal Molecules,'" *Angew. Chem. Int. Ed. Engl.*, vol. 121, pp. 367–371, 2009.
- [35] A. Désert, I. Chaduc, S. Fouilloux, J.-C. Taveau, O. Lambert, M. Lansalot, E. Bourgeat-Lami, A. Thill, O. Spalla, S. Ravaine, and E. Duguet, "High-yield preparation of polystyrene/silica clusters of controlled morphology," *Polym. Chem.*, vol. 3, pp. 1130–1132, 2012.
- [36] A. Désert, "Thèse de l'Université Bordeaux 1: Colloïdes hybrides silice/polystyrène de morphologie contrôlée," 2011.
- [37] K. D. Hartlen, A. P. T. Athanasopoulos, and V. Kitaev, "Facile preparation of highly monodisperse small silica spheres (15 to >200 nm) suitable for colloidal templating and formation of ordered arrays.," *Langmuir*, vol. 24, pp. 1714–1720, 2008.
- [38] A. Perro, S. Reculosa, E. Bourgeat-Lami, E. Duguet, and S. Ravaine, "Synthesis of hybrid colloidal particles: From snowman-like to raspberry-like morphologies," *Colloids Surfaces A Physicochem. Eng. Asp.*, vol. 284–285, pp. 78–83, 2006.
- [39] W. Stöber and A. Fink, "Controlled Growth of Monodisperse Silica Spheres in the Micron Size Range 1," *J. Colloid Interface Sci.*, vol. 26, pp. 62–69, 1968.

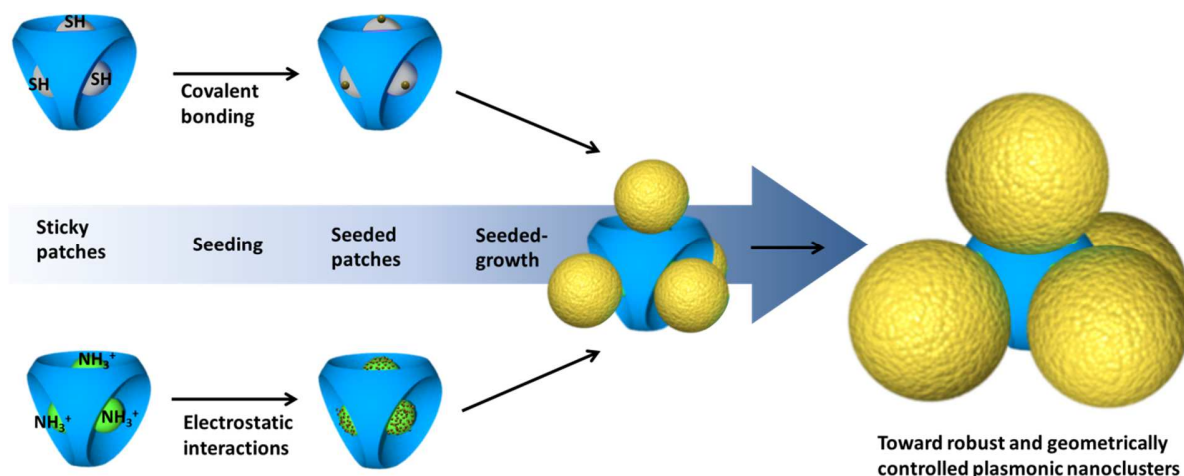
- [40] C. A. Schneider, W. S. Rasband, and K. W. Eliceiri, "NIH Image to ImageJ: 25 years of image analysis," *Nat. Methods*, vol. 9, pp. 671–675, 2012.
- [41] E. Bourgeat-Lami, M. Insulaire, S. Reculosa, A. Perro, S. Ravaine, and E. Duguet, "Nucleation of Polystyrene Latex Particles in the Presence of γ -Methacryloxypropyl-trimethoxysilane: Functionalized Silica Particles," *J. Nanosci. Nanotechnol.*, vol. 6, pp. 432–444, 2006.
- [42] A. Désert, C. Hubert, A. Thill, O. Spalla, J.-C. Taveau, O. Lambert, M. Lansalot, E. Bourgeat-Lami, E. Duguet, and S. Ravaine, "Regioselective Coating of Tetrapod-like Clusters with Silica," *Mol. Cryst. Liq. Cryst.*, vol. 604, pp. 27–32, 2014.
- [43] R. M. Metzger, *The Physical Chemist's Toolbox*. Wiley, p. 667, 2012.
- [44] E. Bourgeat-Lami and G. Fevotte, "Emulsion copolymerization mechanism of 3-trimethoxysilylpropyl methacrylate and styrene," *Acta Polym. Sin.*, vol. 7, pp. 912–916, 2006.
- [45] A. Perro, D. Nguyen, S. Ravaine, E. Bourgeat-Lami, O. Lambert, J.-C. Taveau, and E. Duguet, "Planar submicronic silica–polystyrene particles obtained by substrate-directed shaping," *J. Mater. Chem.*, vol. 19, pp. 4225–4230, 2009.
- [46] D. Yin, Q. Zhang, H. Zhang, and C. Yin, "Fabrication of covalently-bonded polystyrene/SiO₂ composites by Pickering emulsion polymerization," *J. Polym. Res.*, vol. 17, pp. 689–696, 2009.
- [47] A. Guyot and P. Espiard, "Poly(ethyl acrylate) latexes encapsulating nanoparticles of silica: 2 . grafting process onto silica," *Polymer (Guildf.)*, vol. 36, pp. 4391–4395, 1995.
- [48] Z. Zeng, J. Yu, and Z.-X. Guo, "Preparation of Functionalized Core-Shell Alumina/Polystyrene Composite Nanoparticles, 1," *Macromol. Chem. Phys.*, vol. 206, pp. 1558–1567, 2005.
- [49] R. Mueller, H. K. Kammler, K. Wegner, and S. E. Pratsinis, "OH Surface Density of SiO₂ and TiO₂ by Thermogravimetric Analysis," pp. 160–165, 2003.
- [50] G. D. Jones, "Chloromethylation of Polystyrene," *Ind. Eng. Chem.*, vol. 44, pp. 2686–2693, 1952.
- [51] A. Warshawsky and A. Deshe, "Halomethyl Octyl Ethers: Convenient Halomethylation Reagents," *J. Polym. Sci. Polym. Chem. Ed.*, vol. 23, pp. 1839–1841, 1985.
- [52] C. Lü, B. Gao, Q. Liu, and C. Qi, "Preparation of two kinds of chloromethylated polystyrene particle using 1,4-bis (chloromethoxy) butane as chloromethylation reagent," *Colloid Polym. Sci.*, vol. 286, pp. 553–561, 2007.
- [53] V. G. Teixeira, F. M. B. Coutinho, F. R. M. Petrocíniao and A. S. Gomes, "Determination of Accessible Chloromethyl Groups in Chloromethylated," *J. Braz. Chem. Soc.*, vol. 16, pp. 951–956, 2005.
- [54] R. Rodrigo, C. A. Toro, and J. Cuellar, "Preparation of chloromethylated and aminated gel-type poly(styrene- co -divinylbenzene) microparticles with controlled degree of functionalization," *J. Appl. Polym. Sci.*, pp. 4054–4065, 2013.

-
- [55] F. Galindo, B. Altava, M. I. Burguete, R. Gavara, and S. V Luis, "A sensitive colorimetric method for the study of polystyrene merrifield resins and chloromethylated macroporous monolithic polymers.," *J. Comb. Chem.*, vol. 6, pp. 859–61, 2004.
- [56] B. G. P. van Ravensteijn, M. Kamp, A. van Blaaderen, and W. K. Kegel, "General Route toward Chemically Anisotropic Colloids," *Chem. Mater.*, vol. 25, p. 4348–4353, 2013.
- [57] V. K. Sarin, S. B. H. Kent, J. P. Tam, and R. B. Merrifield, "Quantitative monitoring of solid-phase peptide synthesis by the ninhydrin reaction," *Anal. Biochem.*, vol. 117, pp. 147–157, 1981.
- [58] J. S. Fritz and C. A. Burgett, "Titration of Amines in Acetone," *Anal. Chem.*, vol. 44, pp. 1673–1674, 1972.
- [59] M. Whitesides, "Thiol-disulfide interchange," in *Sulphur-Containing Functional Groups*, pp. 633–658, 1993.
- [60] A. Wang, H. P. Ng, Y. Xu, Y. Li, Y. Zheng, J. Yu, F. Han, F. Peng, and L. Fu, "Gold Nanoparticles: Synthesis, Stability Test, and Application for the Rice Growth," *J. Nanomater.*, vol. 2014, pp. 1–6, 2014.
- [61] I. Ojea-Jime, F. M. Romero, N. G. Bastus, and V. Puentes, "Small Gold Nanoparticles Synthesized with Sodium Citrate and Heavy Water: Insights into the Reaction Mechanism," *J. Phys. Chem. C*, vol. 114, pp. 1800–1804, 2010.
- [62] M. Roca, N. H. Pandya, S. Nath, and A. J. Haes, "Linear assembly of gold nanoparticle clusters via centrifugation.," *Langmuir*, vol. 26, pp. 2035–41, 2010.
- [63] N. G. Bastus, J. Comenge, and V. Puentes, "Kinetically Controlled Seeded Growth Synthesis of Citrate-Stabilized Gold Nanoparticles of up to 200 nm: Size Focusing versus Ostwald Ripening," *Langmuir*, pp. 11098–11105, 2011.
- [64] J. Kimling, M. Maier, B. Okenve, V. Kotaidis, H. Ballot, and A. Plech, "Turkevich method for gold nanoparticle synthesis revisited.," *J. Phys. Chem. B*, vol. 110, pp. 15700–15707, 2006.

Chapter 2: Structured plasmonic nanoclusters through the site-specific and seed-mediated growth of the satellites

As shown in Chapter 1, the aminated or thiolated patchy particles offered the possibility to induce regio-selective surface chemistry and in particular to decorate specifically the bottom of the dimples with gold seeds. Here, we describe our effort for promoting and directing their subsequent growth in order to get spherical gold satellites within each dimple and narrow inter-satellites gaps.

Two strategies to promote the seed-mediated growth onto the dimple surface only were employed as sketched in **Scheme 10**. First, an approach driven by direct covalent linkage was explored in order to create a strong interaction in between the preformed metallic seeds and the PS bumps. The second strategy was based on electrostatic association between oppositely charged species. Once immobilized, the seeds were further grown to produce gold spherical satellites onto each concave area forming plasmonic nanoclusters.



Scheme 10: Scheme of the two seed-mediated growth approaches developed in order to fabricate a silica/gold tetrapod-like cluster.

1 Seeded-growth of gold satellites on thiolated patchy particles

Gold surface and thiol molecules are well-known to exhibit strong covalent interactions due to the soft electrophile [1] and nucleophile [2] character respectively (see for example the works of Mulvaney [3] and Whitesides [4] teams). **Figure 30** shows a recent example of original nanostructures that could be engineered through thiol-gold linkages by the incorporation of bio-functionalities such as cysteine on the surface of a cowpea mosaic virus capsid.[5]

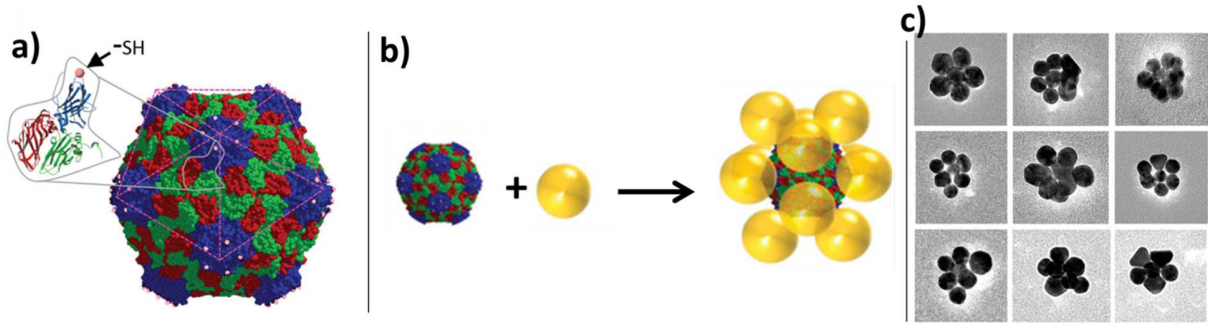


Figure 30: a) Cysteine modified cowpea mosaic virus capsid; b) Assembly of the modified capsid with gold nanosphere; c) TEM images of the as-obtained plasmonic nanoclusters (various morphologies simultaneous obtained in a same batches) scale bar 100 nm. Adapted from reference [5].

Inspired by this work and the previous studies on the well-established strong interactions in between gold and sulfur, we explored the possibility to strongly anchor gold seeds onto thiol-modified dimples and investigate their subsequent growth. Citrate-stabilized gold nanoparticles were chosen as seeds. Their major advantage was that the binding forces of citrate and surface gold atoms are rather weak and the citrate ligands are expected to be readily exchanged by thiol groups.

The following sections describe the several growth approaches used on the 12-nm gold seeds anchored at the bottom of the thiolated dimples (**Figure 29c**).

1.1 Growth of the anchored gold seeds

Despite the low amount of seeds grafted onto the concave areas of the particles, we further proceeded to their growth in order to get gold satellites of large diameter. The seeds are well known to act as efficient redox catalysts for metal ion reduction, which occurs selectively at their surface, as the energetic barrier for heterogeneous nucleation is much lower than that for homogeneous nucleation. For the sake of simplicity the number of gold seeds per dimples was assumed to be 1. In this condition the volume of gold required to grow the particles to a given size can be anticipated thanks to **Eq. 5** where: V_{seeds} = volume of dimpled silica particles seeded by the gold particles; $V_{growth\ sol}$ = volume of growth solution media; $C_{growth\ sol}$ = gold concentration of growth solution media; $M_{(gold)}$ = the molar mass of gold; ΔV_{part} = added volume of gold per particle; $N_{patches}$ = number of sites assumed to contain one gold particle per dimpled silica particle; C_{seeds} = concentration of dimpled silica particle.

$$V_{seeds} = \frac{V_{growth\ sol} * C_{growth\ sol} * M_{(gold)}}{N_{patches} * C_{seeds} * \Delta V_{part}} \quad \text{Eq. 5}$$

In the literature, many seed-mediated recipes based on the use of citrate-capped gold nanoparticles have been reported. Three of them are particularly interesting since they allow to

get size-monodisperse gold nanoparticles of 50-200 nm in diameter. The results of their investigation for our own purpose are described below.[6]–[8]

1.1.1 Seed-mediated growth derived from the Rodriguez-Fernandez's work

In 2006, Rodriguez-Fernandez *et al* published a seeded-growth approach to obtain CTAB-stabilized quasi spherical gold nanoparticles with a narrow size distribution from 12 to 180 nm.[6] It was based on the use of ascorbic acid as reducing agent and cetyltrimethylammonium bromide (CTAB) as surfactant. At this time the method has extended the size range of monodispersed spherical gold particles obtainable. We derived this method to accomplish the growth of the gold seeds within the dimples.

Protocol 16: Seeded-growth method inspired by the Rodriguez-Fernandez's work.

Typically, the thiolated patchy particles seeded by the citrate-stabilized gold nanoparticles are introduced into 250 mL of an aqueous solution containing CTAB (0.015 M), ascorbic acid (1 mM) and HAuCl₄ (0.5 mM). Typically, this solution is prepared from stock solutions of CTAB (0.1 M), ascorbic acid (0.1 M) and HAuCl₄ (25 mM). The volume of solution containing the seeded dimpled silica particles is calculated by using Eq. 5 and by considering that the targeted particle diameter is from 12 to 60 nm.

A special effort was made to work with a known range of particles concentration in order to anticipate the required amount of gold for regrowth. For that purpose, Eq. 5 was quite useful. After the growth, the products were highly irregular (**Figure 31**). Most of the gold nanoparticles were unattached from the concave areas. The detachment phenomenon was probably caused by the presence of the CTAB surfactant. Such a surfactant is suspected to interact detrimentally with the anchorage of the gold nanoparticles into the dimples. Even if the exact mechanism remains unclear, the effect is detrimental for the colloidal stability and the construction of robust nanoclusters. This result led us to disregard this CTAB-based regrowth.

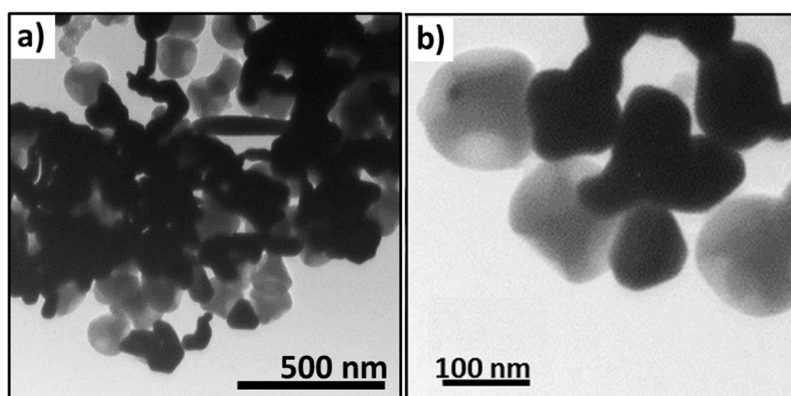


Figure 31: TEM images of the nanoclusters obtained after gold regrowth performed in the condition inspired by the Rodriguez-Fernandez's work a) large view and b) focused view.

1.1.2 Seed-mediated growth derived from the Puentes' work

In 2011, Puentes and coworkers reported another seeded-growth process to realize monodisperse gold nanoparticles up to 200 nm in diameter in an aqueous solution.[7] In the article, an initial dispersion of citrate-stabilized gold nanoparticles was used as seeds. Subsequently, this dispersion was diluted and the regrowth was performed in the presence of citrate at 90°C. This process was repeated until the targeted size of the gold nanoparticles obtained was reached.

Protocol 17: Seeded-growth method inspired by the Puentes' work.

A volume of thiolated patchy silica particles seeded by 12-nm citrate-stabilized gold nanoparticles calculated thanks to the Eq. 5 is centrifuged and dispersed into 15 mL of sodium citrate solution (2.2 mM) and transferred into a 20 mL flask. This solution is heated to 90°C and 0.1 mL of H₂AuCl₄ (25 mM) is introduced, thirty min later the same volume of the same solution is added. The gold nanoparticles concentration is assumed to be around $3 \cdot 10^{12}$ part/ mL. After 30 min, 5.5 mL of the volume are removed from the flask and 5.3 mL of ultrapure water are added with 0.2 mL of citrate sodium solution (60 mM). After temperature stabilization (5 min), a growth cycle of the process is considered as completed. Finally, to stop the process, the solution is allowed to cool down to room temperature after completion of the last cycle.

Figure 32 shows the TEM images and the UV-visible spectra obtained by using this second recipe. As depicted by the TEM images, as the number of iterative step increased, the gold nanoparticles size increased progressively within the dimples. The initial 12-nm seeds turned into nanoparticle exhibiting an average diameter of 19 ± 3 nm; 25 ± 3 nm; 44 ± 6 nm; 91 ± 26 nm after 1, 3, 6 and 9 steps, respectively. Contrarily to the previous approach, the gold nanoparticles remained anchored to the dimples and were relatively spherical. However, the silica cores appeared more and more damaged by the successive treatments. After the ninth step, it was difficult to identify the core morphology. The silica cores seemed progressively to be partially dissolved due to the presence of a significant amount of sodium ions (counter-ions of the citrate precursor) in the reaction suspension. This argument is consistent with what was reported in the literature in some experimental [9] and theoretical [10] investigations. Moreover, the reduction process was operated at 90°C which appeared like harsh conditions for silica, as already observed in previous investigations.[11]

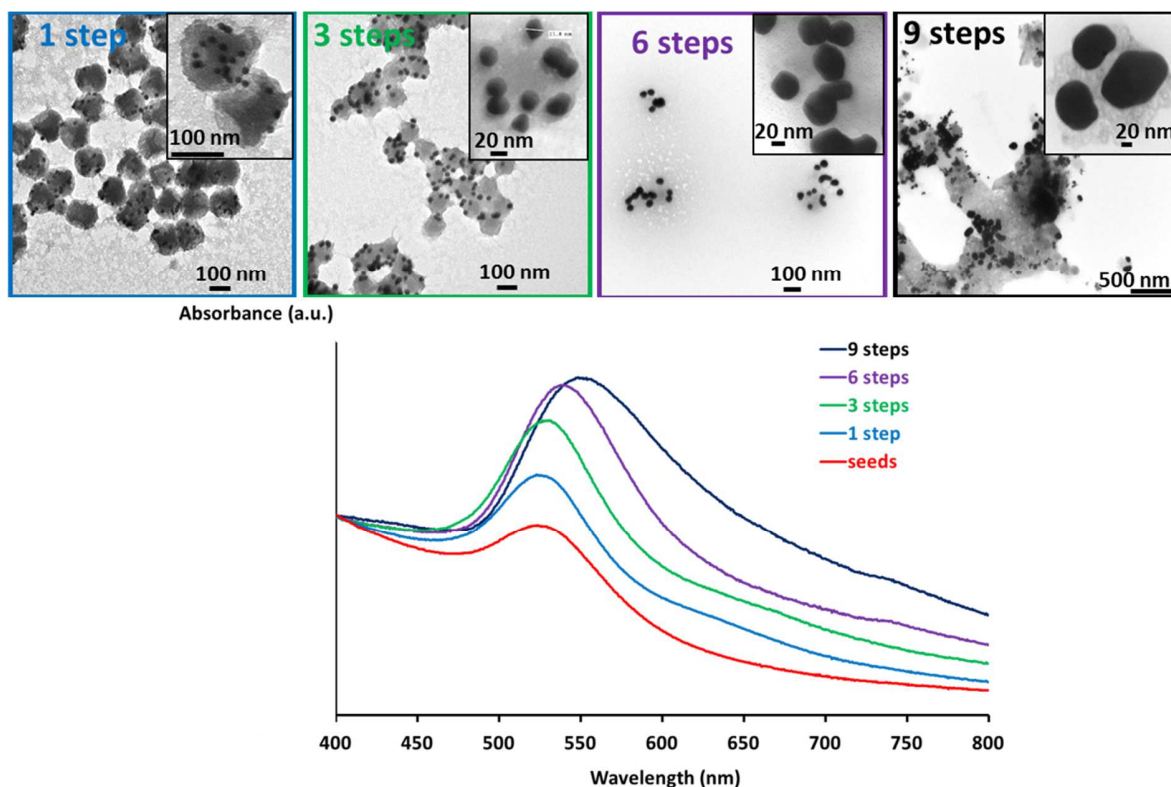


Figure 32: TEM images and the corresponding UV-visible spectra normalized at 400 nm of the plasmonic nanoclusters obtained after 1, 3, 6 or 9 iterative growth steps inspired by the Puntès' work.

The corresponding UV visible spectra of the plasmonic nanoclusters were in agreement with these overall observations. The SPR band red-shifted with increasing particle size: it peaked at 524 nm; 531 nm; 538 nm and 548 nm after 1, 3, 6 and 9 regrowth steps, respectively. A large SPR broadening and scattering were progressively observed during the stepwise reduction growth. The effect was assigned to the increase of the gold particle size as well as their progressive interaction. The progressive dissolution of the silica cores induced an uncontrolled vicinity of the large gold particles yielding into randomly distributed coupling distance broadening the absorption bands.

1.1.3 Seed-mediated growth derived from the Eychmüller's work

A third seed-mediated growth approach in milder reduction conditions was tested. It was a variation of the Eychmüller's recipe enabling to produce gold particles with diameter in the range 15-300 nm.[8] The process consisted in a reduction process performed at ambient temperature thanks to ascorbic acid and sodium citrate as stabilizer. From an experimental point of view, the typical diameter of the products could apparently be doubled in one growth step without detrimentally affecting the morphology. Note that the typical concentration of gold particles for a given experiment was in the range 10^{10} - 10^{12} part/mL. Moreover, the chloride ions concentration should be kept below 15 mM in order to prevent faceting of the growing gold nanoparticles.

Protocol 18: Seeded-growth method inspired by the Eychmüller's work.

In a three-neck round bottom flask, a typical volume of patchy particles seeded by citrate-stabilized gold nanoparticles is introduced. This volume is calculated knowing the concentration of patchy particles, the average number of patches and assuming one gold seed per patch. Taking those considerations into account, the volume of the suspension shall contain from 10^{10} - 10^{12} gold seeds.

The volume of gold precursor solution -concentrated at 5 mM- required to grow the seeds to a final diameter noted D_f is given by **Eq. 6** In a typical synthesis, this volume of gold precursor stock solution is extended to 10 mL and loaded in syringe A. A volume of ascorbic acid stock solution and sodium citrate stock solution corresponding to the volume ratio and concentration described in **Table 7** are mixed together, extended to 10 mL then loaded in syringe B. The two syringes are set on two syringe pumps which are adjusted to deliver their load in 45 min (13.3 mL/h).

$$V_{Au \text{ precursor solution}} = \frac{\rho_{Au}}{C_{gold \text{ precursor}} \cdot M_{Au}} N_{Au} \cdot \frac{\pi}{6} \cdot (D_f^3 - D_i^3) \quad \text{Eq. 6}$$

$C_{solution}$ = concentration of the gold precursor solution; D_f = final diameter noted; D_i = initial diameter of the gold seeds; N_{Au} = the number of gold particles contained in a given volume; M_{Au} = molar mass of gold; ρ_{Au} = gold density.

Table 7: Solutions used to implement the Eychmüller's method.

Type of solution	C gold precursor	C acid ascorbic	C tri-sodium citrate
wt./vol. concentration	0.2 %	1 %	1 %
Molar concentration	5 mM	58 mM	38 mM
Volume ratio in between solutions	1	1/4	1/8

This third recipe gave interesting results as shown on the series of TEM images (**Figure 33**). Indeed, the reduction of the metallic precursor led to the progressive growth of the gold satellites. They remained strongly anchored onto the dimples during the repeated process. The gold nanoparticles could grow up to 120-140 nm for the largest ones.

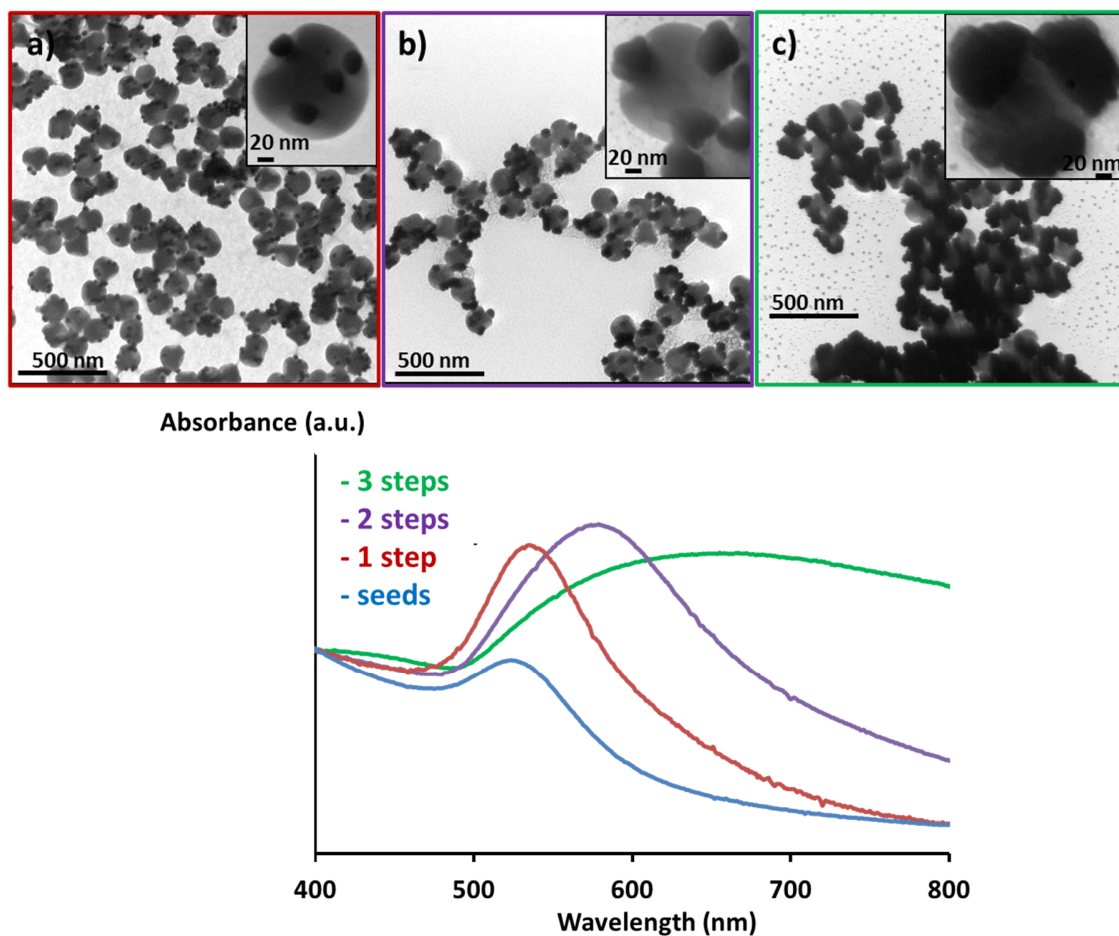


Figure 33: TEM images and the corresponding UV-visible absorption spectra normalized at 400 nm of the plasmonic nanoclusters obtained by the Eychmüller's work after 1, 2 and 3 growth steps.

After the third step, the plasmonic nanoclusters obtained were very large but randomly shaped. The cluster looked aggregated into small networks on the grid. Their colloidal stability was affected probably due to aggregation of the growing gold satellites. The large size and random shape of the gold particles obtained following this route induced a large SPR red-shift and broadening of the band (**Figure 33**). Moreover, the dimpled silica particles seem slightly damaged. This was attributed to the presence of sodium ions in the reactive medium known to be detrimental for silica (as discussed before).

1.2 Closing remarks on this strategy involving thiolated patchy particles

Table 8 compares some of the features of the plasmonic nanoclusters produced by the three previously described seed-mediated growth approaches.

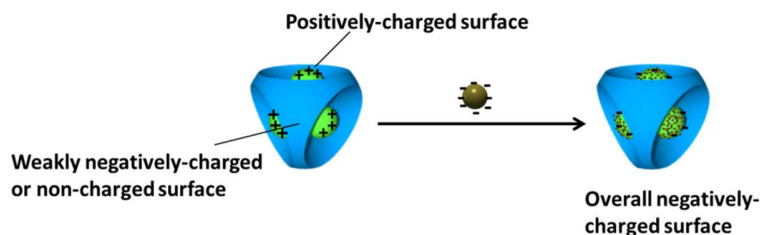
Table 8: Comparison of the features of the plasmonic clusters obtained via the three seed-mediated growth approaches.

Inspired by			
Main features	Rodriguez-Fernandez	Puntes	Eychmüller
Stability of the gold nuclei in the dimple	Unstable	Stable	Stable
Stability of the silica particles core	Stable	Dissolved	Damaged
Shape of the gold nanoparticles within the dimples	Randomly shaped	Spheroidal	Irregular
Production of relevant plasmonic nanoclusters	Impossible	Impossible	Impossible

None of the three methods had been proved to be efficient enough for the production of plasmonic nanoclusters fulfilling all our requirements (robustness, stability, size-monodisperse products with controllable morphology). The types of plasmonic nanoclusters that could be realized were quite primitive and not fully controlled. We believe that the main drawback of the strategy adopted here came probably from the small proportion of seeds grafted within the dimples and the weak interaction in between the thiol and the gold surface. The thiol molecules strongly bound to the gold surface through a covalent bond; but the proportion of thiol group per dimple was probably too low to ensure a strong anchorage of the enlarged seeds. Consequently, easy, large scale gold growth approach that doesn't damage the dimpled silica particles was still required. Surface modification of the dimples with other chemical functions enabling to induce a long range attraction force with gold seeds was explored and is presented in the following section.

2 Seeded-growth of gold satellites on aminated patchy particles

We explored the possibility to anchor gold seeds within the dimples whose PS was previously aminated (Chapter 1). Although the binding forces in between the amine ligands and the gold surface atoms were weaker than the thiol-gold ones, this process offered the possibility to associate the components by electrostatic interactions (**Scheme 11**). One potential advantage of these interactions was their long-range character expected to promote the decoration of the dimples with a larger proportion of gold seeds. Then, the subsequent growth of the anchored seeds was achieved with a mild reductant in the presence of a metal salt precursor.



Scheme 11: How negatively-charged gold nanoparticles were expected to site-specifically adsorb onto the aminated PS bumps within the dimples of a patchy silica particle.

2.1 Impact of the seed size

Figure 34 shows representative images of the dimpled silica particles bearing amino-groups after the incubation step with the citrate-stabilized gold seeds, according to *Protocol 13*. The exposure of 12-nm gold seeds to the amino-functionalized dimples led to a higher coverage of the concave areas (about 2.5 seeds per dimple) than the ones functionalized with thiol-groups (about 1.4 seeds per dimple) (Figure 29). However, the degree of coverage remains moderate.

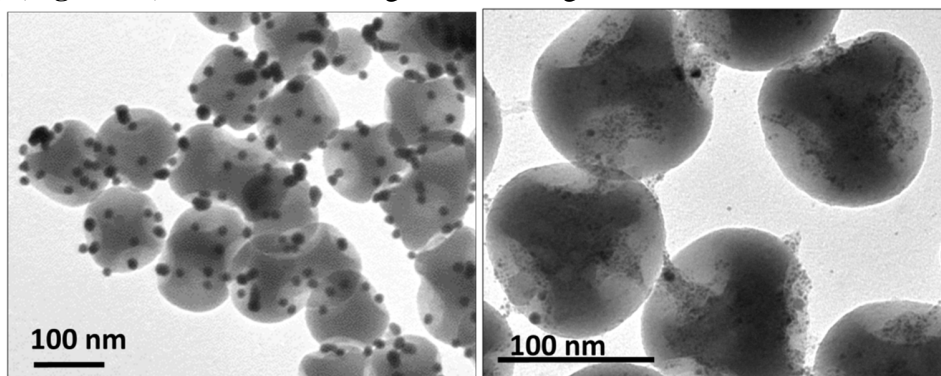
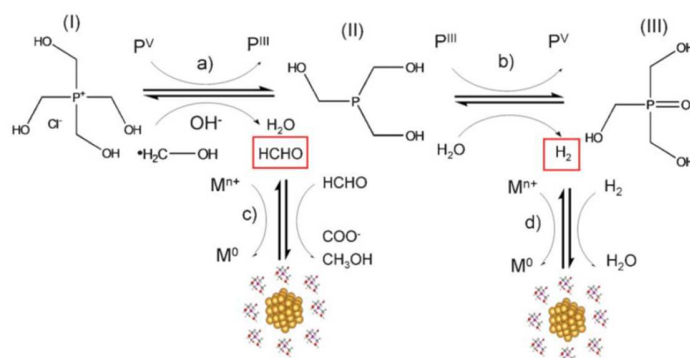


Figure 34: TEM images of the dimpled silica particles chemically modified with amino groups after incubation with 12-nm citrate-stabilized gold seeds (left) or 1-3-nm gold seeds (right).

To increase the surface coverage of gold seeds onto the dimples, the size of the gold seeds was decreased. Tiny gold seeds of about 1-3 nm in diameter were prepared following the *Protocol 19*, derived from the study of Duff and coworkers.[12],[13]. Briefly, the involved mechanism is the reduction of the gold salts from Au^{3+} to Au^0 by the formaldehyde and H_2 produced from tetrakis(hydroxymethyl)phosphonium chloride (THPC) molecules in presence of an excess of OH^- (Scheme 12).

Protocol 19: Synthesis of 1-3-nm gold nanoparticles according to the Duff's recipe.

In a 500-mL flask, 227.5 mL of milliQ water, 7.5 mL of an aqueous solution of NaOH (0.2 M) and 5 mL of THPC aqueous solution (120 μL in 10 mL) are introduced. This solution is homogenized during 15 min. Then, 10 mL of HAuCl_4 (25 mM) are quickly injected in the flask under stirring. The solution turns from pale yellow to brown in few seconds indicating the formation of gold nanoparticles.



Scheme 12: Proposed reaction mechanism describing the role of THPC in the formation of gold nanoparticles: the specie (I) THPC is converted into (III) THPO, producing formaldehyde and H_2 both serving as reducing agents. This illustration comes from reference [14].

The corresponding UV-visible spectrum of the as-obtained colloidal gold dispersion is shown on **Figure 35**. The spectrum exhibits an absorption that decays approximately exponentially into the visible, with a superimposed SPR shoulder at about 500 nm of weak intensity. Such optical signature is characteristic of tiny gold seeds.

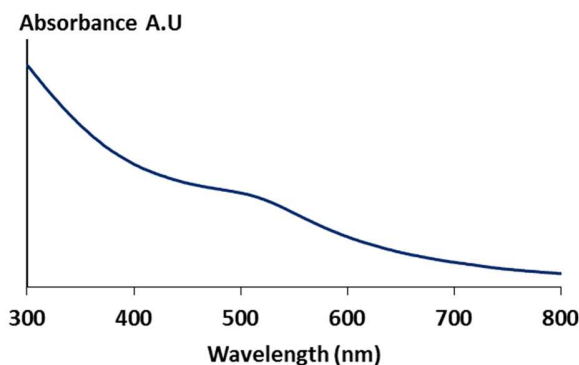


Figure 35: UV-visible spectrum of an aqueous dispersion of 1-3 nm gold nanoparticles as-obtained according to the Duff's method.

These tiny gold nanoparticles were then attached onto the dimpled silica surface according to the **Protocol 20**.

Protocol 20: Adsorption of gold Duff seeds on the dimpled silica particles.

Typically an amount of dimpled silica particles corresponding to $2 \cdot 10^{13}$ particles in water have their medium acidified to pH 3-4 followed by centrifugation at 10 000 g during 15 min and redispersion into 20 mL of ultrapure water. Subsequently, 2 mL of this peptized silica nanoparticles dispersion are mixed with 50 mL of Duff gold seeds dispersion and are let to incubate for 6 h on the roller mixer. Finally, the dispersion is washed three times by centrifugation at 8 600 g during 15 min to eliminate the excess of gold seeds and redispersed in 40 mL of milliQ water. Basically, the minimal volume of Duff seeds required is calculated thanks to **Eq. 7** giving the number of Duff nanoparticles of diameter r required to completely cover the surface of a sphere of radius R . **Eq. 8** gives

an estimation of the minimal volume of Duff solution required to seed the patches, where $N_{patches}$ corresponds to the number of patches per particle and C_{Duff} to the concentration of the Duff solution in part/L.

$$N_{duff} = \frac{2\pi}{\sqrt{3}} \cdot \left(\frac{R}{r} + 1\right)^2 \quad \text{Eq. 7}$$

$$V_{Duff\ sol} = \frac{N_{Duff} \cdot \frac{1}{4} \cdot N_{patches}}{C_{Duff}} \quad \text{Eq. 8}$$

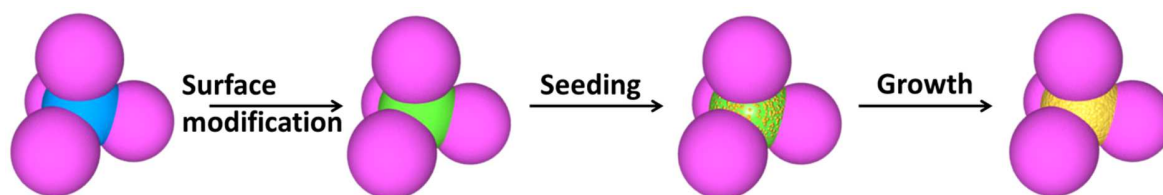
As shown on **Figure 34**, the degree of coverage of the dimpled particles was strongly affected by the size of the gold seeds. By reducing the size of the seeds, the number of seeds covering the concave areas was increased. The seed-mediated growth process, in the following, was thus explored with the dimpled particles chemically functionalized with amino-groups with the assumption that the higher the proportion of adsorbed gold seeds, the smoother the morphology of the gold satellites.

2.2 Optimization of the growth reaction conditions of the tiny gold seeds anchored onto the aminated silica surface

2.2.1 A conventional method applied on atypical colloids

In order to find out the judicious choice of the reaction conditions for the growth process, several control experiments were carried out both on conventional silica particles and multipod-like silica/PS clusters. This avoided us to limit the amount of patchy particles used for these optimization tests.

The strategy adopted to grow the gold seeds of 1-3 nm was based on a standard procedure well-described in the literature.[15]–[17] Briefly, the growth of the gold seeds was ensured with the use of a solution containing $\text{Au}(\text{OH})_4^-$ as gold precursor and formaldehyde as reducing agent. The $\text{Au}(\text{OH})_4^-$ solution was prepared by using an aqueous solution of gold salt (HAuCl_4) with K_2CO_3 . The reaction generated the $\text{Au}(\text{OH})_4^-$ complex. Such solution is often called “gold plating solution” (GPS) in the literature.[18] The use of this solution allowed to remove the chlorides which are well known to induce the sintering of the gold nanoparticles. The reduction occurred in the presence of PVP to sterically stabilize the silica/PS/Au clusters. Depending on the amount of gold precursor added, the gold shell could be holey as well as continuous. In the case of conventional silica particles, the process yielded to the synthesis of silica@gold core-shell particles (not shown). In the case of the silica/PS clusters, it yielded to the synthesis of gold shells with a controlled number of masked areas (**Scheme 13**).



Scheme 13: Strategy to prepare nanoshell over the silica part of the silica/PS clusters by reduction of gold precursor after decoration of the silica core with tiny gold seeds.

Protocol 21: Surface amination of the silica free surface of the silica/PS clusters.

Typically, 50 mL of the dispersion of silica/PS clusters (T-52) obtained after the silica regrowth in ammonia/ethanol medium (**Protocol 2**) are transferred into a 100-mL flask. A volume of APTES calculated as described in the section 2.2 from appendix and corresponding to a surface coverage equivalent to 50 functions /nm² is introduced in one shot; the solution is let to be stirred overnight. Subsequently, the dispersion is heated 1 h at 50°C and washed 3 times by centrifugation at 4000 g during 20 min and redispersed into a solution of 1-mL of NP30 (150 g/L) and 39 mL of water. Finally, the dispersion has to be acidified (pH 4) by using few drops of HCl.

Protocol 22: Adsorption of gold NPs on the silica surface of the silica/PS particles.

In a 50-mL falcon tube, 30 mL of 1-3-nm gold nanoparticles dispersion as-prepared after **Protocol 20** is introduced and 10 mL of the solution of APTES-functionalized silica/PS clusters are added. The solution is incubated for at least 6 h. Finally, the as-obtained clusters are washed three times by centrifugation during 30 min at 2500 g and redispersed in 20 mL of milliQ water.

Protocol 23: Preparation of the GPS.[15]

First, 10 mL of a stock 25-mM solution of gold precursor is prepared from H₂AuCl₄ (99.9 % Sigma-Aldrich) and stored protected from light at 4°C. In a 100-mL flask, 8 mL of the gold stock solution and 300 mg of potassium carbonate K₂CO₃ (1.5 H₂O) are mixed and the flask is completed to 100 mL with milliQ water. The solution is stirred overnight at 4°C.

Protocol 24: Growth of the gold nanoshell on the silica surface of the silica/PS particles.

One mL of the solution of clusters after seeding with gold nuclei (**Protocol 9**) is introduced into a 50-mL falcon tube followed by the introduction of a given volume of the GPS calculated as described in the 2.3 in order to obtain a targeted gold thickness. The mixture is homogenized and 10 mL of PVP solution (10 g/L; $\overline{M}_w = 29\,000$ g/mol) are introduced, the mixture is one more time homogenized and finally a volume of formaldehyde corresponding to 50 μ L/ mL of GPS is added in one shot. The solution is

quickly homogenized by using vortex and let to react under stirring for 12 h. The solution turns from beige to blue/green depending on the thickness of the gold deposited.

The TEM images collected after the activation of the silica core of the silica/PS clusters with the tiny gold seeds are shown on **Figure 36**. The silica coverage was clearly dense and homogeneous. This observation confirmed that the electrostatic attraction in between the silica and the gold surface was a more promising strategy to provide dense metallic coatings.

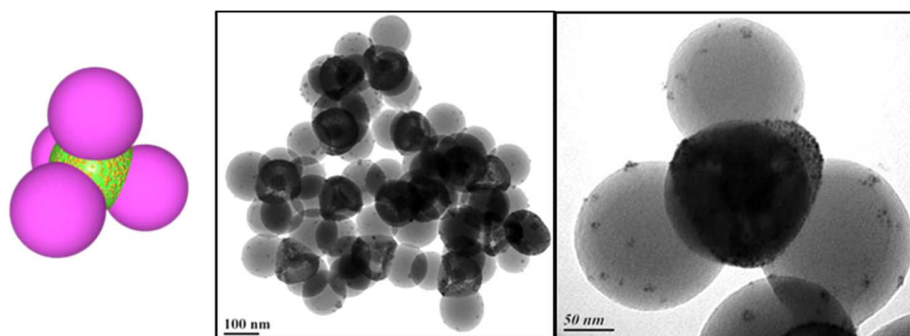


Figure 36: Scheme of the targeted structure and TEM images of tetrapod silica/PS hybrid clusters with gold seeds attached quasi-exclusively to their silica core.

In order to achieve a uniform growth of the gold seeds onto silica surface, several accurately controlled parameters and steps were required:

- control of the concentration of the seeded particles in the growth media. According to previous investigations, it had to be in the range 10^{-4} - 10^{-3} vol.% to avoid any aggregation phenomenon;[16] observed in the case of more concentrated particles and to avoid a too important homogeneous nucleation observed in the too low concentrated suspensions.
- adjustment of the concentration of the GPS and the formaldehyde: it was successful for concentrations in the range 0.5-1 mM and 0.1-0.3 M, respectively;[19]
- size of the silica nanoparticles (or silica/PS clusters). Literature reports revealed that too small silica@Au_n colloids, *e.g.* 40-50 nm in diameter, had a strong tendency to aggregate, because of the size-dependence of the electrostatic double layer potential;[20]
- nature of the stabilizer. PVP was chosen in the following experiments because of its multiple role: it allows to avoid aggregation and precipitation and to slow down the kinetics of the growth reaction. Consequently, it reduced the secondary nucleation of gold nanoparticles. Finally, it helped to obtain a dense pellet, more convenient to handle during the centrifugation washing steps.

Furthermore, a delicate balance had to be achieved between several parameters, such as the pH value of the seed dispersion, the pH of the GPS, the iterative growth process and the rate of reduction on the gold nanoshell formation. These effects are described in the following sections.

2.2.2 Optimization of the pH value of the seed dispersion

Reports in the literature attested that variations in the pH setting of the seed solution affected the fabrication process of gold shells onto conventional silica particles.[19],[21] Preparation of gold seeds colloids was performed in alkaline medium (pH 10.5). The use of the as prepared seed is known to induce their heterogeneous deposition onto the silica surface. Moreover, ageing of this dispersion is known to allow the pH of the dispersion to decrease from 10 to a value in the range 8-9. For that purpose, the seed dispersion required an ageing time of at least four days at 4°C. The effect is attributed to the continuous reduction of residual gold by the remaining THPC species in solution, progressively consuming OH⁻. [17],[21] (**Scheme 12**).

Two experiments were carried out in order to investigate the effect on the subsequent gold growth onto the silica/PS clusters. The tiny gold seeds were introduced into the silica/PS clusters dispersion at pH 3 and 9. The pH was adjusted to 3 by adding HCl while pH 9 corresponded to the natural pH of the gold nuclei dispersion. **Figure 37** shows the TEM images of the as-obtained silica@gold/PS clusters, before and after the metal growth.

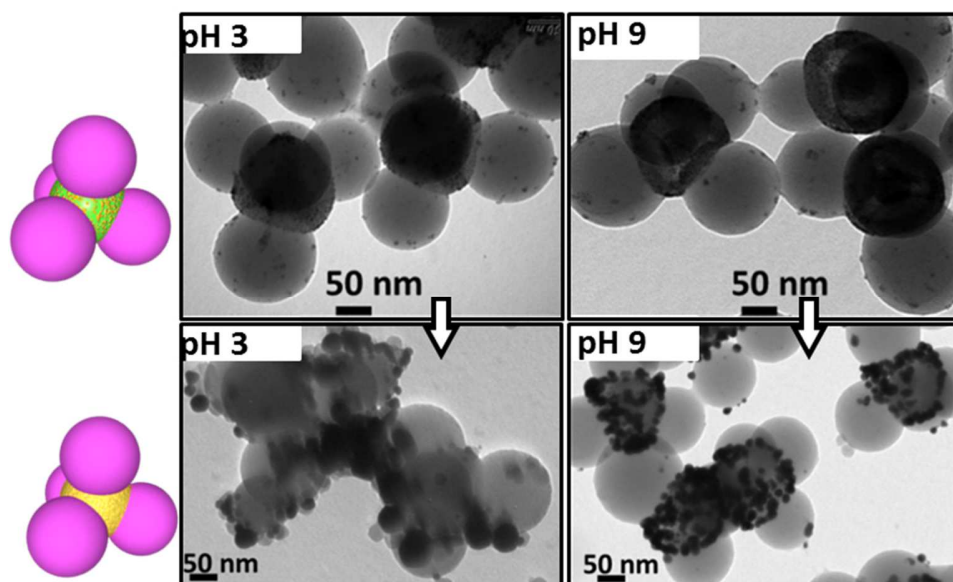


Figure 37: Scheme of the expected silica@gold/PS clusters and TEM images of those clusters before (top) and after (bottom) the gold growth; performed at different pH values.

Depending on the pH of the gold seeds dispersion, the degree of coverage of the silica cores was sparse or high respectively (**Figure 37 top**). Considering the fact that the aminated particles were dispersed in acidified suspension in our case the addition of acidified and so low charged gold nuclei (pH 3) didn't result in an efficient electrostatic interaction. On the contrary, the mix of highly charged gold colloids (pH 9) with highly charged aminated particles (pH 4) resulted in homogeneous coverage. This result was consistent with those reported by Park *et al.*[21] The growth process was strongly affected by the surface coverage of the silica core. Consequently, the growth of the gold seeds yielded into a much denser shell in the case of the core seeded by nuclei dispersion at pH 9 (**Figure 37 bottom**).

2.2.3 Optimization of the pH value of the growth medium

According to Zhongshi Liang *et al*, the pH of the solution during the growth step also had an influence on the uniformity of the coating as shown on **Figure 38**. [22] These authors proposed that, by changing the pH during this step, the gold chloride anions transformed into hydroxychloride anions $\text{AuCl}_{4-x}(\text{OH})_x^-$. As pH increased, the gold speciation were hydrolyzed and formed, for instance $\text{AuCl}(\text{OH})_3^-$ species at pH 9. These changes would affect the kinetic growth rates and the final morphology of the shell.

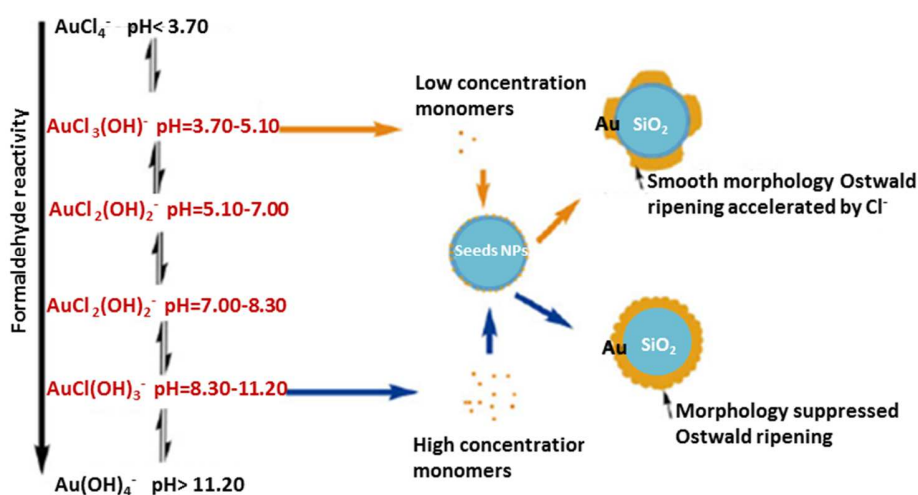


Figure 38: Influence of the pH solution used during the growth step on the gold shell morphology, after reference [22].

The impact of the pH value on the metal deposition was investigated and the results are summarized on **Figure 39**. In this set of experiments, we adjusted the pH of the reactive solution to 4.5, 8.6, 9.5 and 12.0 using HCl or NaOH. The reduction of the gold precursor was then carried out using the *Protocol 24*.

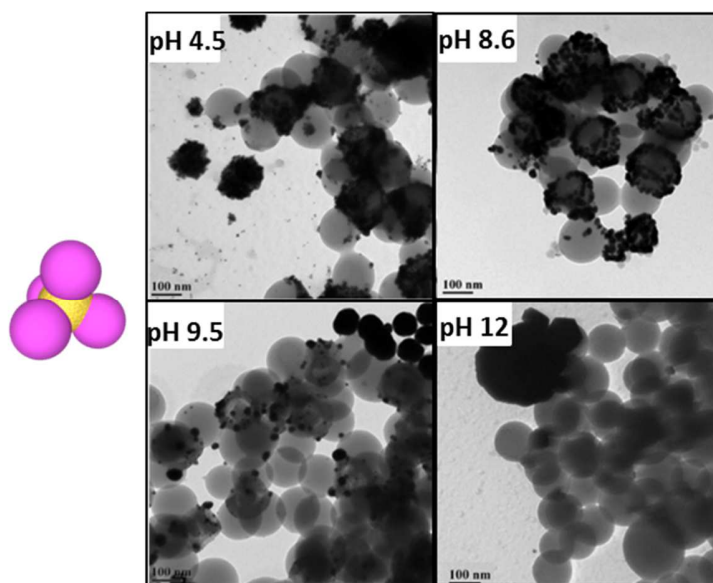


Figure 39: TEM images of silica@gold/PS clusters after gold regrowth using the GPS at different pH values.

TEM images show that the pH value indeed mattered. The growth process at pH 4.5 led to thin and irregular shells with few needle-like particles. At "natural pH", *i.e.* pH 8.6, the growth yielded uniform metallic shell. At higher pH value (*i.e.* 9.5 and 12.0), large gold nanoparticles and non-uniform coating were observed. These results could be attributed to kinetic rate changes in good agreement with the report of Zhongshi *et al.*[22]

2.2.4 Optimization of the reduction procedure: iterative regrowth

We found that the thickness of the metallic coating on the silica surface could be easily tuned by repeating the growth process. After the first growth step in the optimal experimental conditions described above, the solution was washed by centrifugation at 800 g for 15 min. The supernatant was removed and the silica@gold/PS clusters were redispersed in ultrapure water before the subsequent growth stage. **Figure 40** shows the TEM images of the silica@gold/PS cluster prepared after several successive gold growth stages.

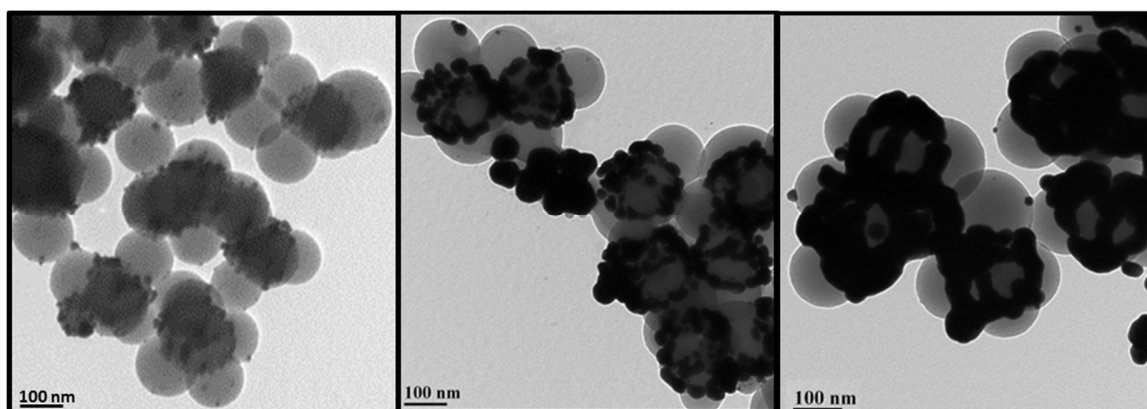


Figure 40: TEM images of silica@gold/PS cluster obtained from seed dispersion at pH 8.6; GPS at pH 9 after one (left) two (center) and three (right) growth steps.

Obviously, as far as the growth process was being repeated, the coverage degree of gold on the silica core gradually increased. Three successive growth stages were thus systematically performed in the following experiments.

On the basis of this study, uniform metallic coating of the core surface of silica/PS clusters could be prepared by adjusting several parameters:

- the pH value of the seed dispersion to get uniform metallic coating. It should be the “natural” pH value (pH 8.6) after an ageing period of at least four days at 4°C;[21]
- the pH value of the growth medium at pH 9;
- for the thickest coatings, the use of a multi-step procedure where iterative growth stages were intercalated with centrifugation/redispersion stages.

Beyond helping us to study the effect of several parameters on the gold shell formation, the silica@gold/PS clusters may be precursors of unusual objects (metal nanocages, etc.) see the section 5 of the appendix.

2.3 Growth of the tiny gold seeds anchored to the aminated PS bumps at the bottom of the patchy particles

By using these optimized conditions, we proceeded to the growth of the tiny gold seeds onto the aminated PS bumps at the bottom of the patchy particles silica/gold multipod-like clusters.

Protocol 25: Seeded growth of the tiny seeds anchored to the aminated PS bumps by formaldehyde reduction method.

Typically, 1 mL of the dispersion of aminated patchy particles decorated by the gold seeds produced after Protocol 19 is introduced in a falcon tube. Subsequently 10 mL of PVP solution (10 g/L; 29 000 g/mol) is added followed by the introduction of a volume of GPS (1 mM) produced according to the Protocol 23. After homogenization an amount of formaldehyde solution 37 % in water (Aldrich) corresponding to 50 μ L per mL of GPS is introduced. The reaction is performed for at least 12 h over the roller mixer device, washed by three cycles of centrifugation at 3 000 g during 15 min and redispersion into 20 mL of milliQ water.

Upon growth, large gold domains were produced within the dimples of the silica particles (**Figure 41a/b**). The gold satellites that formed using tiny gold seeds had a more homogeneous shape than those produced by using the larger seeds (12 nm) (data not shown). However, an accurate observation of the images revealed that gold wasn't exclusively located at the dimple surface. Some metallic nanoparticles also appeared on the inter-patch surface areas. This resulted probably from interactions in between the silanol groups and the seeds. To overcome this drawback, we performed a “passivation” of the silica core surface of silica/PS clusters prior to the PS dissolution and activation steps by using propyltrimethoxysilane (PTMS). This non-polar

propyl graft was expected to be inert toward gold as the PS surface.[23] The amount of PTMS added during the passivated step was calculated as reported in the section 2.2 from the appendix.

Protocol 26: “Passivation” of the inter-patch surface area using propyltrimethoxysilane (PTMS).

Typically the dispersion of the silica/PS clusters obtained after silica regrowth in their ethanol/ammonia medium are maintained in the growth flask and a volume of PTMS corresponding to 50 functions per nm² (section 2.2 from the appendix) is introduced in the flask in one shot. The reaction is let to be completed under stirring at ambient temperature for 12 h. Finally, the suspension is washed by three centrifugation/redispersion cycle in ethanol.

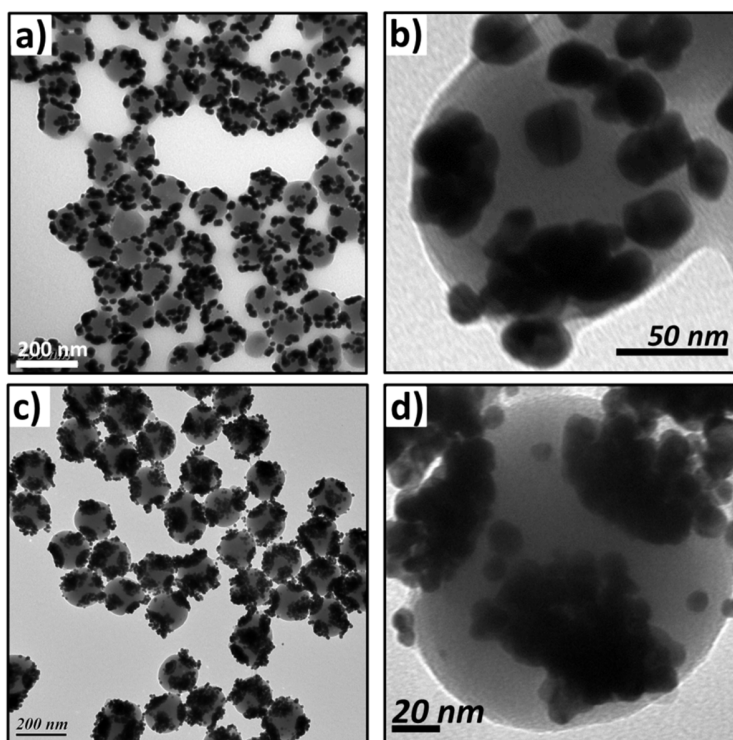


Figure 41: TEM images of the silica/gold multipod-like clusters without (a, b) and with (c, d) the “passivation” stage of the interpatch surface area.

Figure 41 c/d shows TEM images of the clusters obtained by gold seeding and regrowth after the passivation step. The images showed more defined patterns of dark and bright regions corresponding to the gold deposition and the bare silica part. The deposition of gold was clearly more site-specific, because occurring essentially within the dimples. Only very few gold nanoparticles were observed out of the concave areas.

In order to obtain more uniform and dense deposition of gold into the concave areas and to grow larger gold satellites, we changed the amount of GPS in the reaction medium. Several volumes of GPS were used for a given quantity of seeded patchy particles. In **Table 9**, the amount of gold

employed (here from GPS) was expressed in a more meaningful way. Indeed, considering that gold precursor is equally distributed in all the concave sites of the patchy particles, forming spheres, the mean diameter of such sphere was calculated thanks to **Eq. 9** and given in **Table 9**. Those ideal and expected results are compared with the ones obtained experimentally by measuring the average dimension of the gold satellites NPs by TEM.

$$N_{dpls} = 4; N_{parts} = 5^{10}; M_{Au} = 196.96 \rho_{Au} = 19.9 \text{ g/cm}^3$$

$$D_{\text{corresponding sphere}} = 2 \cdot \sqrt[3]{\frac{(V_{GPS} \cdot C_{GPS} \cdot M_{Au}) / \rho_{Au} \cdot 3}{N_{dpls} \cdot N_{parts} \cdot 4\pi}} \quad \text{Eq. 9}$$

Table 9: Equivalent diameter of Au NPs obtainable in nm considering the volume of GPS employed for the regrowth.

V _{GPS} (mL)	2	4	8	16	24	48
Equivalent diameter of Au NPs expected (nm)	57	73	91	115	131	166
Mean dimension of the Au NPS obtained (nm)	46	65	74	90	108	115

Figure 42 shows the TEM images of the silica/gold clusters prepared at different concentrations of seeds. The higher the volume of the GPS, the denser and more homogeneous the coating of the concave areas. This means that the coverage degree and so the size of the gold nanoparticles obtained could be easily tuned by playing with the volume of GPS.

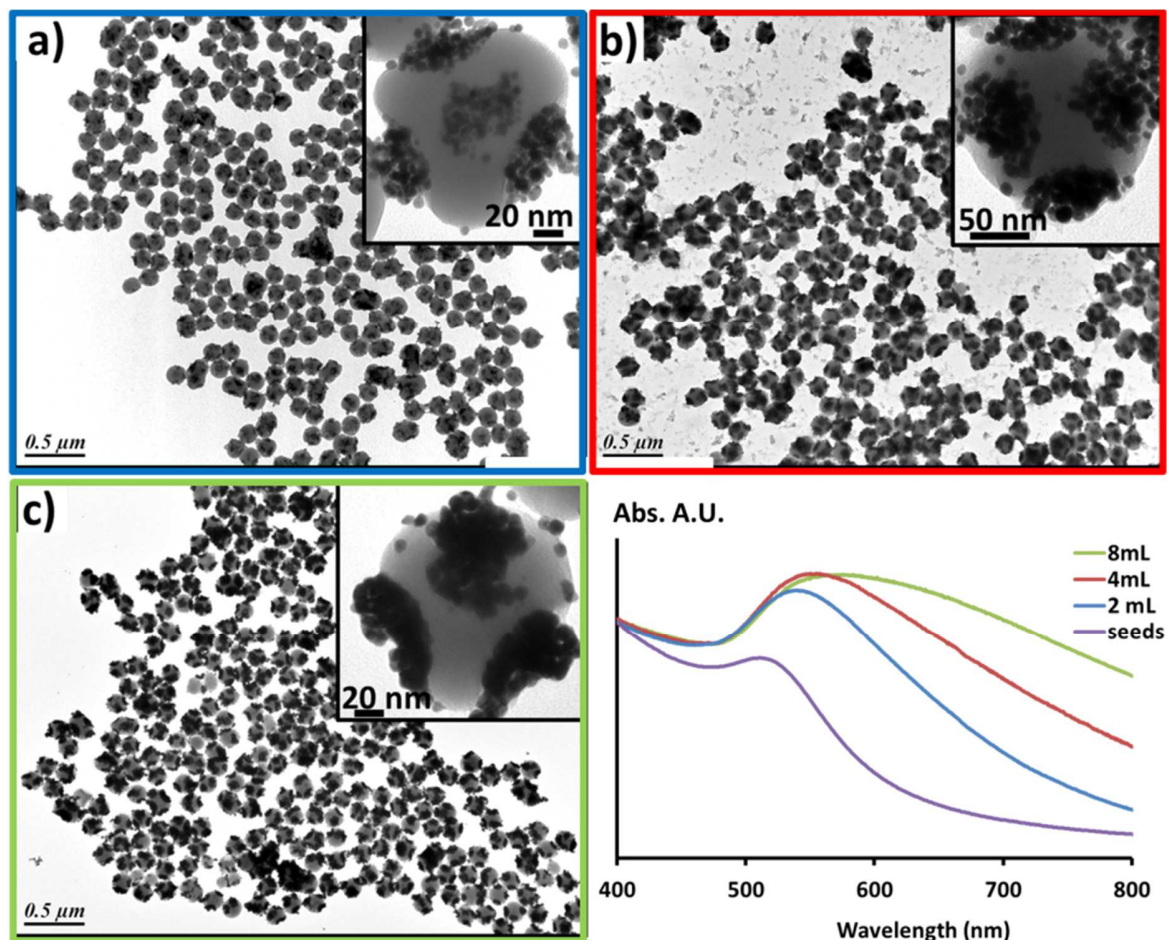


Figure 42: TEM images of the silica/gold clusters obtained by the seeded-growth strategy using aminated PS bumps within the silica dimples for different volume of GPS added in one shot: a) 2 mL; b) 4 mL; c) 8 mL; and the corresponding UV-vis spectra normalized at 400 nm.

Figure 43 further presents the SEM images of silica/gold clusters prepared with larger volume of GPS. Obviously, when the volume of GPS was increased, the size of the particles obtained in the dimples increased gradually. The SEM image with higher magnification showed that the gold entirely fulfilled the concave area of the dimples and shaped the template. The morphology of the gold nanoparticles were not exactly spherical, but rather oblate spheroid. In the case of the systems observed with the highest volume of GPS used, the gold satellites had an average diameter of 115 nm and an intersatellite gap of about 12 nm. Moreover, we can noticed that the obtained size of the gold nanoparticles increased less than expected with the volume of GPS incorporated, because of the secondary nucleation process.

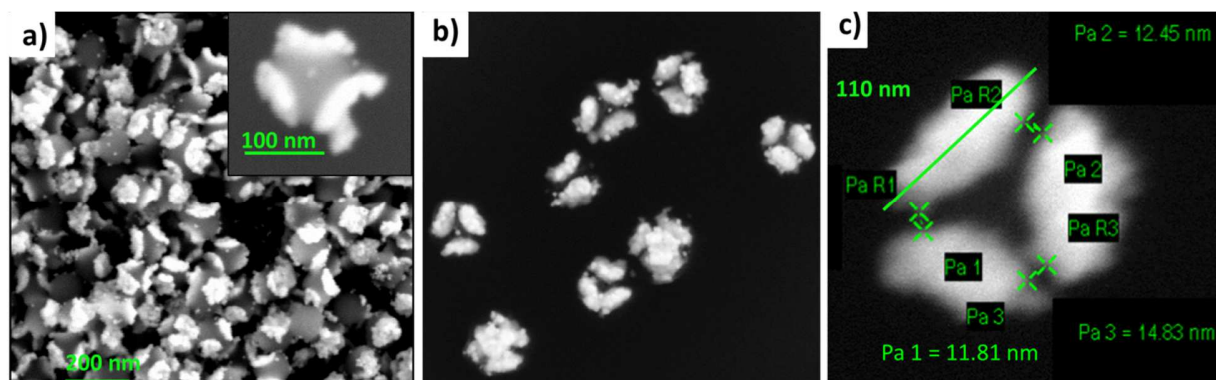
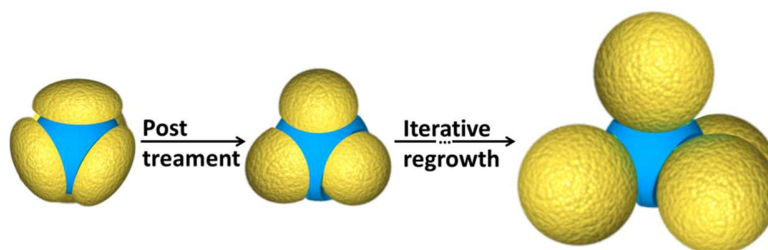


Figure 43: STEM images of the silica-gold clusters obtained by a seeded-growth strategy using aminated PS bumps within the silica dimples for different volumes of GPS added in one shot: a) 16mL; b) 24 mL and c) 48 mL.

The UV-visible absorption spectra of the silica/gold clusters prepared with various amounts of GPS are shown on **Figure 42**. Before the spectroscopic analysis, all the samples were centrifuged to remove the free gold particles. The plasmonic nanoclusters displayed an obvious absorption band at around 520 nm due to the Mie plasmon resonance excitation from the gold nanoparticles. As the dimension of the gold nanoparticles increases, the SPR band is red-shifted gradually, and the band is becoming broader due to the larger nanoparticle size and higher coverage shaping the concave areas.

3 Spheroidization of the gold satellites

Despite the progress in the synthesis of the plasmonic nanoclusters through the seed-mediated process described in the previous section, the rational control of the satellite morphology remained uncomplete. The satellite shapes were quite irregular and far from being perfectly spherical even using three or even more regrowth cycles. Furthermore, the gap between neighboring satellites was too large to induce a strong interparticular coupling. We, thus, explored different routes to reshape the satellites in solution followed by a subsequent regrowth step to further increase the satellite size and to get gap size appropriate to maximize the interactions (**Scheme 14**).



Scheme 14: General strategy for making spherical and larger the gold satellites of the silica/gold multipod-like clusters.

The reshaping of gold nanoparticles in solution might be accomplished by several protocols such as (i) microwave irradiation (ii) thermal annealing [24] and (iii) oxidation/reduction steps.[25]

They have been proven to be efficient on anisotropic nanoparticles dispersed in liquid phase. The challenging target was to achieve the reshaping process on supported gold nanoparticles to the same extent as realized in liquid phase.

To get more dense metallic nanoparticles onto each dimples, we first performed experiments to investigate the effect of microwave irradiation. Its advantage over convective heating is that microwaves can heat a substance quickly and uniformly and generate rapidly more homogeneous nanostructures. Therefore, we might predict that microwaving a colloidal dispersion containing the plasmonic nanoclusters could densify the gold satellites and make the particle more spherical within each dimple.

Protocol 27: Microwave treatment of the silica/gold clusters dispersion.

The plasmonic nanoclusters produced thanks to Protocol 25 after gold growth using 8 mL of GPS are introduced into 20 mL of ultrapure water. This dispersion is transferred into the microwave sample container, set in the microwave oven and the treatment is performed for 45 min. The microwave oven is a MARS 5 from CEM, the reactor used is a XP-1500 used at fixed power of 400W at fixed temperature.

The pressure and temperature were modulated from 100°C at 1 bar and 180°C for 20 bars. However, the microwave appeared to be systematically deleterious. For instance, after treatment at 180°C, the plasmonic nanostructures were seriously damaged, with desorption of the gold satellites, their agglomeration into dense and irregular particles, concomitantly to a serious reshaping of the silica cores which became smaller and more numerous (**Figure 44**). Tuning the temperature didn't modify the shape of the gold satellites. Therefore, the microwave irradiation appeared unsuitable for controlling the morphology of supported gold nanoparticles.

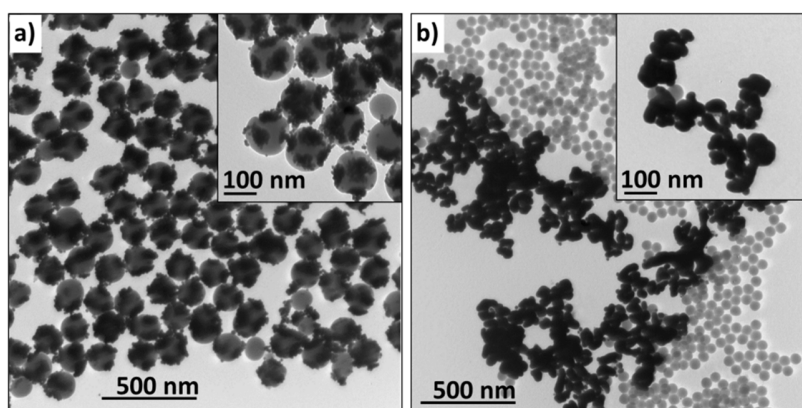


Figure 44: TEM image of the silica/gold clusters (T-52) prepared with 8 mL of GPS before (a) and after (b) microwave irradiation for 45 min at 180°C and 10 bar.

Another way to reshape the morphology of the gold satellites was to heat more conventionally the particles at the expense of transferring the clusters into a high boiling point liquid such as ethylene glycol ($T_b = 197\text{ }^\circ\text{C}$). Moreover, the ethylene glycol isn't known to be a good solvent for

polystyrene and therefore shouldn't swell the modified PS bumps neither destabilize the attached gold seeds.

Protocol 28: Thermal treatment of the silica/gold clusters.

*The dispersion of plasmonic nanoclusters produced thanks to the **Protocol 25** after two successive growth steps using 8 mL of GPS is transferred into 20 mL of ethylene glycol by centrifugation. Subsequently, the dispersion is heated at 190°C for 12 h then diluted into milliQ water and washed three times by using centrifugation (2500 g; 15 min). The treated clusters are finally used as seeds and a gold regrowth is performed after **Protocol 25**.*

Figure 45a/b shows the silica/gold clusters, before and after the thermal annealing. The observations were consistent with the above statements. The annealing treatment drove the densification of the gold into a single and large particle, instead of several small ones. The as-obtained clusters exhibited more dense and spheroidal satellites. However, the interaction of the gold and silica seemed less pronounced than that observed before the treatment. Some gold satellites were indeed off-centered or not anymore in contact with the dimples. This approach was thus rapidly disregarded for those stability reasons.

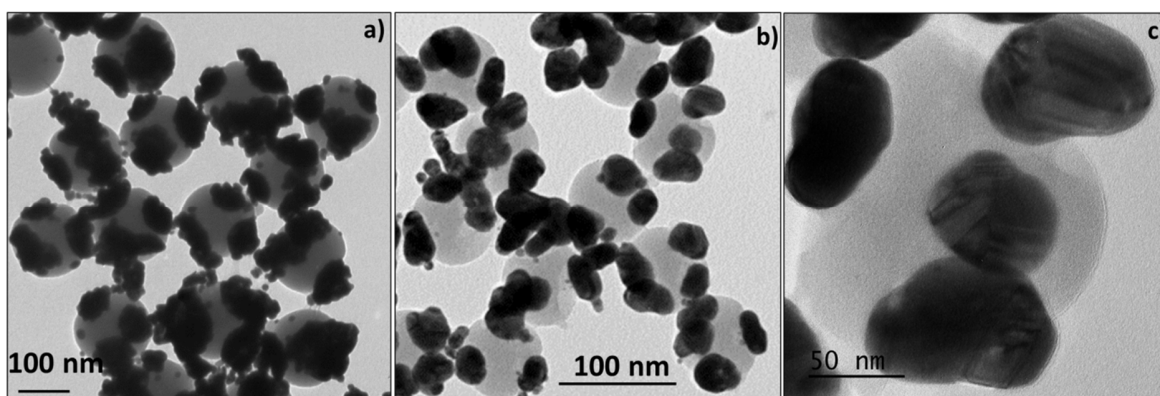


Figure 45: TEM images of the silica/gold clusters before a) and after b), c) annealing in ethylene glycol.

The oxidative etching approach is another important route for controlling nanoparticle morphology. It consists typically in a partial dissolution of the gold particles thanks to a preferential etching of the atoms of smallest coordination number. Thanks to the combination of oxidant conditions (HAuCl₄ serves as an oxidant) with the use of a polyelectrolyte, i.e. able to complex both the AuCl₄⁻ and AuCl₂⁻ ions, e.g. Polydiallyldimethylammonium chloride (PDDA), the oxidation of Au⁰ is promoted.

Indeed, the oxidation of Au⁰ to AuCl₂⁻ or AuCl₄⁻ is normally negligible due to the large negative values of the standard oxidation potentials (-1.154 V and -1.002 V respectively, versus normal hydrogen electrode). However, when PDDA is used to complex both AuCl₄⁻ and AuCl₂⁻ ions as they were formed, the reaction occurred by dissolving metallic gold through a slow process.

Then, the particles were etched. The particles can be regrown with a new growth step and etched again so on so forth. This approach had the advantage of not rising the temperature of the colloidal dispersion, making the gold-silica interaction weakened, as observed above. We thus attempted to study this route to reshape the gold satellites. First, we explored the optimal etching reaction conditions by tuning the molar amount of oxidative agent, i.e. the gold salt, used during the process. The molar amount of gold salt was tuned from 25 % to 75 % (**Figure 46 a/c**).

Protocol 29: Oxidative etching treatment of the silica/gold clusters.

*Typically, 20 mL of the silica/gold clusters dispersion prepared by seeded-growth approach are centrifuged at 3 000 g for 15 min and redispersed into 20 mL of ethylene glycol (JT. Baker, Baker analyzed). 0.4 mL of PDDA ($\overline{M}_w = 400\,000 - 500\,000$ g/mol, Aldrich) solution in water (20 wt.%) is added, the dispersion is stirred during 15 min. A volume of gold etching solution (HAuCl₄.3H₂O Sigma-Aldrich 99.9 %) in water (0.5 M), corresponding to a fraction of the gold amount used to produce the sample is calculated thanks to **Eq. 10** and introduced into the dispersion. Afterward, the mixture is rapidly homogenized using vortex device, and the reaction is performed for 24 h at ambient temperature on the roller mixer. After reaction, the clusters are washed by centrifugation: typically the 20 mL of gold nanoclusters dispersion are diluted into 90 mL of milliQ water, and centrifuged into two 50-mL falcon tubes. The dispersion is centrifuged at 2500 g during 20 min and washed 3 times using milliQ water. At this point, the dispersion is either characterized or used in a new regrowth step.*

$$\frac{V_{GPS} \times C_{GPS} \times F_{gold}}{C_{ES}} = V_{ES} \quad \text{Eq. 10}$$

V_{GPS} = volume of GPS used to produce the plasmonic nanoclusters; C_{GPS} = concentration of the solution (typically 1 mM); F_{gold} = molar fraction of gold etched; C_{ES} = concentration of etching solution (0.5 M typically); V_{ES} = volume of the gold etching solution.

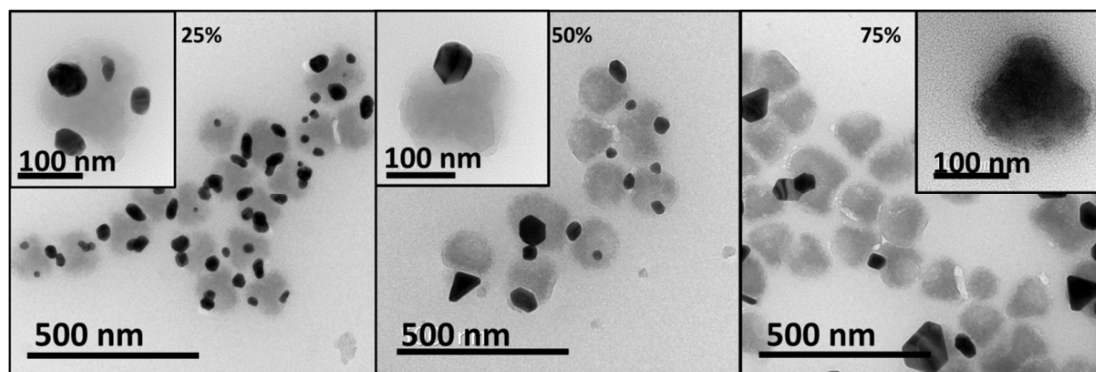


Figure 46: TEM images depicting the shape evolution of silica/gold clusters with the amount of oxidant.

Tuning the precursor ratio did change the morphology of the metallic satellite anchored in the concave area. The etching reaction by using 25 % of the gold precursor amount gave spheroidal nanoparticles, as shown by the TEM image in **Figure 46**. It did sculpt the particle toward a spherical shape. Using 50 % or 75 % of the gold amount led to a serious dissolution of the satellites.

After a subsequent regrowth step (*Protocol 25*), the clusters were “messy” with gold satellites evolving from spheroid-like morphology to randomly shaped ones (**Figure 47**). However the gold satellites were denser and could be reshaped through a subsequent etching step.

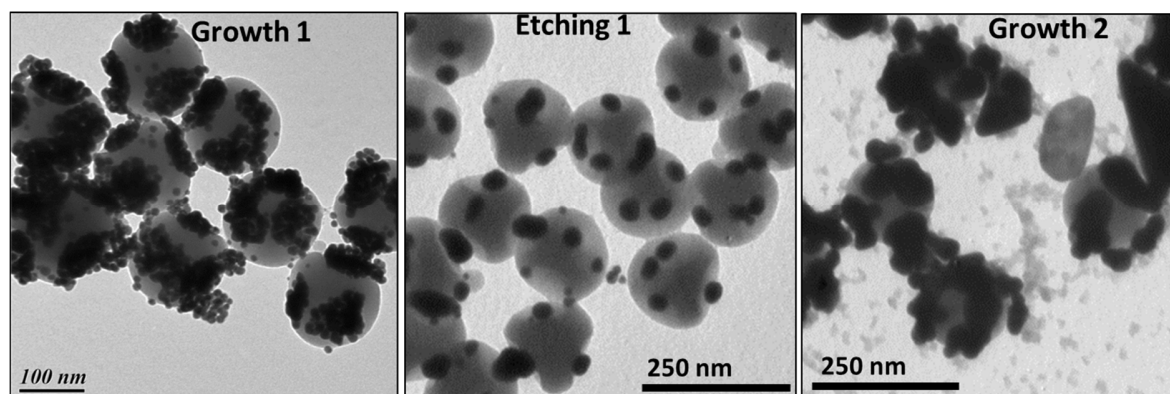


Figure 47: TEM images of silica/gold clusters after growth/etching with 25 % of oxidizing agent and a subsequent growth step.

Such iterative approach consisting in the repetition of the etching process allowed to increase the size of the particles while a spheroidal shape is maintained. Extra studies will be needed in order to fully understand and therefore control the etching and the subsequent regrowth stages on supported gold nanoparticles.

4 Extension to patchy particles bearing 6 and 12 dimples

The optimized method for the preparation of plasmonic nanoclusters described above was generalized for synthesizing clusters bearing 6 and 12 gold satellites. The successful

functionalization of the dimples with amino groups allowed to regioselectively anchor tiny gold seeds (**Figure 48**). The sequential growth of gold on the preformed seed led to the transformation into clusters with a controlled number of gold satellites. Two subsequent etching/regrowth stages yielded to a quite satisfying control of the satellite shapes.

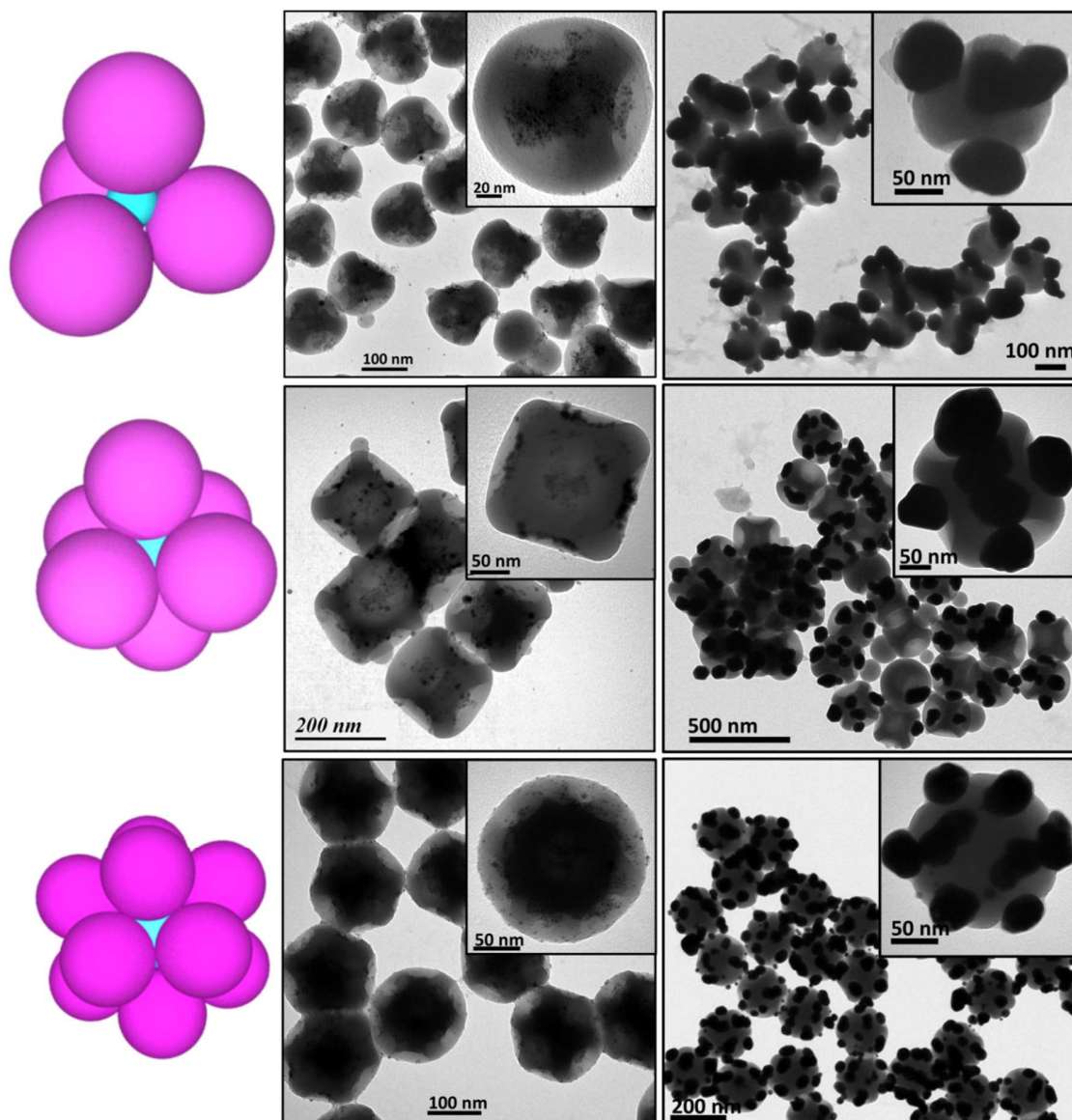


Figure 48: First row: Scheme of the initial silica/PS multipod-like clusters with 4, 6 and 12 PS satellites; Second row: TEM images of silica particles bearing 4, 6 and 12 dimples containing aminated PS bumps decorated by Duff gold seeds. Third row: TEM images of the silica/gold multipod-like clusters obtained using the oxidative etching process coupled with the iterative regrowth.

The plasmonic clusters bearing 6 gold satellites appeared like more regular than the tetrahedral ones and the trend was even more pronounced with the icosahedral ones which were really regular and exhibit few lost satellites. This observation could be explained by the differences, in term of size, of the gold nanoparticles obtained for each of the morphology. Indeed, while the

reshaped gold nanoparticles of the tetrahedral clusters are larger than 70 nm in diameter, the one from the icosahedral one are less than 40 nm. Therefore, the mechanical stress applied on the clusters during centrifugation is probably higher for the large gold nanoparticles of the tetrahedral morphology than the ones of the icosahedra. Consequently, the risk that clusters loose satellites is probably higher. Moreover, one satellite missing over four corresponds to a much important loss of regularity for the tetrahedral morphology than one missing over twelve for the icosahedral one.

5 Conclusion

Along this chapter, the results obtained by seed-mediated growth approaches in order to induce the formation of gold satellites onto each large spherical dimple have been presented. Two anchoring approaches of gold seeds and their subsequent growth were investigated:

- the covalent bonding strategy taking advantage of the thiolated-PS bumps to site-specifically attached citrate-stabilized gold nuclei. Three different methods of regrowth were explored but none of them yielded into relevant clusters;
- the electrostatic interaction using the amino-modified PS bumps strategy. This second approach allowed attaching a larger number of tiny gold nuclei (1-3 nm). This factor was proven to be of pivotal importance to initiate the synthesis of relatively large metallic satellites in a further growth step.

The overall results clearly indicated that this second approach generated more stable and uniform plasmonic nanoclusters with large satellites well located. The size of the gold particles grown into the aminated dimples can be controlled through the amount of GPS. Note that this approach required a passivation step of the interpatch areas to avoid the deposition of gold in between the dimples surface. Nevertheless, this route has some limitations: The lack of control over these $\text{Au}(\text{OH})_4^-$ satellites shape that remain oblate spheroid as well as the lack of control over the interparticles distance. Post-treatment performed at ambient temperature by alternating etching and regrowth approach, yielded to the nanoclusters exhibiting more regular morphologies and more spheroidal satellites. This result was confirmed for the three main morphologies investigated: tetrahedral, octahedral and icosahedral. These overall results obtained can be considered like a relevant step toward the production of geometrically controlled plasmonic nanoclusters. Taking advantage of the controlled surface chemistry of the patchy particles, it was possible to successfully obtain stable and robust plasmonic nanoclusters in a reproducible way. On the basis of this approach many kinds of complex hybrid particles could be possibly obtained and used in optical sensor devices.

6 References

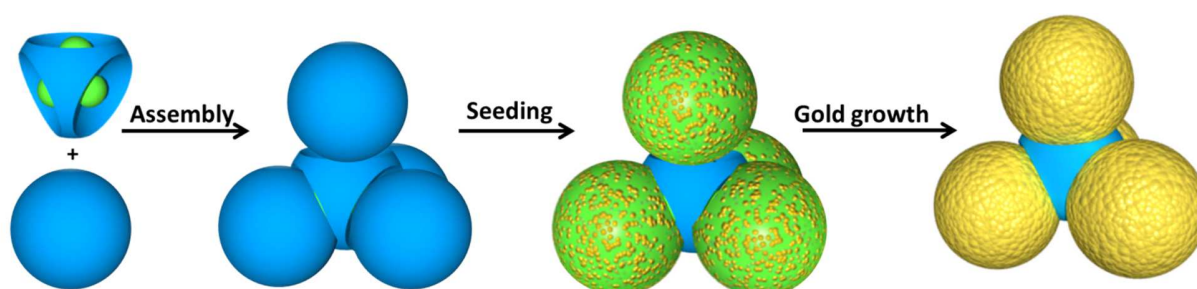
- [1] P. F. Geydar, G. A. Gardashchan, and A. T Mahmood, "The Study of Gold Nanoparticles in basis of Slater Functions," *J. Nano. Adv. Mat*, vol. 2, pp. 35–41, 2014.

-
- [2] M. Lo Conte and K. S. Carroll, "The chemistry of thiol oxidation and detection.," in *Oxidative Stress and Redox Regulation*, pp. 1–42, 2013.
- [3] M. Giersig and P. Mulvaney, "Preparation of Ordered Colloid Monolayers by Electrophoretic Deposition," *Langmuir*, vol. 9, pp. 3408–3413, 1993.
- [4] S. Weisbecker, V. Merritt, C. S. Weisbecker, M. V Merritt, and G. M. Whitesides, "Molecular of Aliphatic Thiols on Gold Colloids," *Langmuir*, vol. 12, pp. 3763–3772, 1996.
- [5] J. Fontana, W. J. Dressick, J. Phelps, J. E. Johnson, R. W. Rendell, T. Sampson, B. R. Ratna, and C. M. Soto, "Virus-Templated Plasmonic Nanoclusters with Icosahedral Symmetry via Directed Self-Assembly.," *Small*, vol. 10, pp. 3058–3063, 2014.
- [6] J. Rodríguez-Fernández, J. Pérez-Juste, F. J. García De Abajo, and L. M. Liz-Marzán, "Seeded growth of submicron Au colloids with quadrupole plasmon resonance modes.," *Langmuir*, vol. 22, pp. 7007–7010, 2006.
- [7] N. G. Bastus, J. Comenge, and V. Puntès, "Kinetically Controlled Seeded Growth Synthesis of Citrate-Stabilized Gold Nanoparticles of up to 200 nm: Size Focusing versus Ostwald Ripening," *Langmuir*, pp. 11098–11105, 2011.
- [8] C. Ziegler and A. Eychmüller, "Seeded Growth Synthesis of Uniform Gold Nanoparticles with Diameters of 15-300 nm," *J. Phys. Chem. C*, vol. 115, pp. 4502–4506, 2011.
- [9] E. Mahon, D. R. Hristov, and K. A Dawson, "Stabilising fluorescent silica nanoparticles against dissolution effects for biological studies.," *Chem. Commun.*, vol. 48, pp. 7970–7972, 2012.
- [10] P. M. Dove, N. Han, A. F. Wallace, and J. J. De Yoreo, "Kinetics of amorphous silica dissolution and the paradox of the silica polymorphs.," *Proc. Natl. Acad. Sci. U. S. A.*, vol. 105, pp. 9903–9908, 2008.
- [11] Y. J. Wong, L. Zhu, W. S. Teo, Y. W. Tan, Y. Yang, C. Wang, and H. Chen, "Revisiting the Stöber Method: Inhomogeneity in Silica Shells," *J. Am. Chem. Soc.*, vol. 133, pp. 11422–11425, 2011.
- [12] D. G. Duff, A. Baiker, and P. P. Edwards, "A New Hydrosol of Gold Clusters . 1 . Formation and Particle Size Variation," *Langmuir*, vol. 272, pp. 2301–2309, 1993.
- [13] D. G. Duff, A. Baiker, I. Gameson, and P. P. Edwards, "A new hydrosol of gold clusters. 2. A comparison of some different measurement techniques," *Langmuir*, vol. 9, pp. 2310–2317, 1993.
- [14] J. L. Hueso, V. Sebastián, Á. Mayoral, L. Usón, M. Arruebo, and J. Santamaría, "Beyond gold: rediscovering tetrakis-(hydroxymethyl)-phosphonium chloride (THPC) as an effective agent for the synthesis of ultra-small noble metal nanoparticles and Pt-containing nanoalloys," *RSC Adv.*, vol. 3, pp. 10427–10433, 2013.
- [15] S. Oldenburg, R. Averitt, S. Westcott, and N. Halas, "Nanoengineering of optical resonances," *Chem. Phys. Lett.*, vol. 288, pp. 243–247, 1998.

- [16] T. Pham, J. B. Jackson, N. J. Halas, and T. R. Lee, "Preparation and Characterization of Gold Nanoshells Coated with Self-Assembled Monolayers," *Langmuir*, vol. 18, pp. 4915–4920, 2002.
- [17] B. J. Jankiewicz, D. Jamiola, J. Choma, and M. Jaroniec, "Silica-metal core-shell nanostructures.," *Adv. Colloid Interface Sci.*, vol. 170, pp. 28–47, 2012.
- [18] J. L. Cardoso and S. G. Dos Santos Filho, "Electrodeposition of gold from formaldehyde-sulfite baths: bath stability and deposits characterization," *Quim. Nov.*, vol. 34, pp. 641–645, 2011.
- [19] S. E. Park, M. Park, P. K. Han, and S. W. Lee, "Relative Contributions of Experimental Parameters to NIR-Absorption Spectra of Gold Nanoshells," *J. Ind. Eng. Chem.*, vol. 13, pp. 65–70, 2007.
- [20] M. R. Rasch, K. V. Sokolov, and B. A. Korgel, "Limitations on the optical tunability of small diameter gold nanoshells.," *Langmuir*, vol. 25, pp. 11777–11785, 2009.
- [21] S. E. Park, M. Y. Park, P. K. Han and S. W. Lee. "The effect of pH adjusted Gold Colloids on the formation of Gold Clusters over APTMS-Coated Silica Cores," *Bull. Korean Chem. Soc.*, vol. 27, pp. 1341–1345, 2006.
- [22] Z. Liang, Y. Liu, S. S. Ng, X. Li, L. Lai, S. Luo, and S. Liu, "The effect of pH value on the formation of gold nanoshells," *J. Nanoparticle Res.*, vol. 13, pp. 3301–3311, 2011.
- [23] S. L. Westcott, S. J. Oldenburg, T. R. Lee, and N. J. Halas, "Formation and Adsorption of Clusters of Gold Nanoparticles onto Functionalized Silica Nanoparticle Surfaces," *Langmuir*, vol. 14, pp. 5396–5401, 1998.
- [24] H. R. Vutukuri, A. Imhof, and A. van Blaaderen, "Fabrication of polyhedral particles from spherical colloids and their self-assembly into rotator phases.," *Angew. Chem. Int. Ed. Engl.*, vol. 53, pp. 13830–13834, 2014.
- [25] Q. Ruan, L. Shao, Y. Shu, J. Wang, and H. Wu, "Growth of Monodisperse Gold Nanospheres with Diameters from 20 nm to 220 nm and Their Core/Satellite Nanostructures," *Adv. Opt. Mater.*, vol. 2, pp. 65–73, 2014.

Chapter 3: Structured plasmonic nanoclusters through the assembly of preformed dimpled particles and satellites

This chapter is dedicated to the fabrication of the multipod-like plasmonic clusters through the assembly of preformed (metal) satellites within the dimples of patchy particles as prepared in Chapter 1. First, a state-of-the-art regarding the assembly of colloidal particles is the opportunity to describe the different forces involved and the main self-assembly routes reported in the literature, and then to select *a priori* the most efficient one(s). The second part of this chapter is dedicated to the description of the assembly experiments, the issues that were overcome and the extent in which the morphology of the final assemblies may be controlled (**Scheme 15**) In particular, it is shown that the direct assembly route of metallic satellites was tricky and the best results were obtained by combining an extra-stage of nucleation/growth of the plasmonic counterparts from the knowledge learnt in Chapter 2.



Scheme 15: The representation of the other strategy developed to get plasmonic nanoclusters. First, one induced a self-assembly of silica satellites and patchy particles and then a seeded mediated growth approach to deposit gold onto the satellite.

1 Assembly of (nano)particles: state-of-the-art

The assembly of colloidal particles is nowadays considered as an efficient way to produce materials,[1] at the condition to be able to initiate, drive and control the assembly process. For this purpose, the main forces to be fought against or to be taken advantage of during the assembly of particles are briefly described.[2] Then, some representative examples found in the literature are discussed in the cases of 2-D and 3-D arrays, and also discrete clusters.

1.1 Forces involved in the assembly of particles

Firstly, we consider the forces stabilizing a dispersion of identical colloids. In a simple model of two identical particles, the attractive van der Waals (VdW) forces are counterbalanced by two main kinds of repulsive forces:

- in the case of surface-charged particles, the repulsive forces are electrostatic and described by the DLVO (Derjaguin-Landau-Verwey-Overbeek) theory;[3],[4]
- in the case of particles decorated by uncharged macromolecules, the solvation of the chains act as an efficient steric stabilization layer. This phenomenon occurs in good solvent conditions, where the macromolecules are extended.

Depending if we consider small (1-10 nm) or large colloids (up to micron-scaled ones), the interaction length scales differ. While small nanoparticles are influenced by strong attractive VdW forces and by relatively long-range interactions compare to their sizes, larger colloids experience short range interaction relative to their dimensions. Consequently, the strategy adopted to control the assembly can be different for each size range. In this study, we were interested in the size range of 100-200 nm.

1.1.1 Van der Waals forces

VdW forces are electromagnetic long-range forces arising from three origins: (i) Keesom forces corresponding to attractive or repulsive interactions coming from permanent dipole orientations, (ii) Debye forces coming from the interaction in between a permanent dipole and an induced one and (iii) London dispersion forces coming from the interaction of instantaneous dipoles.

For two spheres of a radius R , density ρ , separated by a distance r , the potential can be written as **Eq. 11**.

$$U_{tot}(r) = -\frac{A}{12} \frac{R}{r - 2R} \quad \text{Eq. 11}$$

where $A = \pi^2 C \rho^2$ is the Hamaker constant depending on the interaction pair coefficient parameter (C) which are related to the chemical nature of the surface's sphere surface and the dispersion medium. The A value set the intensity order of magnitude for the VdW interactions and is most of the time comparable to the thermal agitation at the ambient temperature. The VdW interaction in between two particles generally exhibits an effective range of several tens of nm. This force is attractive for two identical particles but can be repulsive in the case of particles of different chemical nature.[5],[6]

1.1.2 Electrostatic forces

The electrostatic forces arise from the charges existing at the particle surface. In a polar medium, the ions pairs are dissociated and the counter ions form a double layer surrounding the charged surface. The presence of such a double layer induced a strong repulsion with an entropic origin. The effective range of this interaction is given by the Debye length, κ^{-1} , directly related to the ionic species concentration. The sum is done on the whole ionic species present in the system as described by **Eq. 12**.

$$\kappa = \left(\sum \frac{p_{\infty i} e^2 Z_i^2}{\epsilon \epsilon_0 k T} \right)^{\frac{1}{2}} \quad \text{Eq. 12}$$

Where $p_{\infty i}$ is the concentration of the ions i at an infinite distance of the surface and Z_i the valence of the ionic specie i .

The electrostatic repulsion in between two charged spherical particles exhibiting a R radius and separated with a distance r is calculated by using the Poisson-Boltzmann **Eq. 13**.

$$U_{\text{electrostatic repulsion}}(r) = \left(\frac{64\pi kTRP\rho_{\infty}\xi^2}{\kappa^2} \right) e^{-\kappa(r-2R)} \quad \text{Eq. 13}$$

$$\text{With } \xi = \tanh\left(\frac{ze\Psi_0}{4kT}\right)$$

In this case, Ψ_0 is the surface potential of the particles and ρ_{∞} the sum of ion concentration far from the surfaces. In such conditions, the repulsion potential followed a decreasing exponential law with r .

The total interaction energy can be written as $V_T = V_A + V_R$ corresponding to the DLVO interaction potential which is the sum of attractive and repulsive potentials. **Figure 49** shows the potential energy as a function of the distance between the surfaces. The secondary minimum is attributed to the dominance of the VdW interactions at long distance inducing reversible colloidal destabilization. The primary minimum is not an infinite one due to the repulsion forces existing at short distances and attributed to the Born repulsion while the value of V_T corresponds to the kinetic barrier describing the colloidal stability of the particles.

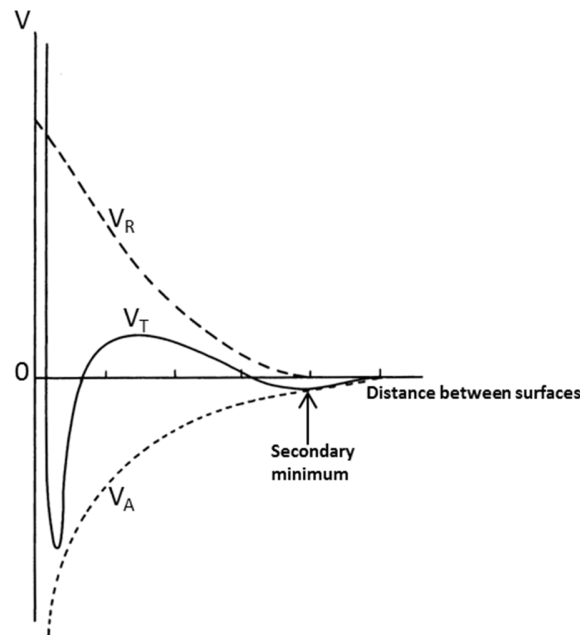
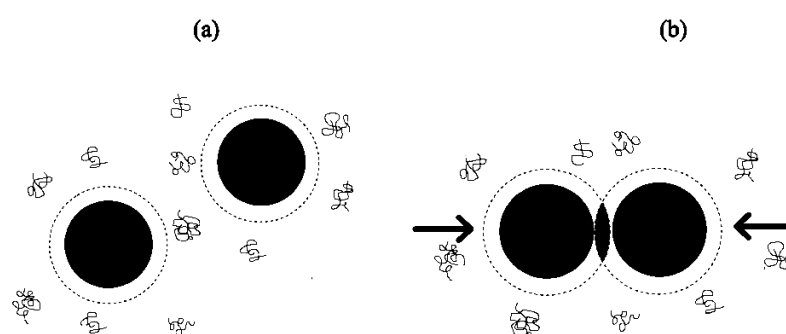


Figure 49: Energy potential diagram as a function of the distance between colloids surface. Adapted from reference [7].

1.1.3 Depletion forces

The depletion forces rely on the principle of maximum entropy of the solvent. Entropic excluded volume effects induced an overcoming of the short-range repulsive interparticular interactions. This leads to the particles attraction and assembly.[8],[9] Methods to induce depletion conditions

are based on the adjunction of a species, called depletant: small particles, molecules or the most often macromolecules. In order to induce a depletion effect useful for an assembly purpose, it's important to consider a depletant presenting a repulsive attraction for the colloids surface. In such conditions, a depletion layer can be formed on the surface of the particles where the polymer is excluded, leading to the destabilization of the dispersion (case of the flocculation induced by depletion) **Scheme 16**. The case of particles exhibiting a shape complementarity is a particular way to maximize the overlapping [10] and studied by computer simulation.[11] The results showed that indented particles can be self-assembled into chain or branched structures, depending of the colloid shape and depletion conditions. This behavior is also true in the biochemistry field where it's a major concern in the case of the protein-protein interactions.[12]



Scheme 16: Scheme of two colloidal spheres in a solution of non-adsorbing macromolecules; The depletion layers are indicated by short dashes. (a) Without overlap, the osmotic pressure on the spheres due to the polymer solution is isotropic. b) For overlapping depletion layers, osmotic pressure on the spheres is unbalanced; pressure is indicated by the arrows. Reproduced from reference [13].

1.1.4 Hydrophobic effect

The commonly named hydrophobic effect (hydrophobic attraction) is the strongest non-covalent, non-electrostatic binding force occurring between particles dispersed in water. According to several authors, this designation could be a misnomer for a mechanism which is, so far, driven by the free energy of cohesion of water molecules.[14] The origin of hydrophobic interactions is therefore supposed to be an effect mostly entropic originating from the disruption of the hydrogen bonding.[15]

1.1.5 Chemical coupling between particle surface through reactive species

The coupling in between particles can't be considered as a force applied directly on particles, but it is a way to link particles through their surfaces. It consists into the reaction of two complementary chemical species which are allowed to react together when the proper conditions are induced in the medium. It consists into short-range attractive forces at the molecular level, corresponding to enthalpic mechanisms.

1.2 Assembly in 2-D or 3-D arrays

Over the last few decades, particles have served as hard sphere models for atoms and within this context they may be called colloidal atoms (CAs). This analogy has turned out to be most rewarding and the origin of several major developments. For instance, self-assembly of size-monodisperse isotropic CAs in aqueous dispersions helped to clarify crystallization and phase transition mechanisms.[16]–[18] Thanks to their mesoscopic size, CAs can indeed be studied in detail at the single-particle level and their dynamics are slowed down sharply in comparison with atomic systems, such that the formation of a crystal nucleus can be followed in detail. Crystallization of CAs in colloidal crystals (CCs) is an entropy-driven process in which configurational entropy and free volume entropy at low and high concentrations, respectively dominate. Concentrating the dispersions allows the disorder-to-order transition; face-centered cubic (*fcc*) and hexagonal-close packed (*hcp*) structures are thermodynamically favored, as they gain more free volume entropy than other packing symmetries. Nevertheless, it requires a long time because of the slow relaxation of large CAs and the high viscosity of concentrated suspensions. So metal crystals and crystallization are quite easily mimicked from CAs self-assembly, especially for evidencing formation of defects such as vacancies, macroscopic cracks, polycrystalline domains, and stacking faults. For instance, depletion forces were used to form extended cubic array of cubic CAs.[19]

Electrostatic forces were used for mimicking ionic crystals, *i.e.* crystals made of cations and anions, achieved through the self-assembly of binary mixtures of CAs.[20] For instance, mixing oppositely surface-charged and differently-sized CAs and tuning the coulombic attraction through the nature and length of the capping agents enable the fabrication of binary CCs with AB, AB₂, AB₃, AB₄, AB₅, AB₆ and AB₁₃ symmetries, providing a mesoscale embodiment of NaCl, AlB₂, MgZn₂, CaB₆, NaZn₁₃, *etc.* crystals.[21] Two dimensional arrays were also obtained thanks to similar electrostatic interactions in between Janus-like particles and charged substrate in order to confine the assembly in two dimensions.[22]

Recent improvements concerning the surface modification of CAs allowed high density grafting of DNA strands. Such a high density lead to an increasing control over the crystallization of CAs by playing on DNA strand melting temperature.[23],[24]

Mimicking covalent crystals, *i.e.* crystals made of pure covalent bonds such as diamond, Si, Ge, SiC crystals, necessitates highly directional interactions between CAs and therefore the implementation of their patchiness, as plentifully numerically demonstrated.[25]–[27] As far as we know, any similar array obtained experimentally has been yet reported.

1.3 Assembly into discrete clusters

Over the last decade, both experimental and simulation works have tremendously explored the assembly laws of extended arrays of particles. On the contrary, the formation of discrete clusters

has been quite well explored experimentally [28] while numerical studies have remained a minority and concerned most of the time Janus-like or patchy particles.[29],[30] The assembly strategies are classified according to the driving force used to promote the clusters formation.

1.3.1 Assembly route exploiting electrostatic interactions

Electrostatic interactions in between negatively-charged (citrate-stabilized) gold nanoparticles (10-50 nm) and positively-charged silica core (100 nm) were used to produce raspberry like-structures.[31] The silica cores were previously surface-modified by using amino silane as well as polyelectrolyte multilayers. By playing on the overall surface charges of the colloids, the density of coverage could be tuned in a certain range. The raspberry like nano-objects obtained by varying the size of the gold satellites showed the weakness of the interactions. The largest the satellites are, the weaker the attraction is. Consequently, the largest satellites have a strong tendency to collapse from the core surface once dried on a substrate (**Figure 50**); this issue was overcome by the deposition of a thin silica coating on the raspberry-like assemblies.

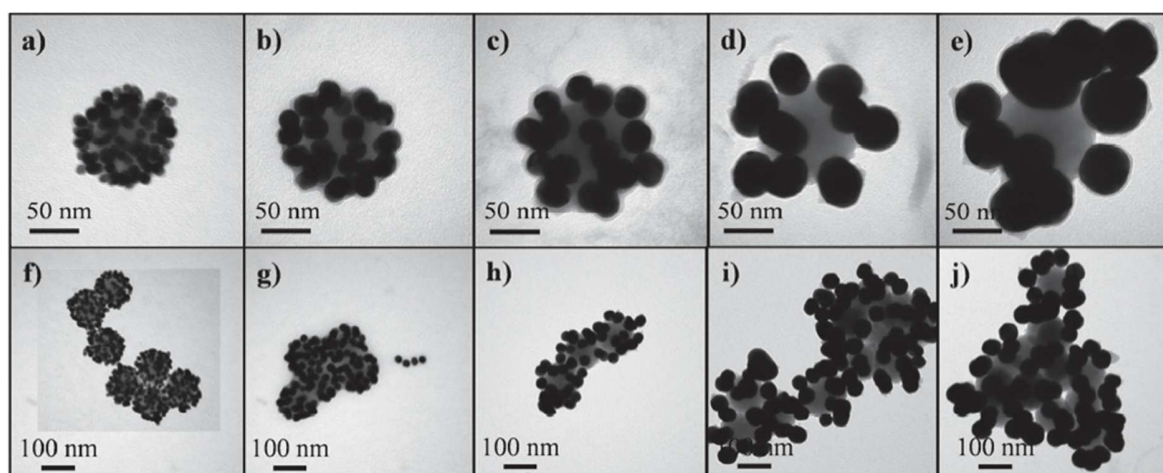


Figure 50: TEM-images of the nanoclusters obtained by assembling gold nanoparticles of different diameters of (a, f) 10, (b, g) 20, (c, h) 30, (d, i) 40 and (e, j) 50 nm on the polyelectrolyte-modified silica beads after encapsulation with a thin silica shell.[31]

1.3.2 Assembly route exploiting hydrophobic effect

The clusterization of identical particles generated by hydrophobic effects was exploited to produce plasmonic nanoclusters.[32] Thiol-ended PS macromolecules were grafted onto the surface of citrate-stabilized 15-nm gold nanoparticles and those particles were incubated with amphiphilic PS-*block*-poly(acrylic acid) copolymer in DMF at 60°C. The quality of the DMF solvent for PS was then decreased by adding an increasing amount of water promoting the aggregation of the gold nanoparticles within the PS domains of the copolymer and then the solidification of the assembly (**Figure 51**).

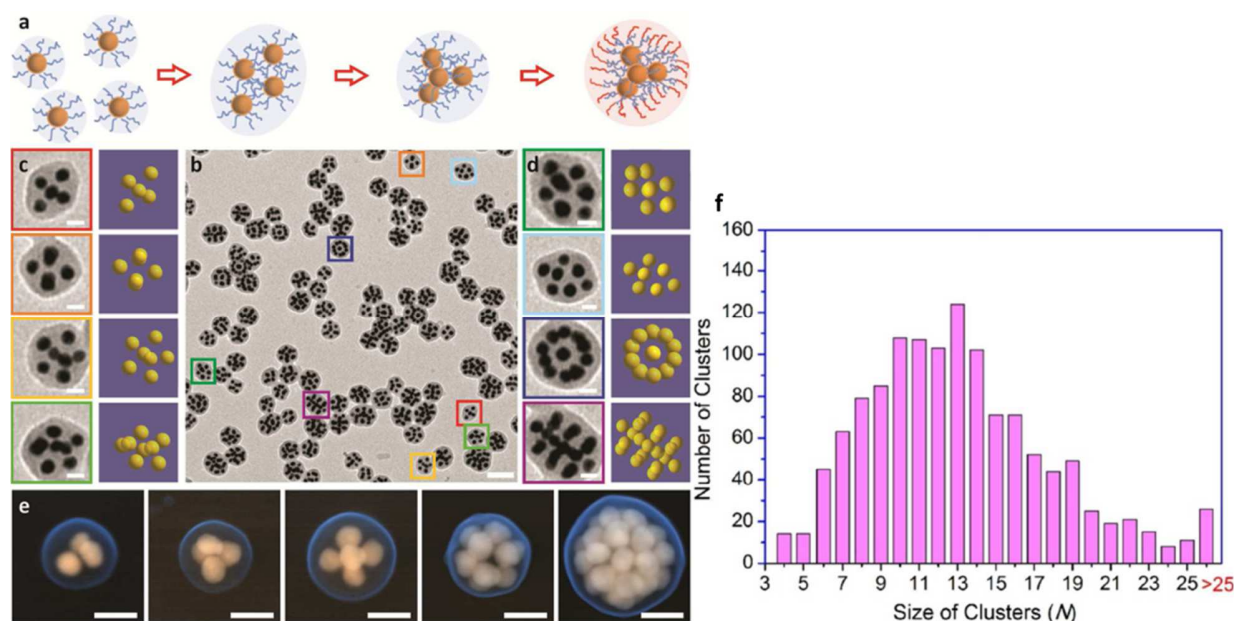


Figure 51: a) Scheme of the clusterization of Au nanoparticles thanks to a progressive addition of water into DMF and use of PS-*block*-poly(acrylic acid) macromolecules as stabilizing agents; b-d) TEM images for various plasmonic nanoclusters and focused views in the inserts and e) SEM images for various plasmonic nanocluster morphologies f) distribution of the nanoclusters size considering the number of plasmonic particles (N).[32]

The same strategy was reported by Liz-Marzan and coworkers.[33]–[35] Using PS-*block*-poly(acrylic acid) and gold nanoparticles surface-modified with HS-ended PS macromolecules, and playing on the solubility condition of the different blocks, they succeeded in obtaining gold nanoclusters mostly made from 3 to 25 nanoparticles.

Another paper from the same team proposed to use a strategy based on the formation of plasmonic nanoclusters prepared by using a non-ionic surfactant called pluronic F 68 to stabilize and cluster gold nanoparticles.[36] Typically, gold nanoparticles initially capped with CTAB and were transferred into a solution of Pluronic F 68. Subsequently the colloidal dispersion was emulsified with toluene using ultrasonic homogenizer. The emulsion droplets bearing nanoparticles were evaporated using a rotary evaporator yielding clusters. Finally the separation of the different populations of clusters was achieved by gradient density centrifugation. In this case hydrophobic interactions drove the assembly.

1.3.3 Assembly route exploiting depletion forces

Depletion forces were used in the concept of lock-and-keys colloids developed by Pine and coworkers.[37]–[39] Using micron-sized monodimpled particles, spherical particles and poly(ethylene oxide) ($\overline{M}_w = 600\,000$ g/mol; 0.5 g/L) as depletant, dimeric, trimeric and tetrameric assemblies were obtained with the unique feature of having flexible bonds. More recently, the same concept was extended to multidimpled lock colloids obtained by the clusterization route already described in **Figure 12**. [40]–[44] The lock particles were added with an excess of 5 fold keys to promote a complete fulfillment of the lock. Another important concern was the size of the

keys (**Figure 12, Figure 52**). Indeed, the best results in term of assembly were obtained when the radius of the keys was matching the curvature radius of the lock, confirming the importance of the shape complementarity.

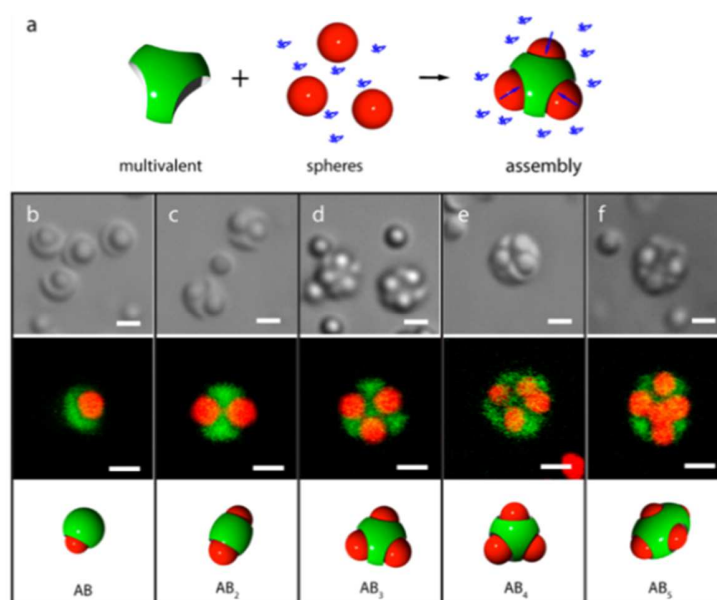


Figure 52: Lock-and-key assemblies from lock particles made of a varying numbers of dimples. a) Schematic illustration showing a trivalent particle with three assembled spheres using depletion interaction. The depletant (blue coil) causes osmotic pressure (arrows) between adjacent colloids, which is maximized when a sphere assembles into a cavity. (b–f) Bright field images (top panel), confocal images (middle panel), and cartoons (bottom panel) showing multivalent lock particles with b) one, c) two, d) three, e) four, and f) five cavities binding to red fluorescent spheres stoichiometrically. Scale bars: 1 μm .^[40]

1.3.4 Assembly routes exploiting supramolecular or covalent coupling

The assembly of particles thanks to supramolecular or covalent coupling has been reported in the literature. For instance, it was described the fabrication of raspberry-like structures made of a 90-nm PS core and 36-nm silver satellites, previously surface-decorated with streptavidin and biotin-terminated ligands, respectively.^[45] For avoiding the formation of aggregates and promoting a maximum grafting density, the silver nanoparticles were surface-modified with a mixture of 60/1 HOOC-PEG-SH/biotin-PEG-SH. The particles were mixed in a silver-to-PS nanoparticle ratio of 100. An average inter-satellites spacing of 3.8 nm was spontaneously obtained (**Figure 53a**). The authors didn't precise the average number of satellites attached per core particle, however they considered clusters made of 32 satellites per core for the simulation experiments.

Another approach, which had been envisioned for controlling the satellite number and positions was to take the inherent icosahedral symmetry exhibited by some virus capsids as an advantage. Chemical-modification was performed by attaching cysteine groups on the twelve specific sites situated at the vertices of the icosahedral capsid structure. The use of an excess of gold-particles was critical. A gold-to-capsid nanoparticles ratio of (240/1), i.e. 20 gold particles per icosahedral

site was used. Thanks to those thiolate amino-acids, the authors succeeded in directing the assembly of gold nanoparticles at the specific locations of the virus surface.[46],[47]

The DNA patches produced thanks to the clusterization of amidinated PS microspheres, as already described in Chapter 1 (**Figure 11**), were used for assembly purpose with particles exhibiting complementary DNA strands.[44] The formation of a range of discrete structures, controlled by the valence of the patchy particles, was observed by optical microscopy (**Figure 53c**). When the assembly was carried out with stoichiometric amounts of particles, only 50 % of the sites were occupied after few days of reaction. The use of a five folds excess lead to 80 % of sites occupied after the same reaction time. Moreover, it was suggested that the use of stronger DNA bonding (obtained by increasing the length of the DNA strand) should increase the reaction rate. The stability of the clusters was quite good at ambient temperature. However, some disassembly phenomena were observed while the suspensions were warmed over the melting temperature of DNA.

A covalent coupling method was employed to attached silica particles on the tips of silica tetrapods prepared by colloidal templating.[48] Controlled clusters of colloidal particles were obtained through a reductive amination reaction between amino-modified satellites and aldehyde-modified tips (**Figure 53b**). The article gave any insight about the amount of particles necessary for completing the assembly.

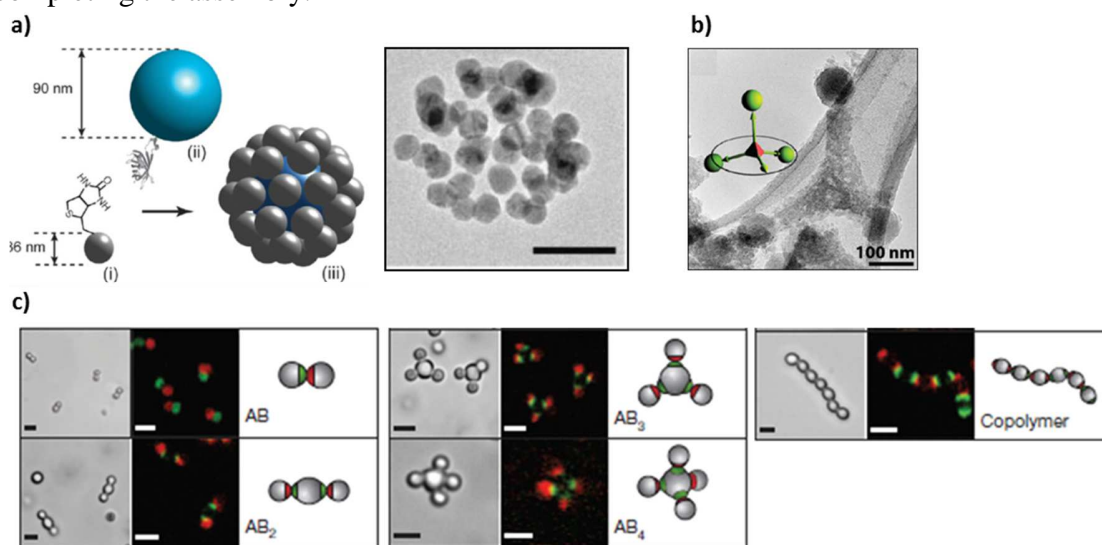


Figure 53: a) (i) Biotin-functionalized silver nanoparticles; (ii) streptavidin functionalized PS nanoparticles; (iii) raspberry like cluster; TEM image of the raspberry-like structure prepared according to the streptavidin-biotin method. Scale bar: 100 nm.[45] b) Site-specific assembly of colloidal silica spheres on tethered silica tetrapods.[48] c) Specific directional bonding between patchy particles observed by optical microscopy: bright-field (left panels), confocal fluorescent (middle panels), and corresponding schematic structures (right panels). Scale bars: 2 μm .[49]

1.4 Conclusion and assembly strategy taken on for this study

Our objective being to promote the fulfillment of the dimples of silica cores by satellite gold particles, with diameter that are of the same order, for finally getting robust silica/gold multipod-like clusters, most of the already-reported assembly routes were initially discarded:

- ionic interactions between oppositely surface-charged particles, because it had been shown that they aren't strong enough for mechanically anchoring large and dense metallic satellites;

- depletion interactions, because their efficiency had been only demonstrated with micron-sized particles exhibiting shapes which were exactly complementary. But the bottom of our dimples was indeed convex, due to the reminiscence of the original silica seed and the presence of the PS bump, therefore unsuitable for welcoming ideally spherical satellites. Moreover, the assemblies obtained by depletion interactions are supposed to be reversible as a function of the depletant concentration variation. Moreover, it's actually known that the roughness or more generally the topographic irregularities of the surface is detrimental to depleted assembly purpose;[50]–[52]

- hydrophobic effects, even if the presence of the PS bumps could have been an excellent opportunity for interacting with gold satellites previously surface-modified with end-grafted PS macromolecules. If there exists numerous routes for such a grafting, the main reluctances were that (i) the previously-reported assemblies were made of gold colloids which didn't exceed a diameter of 60 nm and (ii) the control of the number of gold colloids constituting the clusters wasn't so easy. In order to simultaneously promote the interactions with the PS within the dimples and avoid a self-aggregation of the gold colloids, an alternative would have been to make preliminarily the gold colloids Janus-like, *i.e.* with one patch made of PS grafts. This promising route appeared to be too time-consuming in the context of the present study, leading us to disregard this method;

- DNA strands interactions, because despite their high specificity, the DNA chemistry is quite expensive and the stiffness of the DNA linkage is lacking;

- biotin-streptavidin coupling, because of the cost of reagents and the high sensitivity of streptavidin (and more generally of any protein) to the dispersion medium making them destroyed or under unreactive conformation in the improper conditions.

As a consequence, the chemical coupling strategy appeared to be a simple and straightforward method to assemble particles through the creation of covalent bonds between complementary groups grafted onto their respective surface. Indeed, we have already described in Chapter 1 that the PS residue at the bottom of the dimples might be readily made reactive, *e.g.* with amino groups. Therefore the use of satellite spheres surface-modified with antagonist chemical functions appeared to be a promising route and was considered as a first-line route. Here, we

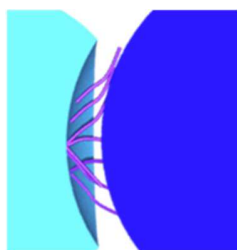
chose to use a peptidic-coupling method instead of the reductive amination process proposed by Li.[48] The reason is simple: even if the process could be envisioned thanks to several adaptations, the main coupling reaction had been carried out in toluene which is a medium in which the patchy particles are not colloidally stable.

A common drawback of all the assembly routes previously cited is the need for a large excess as well as high concentration of satellite particles in order to promote a rapid reaction of a majority of reaction sites. Those conditions arise from two main concerns. The first one is to increase the probability of inter-particle collisions. The second one is to keep the clusters discrete, by avoiding the formation of bridged clusters or arrays of particles.[53] Those major considerations led us to disregard the direct assembly of gold satellites, because of the cost of their fabrication at large scale. Instead, we preferred an approach based on the assembly of silica satellites which could be later coated with a gold shell in a way similar to that investigated in Chapter 2.

Therefore the synthesis strategy of the silica/gold multipod-like clusters investigated in this Chapter is summarized in. We first investigated the assembly of spherical silica satellites within the dimples of the patchy particles prepared in Chapter 1 (**Scheme 15**). Then, we performed the discriminatory tagging of the satellites by gold colloids followed by their regrowth in order to get a thick coating of gold larger than the skin depth of gold (20-25 nm of thickness). Contrarily to the strategy developed in Chapter 2, where the coupling was performed in water, we took advantage of the possibility for the PS macromolecules of the bumps to be extended and therefore more reactive in an organic solvent.

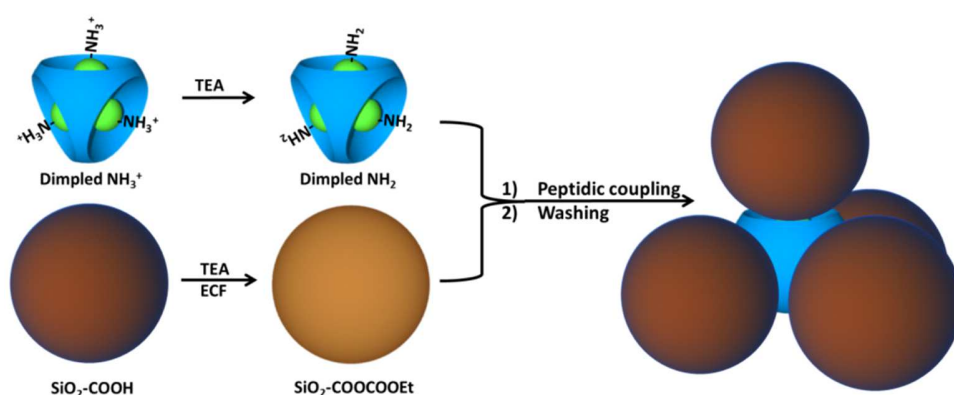
2 Synthesis of silica/silica multipod-like clusters by assembly

The purpose of this part is to describe a pathway for the assembly of colloids and dimpled silica particles in a good solvent for PS chains. Also, for convenience, we focused on the use of the aminated PS chains as-described in Chapter 1 (**Scheme 17**). We used DMF as dispersion liquid because of its aprotic and polar properties as well as good solvent for PS. We proposed to use a peptidic coupling to attach the silica satellites into the aminated dimples. This kind of reaction is well known in the literature and has been extensively studied in the biochemistry field dealing with the amino-acid modifications[54],[55] The first stage was to prepare silica particles covered with reactive carboxylic acid functions.



Scheme 17: Cross section of the possible contact in between the silica satellite and the dimpled silica particles in a good solvent for polystyrene.

The carboxylic groups are not highly reactive toward amino groups in aqueous media. Indeed, carboxylic groups are known to react in very particular conditions such as high temperature treatment in anhydrous or enzymatic conditions depending if we consider synthetic or biological points of view. But, a simple and well-known approach consists into the activation of the carboxylic groups into more reactive groups. Basically, the reactivity scale is the following: acyl halides > anhydrides > esters or carboxylic acids > amides. We chose to use chloroformate [56] derivatives to get mixed anhydrides by reaction with carboxylate groups. Here, we selected the ethyl chloroformate (ECF) to activate the COOH group, which is well-known and cheap; ECF was expected to release ethanol during the reaction which is a convenient side-product. Triethylamine (TEA) was used as a base to deprotonate both amino and carboxylic groups (Scheme 18).

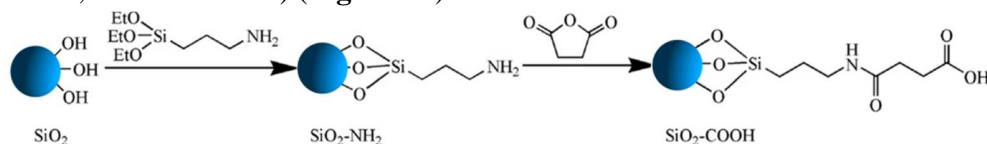


Scheme 18: The peptidic coupling investigated in this study: The aminated PS within the dimples of the patchy particles are deprotonated by TEA meanwhile carboxylic-modified silica particles are deprotonated by TEA and activated by ECF.

The formation of mixed anhydride species, much more reactive toward the amine than the initial carboxylic group, should promote the formation of amide bonds. Here, this approach results from the search for a balance in term of reactivity. Indeed, while a carboxylic acid is probably not reactive enough for an assembly purpose, the acyl halide formed is so reactive that it became sensitive toward the water traces present in the solvent or in ambient atmosphere and became hard to handle. Taking such considerations into account, the use of a reaction forming the mixed anhydride at the silica surface few minutes prior to the assembly should be a relevant compromise.[57],[58]

2.1 Synthesis of silica particles bearing carboxylic acid groups

The synthetic pathway for chemically functionalized silica particles with carboxyl group is summarized on **Scheme 19**. It was applied to batches of silica particles as prepared in Chapter 1 (diameter of 55, 85 and 137 nm) (**Figure 17**).



Scheme 19: The surface functionalization of the silica nanoparticles with carboxylic acid groups.

2.1.1 First stage: synthesis of amino-modified silica particles

Several recipes, more or less successful regarding the isoelectric point (IEP) value, the colloidal stability and the grafting density, could be used to perform the silica modification by aminopropyltriethoxysilane (APTES).[59],[60] We chose to use a recipe which had been proved to be the most efficient in our group.[61] The silica particles were modified just after their growth and a thermal treatment stage in a high boiling point dispersion liquid serving as wetting agent was carried out for completing the condensation reaction.

Protocol 30: Amino modification of the silica particles surface.

Silica particles produced thanks to Protocol 2 from Chapter 1 are typically used in their growth media (ethanol/ammonia). An amount of APTES (98 % Sigma Aldrich) corresponding to 20 functions per nm² of available silica surface is added the reactor. The dispersion is stirred for 12 h. A volume of glycerol (99 % Sigma Aldrich) corresponding to 10 % of the total volume of the dispersion is added. Ethanol and water are evaporated using rotary evaporator device set at 90°C. The dispersion, from now in glycerol, is heated by an oil bath set at 105°C for a subsequent 2 h thermal treatment conducted under the vacuum produced by a rotary vane pump. Finally the dispersion is washed by 4 cycles of centrifugation/redispersion in ethanol (12 000 g; 20 min).

In brief, **Figure 54** presents the typical evolution of the zeta potential of the as-obtained aminated silica particles as a function of pH, before and after thermal treatment. The value of IEP was strongly affected by the thermal treatment increasing from pH 7 to a value not measured because of the device limitation, but certainly higher than pH 10. Knowing that the pKa of a primary amine such as that of APTES is between 10.5 and 11, the IEP value obtained after the thermal treatment was the proof that the majority of the charge carriers were amino groups. It means not only that they were available for further reactions, but also that the original negatively-charged silanolates had properly reacted. This evidenced that the APTES surface density was high. Indeed, it was previously demonstrated that APTES molecules first interact through their amino groups with the surface silanols and that the dehydration phenomenon induced by the thermal treatment is an efficient way for the APTES molecules to turn over and condense through their alkoxy silane moiety.[62],[63]

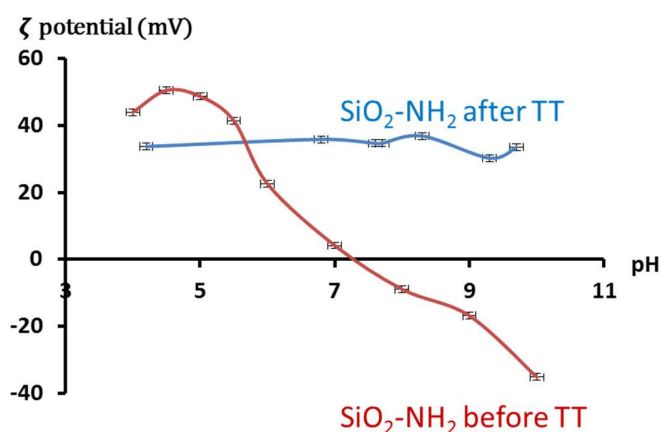


Figure 54: Zeta potential measurement as a function of the pH for amino-modified 55-nm silica particles prepared with (blue) and without (red) thermal treatment (TT).

2.1.2 2nd stage: derivatization of the amino groups into carboxylic acid ones

It involved the use of succinic anhydride to convert the surface amino groups - deprotonated by TEA (acting here as a base) - into carboxylic acid ones through the creation of amide bonds. The carboxylic modified particles are schematized by the brown color for the rest of this dissertation.

Protocol 31: Functionalization of silica particles with carboxylic groups.

The aminated silica particles as obtained from Protocol 30 are transferred into DMF by two centrifugation cycle at 12 000 g during 20 min. Subsequently an amount of triethylamine (TEA) corresponding to 50 functions per nm² of available silica surface is introduced into the dispersion which is centrifuged one more time at 12 000 g during 20 min and dispersed in DMF. The dispersion is transferred into a round bottom flask set in an oil bath at 60°C and dehydrated during 2 h under vacuum generated by a rotary vane pump. Subsequently an amount of succinic anhydride corresponding to 50 functions per nm² of available silica surface is introduced and let to react overnight at 60°C. The dispersion is washed 2 times by centrifugation in ethanol and 2 times in DMF, an amount of TEA corresponding to 50 functions per nm² is introduced and the dispersion is washed one more time at 12 000 g for 20 min and finally dispersed in DMF and dehydrated under vacuum using rotary vane pump (RV5 from Edwards).

Figure 55 presents typical infrared spectra of the silica particles with a reaction performed at ambient temperature without dehydration or with dehydration at 60°C. As expected, the presence of amino groups was evidenced by the N-H bending at 1635 cm⁻¹ on the first spectrum while the amide C=O stretching at 1650 cm⁻¹ and the carboxylic C=O stretching at 1730 cm⁻¹ are clearly visible on the second spectrum.

Moreover, zeta potential measurement was performed on the carboxylic-modified silica particles with or without the thermal treatment. Basically, a typical carboxylic group exhibits a pK_a value around 3-3.5; in such conditions, a silica surface covered by carboxylic groups should exhibit an

IEP around pH 3-3.5. As shown on **Figure 56**, the IEP measured for the carboxylic-modified silica particles obtained with and without thermal treatment are around pH 3.5 and pH 6, respectively. Those measurements have pointed the efficiency of the thermal treatment performed during the conversion. It is assumed that the thermal treatment is useful to remove the side-produced ethanol. This is considered as being doubly useful, first to avoid undesired reaction in between succinic anhydride and ethanol and second to drive the reaction to completion.

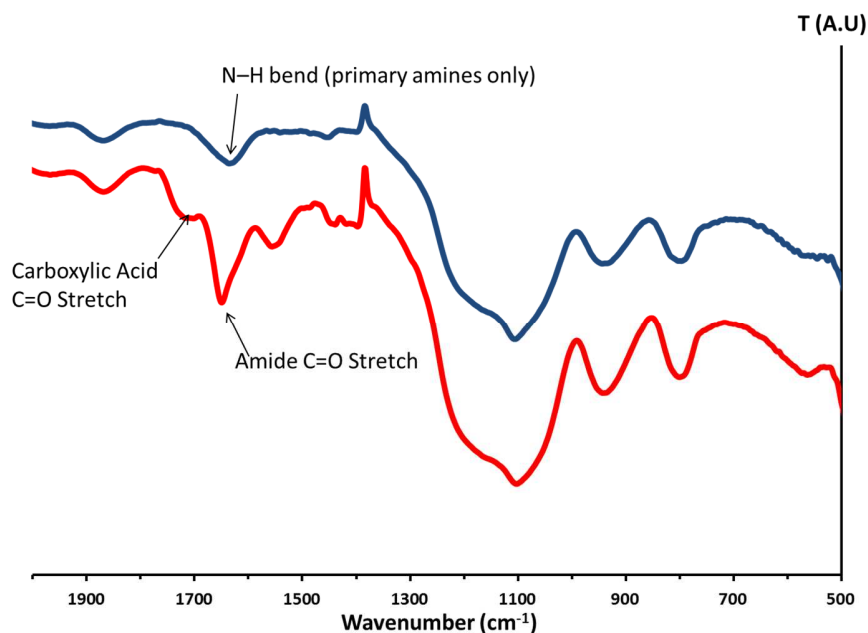


Figure 55: IR-spectra of the amino-modified and carboxylic-modified 55-nm silica nanoparticles.

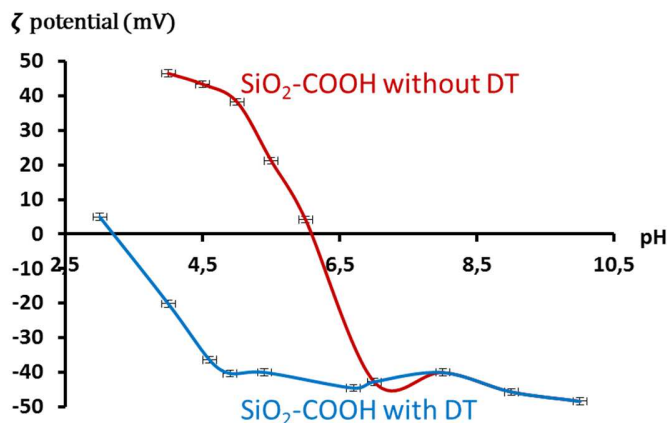
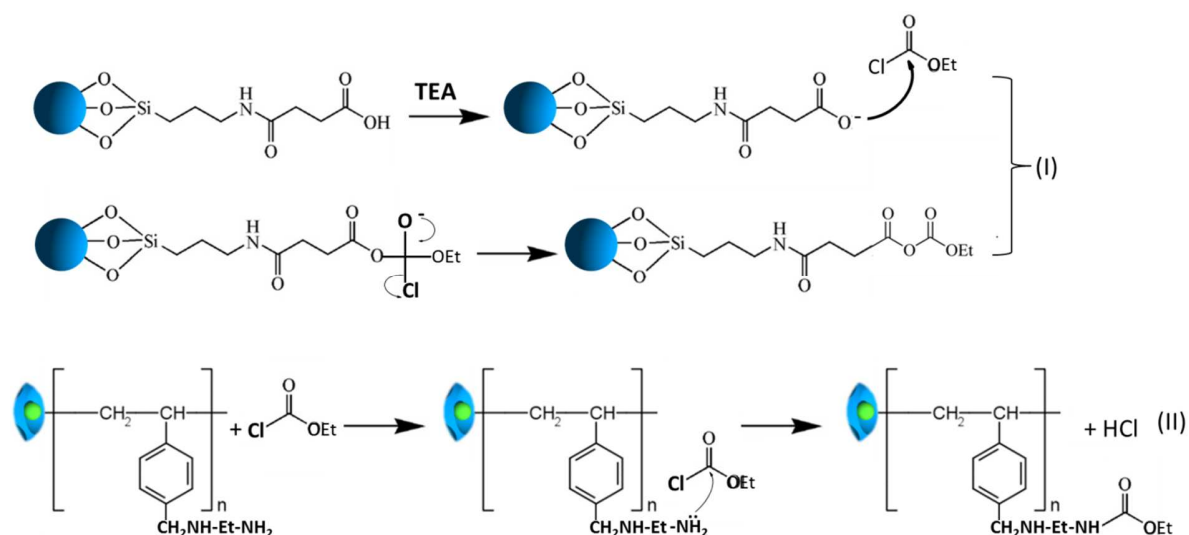


Figure 56: Zeta potential measurement of 55 nm silica nanoparticles in water surface modified with carboxylic group with or without dehydration treatment.

In the literature, various approaches exist for modification from aminated particles to carboxylic modified ones [64],[65]. The multi-functionality of the particle i.e, simultaneous presence of amino and carboxylic groups, is a well-known phenomenon.[66] Here we showed that a thermal treatment can dramatically change the IEP value of the COOH-modified particles. This result was attributed to an increase in the density of carboxylic groups.

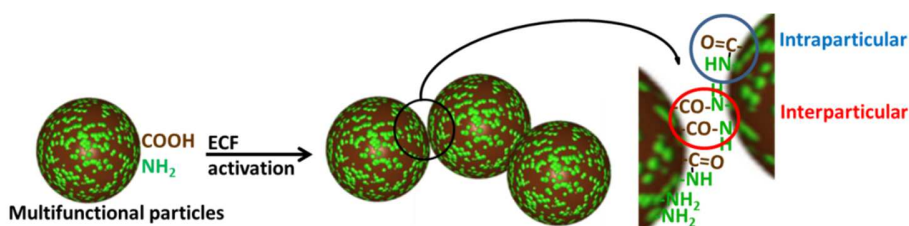
2.2 Assembly of carboxylic-modified silica particles with aminated patchy particles

The assembly process depends upon several important details. First of all, the silica particles as well as the dimples needed to be deprotonated to be reactive during the coupling (**Scheme 20 (I)**). This is typically the case when an excess of TEA is used. Moreover, due to the peptide coupling reaction in itself, the amount of ECF manipulated needed to be carefully controlled. An excess could be very detrimental for the targeted assembly reaction. Indeed, ECF is reactive towards the amine group leading to the formation of urethane-like molecule. The use of a stoichiometric amount of ECF molecules regarding the amount of carboxylic groups avoided the side reaction of residual ECF susceptible to inhibit the amine reactivity upon mixing (**Scheme 20 (II)**).



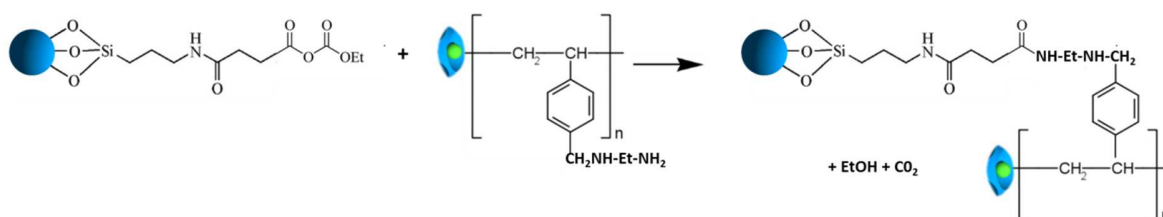
Scheme 20: The activation reaction of the carboxylic-modified silica particles (I); the undesired reaction that could occur in between amine and chloroformate forming an urethane-like molecule (II).

As previously mentioned, the use of carboxylic silica particles without residual amino groups is of major importance considering the coupling reaction in itself. Indeed, during the activation process carboxylic and amine are susceptible to react with ECF. However, carboxylic groups could also react once activated with the amine groups remaining on neighboring particles leading to the formation of an aggregated state following the activation step. In parallel, a deactivation of the surface by intra-surface reactions is also possible yielding also in the destabilization of particles by the loss of surface charge (**Scheme 21**). In those conditions, a controlled and defined assembly would be no more possible.



Scheme 21: How multifunctional particles, i.e. when amino groups would have been uncompletely converted into carboxylic groups, could self-assemble at the time of the activation by ECF.

If the requirements previously listed are fulfilled, the assembly reaction as schematized on the **Scheme 22** should be promoted.



Scheme 22: The peptide bonding reaction used for the assembly of activated carboxylic particles into aminated dimples.

Protocol 32: Assembly of the carboxylic-modified silica particles with aminated dimples.

A dispersion of aminated dimpled silica particles prepared according to **Protocol 11** is transferred in DMF by 2 centrifugation cycles at 12 000 g during 20 min. An amount of TEA corresponding to fifty functions per nm^2 of surface of a sphere of similar diameter is introduced and the solution is washed one more time with DMF. Finally, the remaining water is removed from the dispersion, by heating at 50°C under stirring and vacuum generated by a rotary vane pump for 1 h. Meanwhile, 1 mL of the dispersion of carboxylic surface modified silica nanoparticles is introduced in an Eppendorf (55 nm in diameter 70 g/L). A volume of TEA ($6.2 \mu\text{L}$) corresponding to 8 functions per nm^2 is introduced and the solution is homogenized using vortex device. The activation of the carboxylate groups into anhydride carbonate is performed by adding $2.4 \mu\text{L}$ of ethyl chloroformate corresponding to 4 functions per nm^2 of available silica surface. The dispersion is mixed upon vortex device and homogenized on the roller mixer for 2 min. Finally 0.1 mL of the dehydrated dispersion of dimpled silica particles in DMF containing approximately 6×10^{11} dimpled silica particles is introduced in one shot into the Eppendorf containing the activated silica spheres. Then, the solution is homogenized and let to react over the roller mixer overnight. The dispersion is typically transferred in 40 mL of water and washed 3 times with 40 mL of water and 0.1 mL of TEA by using 3 cycles of centrifugation/redispersion at 500 g during 20 min.

The first experiments concerned the assembly of 55-nm carboxylic-modified silica particles with the aminated dimpled silica particles deriving from H-86 used in an excess of approximately 600/1 in term of satellites per core particles. As shown on **Figure 57**, it was successful leading to

robust silica/silica multipod-like clusters. No aggregation phenomenon was observed in water. Moreover, due to the important size difference between the assembled clusters and the silica particles, the washing steps allowed an efficient removal of the free silica spheres.

At this point, we understood what the key-parameters were for the assembly of satellites onto the dimpled particles: the high density of carboxylic acid groups on the satellites, the amount of TEA to deprotonate the amino and carboxylic groups, the amount of ECF that shall equal the amount of carboxylate groups and finally the mixing stage that shall be performed after the activation steps.

Moreover, it was important to find how to promote the complete assembly of particles that is why we studied the effect of the concentration of particles as well as the contact time which are intuitively related to the collision probability.

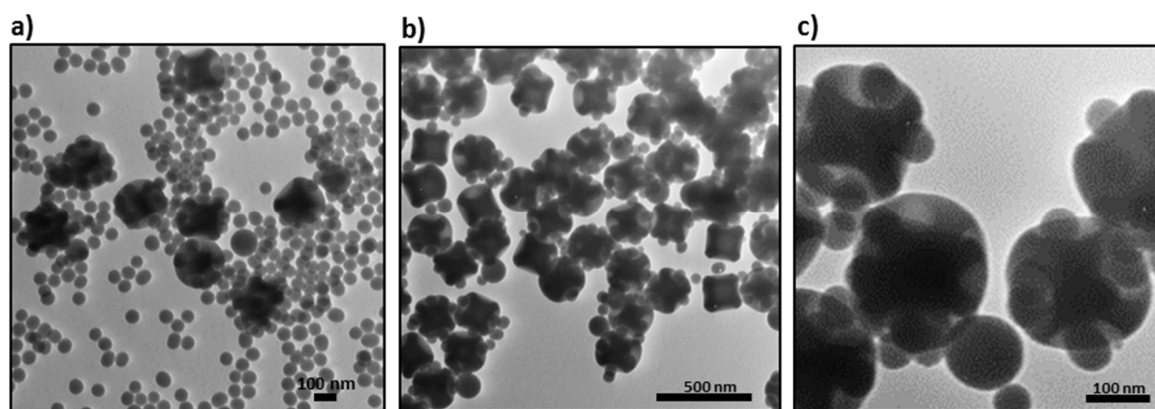


Figure 57: TEM images at different magnifications of the silica/silica multipod-like clusters obtained by assembly in between ECF-activated carboxylic-modified 55-nm silica nanoparticles and aminated dimpled particles (H-86) deriving from (H-86) a) and b) before elimination of the excess of satellites and c) after.

2.2.1 Effect of the concentration on the assembly

In order to determine the effect of the satellite-to-core ratio over the assembly efficiency, we performed assemblies varying the amount of satellites for a concentration of cores kept constant. From an experimental point of view, an amount of activated satellite dispersion was prepared and various volumes of this dispersion were introduced onto a constant volume of deprotonated amino dimpled silica particles. To maintain the volume of the total dispersion constant, we completed the volume with pure DMF. After an overnight reaction, the as-obtained particles were washed as previously described.

According to the results presented on **Figure 58**, the assembly success seemed to be directly influenced by the concentration of colloids. The observed trend was as following: the more concentrated the dispersion, the more fulfilled the dimples.

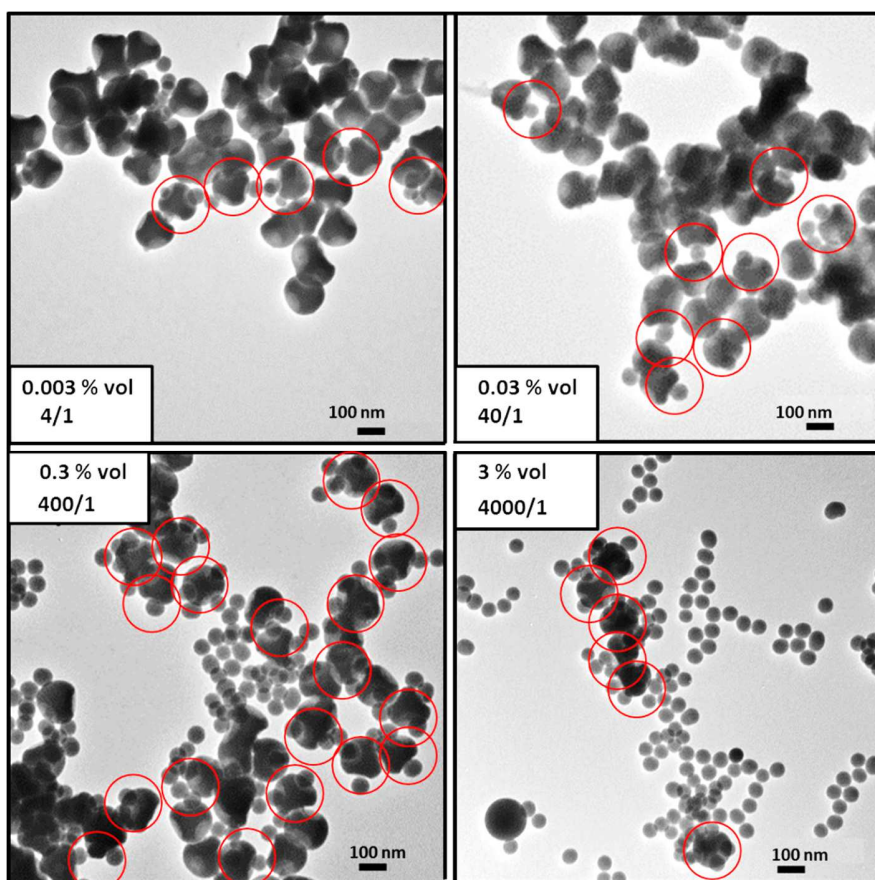


Figure 58: TEM images series of silica/silica multipod-like clusters (T-86) showing the effect of the silica satellite concentration over the assembly efficiency in the dimples; the fulfilled dimples are highlighted by the red circles.

We didn't push forward this investigation, knowing that we could produce sufficiently highly concentrated dispersion of colloids simply by concentrating them using centrifugation. Statistics weren't attempted on these experiments, because during the washing steps the assembled silica/silica clusters with a low amount of satellites could be removed with the excess of satellites yielding to statistics distortion. Moreover, statistical analysis of the raw mixture wasn't realistic due the large excess of satellites. That is why we decided to move forward and to investigate the required reaction times for the set of conditions we used. For this investigation, the experiments were conducted at volume fraction of colloids typically higher than 3 %.

2.2.2 Effect of reaction time on the assembly

Typically, the success of such an assembly could be expected like strongly dependent on the collision probability existing in between the particles. To elucidate if this assembly required almost one day, which is the time used for the previous experiments, or shorter time scale we extracted aliquots of the dispersion at different time intervals and took the precaution to stop the assembly reaction by diluting the sample in water, followed by centrifugation. The corresponding results are presented on **Figure 59**.

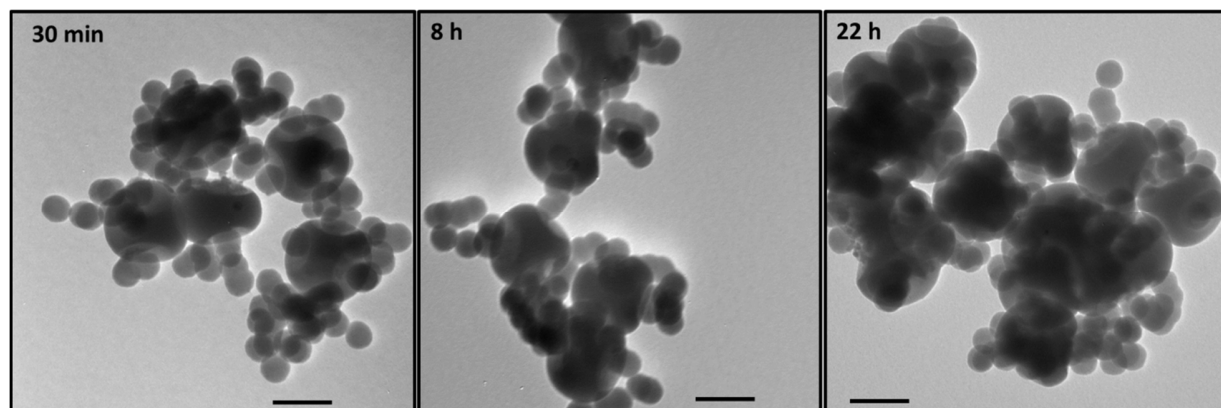
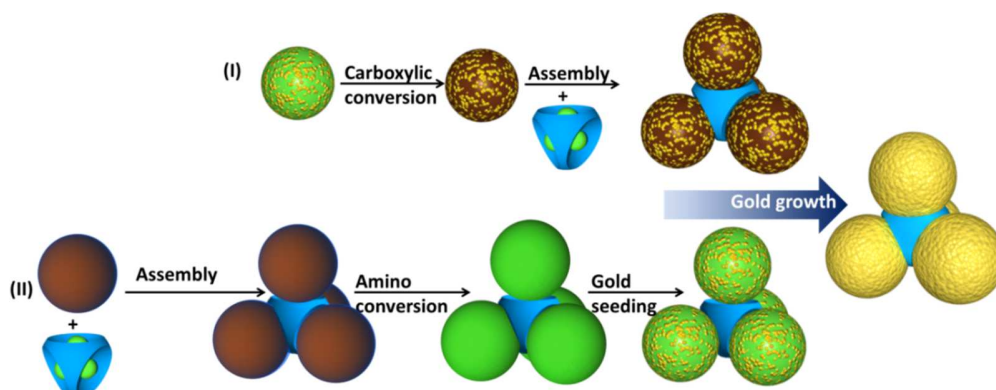


Figure 59: TEM images showing the effect of reaction times over the assembly of aminated patchy particles (T-52) with and ECF activated carboxylic-modified 55-nm silica particles. Scale bar: 100 nm.

By observing the TEM pictures, it was evidenced that the contact time required for the assembly was shorter than 30 min. Indeed, longer reaction times didn't seem to lead to more fulfilled dimples.

3 Derivatization of the silica/silica clusters into silica/silica@gold clusters

The formation of the gold layer over the silica satellites after the assembly appeared to be a relevant alternative to the attachment of pure gold satellites. However, the question was: how the silica satellites should be labelled by gold nuclei to promote an efficient gold layer formation while preserving the morphology, *i.e.* an exclusive growth on the satellites. Two main routes were possible: performing the labelling before or after the assembly, called strategy **(I)** and **(II)**, respectively (**Scheme 23**). Both strategies had a priori their own drawbacks: the possible perturbation of the assembly process due to the gold nuclei presence for the strategy **(I)**, and the tricky gold labelling supposed to be discriminatory between the satellites and the core for the strategy **(II)**. That is why we investigated both routes in a pragmatic spirit.



Scheme 23: **(I)** Strategy consisting in the decoration of amino-modified particles by Duff gold nuclei then conversion in carboxylic surface and assembly in between amino patchy particles and silica particles decorated by gold nuclei. **(II)** Assembly in between carboxylic-modified silica particles and amino patchy particles, in a second step the carboxylic groups are converted into amino group, finally the particles are seeded by gold nuclei.

3.1 Strategy (I): assembly with silica satellites previously decorated by gold nuclei

85-nm silica spheres modified with APTES were decorated with “Duff” gold nuclei. The process was a variation of the seeding step described in Chapter 2 (**Protocol 19**) where the aminated silica particles were positively charged thanks to acidic pH condition and then mixed with an excess of gold nuclei dispersion. However, in this approach, the elimination of the excess of gold nuclei was followed by a transfer in DMF. Then the amino groups were typically converted into carboxylic ones by reaction with succinic anhydride as described in this Chapter (**Protocol 31**).

Protocol 33: Seeding of the amino-modified silica particles by gold nuclei followed by conversion of the amino groups into carboxylic ones.

*Typically, a volume of amino-modified silica particles as obtained after **Protocol 30** are transferred into water acidified by HCl (pH 4) by using two centrifugation/redispersion cycles (12 000 g; 15 min). A volume of gold nuclei prepared according to **Protocol 19** from chapter 2 is added. The solution is stirred overnight and finally washed from the free gold nuclei by three centrifugation/redispersion cycles (10 000 g during 20 min) in DMF. Then the **Protocol 31** is applied.*

During this process we noticed that the dispersion obtained after the seeding process was turning from the initial “cola” brownish color to a much more burgundy color. The process was anyway pursued in order to attempt an assembly of the seeded particles into the dimples of the aminated patchy particles according to the **Protocol 32**.

As shown on **Figure 60**, the assembly failed. Indeed, most of the silica particles weren’t attached to the dimples. Moreover the gold nuclei seemed to have moved from the silica spheres to the patchy particles where they were stuck into the dimples.

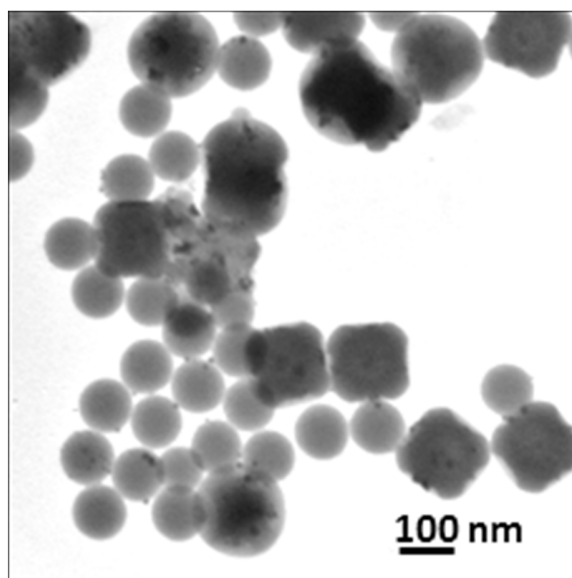


Figure 60: TEM image of the assembly of silica particles decorated by gold nuclei prior to the conversion of the amino groups into carboxylic ones with aminated dimples (H-86).

We think that the thermal treatment performed during the conversion of the amino groups into carboxylic ones had induced a certain coalescence of the gold nanoparticles as well as a loosening of the electrostatic interactions in between the amine and gold nuclei. At some point, it might be envisioned that a fraction of the amines “holding” the nuclei was converted into carboxylic groups. In such conditions, the silica particles could be easily stripped of their gold nuclei by the amine groups of the dimples giving structures similar those studied in Chapter 2.

In order to determine if the assembly failure as well as the loosening of the gold nuclei was both due to the thermal treatment, we repeated the experiment without the thermal treatment stage performed during the *Protocol 31*. Afterwards, the particles were put in contact with the aminated dimpled particles according to the *Protocol 32*. Subsequently, the assembly formed were used for a regrowth process similar to the one described in the section 2.3 of Chapter 2 in order to promote a gold layer formation over the decorated silica particles.

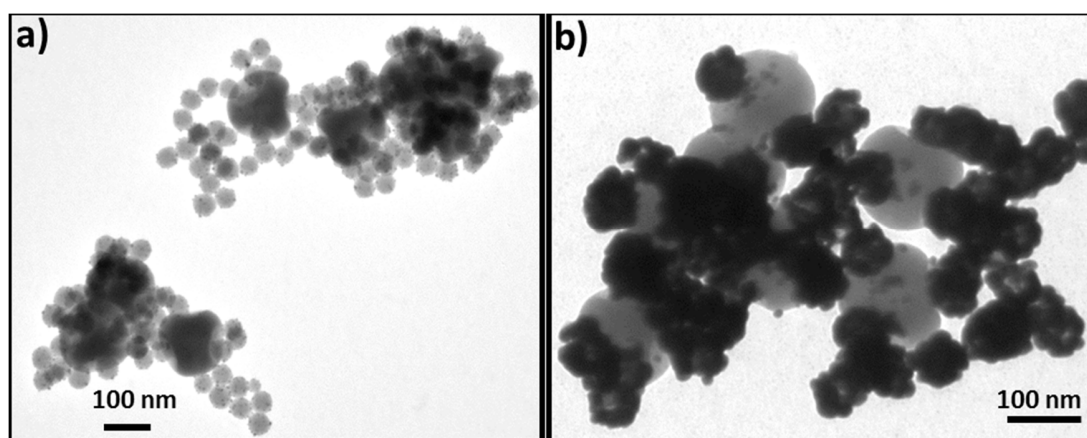


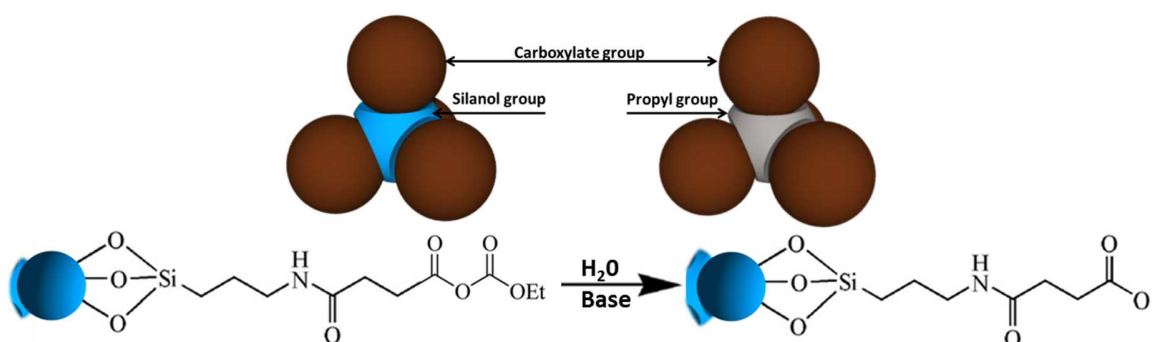
Figure 61: TEM images of the assembly of Duff decorated amino silica converted into carboxylic surface groups assembled with aminated dimples (T-86) a) and after gold growth b).

The typical kind of assembly obtained is shown on **Figure 61a**. The assemblies exhibited string-beads like formation instead of anchorage of individual silica particles. Indeed, the silica satellites seemed linked in between each other and this aspect became more obvious after the gold growth as seen on **Figure 61b**. This observation was attributed to the formation of chemical bonds in between the satellites due to their multi-functionality as explained before (**Scheme 21**). Indeed, we showed that the absence of thermal treatment to convert the amino groups into carboxylic ones gave particles with IEP at pH 6 meaning that the surface coverage in term of COOH groups wasn't total with remaining NH₂ groups. In such conditions, the undesired assembly in between the satellites during the activation step became a real issue as highlighted by those results.

3.2 Strategy (II): post-assembly decoration of the silica satellites by gold nuclei

The second strategy developed to obtain plasmonic nanoclusters from self-assembled silica/silica multipod-like clusters took advantage of the discrepancy existing in term of surface chemistry between the satellites and the core.

We can consider the surface as schematized on **Scheme 24**. The left scheme represents the assembly with unmodified patchy particle whereas the right one deals with the assembly performed with "passivated" patchy particle, *e.g.* after grafting of propyl groups as described in Chapter 2. It was important to keep in mind that the washing step performed in alkaline aqueous media converted the remaining mixed anhydride groups located at the surface of the silica particles into carboxylate ones (**Scheme 24**). Considering such structures, there were two main surface areas available to work with: an inter-patch area covered with silanols or propyl groups, and satellite surface area with carboxylate groups.

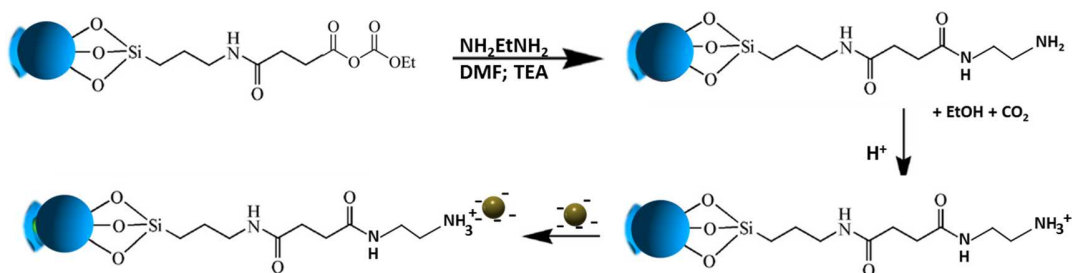


Scheme 24: The assembled structure with the nature of their chemical surface groups in the case of a raw assembly (left) or an assembly performed with dimpled silica particles previously surface-passivated (right); scheme of the reaction occurring during the washing of the assembly dispersion (bottom).

3.2.1 Amination of the silica satellites attached to the patchy silica core and their subsequent decoration with gold nuclei

The strategy consisted first in the modification of the surface of the silica satellites with amino groups. During this process, the passivated inter-patch surface area shouldn't be affected. The

silica satellites surface became ready to be seeded by gold nuclei, supposed to promote the formation of a gold shell over the satellites but not over the core. For that purpose, we attempted to convert the carboxylate groups specifically present on the satellite surface into amino ones (**Scheme 25**). Indeed, it was expected to derivatize the carboxylic groups into amine ones through a re-activation step of the carboxylates into mixed anhydrides thanks to the use of ethyl chloroformate followed by the reaction with a molecule such as the ethylene diamine.



Scheme 25: The reaction involved in the amino modification of the silica satellites of the self-assembled silica/silica multipods. The second step represents the protonation reaction of the amino group followed by the adsorption of negatively-charged gold nanoparticles.

Protocol 34: Site specific decoration of the self-assembled silica/silica clusters with gold nuclei.

Typically, 20 mL of the dispersion of patchy particles assembled with the silica COO^- activated particles are washed in water and then deprotonated using TEA. The clusters are transferred into DMF by centrifugation and the COO^- groups are reactivated through the addition of an amount of ECF corresponding to 10 functions / nm^2 of the total silica satellite surface used for the assembly. After 5 min, an amount of ethylene diamine corresponding to 50 functions / nm^2 of the total silica satellite surface is added and the mixture is let to react overnight. Then, the dispersion is washed three times by centrifugation/redispersion in milliQ water, then acidified using few drops of HCl to protonate the amino group and washed one more time with milliQ water. This dispersion containing the assembly is mixed with gold dispersion as prepared **Protocol 19** and let over roller mixer for at least 4 h. Finally, the dispersion corresponding to the assembly decorated by gold nuclei is washed three times by centrifugation/redispersion in milliQ water (2 000 g; 10 min).

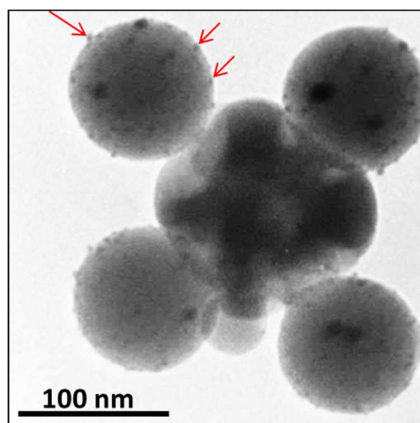


Figure 62: TEM image of a self-assembled silica/silica cluster made from 86-nm silica satellites and aminated dimpled particle deriving from H-86. The 86 nm satellites were amino-modified in order to assemble Duff gold nuclei at the surface (some nuclei are highlighted by red arrows).

Following the described strategy, the assembly of silica particles into the aminated patches of passivated silica particles could be amino modified and decorated by gold nuclei as shown on **Figure 62**. The results observed are in good agreement with the expected ones because the seeding occurred in a site-specific way.

3.2.2 Growth of the gold nuclei to get silica@gold satellites

Once seeded by gold nuclei, the satellite was coated by a gold layer thanks to a gold growth performed in conditions similar to those used in Chapter 2.

Protocol 35: Growth of a gold layer over the silica satellites of the self-assembled silica silica clusters.

*Typically, 0.5 mL of the dispersion containing the self-assembled silica-silica clusters decorated with Duff gold nuclei are introduced into a 50-mL falcon tube. A volume of PVP solution (10 g/L $\overline{M}_n = 29\,000$ g/mol) is added and mixed using the vortex and the adsorption is completed to occur over the roller mixer for 5 min. Subsequently a volume of the gold plating solution prepared according to the **Protocol 23** is added and mixed with a volume of 50 μ L of formaldehyde per mL of gold plating solution.*

Typically, the satellites obtained after gold growth exhibited an aspect varying from raspberry-like to core-shell morphology depending on the amount of gold used for the regrowth (**Figure 63**). Interestingly, it was possible to control the morphology of the clusters by playing with the size of the silica clusters and the thickness of the gold deposited. Moreover, this approach was relevant in term of amounts of gold used. Indeed, we used a gold plating solution to coat silica with gold. Firstly that means that the excess of particles required to obtain the proper assembly condition are the silica one which are easy to produce. Secondly, when the assembly sites are fulfilled by silica, gold is employed to coat the surface. The results presented were obtained by

using a batch of silica particles with six dimples in average and a batch of 86 nm silica particles presented in the Chapter 1.

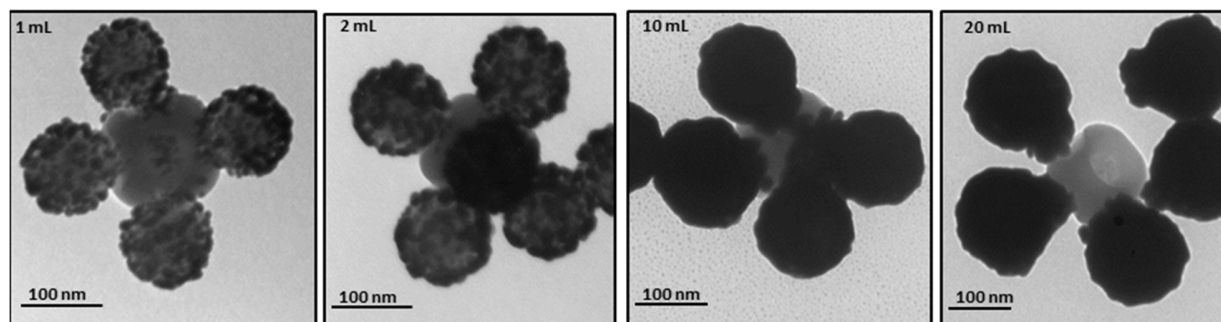


Figure 63: TEM images of the silica/silica@gold clusters. The amount of gold plating solution used for the growth is specified at the top left corner of the pictures. The dimpled particles were obtained deriving H-86 batches.

The inter-patch area passivation was mandatory to get a sharp discrepancy in terms of surface chemistry. **Figure 64** presents the results obtained in the case of an assembly made with non-passivated patchy particles. Typically, the satellites were covered by gold nuclei as well as the inter-patch area (sparsely coverage due to non-specific adsorption).

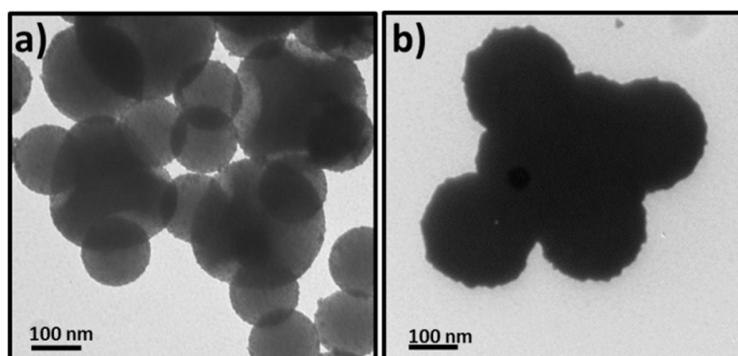


Figure 64: TEM images of the plasmonic clusters obtained without passivation of the interpatches areas: after decoration by Duff gold nuclei a) and b) after the stage of gold growth. This sample is made from 86 nm silica satellites with dimpled particles deriving from (T-86).

3.2.3 Toward the control of the inter-satellites distance

We were looking for plasmonic nanoclusters exhibiting tight intersatellites gap. The clusters exhibiting a high degree of geometry with size-monodisperse satellites, we used a geometrical approach to optimize the morphology.

We have prepared carboxylic-modified silica particles with a diameter of 137 nm and we assembled them to 6 dimples patchy particles H-86. As seen on **Figure 65**, the assembly of silica satellites into the dimples was efficient as well as the gold nuclei decoration.

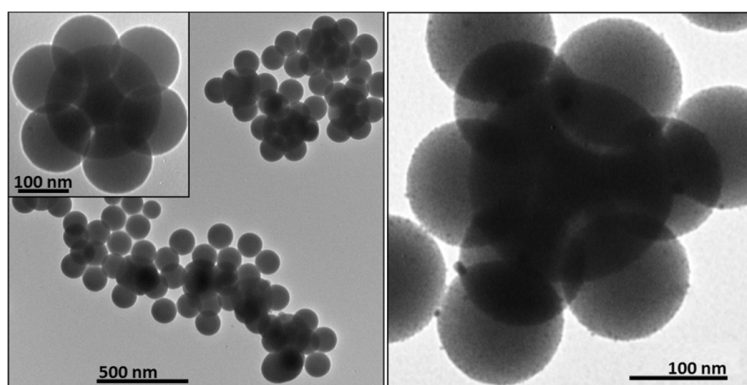


Figure 65: TEM images of self-assembled silica/silica clusters from 137-nm satellites attached to the six-dimples of a silica core (left) with a focused view in the insert, and the same batch after satellite decoration by gold nuclei (right).

In order to easily determine the geometrical parameters of the clusters, we exploited the TEM picture of a silica/silica hexapod with a missing satellite (**Figure 66a**). In this situation, the “hexapod” was deposited on a square section then the distance was quite precisely determined. The distance from edge to edge of the cluster was about 400 nm and the spacing in between the satellites was about 50 nm.

Considering the diameter of the silica sphere (137 nm) and the initial diameter of the patchy core (86 nm) the edge to edge distance should exhibit a dimension of $(137 \times 2) + 86 = 360$ nm. Here the dimensions, 40 nm larger than the expectation, were attributed to the presence of the PS bumps into the dimples. Considering those PS bumps, the structure could be represented as the one on **Figure 66b** (drawn to scale) which is in good agreement with the result presented on **Figure 66c** corresponding to the case of an assembly performed with dimpled silica particles exhibiting not very deep dimples. In such conditions, it became easier to see the presence of the PS bumps into the dimples. Thanks to this geometrical analysis, we determined the value of the diagonal of the blue square represented **Figure 66b**, and hence we calculated the distance corresponding to the edge of the square.

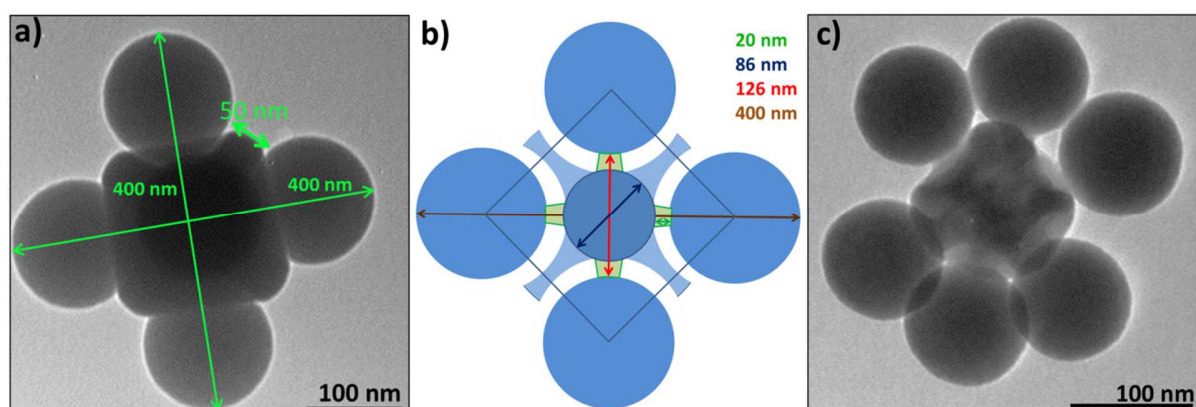


Figure 66: a) TEM picture with measurement annotation of an octahedral cluster with a missing satellite, in that case the cluster is sat on the square defined by four of the five satellites; b) a scheme representing a cross-section of the cluster drawn at true scale; c) assembly performed with dimpled silica particles with not deep dimples allowing to see the PS bumps connected to the satellites.

Here this distance corresponds to $\sqrt{2}$.diagonal so $\sqrt{2} \cdot (137 + 40 + 86) \cong 187 \text{ nm}$ that means that the inter-satellites gap existing in between the two silica particles was about 50 nm. Thanks to this piece of information it became possible to evaluate the inter-particles distances in between particles for various gold thicknesses. The growth of the gold layer was performed varying the amount of gold plating solution added. By doing so, the thickness of the gold layer was tuned modifying the inter-satellite gap. Basically, **Figure 67** and **Table 10** summarized the geometrical characteristics of the plasmonic nanoclusters prepared. The structures presented on **Figure 67** correspond to octahedral patchy (H-86) particles with 5 satellites attached to the dimples (images **a**), **b**), **c**), **d**). The images **e**) corresponds probably to the situation where only 4 satellites were attached onto the hexavalent dimpled core.

The value of $D_{\text{core shell}}$ measured was extracted from the analysis of the TEM images. The gold shell thickness deduced is the difference between the average diameter of the core-shell measured and the diameter of the silica satellite particles. The expected inter-particles distances are the average distances in between satellites. Those distances were calculated considering the geometrical configuration as presented on **Figure 66b** and using the value of the mean gold shell thickness measured; $D_{\text{silica satellites}}$; $D_{\text{inner silica particles}}$, and the mean size of the PS bumps attaching the satellites.

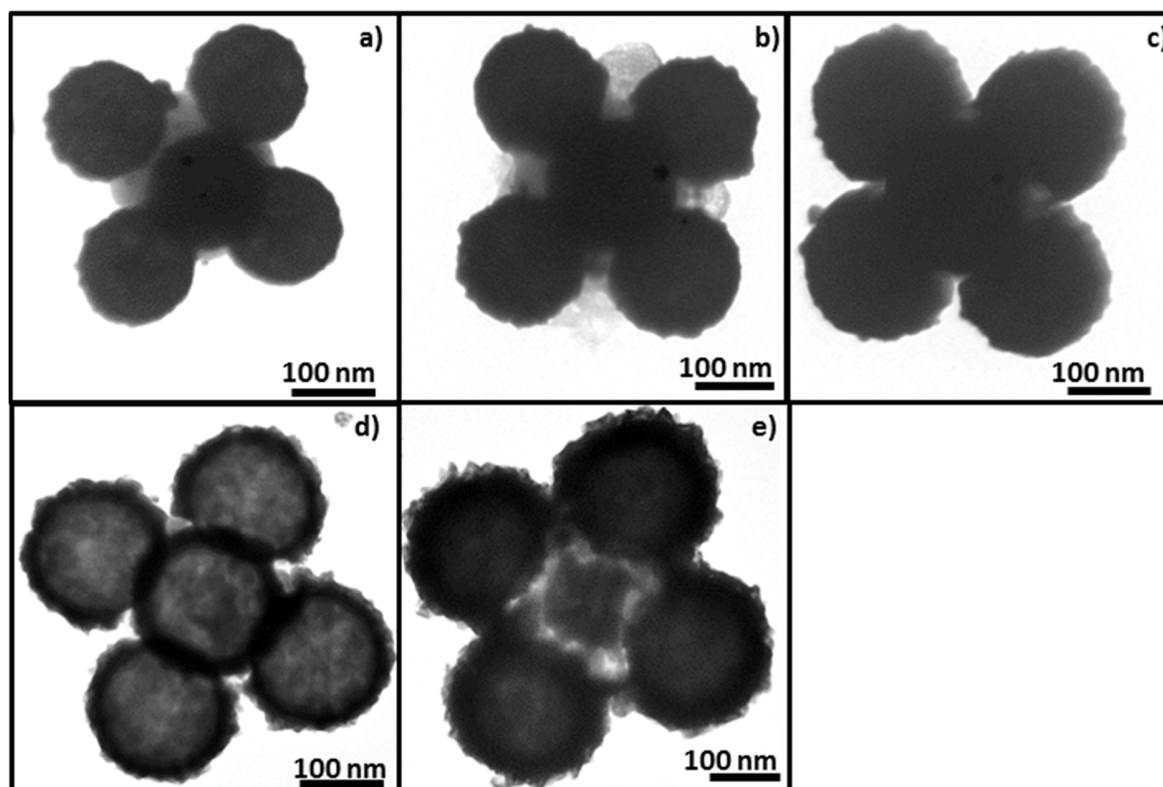


Figure 67: TEM images of silica/silica@gold clusters corresponding to various gold regrowth obtained for several amounts of gold precursor: a) 5 mL; b) 10 mL; c) 20 mL; d) 25 mL and e) 35 mL.

Table 10: Geometrical features of the silica/silica@gold clusters for different thicknesses of the gold layer.

TEM images on Figure 67	a)	b)	c)	d)	e)
V_{GPS} (mL)	5	10	20	25	35
$D_{core\ shell}$ measured (nm)	150	165	180	185	220
Gold shell thickness deduced (nm)	7	14	22	24	41
Expected inter-satellites gap (nm)	37	22	7	2	0 (contact)
Measured inter-satellite gap (nm)	35	20	7-10	2-5	0 (contact)

The measured inter-particles distances were in good agreement with the expected ones considering the gold thicknesses. The core-shell satellites could be considered as properly separated from each others for a range of shell regrowth simply due to their geometry. For the smallest inter-particle distances and so the thickest shells, the value can be distorted due to the roughness of the shell. The sample obtained by using 35 mL of gold plating solution give so big plasmonic particles that they merged or they were deattached from the patchy particles.

The calculated amount of gold required for a given shell thickness could be easily determined in the case of a dispersion of octahedral clusters at a known concentration. However, here we had only a very rough idea of the cluster concentration and furthermore the dispersion contained a significant amount of free silica spheres seeded by gold nuclei that could be coated by gold during the regrowth. Those limitations could be overcome by a gradient density washing steps allowing the removal of the free particles remaining in the dispersions. However, due to a lack of time, this improvement through the purification step wasn't performed. Despite the presence of free silica@gold particles shown on the SEM and TEM picture of **Figure 68**, the formation of plasmonic clusters with a good control over the inter-particles distances was achieved.

The conditions corresponding to a gold growth done from 25 mL of the plating solution appeared like the most relevant in term of geometrical features. This sample was studied by EDX mapping as shown on **Figure 69**. This observation highlighted the presence of a gold layer specifically deposited on the silica satellites and confirms the TEM observation showing that there is no gold deposited on the core particles.

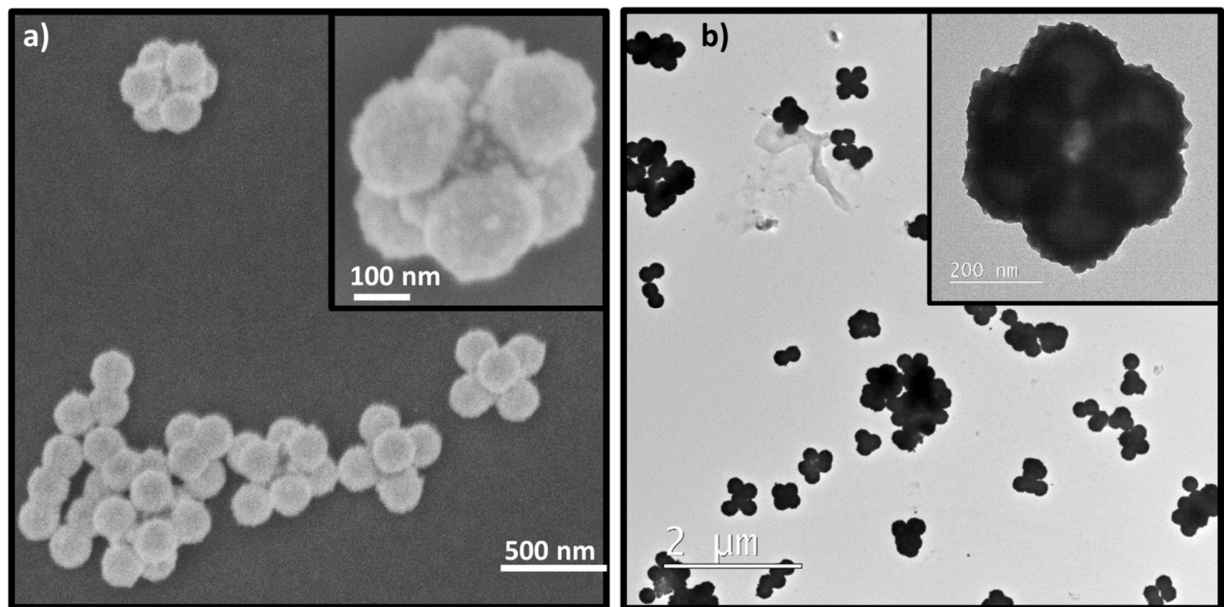


Figure 68: SEM (left) and TEM images (right) of the self-assembled silica/silica@gold clusters after gold growth with 25 mL and 35 mL of plating solution, respectively.

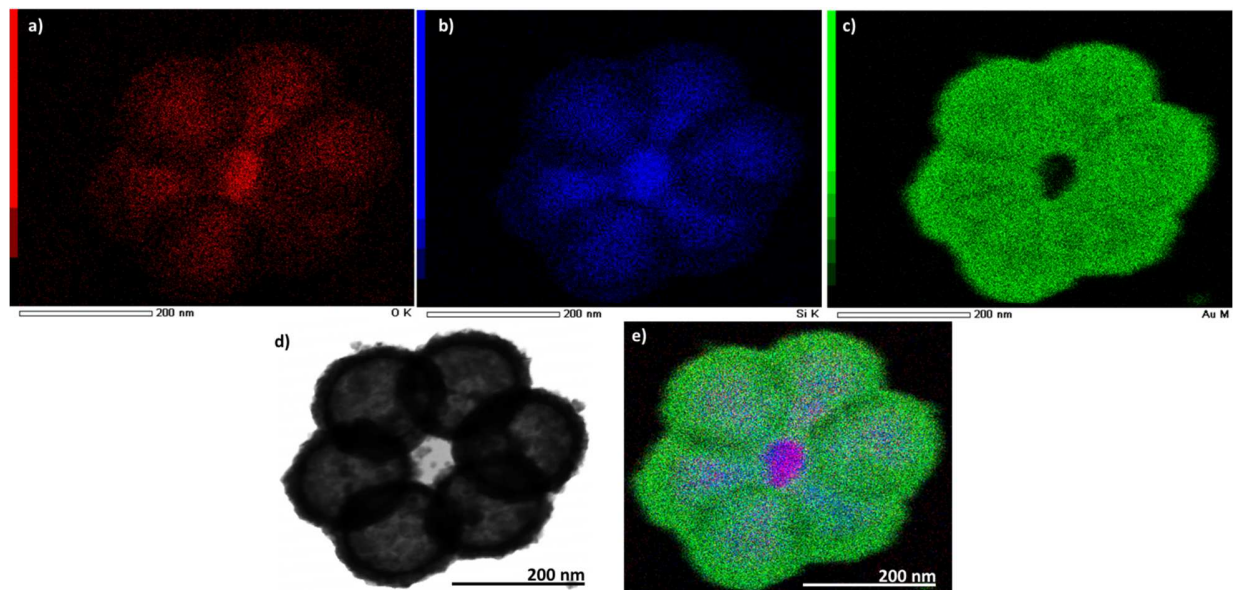


Figure 69: EDX mapping of the silica/silica@gold clusters: a) oxygen mapping; b) silicon mapping; c) gold mapping; d) corresponding high resolution TEM image; and e) superimposition of the previous maps.

4 Conclusion

In this chapter, another strategy to synthesize the plasmonic nanoclusters and get short inter-satellite separation was investigated. One explore the possibility to elaborate the nanoclusters via self-assembly approach of pre-formed colloidal particles. Several attraction forces to self-assemble pre-formed colloids are currently under investigation into the literature. In this work, one demonstrates that the covalent coupling approach via peptide bonding is an efficient way to immobilize pre-formed satellites onto the concave areas of the patchy particles. It was difficult to directly anchor plasmonic nanoparticles of few tens of nanometer diameters onto the dimples surface, but we were able to assemble large pre-formed silica particles onto the dimpled particles. Once the silica particles were held together, gold nanoshells were grown on the satellites surface. One was able to precisely tune the interparticle separation by controlling the thickness of the Au shell.

We have identified two main factors to efficiently direct the assembly of silica satellites onto the concave areas of the particles: (i) control of the surface functionalization experimental conditions (ii) control of the satellites /core concentration ratio. In these optimized experimental conditions, this route yields spectacular results to produce plasmonic nanoclusters in high yield. It offers interesting strengths to control the interparticle spacing within the cluster which is a crucial dimension for plasmonic coupling.

Based on the results of the present research, there is a clear direction that future investigation should focus on synthesis of novel plasmonic nano-objects. If one could replace the gold layer by a thin silver layer, it could provide an efficient method to develop novel hybrid nano-objects with interesting optical properties. If one could functionalize differently each dimple one could develop the formation of chiral colloidal particles.

5 References

- [1] F. Li, D. P. Josephson, and A. Stein, "Colloidal assembly: the road from particles to colloidal molecules and crystals.," *Angew. Chem. Int. Ed. Engl.*, vol. 50, pp. 360–388, 2011.
- [2] Y. Min, M. Akbulut, K. Kristiansen, Y. Golan, and J. Israelachvili, "The role of interparticle and external forces in nanoparticle assembly.," *Nat. Mater.*, vol. 7, pp. 527–538, 2008.
- [3] B. Derjaguin and L. Landau, "Theory of the stability of strongly charged lyophobic sols and of the adhesion of strongly charged particles in solutions of electrolytes," *Acta Phys. Chem. URSS*, vol. 14, p. 633, 1941.
- [4] E. J. W. Verwey and J. T. G. Overbeek, *Theory of the stability of lyophobic colloids*. 1948.
- [5] J. N. Israelachvili, *Intermolecular and surface forces*, Academic P. 1991.
- [6] J. Lyklema, *Fundamentals of interface and colloid science*. 1991.

-
- [7] R. J. Hunter, *Foundations of colloid science*. 2001.
- [8] A. D. Dinsmore, D. T. Wong, P. Nelson, and A. G. Yodh, “Hard Spheres in Vesicles: Curvature-Induced Forces and Particle-Induced Curvature,” *Phys. Rev. Lett.*, vol. 80, pp. 409–412, 2000.
- [9] P.-M. König, R. Roth, and S. Dietrich, “Lock and key model system,” *EPL Europhys. Lett.*, vol. 84, pp. 68006–68011, 2008.
- [10] R. J. Macfarlane and C. A. Mirkin, “Colloidal assembly via shape complementarity,” *Chemphyschem*, vol. 11, pp. 3215–3217, 2010.
- [11] D. J. Ashton, R. L. Jack, and N. B. Wilding, “Self-assembly of colloidal polymers via depletion-mediated lock and key binding,” *Soft Matter*, vol. 9, pp. 9661–9666, 2013.
- [12] Y. Li, X. Zhang, and D. Cao, “The role of shape complementarity in the protein-protein interactions,” *Sci. Rep.*, vol. 3, pp. 3271–3278, 2013.
- [13] R. Tuinier, J. Rieger, and C. G. de Kruijff, “Depletion-induced phase separation in colloid-polymer mixtures,” *Adv. Colloid Interface Sci.*, vol. 103, pp. 1–31, 2003.
- [14] C. J. Van Oss, “Long-range and short-range mechanisms of hydrophobic attraction and hydrophilic repulsion in specific and aspecific interactions,” *J. Mol. Recognit.*, vol. 16, pp. 177–190, 2003.
- [15] T. P. Silverstein, “The Real Reason Why Oil and Water Don’t Mix,” *J. Chem. Educ.*, vol. 75, pp. 116–118, 1998.
- [16] W. B. Rogers and V. N. Manoharan, “Programming colloidal phase transitions with DNA strand displacement,” *Science*, vol. 347, pp. 639–642, 2015.
- [17] U. Gasser, “Crystallization in three- and two-dimensional colloidal suspensions,” *J. Phys. Condens. Matter*, vol. 21, pp. 203101–203125, 2009.
- [18] V. J. Anderson and H. N. W. Lekkerkerker, “Insights into phase transition kinetics from colloid science,” *Nature*, vol. 416, pp. 811–815, 2002.
- [19] L. Rossi, S. Sacanna, W. T. M. Irvine, P. M. Chaikin, D. J. Pine, and A. P. Philipse, “Cubic crystals from cubic colloids,” *Soft Matter*, vol. 7, pp. 4139–4142, 2011.
- [20] H. Zhang, E. W. Edwards, D. Wang, and H. Möhwald, “Directing the self-assembly of nanocrystals beyond colloidal crystallization,” *Phys. Chem. Chem. Phys.*, vol. 8, pp. 3288–3299, 2006.
- [21] E. V. Shevchenko, D. V. Talapin, C. B. Murray, and S. O’Brien, “Structural characterization of self-assembled multifunctional binary nanoparticle superlattices,” *J. Am. Chem. Soc.*, vol. 128, pp. 3620–3637, 2006.
- [22] C. E. Snyder, A. M. Yake, J. D. Feick, and D. Velegol, “Nanoscale functionalization and site-specific assembly of colloids by particle lithography,” *Langmuir*, vol. 21, pp. 4813–4815, 2005.

- [23] Y. Wang, Y. Wang, X. Zheng, É. Ducrot, J. S. Yodh, M. Weck, and D. J. Pine, “Crystallization of DNA-coated colloids.,” *Nat. Commun.*, vol. 6, pp. 1–8, 2015.
- [24] Y. Wang, Y. Wang, X. Zheng, E. Ducrot, M. G. Lee, G.-R. Yi, M. Weck, and D. J. Pine, “Synthetic Strategies Toward DNA-Coated Colloids that Crystallize.,” *J. Am. Chem. Soc.*, vol. 137, pp. 10760–10766, 2015.
- [25] Z. Zhang, A. S. Keys, T. Chen, and S. C. Glotzer, “Structures through Molecular Mimicry,” *Langmuir*, vol. 21, pp. 409–413, 2005.
- [26] F. Smallenburg and F. Sciortino, “Liquids more stable than crystals in particles with limited valence and flexible bonds,” *Nat. Phys.*, vol. 9, pp. 554–558, 2013.
- [27] G. Van Anders, N. K. Ahmed, R. Smith, M. Engel, and S. C. Glotzer, “Entropically Patchy Particles: Engineering Valence through Shape Entropy,” *ACS Nano*, vol. 8, pp. 931–940, 2014.
- [28] J. M. Romo-Herrera, R. A. Alvarez-Puebla, and L. M. Liz-Marzán, “Controlled assembly of plasmonic colloidal nanoparticle clusters.,” *Nanoscale*, vol. 3, pp. 1304–1315, Apr. 2011.
- [29] L. Hong, A. Cacciuto, E. Luijten, and S. Granick, “Clusters of charged Janus spheres.,” *Nano Lett.*, vol. 6, pp. 2510–2514, Nov. 2006.
- [30] L. Hong, A. Cacciuto, E. Luijten, and S. Granick, “Clusters of amphiphilic colloidal spheres.,” *Langmuir*, vol. 24, pp. 621–625, 2008.
- [31] A. Le Beulze, “Ph.D dissertation of the university Bordeaux 1: Synthesis and characterization of nanoresonators for metamaterials application in the visible range,” 2013.
- [32] A. S. Urban, X. Shen, Y. Wang, N. Large, H. Wang, M. W. Knight, P. Nordlander, H. Chen, and N. J. Halas, “Three-dimensional plasmonic nanoclusters.,” *Nano Lett.*, vol. 13, pp. 4399–4403, 2013.
- [33] J. E. Galván-Moya, T. Altantzis, K. Nelissen, F. M. Peeters, M. Grzelczak, L. M. Liz-Marzán, S. Bals, and G. Van Tendeloo, “Self-organization of highly symmetric nanoassemblies: a matter of competition.,” *ACS Nano*, vol. 8, pp. 3869–3875, 2014.
- [34] A. Sánchez-Iglesias, M. Grzelczak, T. Altantzis, B. Goris, J. Pérez-Juste, S. Bals, G. Van Tendeloo, S. H. Donaldson, B. F. Chmelka, J. N. Israelachvili, and L. M. Liz-Marzán, “Hydrophobic interactions modulate self-assembly of nanoparticles.,” *ACS Nano*, vol. 6, pp. 11059–11065, 2012.
- [35] M. Grzelczak, A. Sánchez-Iglesias, and L. M. Liz-Marzán, “Solvent-induced division of plasmonic clusters,” *Soft Matter*, vol. 9, pp. 9094–9098, 2013.
- [36] N. Pazos-Perez, C. S. Wagner, J. M. Romo-Herrera, L. M. Liz-Marzán, F. J. García de Abajo, A. Wittemann, A. Fery, and R. A. Alvarez-Puebla, “Organized plasmonic clusters with high coordination number and extraordinary enhancement in surface-enhanced Raman scattering (SERS).,” *Angew. Chem. Int. Ed. Engl.*, vol. 51, pp. 12688–12693, 2012.

- [37] S. Sacanna, W. T. M. Irvine, P. M. Chaikin, and D. J. Pine, “Lock and key colloids,” *Nature*, vol. 464, pp. 575–578, 2010.
- [38] S. Sacanna, W. T. M. Irvine, L. Rossi, and D. J. Pine, “Lock and key colloids through polymerization-induced buckling of monodisperse silicon oil droplets,” *Soft Matter*, vol. 7, pp. 1631–1634, 2011.
- [39] L. Colón-Meléndez, D. J. Beltran-Villegas, G. van Anders, J. Liu, M. Spellings, S. Sacanna, D. J. Pine, S. C. Glotzer, R. G. Larson, and M. J. Solomon, “Binding kinetics of lock and key colloids,” *J. Chem. Phys.*, vol. 142, pp. 174909–174918, 2015.
- [40] Y. Wang, Y. Wang, X. Zheng, G.-R. Yi, S. Sacanna, D. J. Pine, and M. Weck, “Three-dimensional lock and key colloids,” *J. Am. Chem. Soc.*, vol. 136, pp. 6866–6869, 2014.
- [41] D. Zerrouki, B. Rotenberg, S. Abramson, J. Baudry, C. Goubault, F. Leal-Calderon, D. J. Pine, and J. Bibette, “Preparation of doublet, triangular, and tetrahedral colloidal clusters by controlled emulsification,” *Langmuir*, vol. 22, pp. 57–62, 2006.
- [42] G.-R. Yi, V. N. Manoharan, E. Michel, M. T. Elsesser, S.-M. Yang, and D. J. Pine, “Colloidal Clusters of Silica or Polymer Microspheres,” *Adv. Mater.*, vol. 16, pp. 1204–1208, 2004.
- [43] Y.-S. Cho, G.-R. Yi, J.-M. Lim, S.-H. Kim, V. N. Manoharan, D. J. Pine, and S.-M. Yang, “Self-organization of bidisperse colloids in water droplets,” *J. Am. Chem. Soc.*, vol. 127, pp. 15968–15975, 2005.
- [44] Y. Wang, Y. Wang, D. R. Breed, V. N. Manoharan, L. Feng, A. D. Hollingsworth, M. Weck, and D. J. Pine, “Colloids with valence and specific directional bonding,” *Nature*, vol. 491, pp. 51–55, 2012.
- [45] S. N. Sheikholeslami, H. Alaeian, A. L. Koh, and J. A. Dionne, “A Metafluid Exhibiting Strong Optical Magnetism,” *Nano Lett.*, vol. 13, pp. 4137–4141, 2013.
- [46] J. Fontana, W. J. Dressick, J. Phelps, J. E. Johnson, R. W. Rendell, T. Sampson, B. R. Ratna, and C. M. Soto, “Virus-Templated Plasmonic Nanoclusters with Icosahedral Symmetry via Directed Self-Assembly,” *Small*, vol. 10, pp. 3058–3063, 2014.
- [47] A. S. Blum, C. M. Soto, C. D. Wilson, J. D. Cole, M. Kim, B. Gnade, A. Chatterji, W. F. Ochoa, T. Lin, J. E. Johnson, and B. R. Ratna, “Cowpea Mosaic Virus as a Scaffold for 3-D Patterning of Gold Nanoparticles,” *Nano Lett.*, vol. 4, pp. 867–870, 2004.
- [48] F. Li, W. C. Yoo, M. B. Beernink, and A. Stein, “Site-specific functionalization of anisotropic nanoparticles: from colloidal atoms to colloidal molecules,” *J. Am. Chem. Soc.*, vol. 131, pp. 18548–18555, 2009.
- [49] W. Yufeng, W. Yu, D. R. Breed, and M. Vinathan N, “Colloids with valence and specific directional bonding,” *Nature*, vol. 491, pp. 51–56, 2012.

- [50] K. Zhao and T. G. Mason, "Directing Colloidal Self-Assembly through Roughness-Controlled Depletion Attractions," *Phys. Rev. Lett.*, vol. 99, pp. 268301–268304, 2007.
- [51] D. J. Kraft, R. Ni, F. Smallenburg, M. Hermes, K. Yoon, D. A. Weitz, A. van Blaaderen, J. Groenewold, M. Dijkstra, and W. K. Kegel, "Surface roughness directed self-assembly of patchy particles into colloidal micelles," *Proc. Natl. Acad. Sci. U. S. A.*, vol. 109, pp. 10787–10792, 2012.
- [52] S. Badaire, C. Cottin-Bizonne, and A. D. Stroock, "Experimental Investigation of Selective Colloidal Interactions Controlled by Shape, Surface Roughness, and Steric Layers," *Langmuir*, pp. 11451–11463, 2008.
- [53] N. B. Schade, M. C. Holmes-Cerfon, E. R. Chen, D. Aronzon, J. W. Collins, J. Fan, F. Capasso, and V. N. Manoharan, "Tetrahedral Colloidal Clusters from Random Parking of Bidisperse Spheres," *Phys. Rev. Lett.*, vol. 110, pp. 148303–148308, 2013.
- [54] E. Valeur and M. Bradley, "Amide bond formation: beyond the myth of coupling reagents," *Chem. Soc. Rev.*, vol. 38, pp. 606–631, Feb. 2009.
- [55] C. A. G. N. Montalbetti and V. Falque, "Amide bond formation and peptide coupling," *Tetrahedron*, vol. 61, pp. 10827–10852, 2005.
- [56] H. S. Rho, H. S. Baek, D. H. Kim, and I. S. Chang, "A Convenient Method for the Preparation of Alkanolamides," *Bull. Korean Chem. Soc.*, vol. 27, pp. 584–586, 2006.
- [57] D. R. Burfield and R. H. Smithers, "Desiccant efficiency in solvent drying. 3. Dipolar aprotic solvents," *J. Org. Chem.*, vol. 43, pp. 3966–3968, 1978.
- [58] F. M. F. Benoiton, N. Leo. Chen, "Peptide synthesis in partially aqueous solution preparation of a Leu-Ala-Gly-Val using symmetrical anhydrides of N-afkoxy-carbonylamino acids in aqueous NJ-dimethylformamide," *Febs Lett.*, vol. 125, pp. 104–106, 1981.
- [59] J. A. Howarter, J. P. Youngblood, R. V May, I. Final, and F. September, "Optimization of Silica Silanization by 3-Aminopropyltriethoxysilane," *Langmuir*, vol. 47907, pp. 11142–11147, 2006.
- [60] R. G. Acres and G. G. Ellis, Amanda V. Alvino, Jason Lenahan, Claire E. Khodakov, Dmitriy a. Metha, Gregory F. Andersson, "Molecular Structure of 3-Aminopropyltriethoxysilane Layers Formed on Silanol-Terminated Silicon Surfaces," *J. Phys. Chem. C*, vol. 116, pp. 6289–6297, 2012.
- [61] N. Reinhardt, L. Adumeau, O. Lambert, S. Ravaine, and S. Mornet, "Quaternary ammonium groups exposed at the surface of silica nanoparticles suitable for DNA complexation in the presence of cationic lipids," *J. Phys. Chem. B*, vol. 119, pp. 6401–6411, 2015.
- [62] N. M. E. Reinhardt, "Thèse de l'université de Bordeaux 1 : Modification chimique de surface de nanoparticules de silice pour le marquage d'ADN dans des lipoplexes." 2013.
- [63] C. Elissalde, O. Bidault, E. Sellier, O. Nguyen, and M. Maglione, "Ferroelectric-Based Nanocomposites : Toward Multifunctional Materials," *Chem. Mater.*, vol. 19, pp. 987–992, 2007.

- [64] S. C. Feifel and F. Lisdat, “Silica nanoparticles for the layer-by-layer assembly of fully electro-active cytochrome c multilayers.,” *J. Nanobiotechnology*, vol. 9, pp. 1–12, 2011.
- [65] Y. An, M. Chen, Q. Xue, and W. Liu, “Preparation and self-assembly of carboxylic acid-functionalized silica.,” *J. Colloid Interface Sci.*, vol. 311, pp. 507–513, 2007.
- [66] M. Cano and G. de la Cueva-Méndez, “Self-assembly of a superparamagnetic raspberry-like silica/iron oxide nanocomposite using epoxy-amine coupling chemistry.,” *ChemComm*, vol. 125, pp. 3620–3622, 2015.

Chapter 4: Measurement of the optical response of an unique plasmonic nanocluster using dark-field spectroscopy

When shining light on a metallic object, its electrons population starts vibrating as a whole, generating plasmon excitations. These plasmons do emit light whose spectrum is a unique signature of the object morphology. The optical signatures are directly connected to the size, geometry, structure and compositions of the nano-objects. Precise determination of these connections and elucidation of the fundamental mechanism at the origin of the observed properties are thus necessary advances for fully exploiting nanosystems and designing new ones for specific applications. However, such investigations are difficult to perform in ensembles of nano-objects because the unavoidable variation of their characteristics translates into fluctuations of their individual properties. To avoid these statistical effects, one has to combine measurement of the properties of a single nano-object with the morphological characterization **Figure 70**. The aim of this chapter is to develop and to use an approach to both perform a morphological characterization of a single nanocluster as obtained in the chapter 3, and to determine its optical properties. The development of this combined approach was performed on an octahedral nano-system made of a silica core and core-shell satellites. The observed optical properties of an individual particle were compared to the prediction of theoretical models using its 3D morphological characteristics as an input.

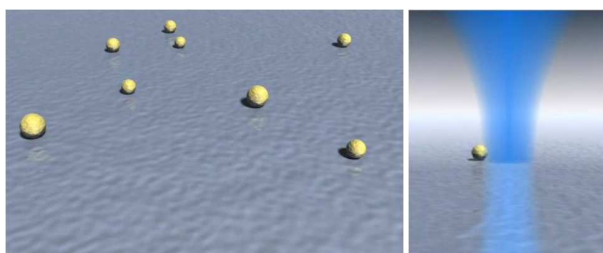


Figure 70: Artist view of isolated gold nanoparticles dispersed on a substrate and studied under focused electromagnetic beam (reproduced from GdR Or-nano team Femto-nano-optics).

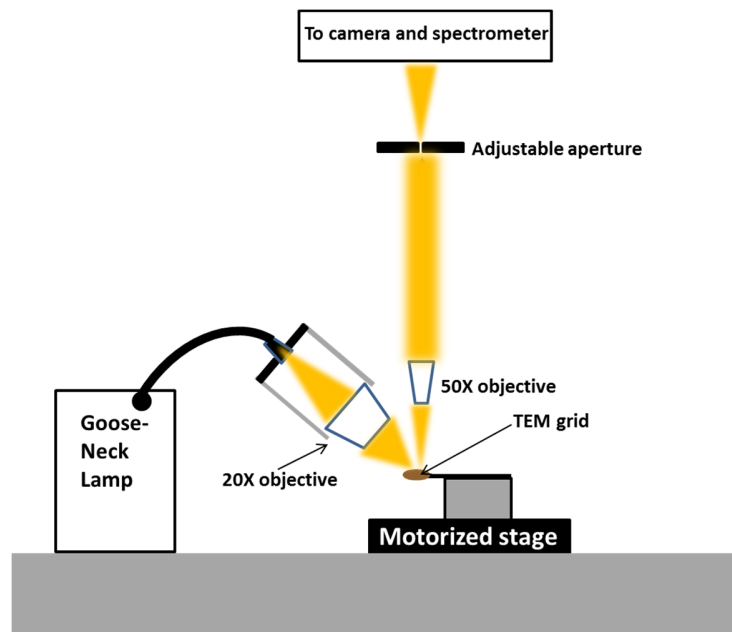
The controlled synthesis of the plasmonic nanoclusters using the concept of the patchy particles allowed us to produce different objects with nanoscale interaction between the satellites. Such nanoclusters exhibit various resonance modes: dipolar modes, multipolar modes as well as magnetic modes.[1]–[4] The magnetic mode is due to the arrangement of closely packed nanoparticles in a circular loop.[5]–[10] Furthermore an interference mode known as Fano-resonance could also appear when the proper coupling conditions are satisfied.[9],[11]–[13] Studying the optical properties of plasmonic nanoclusters at the single-particle level is challenging, since measuring and identifying the several modes is not trivial. Indeed, overlaps between, for example, electric and magnetic modes are frequently encountered. In such situations, identifying their nature generally requires a study correlating simulation and experimental characterizations.

From an optical point of view, different approaches have been developed for optically detecting and investigating single nano-objects. Optical study of the latter requires detection of their light absorption or their scattering. In this context, the high spatial resolution of near field optical techniques is very interesting. However, particle-tip coupling that makes the interpretation of the

experimental data difficult.[14] This has fostered the development of far-field spectroscopy techniques whose lower intrinsic spatial resolution is overcome by using dilute systems so that only one particle is in the probed zone (typically one particle per μm^2). Scattering based-dark field- methods are now well established [15],[16] and allow to investigate the properties of large particles, of typically tens of nanometers. We describe in the following the dark-field setup used to determine the optical properties of an octahedral nanocluster. The measured optical properties will be compared to the computed ones using the measured particle characteristics as an input to the theoretical model.

1 The dark field set-up used for the optical measurement

Optical measurement of a single nanocluster was performed using the dark-field spectroscopy. A spectrometer coupled with a confocal microscope was used in a dark field configuration to track down a cluster, to measure its optical properties and discriminate the electrical resonance from the magnetic one. **Scheme 26** illustrates the configuration that we used to record optical spectra of the nanoclusters. All the measurements were performed in the Manoharan Lab at Harvard University with the help of Nabila Tanjeem and Nicholas B. Schade. The design was very similar to the one used in previous studies.[5],[6] Typically, an incident white light beam from a halogen goose neck lamp is focused on the sample using a 20X long working distance Olympus objective. The incidence angle in our set-up was about 65° which ensured that reflected light did not go into the collection objective. The sample was mounted on a rotation stage itself mounted on a motorized stage connected to the microscope-spectrometer (LabRAM HR Evolution RAMAN SPECTROMETER from HORIBA Scientific) set up and controlled by the software. Scattered light from the sample was collected using a 50X long working distance Olympus objective. Furthermore, an adjustable aperture was situated in the optical path of the spectrometer and could be adjusted in order to screen all the collected light except the one scattered by a narrow area surrounding the cluster.



Scheme 26: Dark-field single object spectrometer set up: Halogen goose neck lamp send a white light beam into a condenser made of a polarizer and a 20X objective. Light is focused on the sample mounted on a rotational stage fixed on a motorized stage. The scattered light is collected into a 50X objective collimating the beam before going through an adjustable aperture narrowing the spot size collected by camera and spectrometer.

2 Modeling of the optical properties of a plasmonic nanocluster

The finite difference time domain (FDTD) Lumerical software was used to model the optical response of the plasmonic nanoclusters. It's based on a numerical analysis technique used for modeling computational electrodynamics. **Figure 71a** shows an example of investigations performed on an octahedral plasmonic cluster as obtained in the Chapter 3. The morphology, structure and composition of the nanocluster are described in the **Figure 71b**. The satellites are composed of a silica core almost completely covered by a thin shell of gold.

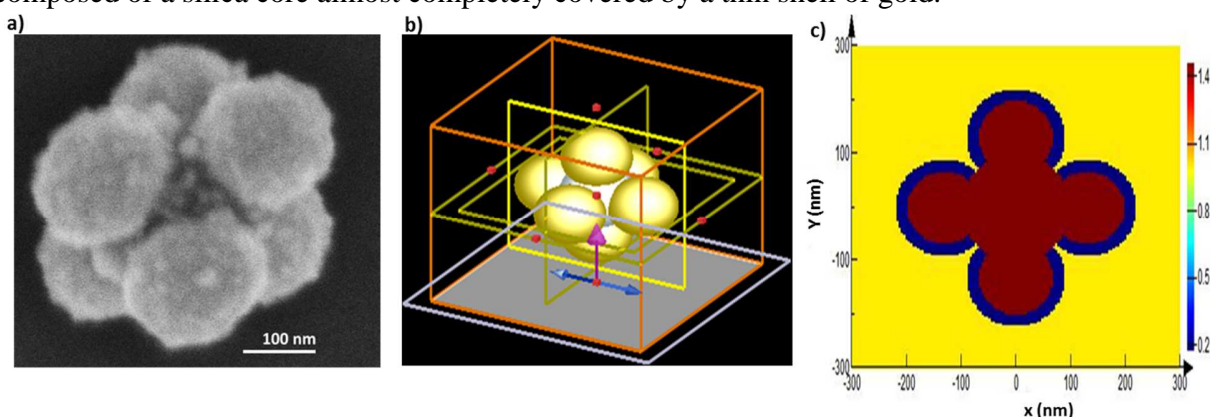


Figure 71: a) SEM images of the studied octahedral plasmonic nanoclusters b) representation of the overall cluster structures in the FDTD lumerical design mode c) map of the (xy plane) obtained using the index monitor: The blue shells correspond to gold; the burgundy area corresponds to the silica patchy particles and satellites

The structure corresponds to the nanoscale organization of the two material components in a nanocluster, i.e. silica core and silica@gold satellites (**Figure 71c**). Blue shells are metal (gold) component while the central burgundy area is silica one. The presence of the PS bumps, inherent to the patchy particles, was neglected for the simulation since we didn't expect that the PS dramatically influence the optical response of the nanocluster. **Figure 72** presents the simulated cross-section obtained considering the cluster structure as described in **Figure 71**. The result was obtained using the "total field scattered field" analysis method of Lumerical software. For all the simulations presented here, an incident electromagnetic beam with the electric field oriented along z axis was defined.

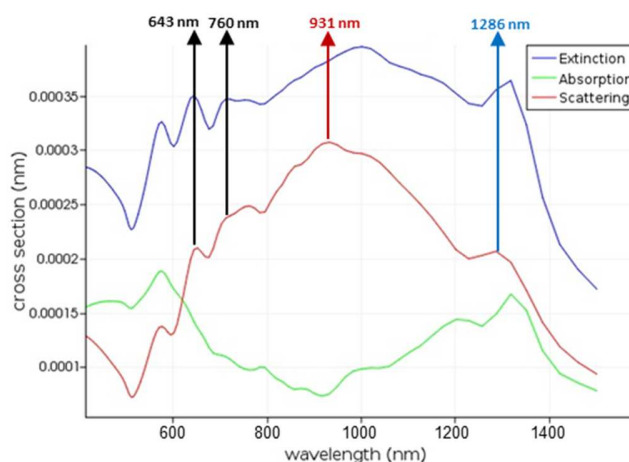


Figure 72: Simulated cross section spectra for the considered cluster structure; the main resonance band are tagged with arrows.

The simulated spectra present several resonances in the visible and in the IR ranges. The scattered spectrum was expected to predict the optical response as collected using the dark field set up. In order to determine the origin of each resonance band, a simulated mapping of the electric field vector was performed for the labelled bands.

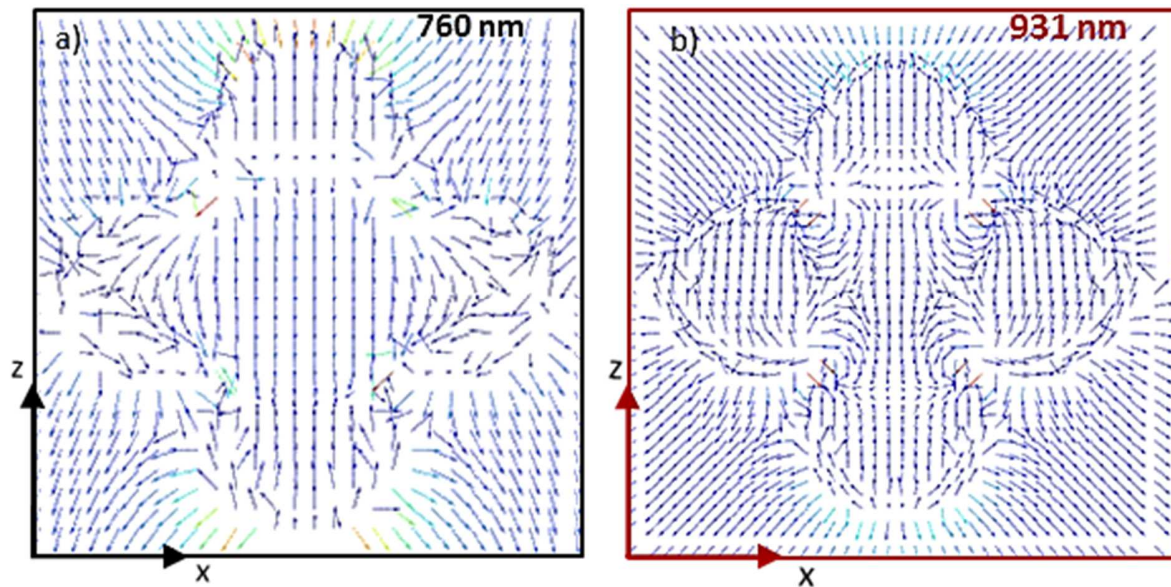


Figure 73: Simulated map of the electric field vector orientation in the (xz) plane at 760 nm a) and 931nm b).

The simulated mapping of the electric field as presented on **Figure 73** was useful to identify the origin of each resonance. The mapping performed considering the resonance at 931 nm exhibited a typical electric dipole mode where the overall distribution of electric vector orientation seems to be driven from one pole of the structure to another. The mapping performed for the resonance located at 760 nm shows a more complex behavior of the electric field vector orientation that are generally attributed to higher resonance mode. Moreover the overall dimension of the cluster (450 nm) is larger than half of the wavelength of the considered resonance (760 nm). For this reason, some part of the structure could be out of phase inducing complex resonances such as multipolar ones.

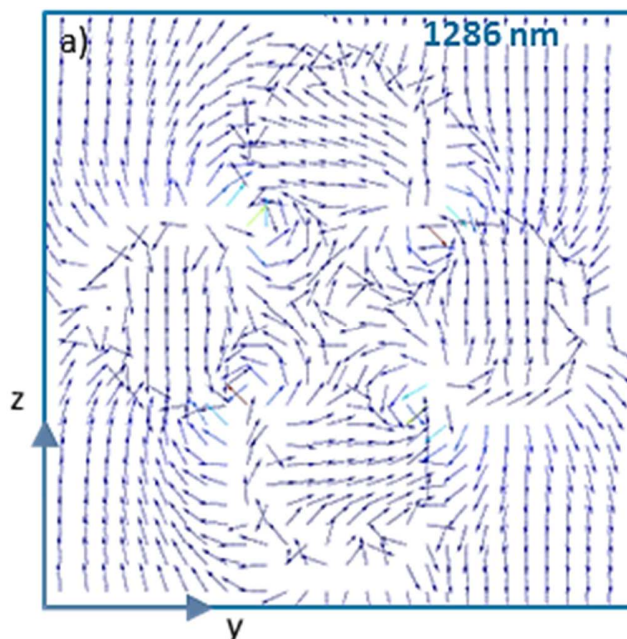


Figure 74: Simulated map of the electric field vector orientation in the (yz) plane at 1286 nm

Figure 74 presents a mapping of the electric field vector orientation in the yz plane considering the resonance band located at 1286 nm. The orientation of the electric field vectors clearly indicates that circulating current loop existed into the structure. Such behavior is typical for the magnetic dipole resonance. Moreover a representation of the magnetic field intensity at the center of the structure (**Figure 75**) indicated that beyond the pure magnetic dipole resonance (1286 nm) other modes could exhibit a magnetic contribution (510 nm and 643 nm).

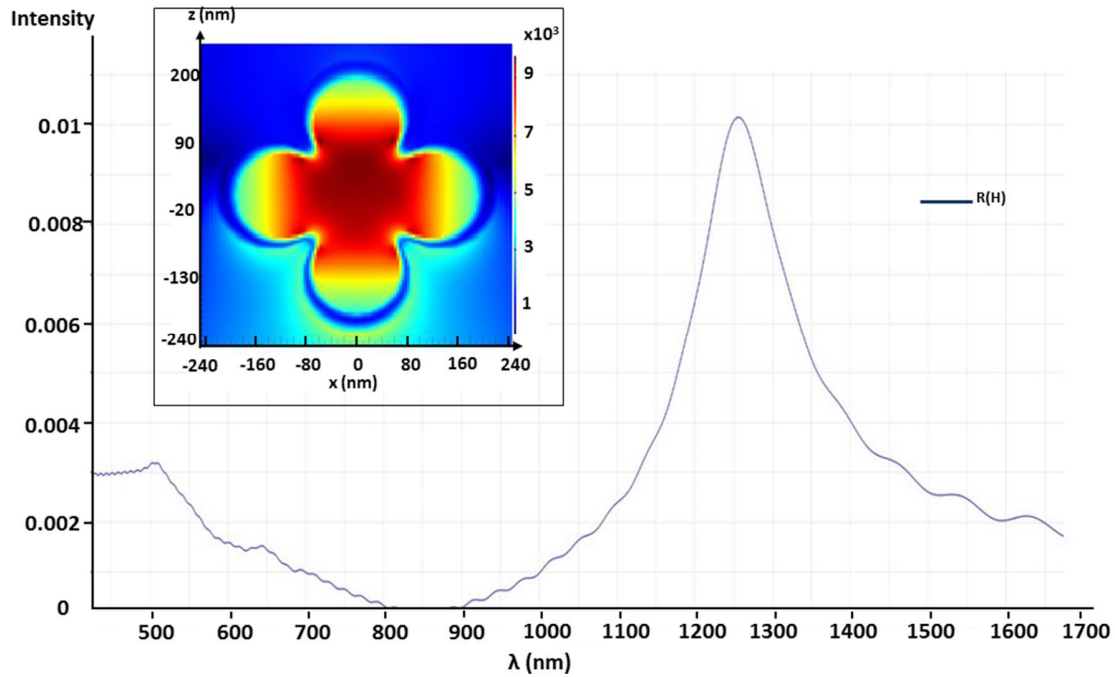


Figure 75: Simulated spectrum of the intensity of the magnetic resonance located at the center of the octahedral structure as a function of the wavelength; The insert presents the mapping of the magnetic field intensity at 1286 nm.

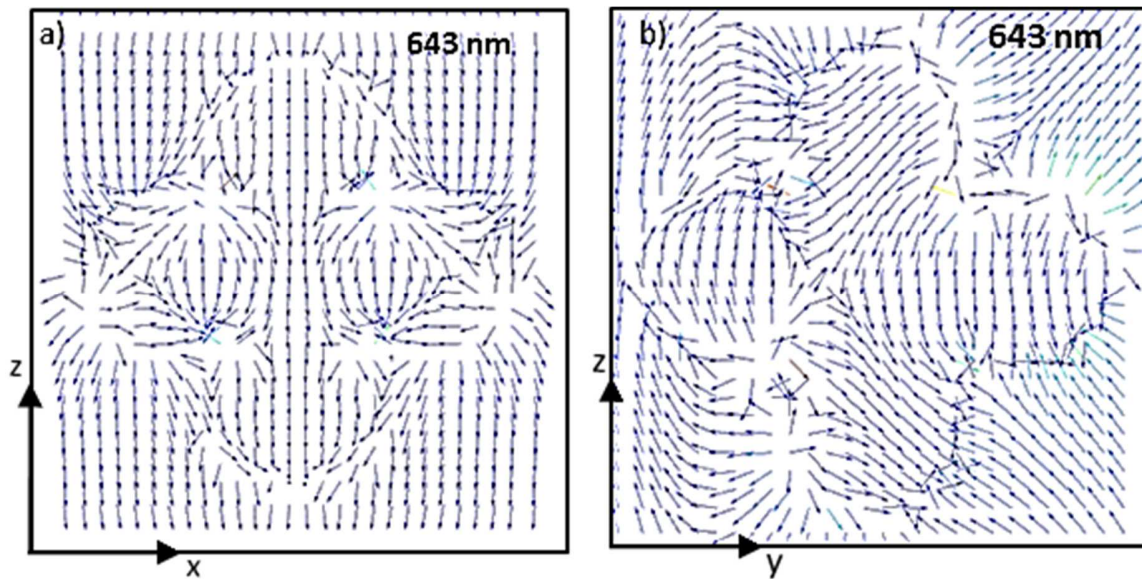


Figure 76: Simulated map of the electric field vector orientation for the resonance located at 643 nm in the (zx) plane a) and (zy) plane b).

A simulated map of the electric field vector orientation is presented on **Figure 76**. This mapping showed that an electric field vector orientation, typically observed for multipolar mode existed in the (zx) plane. In that particular case, this mode was suspected to induce a weak multipolar magnetic contribution in the (zy) plane where circulating current loops were visible.

According to those preliminary calculations, the optical response of such a nanocluster showed that the electric and the magnetic responses should be observable with the experimental setup available in the laboratory. **Figure 73** and **Figure 76b** present the electric field vector orientation in the plane orthogonal to the magnetic field (zy) both representations showed that circulating currents existed around the cluster. This result was typical for closely packed plasmonic particles forming a circular loop. Indeed, such a cluster can be considered as a combination of nano-inductors (the satellites) separated by nano-capacitors (the gap between them). This kind of circular current loop would be responsible of the magnetic resonance induced in the normal plane of the electric field.

Simulation results concerning octahedral nanoclusters made of silver nanoparticles (about 27 nm in diameter) were also reported by Alù and Engheta where a magnetic dipole was expected at shorter wavelength (about 500 nm).[10] Those simulations also predicted electric current loops surrounding the cluster. The authors presented simulations carried out for plasmonic nanoclusters made of 6 silver nanoparticles arranged with an octahedral geometry around a central dielectric core. This kind of structures can be seen as the optical or IR equivalent meta-atoms equivalents to those used for GHz frequencies (cubic SRR).[17] Furthermore, such plasmonic nanoclusters are isotropic and orientation independent meta-atoms. The magnetic field maximum intensity (red area) of **Figure 75** represented in the xz plane at 1286 nm was located at the center of the structure. Several investigations reported simulation experiments highlighting the presence of magnetic dipole resonance at the center of isotropic plasmonic meta-atoms (tetrahedra, icosahedra and raspberry-like).[18]–[20]

3 Optical response of a single nanocluster

Preliminary results were obtained on nanoclusters from sample 25 (**Figure 67**) from chapter 3. Diluted colloidal solutions of the nanoclusters were first prepared and a drop was deposited and dried on "finder" grids. The "finder grids" contained annotated squares and were covered by a thin layer of Formvar, a hydrophobic polymer.

Protocol 36: Single object spectroscopy sample preparation.

*10 μ L of a dispersion of gold octahedral clusters as obtained after **Figure 67** is introduced in an Eppendorf and 450 μ L of ultrapure water are added. The dispersion is homogenized using vortex and ultrasonic bath. 3 μ L of this suspension is deposited on a labelled Formvar TEM grid and left to dry. Afterwards, the sample is observed by TEM and isolated clusters are targeted. Their locations are identified using the tag of the labelled grid. A series of TEM picture at several magnifications (from the highest to the*

lowest) are taken. Those pictures are subsequently used to track down the clusters when the sample is observed under optical microscope.

Figure 77 shows a series of typical TEM images used for locating the nanoclusters. Their relative x-y positions in the square of the "finder grid" were first identified. The different investigated grid windows were identified using their lettering and each one was mapped out optically. This investigation permitted detection of the particles present in the studied zone as well as their position.

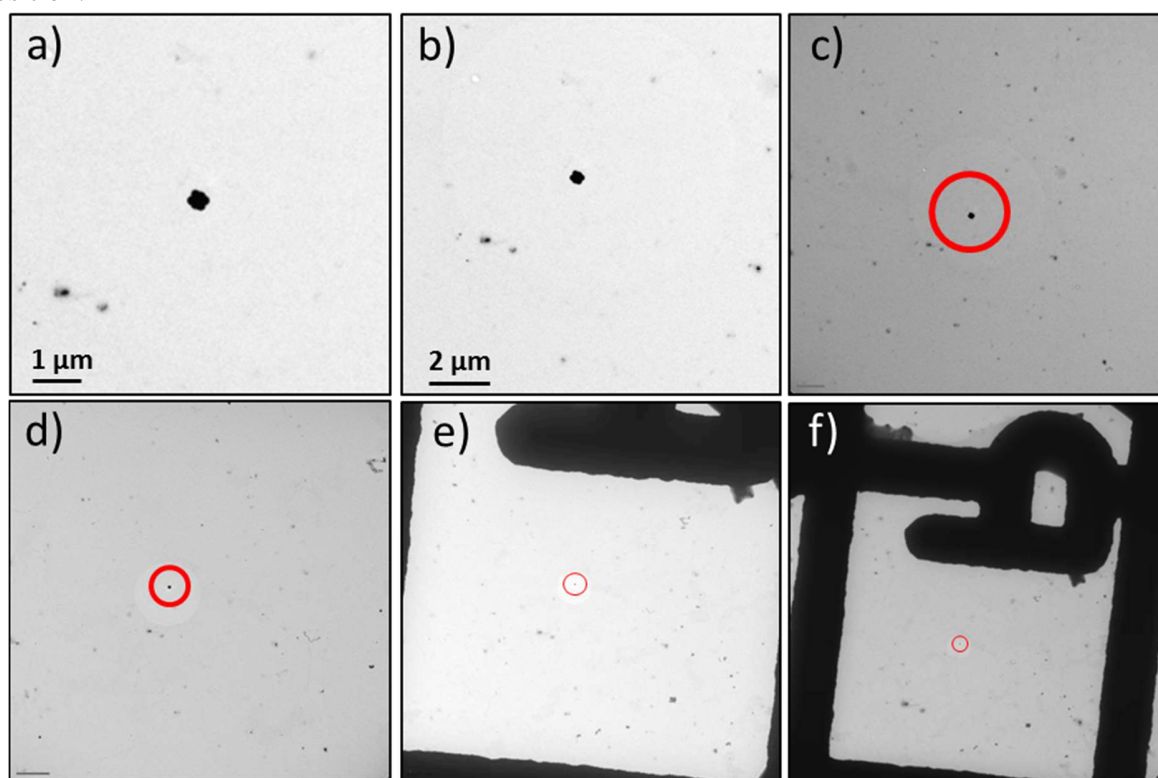


Figure 77: Series of TEM images of an octahedral cluster at various magnification a), b), c), d), e) and f) used for the targeting on labelled TEM grid. This cluster is tagged as P_L.

After identification of the relevant window and the relative position of the particle to the window corners, optical measurements were performed. Each particle had to be at least few microns away from anything that could interfere with the optical measurement, such as a grid bar, other cluster or particles.

Protocol 37: Single object dark field spectroscopy measurement.

A targeted TEM sample as prepared according to Protocol 36 is set on the sample stage of the dark field set up. The spectrometer is a LabRAM HR from Horiba Scientific used with an Olympus optical microscope, the sample stage is disposed on a motorized stage. The light beam from the condenser is focused on the grid and the angle between the incoming light and the sample plane is measured. The sample is set at the focal plane of the 50X objective and clusters are located using the tag. The aperture size is set at 50 μm. The surface area on which the signal is collected can be imaged by activating the

photodiode. The isolated targeted clusters have to be centered into this area. Sample measurements are performed then the same is done for background (typically an area of the Formvar film without any cluster deposited and also away from grid bar glare). Finally, a reference measurement is recorded using Spectralon® Diffuse Reflectance Standards from Labsphere. Depending on the wavelength range measured, two different detectors are used.

Typical spectra of nine different single octahedral nanoclusters are shown in **Figure 78**. The spectra were recorded without any polarizer or cross polarizer contrary to previous studies.[5]

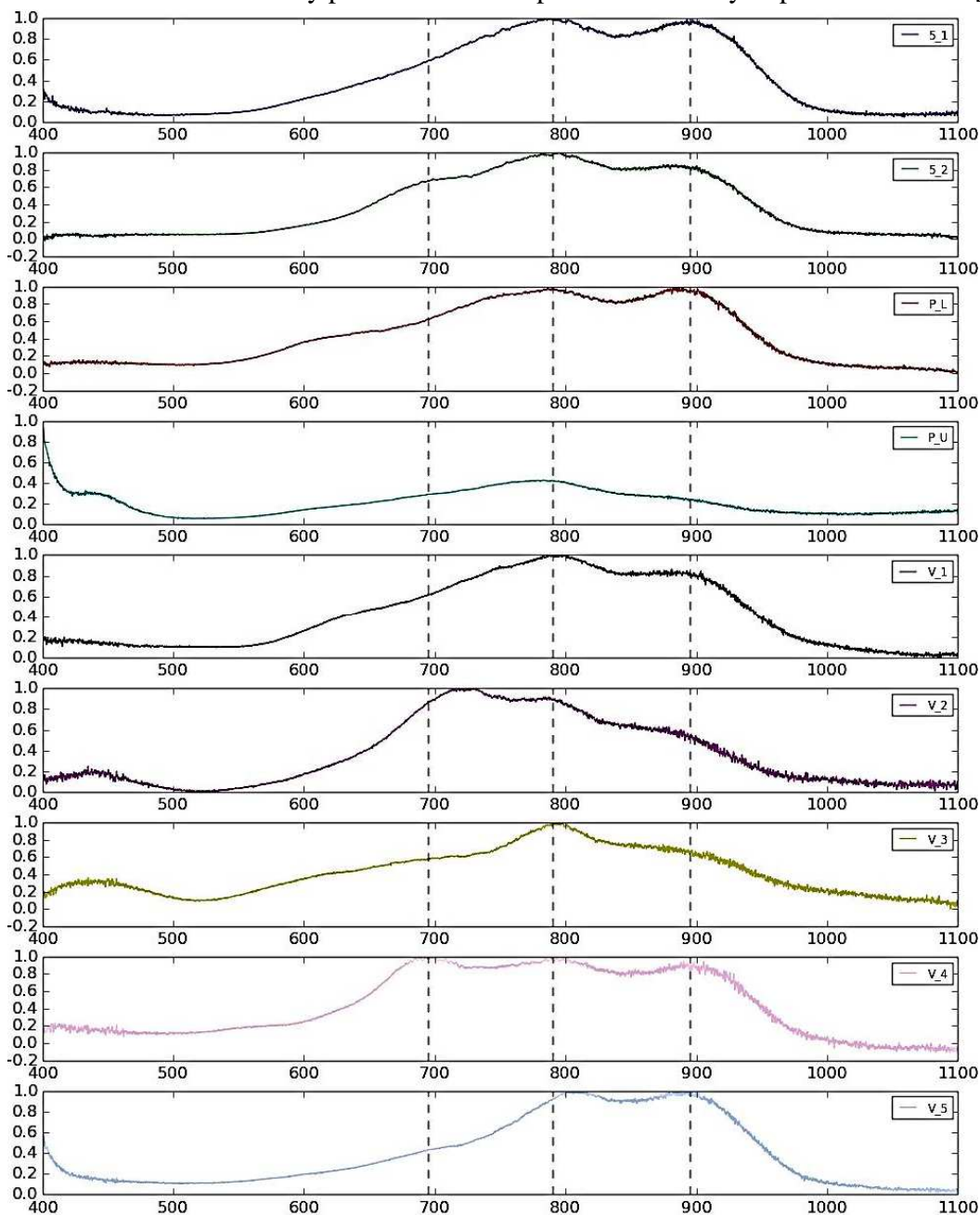


Figure 78: Dark field spectra measured without polarization for several isolated octahedral clusters; the intensities are normalized.

Spectra of nine clusters from the same batch present a similar optical response. They exhibit two bands and a shoulder in the range 600-900 nm. This confirms their isotropic character. This was consistent with the expectation for isotropic clusters since the spectra were reproducible from one cluster to another and that the spectra are orientation-independent since each cluster was oriented randomly with respect to the light source.

Moreover, the fact that the spectra were almost identical highlighted the isotropic features of the clusters and more especially the fact that the synthetic method yielded into clusters presenting reproducible spectra.

Several modes, not completely identified yet, are noticeable. Their clear identifications will require more extensive simulation work. However, according to the first simulations presented in the previous section the main resonance located around 910 nm could be attributed to the electric dipole resonance mode, while the other band and shoulder at about 780 nm and 680 nm respectively could be attributed to multipolar resonance.

4 Optical signature of a nanocluster in the near infra-red region

Measurement was performed on the cluster tagged as P_L (**Figure 77**) in the 400-1100 nm region using the CCD detector and in 1000-1400 nm region using InGaAs detector (**Figure 79**). The measurement obtained in the near infrared region shows a band around 1150 nm which may be attributed to a magnetic resonance according to the simulated results **Figure 75**.

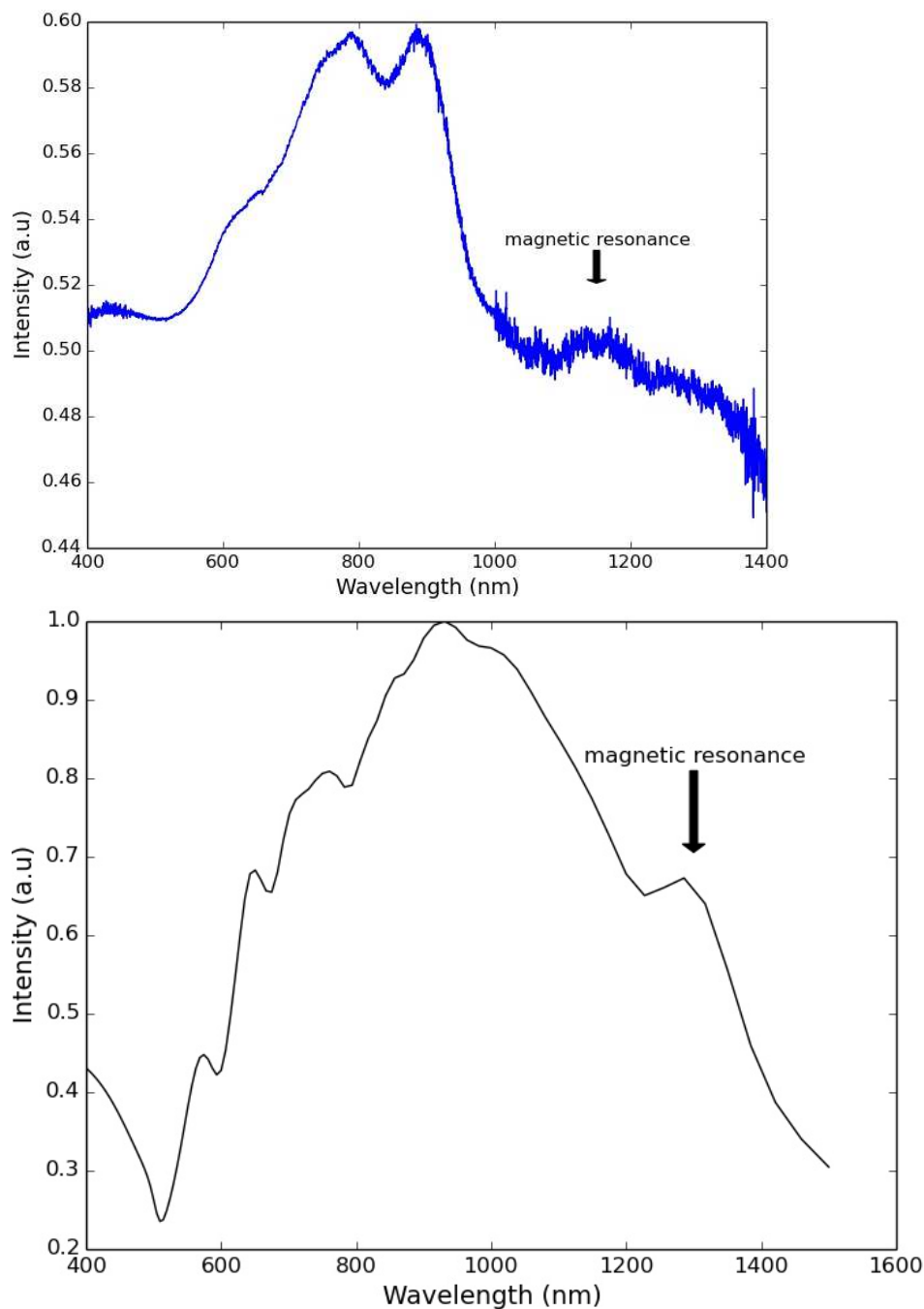


Figure 79: On top: Dark field spectra obtained for an isolated octahedral cluster (tagged as P_L) measured without polarization in the Vis-IR region. On the bottom: the simulated spectra for the corresponding structure.

5 Conclusion and perspectives

Dark field single object measurements on octahedral gold nanocluster exhibiting tight inter-satellites distances were performed. The results obtained on several clusters allowed us to confirm the isotropic nature of such clusters as well as their non-orientation dependence. The clusters exhibit a band around 910 nm assigned to an electric dipole mode while the smaller band

at 780 nm and the shoulder around 680 nm are assigned to multipolar modes. The clusters exhibit another band in the near infrared, at about 1150 nm, that may be attributed to a magnetic dipole resonance.

In the future, further simulation will have to be performed in order to confirm the origin of the different resonance modes observed. Moreover, optimizations of the experimental set up will have to be accomplished to improve the overall signal over noise ratio. Indeed, even using InGaAs IR-detector for the 1100-1400 nm range, the number of counts in the collected signal remains very low. This is one of the main drawbacks of the dark field IR-spectroscopy technique. To overcome such limitation, the use of light source presenting higher intensity in the IR could be envisioned. Moreover, changing the microscope optics for almost 100 % non-IR-absorbent ones could be helpful to improve the photons gathering. The use of oil immersion objectives seems to be a solution already implemented by some groups to avoid unexpected optical issues.[7], [21], [22]

Measurement of various batches of clusters presenting several interparticle distances will have to be performed. The coupling interactions depend on the separation gap between the satellites and consequently have a strong influence on the expected optical properties. In our system, a simple and convenient way to control the interparticle distance is to play with the gold shell thicknesses. However, it's important to take into account that the gold shell thickness usable for plasmonic purposes has to be larger than the skin depth of gold. Consequently, the range of gap accessible is determined by the size of the silica satellites on which gold is growing.

In the mean time, the studies on clusters presenting some irregularities will have to be conducted. Some of the octahedral clusters, prepared with our approach, present some irregularities, such as missing satellites, forming for example a three dimensional pentamer.[22] Other irregularities also exist, such as unexpected satellites positioning or size. Studying their effect on the optical properties could be of great importance, especially since large amount of clusters are required for metafluid applications. Indeed, from an experimental view point, obtaining exactly pure batches of ideal clusters is not realistic. However, quantifying the acceptable degree of imperfection[19], [20] for given target property is at the same time realistic and pragmatic and could be studied with our system.

6 References

- [1] N. Liu and H. Giessen, "Coupling effects in optical metamaterials.," *Angew. Chem. Int. Ed. Engl.*, vol. 49, pp. 9838–9852, 2010.
- [2] E. A. You, W. Zhou, J. Y. Suh, M. D. Huntington, and T. W. Odom, "Polarization-dependent multipolar plasmon resonances in anisotropic multiscale Au particles.," *ACS Nano*, vol. 6, pp. 1786–1794, 2012.

- [3] K. Kolwas and A. Derkachova, “Plasmonic abilities of gold and silver spherical nanoantennas in terms of size dependent multipolar resonance frequencies and plasmon damping rates,” *Opto-Electronics Rev.*, vol. 18, pp. 1–16, 2010.
- [4] J. Rodríguez-Fernández, J. Pérez-Juste, F. J. García de Abajo, and L. M. Liz-Marzán, “Seeded growth of submicron Au colloids with quadrupole plasmon resonance modes,” *Langmuir*, vol. 22, pp. 7007–7010, 2006.
- [5] J. Fan, C. Wu, K. Bao, J. Bao, R. Bardhan, N. J. Halas, V. N. Manoharan, P. Nordlander, G. Shvets, and F. Capasso, “Self-assembled plasmonic nanoparticle clusters,” *Science*, vol. 328, pp. 1135–1138, 2010.
- [6] J. Fan, Y. He, K. Bao, C. Wu, J. Bao, N. B. Schade, V. N. Manoharan, G. Shvets, P. Nordlander, D. R. Liu, and F. Capasso, “DNA-enabled self-assembly of plasmonic nanoclusters,” *Nano Lett.*, vol. 11, pp. 4859–4864, 2011.
- [7] A. S. Urban, X. Shen, Y. Wang, N. Large, H. Wang, M. W. Knight, P. Nordlander, H. Chen, and N. J. Halas, “Three-dimensional plasmonic nanoclusters,” *Nano Lett.*, vol. 13, pp. 4399–4403, 2013.
- [8] S. N. Sheikholeslami, H. Alaeian, A. L. Koh, and J. A. Dionne, “A Metafluid Exhibiting Strong Optical Magnetism,” *Nano Lett.*, vol. 13, pp. 4137–4141, 2013.
- [9] F. Monticone and A. Alù, “Strong Optical Magnetism and Fano Resonances in Asymmetric Plasmonic Metamolecules,” pp. 492–493, 2013.
- [10] A. Alù and N. Engheta, “The quest for magnetic plasmons at optical frequencies,” *Opt. Express*, vol. 17, pp. 5723–5730, 2009.
- [11] J. B. Lassiter, H. Sobhani, M. W. Knight, W. S. Mielczarek, P. Nordlander and N. J. Halas “Designing and Deconstructing the Fano Lineshape in Plasmonic Nanoclusters,” *Nano Lett.*, pp. 1058–1062, 2012.
- [12] F. Shafiei, F. Monticone, K. Q. Le, X.-X. Liu, T. Hartsfield, A. Alù, and X. Li, “A subwavelength plasmonic metamolecule exhibiting magnetic-based optical Fano resonance,” *Nat. Nanotechnol.*, vol. 8, pp. 95–99, 2013.
- [13] J. Fan, K. Bao, C. Wu, J. Bao, R. Bardhan, N. J. Halas, V. N. Manoharan, G. Shvets, P. Nordlander, and F. Capasso, “Fano-like interference in self-assembled plasmonic quadrumer clusters,” *Nano Lett.*, vol. 10, pp. 4680–4685, 2010.
- [14] A. Liu, A. Rahmani, G. W. Bryant, L. J. Richter, and S. J. Stranick, “Modeling illumination-mode near-field optical microscopy of Au nanoparticles,” *J. Opt. Soc. Am. A*, vol. 18, p. 704, 2001.
- [15] J. J. Mock, M. Barbic, D. R. Smith, D. A. Schultz, and S. Schultz, “Shape effects in plasmon resonance of individual colloidal silver nanoparticles,” *J. Chem. Phys.*, vol. 116, p. 6755, 2002.

- [16] A. M. Michaels, M. Nirmal, and L. E. Brus, "Surface Enhanced Raman Spectroscopy of Individual Rhodamine 6G Molecules on Large Ag Nanocrystals," pp. 9932–9939, 1999.
- [17] J. D. Baena, L. Jelinek, and R. Marqués, "Towards a systematic design of isotropic bulk magnetic metamaterials using the cubic point groups of symmetry," *Phys. Rev. B*, vol. 76, p. 245115, 2007.
- [18] Y. A. Urzhumov, G. Shvets, J. Fan, F. Capasso, D. Brandl, and P. Nordlander, "Plasmonic nanoclusters: a path towards negative-index metafluids.," *Opt. Express*, vol. 15, pp. 14129–14145, 2007.
- [19] A. Vallecchi, M. Albani, and F. Capolino, "Collective electric and magnetic plasmonic resonances in spherical nanoclusters.," *Opt. Express*, vol. 19, pp. 2754–2772, 2011.
- [20] A. Vallecchi, M. Albani, and F. Capolino, "Effect of irregularities of nanosatellites position and size on collective electric and magnetic plasmonic resonances in spherical nanoclusters.," *Opt. Express*, vol. 21, pp. 7667–7685, 2013.
- [21] N. Pazos-Perez, C. S. Wagner, J. M. Romo-Herrera, L. M. Liz-Marzán, F. J. García de Abajo, A. Wittemann, A. Fery, and R. A. Alvarez-Puebla, "Organized plasmonic clusters with high coordination number and extraordinary enhancement in surface-enhanced Raman scattering (SERS).," *Angew. Chem. Int. Ed. Engl.*, vol. 51, pp. 12688–12693, 2012.
- [22] S. J. Barrow, X. Wei, J. S. Baldauf, A. M. Funston, and P. Mulvaney, "The surface plasmon modes of self-assembled gold nanocrystals.," *Nat. Commun.*, vol. 3, pp. 1–9, 2012.

Conclusion and future work

1 Main achievements

The main objective of this work was to synthesize and study isotropic plasmonic meta-atoms for optical metamaterials application. The main tasks were the design and the synthesis of plasmonic nanoclusters with an accurate control of their morphology, as well as the subsequent measurement of their optical properties. Our strategy consisted in the use of patchy silica particles and their combination with gold satellites to get isotropic multipod-like clusters for tuning their plasmonic response and validating the results of numerical simulations reported by others.

We first checked that the use of silica/PS clusters as precursors proposed by Désert and coworkers was a suitable route for fabricating dimpled particles at the gram scale with a good control over the dimple number and positions. Then, we showed how to activate the PS bumps at the bottom of the dimples for making them sticky to gold colloids. The main achievements and lessons to be learnt from this preliminary work concerned:

- the control to the nanometer of the silica cores regrowth;
- the high efficiency of the conversion of silica/PS multipod-like clusters into dimpled particles making only the emulsion polymerization stage limiting for controlling the number of dimples per particle;
- the mandatory role of the copolymerizable methacrylate group of the MMS grafts for getting residual PS bumps at the bottom of the dimples;
- the estimation of the average molar masses and average amount of PS constituting the bumps;
- the efficient amination and thiolation of these PS macromolecules, even though the yield of these stages remained unquantified.

Then, we investigated the site-specific and seed-mediated growth of gold satellites within these activated dimples. Two types of interactions in between the PS bumps and the gold seeds were investigated: covalent-like bonding from thiolated bumps or electrostatic interactions from aminated bumps. The former was rapidly disregarded for stability reasons while the latter offered the possibility to generate stable and uniform plasmonic nanoclusters with large well-located gold satellites. Their final size was controlled through the amount of the gold plating solution and the site-specificity of the deposition growth was optimized through the preliminary “passivation” of the inter-patch surface area. Because of the lack of control over their morphologies, which were as oblate spheroids, the satellites were reshaped thanks to a successful iterative etching/regrowth post-treatment performed at ambient temperature applied for the very first time on supported gold colloids. This approach allowed to fabricate silica/gold tetrapod-like, hexapod-like and dodecapod-like clusters which were hitherto unseen nanoparticles. Nevertheless, the inter-satellite gap remained difficult to control because achieving a tight distance would need a large number of the iterative etching/regrowth post-treatment stages, increasing the risk of the definitive detachment and loss of one or several satellites.

A more successful alternative was found through the preliminary assembly of silica satellites in every dimple and the site-specific growth of a gold shell on each of these satellites. For that purpose, we took advantage of the aminated PS macromolecules within the dimples and their ability to be extended in a good solvent such as DMF for creating efficiently peptide-like bonds with the silica satellites previously surface-modified with carboxylic acid groups. We evidenced the importance of the surface modification conditions and the use of a high satellite concentration and high satellite-to-core particles ratios. The silica satellites attached to the patches were derived into plasmonic silica@gold ones, by taking advantage of the sharp discrepancy in term of surface chemistry existing in between the silica satellites and silica cores. The optimal results were achieved when the inter-patch surface area was passivated prior to the assembly step. By an appropriate choice of satellite-to-core size ratio as well as gold layer thickness, we demonstrated the possibility to obtain plasmonic nanoclusters with a tight gap between the core@shell satellites.

Because of the unavoidable geometrical, structural and compositional dispersions of such synthesized plasmonic nanoclusters, interpretation of the measured optical properties and their modeling could only be performed on single nanoparticle. One measured the linear optical properties of a ten of cluster by dark field spectroscopy. Such investigation avoided the statistical effects and allowed to get a precise determination of the fundamental mechanisms at the origins of the observed properties (the spectral characteristics (wavelength and linewidth) of the individual clusters). The morphology of the each individual cluster has been determined by TEM. The results have been interpreted with a numerical model using the TEM measured characteristics of the particles as an input. The results reveal a fairly weak polarization dependence of the optical signature of the nanoclusters confirming their isotropic characteristics.

Dark field single-object measurements on octahedral gold nanoclusters presenting tight inter-satellite gaps were performed. The results obtained on a significant number of clusters (nine) allowed noticing a non-orientation dependence of the optical measurement confirming the isotropic nature of such clusters and consequently the efficiency of the synthetic pathway to produce homogeneous batches of clusters. Moreover, the acquisition of those spectra combine with the simulation work allowed to assign the several electric modes (dipolar and multipolar) in the visible and near IR ranges. The first measurements in the infra-red region with InGaAs detector (1100-1400 nm) evidenced a band that could be assigned to the magnetic dipole resonance.

Optical measurements were performed on single objects, because the composition of the batches of silica/gold multipod-like clusters were too complex, due to the accumulation of side-products at almost each step. The main improvements to be considered will consist in restricting the variability and amounts of these side-products and/or intercalating efficient purification stages. With regard to the more efficient route which was through the intermediary step of silica satellite assembly, optimization efforts should be focused on:

- the synthesis of the precursor silica/PS multipod-like clusters, whose purity was hitherto restricted to 80 %. This value could be certainly overreached through a rationalization of the experimental conditions of the seeded-growth emulsion polymerization step by using a predictive model, which is *a priori* capable to help in tuning the monomer concentration, SDS fraction in the surfactant mixture, silica seed concentration, monomer-to-polymer conversion, *etc.* for optimizing the morphology yield;[1]

- the assembly stage between the dimpled silica particles and silica satellites, which requires a high excess of silica satellites. A systematic study supported by extensive statistical analysis should help in finding the best conditions for completing the assembly in every dimple, *i.e.* minimizing the formation of incomplete silica/silica clusters, by using a minimal amount of silica satellites, whose excess fraction constituted also a large source of side-products, *i.e.* free silica@gold particles in the final batches. For instance, improving the PS modification could be of great help to get more efficient coupling reactions. Moreover, there will be also a great interest in developing a numerical model for predicting the optimal conditions for the assembly in terms of particle concentration, addition order, contact time, temperature, *etc.*;

- the implementation of sorting steps, which could obviously be of great help to reach higher batch purity. The technique of centrifugation in density gradient would be a relevant method for the fractionation of the silica/PS clusters – before or after the silica regrowth stage – because of the expected difference of apparent densities of each cluster type.[2] For sorting the silica/silica clusters, a viscosity gradient could be preferred – even if viscosity and density are most of the time strongly related in aqueous solutions.[3] Indeed, it could be taken advantage of the discrepancy of friction forces.

Extension to combination of dark field spectroscopy with TEM tomography is also very promising as a more precise particle characterization would be obtained. Moreover, studying the effect of the substrate on the optical properties would be necessary to go deeper in the comprehension of the system.

Beyond these optimization propositions, similar measurements in silver based nanoclusters would be particularly interesting as it would permit to improve the optical properties. From a chemical viewpoint, it would essentially alter the last steps, and it seems that the transposition could be easy. Moreover, PS macromolecules could be easily derivatized for getting other chemical functionalities and therefore allowing other coupling strategies such as click-chemistry, thiol-ene chemistry, DNA-strand coupling, *etc.*

Concerning the dark-field spectroscopy, the next step is to accumulate measurements on the as produced clusters in the range of wavelength where magnetic dipole is expected. For that, overcoming the low signal to noise ratio obtained in the IR is the next challenge. The use of IR-transparent optics or oil immersion objectives - depending on which offer the best results - coupled with longer acquisition time using InGaAs detector could be the solution. Once those

measurement conditions optimized, the optical properties of various batches of clusters exhibiting several intersatellites gap could be investigated. Moreover, studying the effect of clusters irregularities could be also possible.

From a more conceptual viewpoint, this study showed that it is possible to design and fabricate particles whose patches are simultaneously enthalpic and entropic. However, we just barely evidenced that purely entropic or purely enthalpic patchy particles were also obtainable depending on how the derivatization of the silica/PS clusters are performed. Purely enthalpic patches could be also produced by reversing the PS satellite dissolution and silica regrowth steps. Moreover, we showed that AMS could be used instead of MMS to activate silica seeds prior to the emulsion polymerization step to obtain dimpled silica particles with any PS bump. In that situation, the as-obtained “empty” dimples could be considered as purely entropic patches. This should also open a new avenue for getting non-discrete assemblies such as 3-D arrays.[4], [5].

2 References

- [1] A. Thill, A. Désert, S. Fouilloux, J.-C. Taveau, O. Lambert, M. Lansalot, E. Bourgeat-Lami, O. Spalla, L. Belloni, S. Ravaine, and E. Duguet, “Spheres growing on a sphere: a model to predict the morphology yields of colloidal molecules obtained through a heterogeneous nucleation route.,” *Langmuir*, vol. 28, pp. 11575–83, 2012.
- [2] V. N. Manoharan, T. E. Mark, and D. J. Pine, “Dense packing and Symmetry in Small clusters of microspheres,” *Science*, vol. 301, pp. 483–487, 2003.
- [3] P. Qiu and C. Mao, “Viscosity Gradient as a Novel Mechanism for the Centrifugation- Based Separation of Nanoparticles,” *Adv. Mater.*, vol. 23, pp. 4880–4885, 2011.
- [4] G. Van Anders, N. K. Ahmed, R. Smith, M. Engel, and S. C. Glotzer, “Entropically Patchy Particles: Engineering Valence through Shape Entropy,” *ACS Nano*, vol. 8, pp. 931–940, 2014.
- [5] F. Smallenburg and F. Sciortino, “Liquids more stable than crystals in particles with limited valence and flexible bonds,” *Nat. Phys.*, vol. 9, pp. 554–558, 2013.

Appendices

1 Appendix: characterization techniques

1.1 UV-Visible spectroscopy

Metal nanoparticles exhibit specific color and resonance modes in the visible range. UV-visible spectroscopy provides valuable information regarding size, shape and aggregation of nanoparticles. The absorption spectra were recorded in the range of 300-1300 nm with an UV-3600 Shimadzu UV-Vis-NIR spectrophotometer. Ten-mm optical path length plastic or quartz cells were used. The data were recorded and treated with the UVProbe software.

1.2 Diffuse Reflectance Infrared Fourier Transform Spectroscopy (DRIFT)

The DRIFT spectroscopy allows to characterize the different species adsorbed and/or grafted on the surface of the nanoparticles by measuring the bending and stretching vibrations of the bonds when they are excited by an infrared beam. These vibrations produce bands in well-defined regions characteristic of specific class of compounds. A volume of the as-modified PS or silica nanoparticles suspension was dried at 100 °C. 9 mg of the dried sample were added to 281 mg of desiccated KBr (spectroscopy grade). The mixture was grinded in an agate mortar and the powder was deposited on the conical sample holder. The sample was then introduced into the Bruker IFS Equinox 55 spectrometer and the measurements were performed in a Selector Graseby Specac reflection cell. After 30 min of degassing, the infrared spectrum was recorded by the acquisition of 120 measurements with a resolution of 2 cm⁻¹.

1.3 Energy-dispersive X-ray Spectroscopy (EDX)

The composition of the patchy particles surface was evaluated by EDX spectroscopy. This technique allowed to determine the qualitative elementary composition of the sample by investigating its emitted X-ray spectrum when it is excited with a focused electron beam. All elements can be detected since each one has a unique atomic structure allowing unique set of peaks on its X-ray spectrum. The energy of the X-rays photons resulting from the electron transitions between inner orbits (K, L or M) is typical for each element. The number and energy of the X-rays emitted from the sample are measured by an energy-dispersive spectrometer. An element distribution image or “map” can be produced by scanning the sample with the incident beam.

1.4 Implementation of the TEM, HRTEM, STEM, EDX

The conventional TEM experiments were performed on a Philips CM20 microscope operating at 75 kV at the Centre de Recherche Paul Pascal (CRPP, Pessac), on a Hitachi H7650 microscope operating at an acceleration voltage of 80 kV at the Bordeaux Imaging Center (BIC, Bordeaux) and on a FEI Tecnai Cryo-Bio 200KV FEG at the center for nanoscale system (CNS) at Harvard. The HRTEM, STEM and EDX analyses were performed with a JEOL 2200FS microscope operating at 200 kV at the Plateforme de Caractérisation des

Matériaux d'Aquitaine (PLACAMAT). For EDX analysis, a 1-nm probe was used in the bright field STEM mode and the Analysis program software from JEOL was used. All the samples characterized by TEM and STEM were prepared as follow: one drop of the colloidal solution was deposited on carbon-coated copper grids. The particles were dried on the grid and placed in a box away from dust.

1.5 Scanning Electron Microscopy (SEM)

The SEM was used to visualize the elaborated nanoclusters by scanning them with an electron beam. The primary electrons interact with the atoms of the sample surface, causing emission of energetic electrons which are collected by a detector producing an image. High Resolution SEM was performed with a JSM 6700F microscope at the PLACAMAT on a pretreated silicon wafer and on a Zeiss Ultra 55 at the (CNS). Firstly, the wafer was first cleaned in hydrofluoric acid solution (HF, 40 %, VWR Prolabo) during 5 min to dissolve the protective layer of silica. Then it was amply rinsed with deionized water. Finally, one drop of the nanoclusters suspension was deposited on wafer then dried on the support and placed in a box away from dust.

1.6 Zetametry

The ζ -potential measurements were performed on a Zeta Potential WALLIS from CORDOUAN Technologies. The device measure the electrophoretic mobility noted μ_e . The electrophoresis measurement principle is, by optical means, to measure the Doppler frequency shift generated by the speed of the particles. In such conditions, the speed direction is determined and knowing the electric field, the electrophoretic mobility is calculated (**Eq. 14**).

$$\vec{v}_{lim} = \mu_e \vec{E} \quad \text{Eq. 14}$$

The software calculate the ζ -potential as shown from the measured electrophoretic mobility with the dielectric constant ϵ , the viscosity η and b a constant (**Eq. 15**).

$$\zeta = b \mu_e \frac{\eta}{\epsilon} \quad \text{Eq. 15}$$

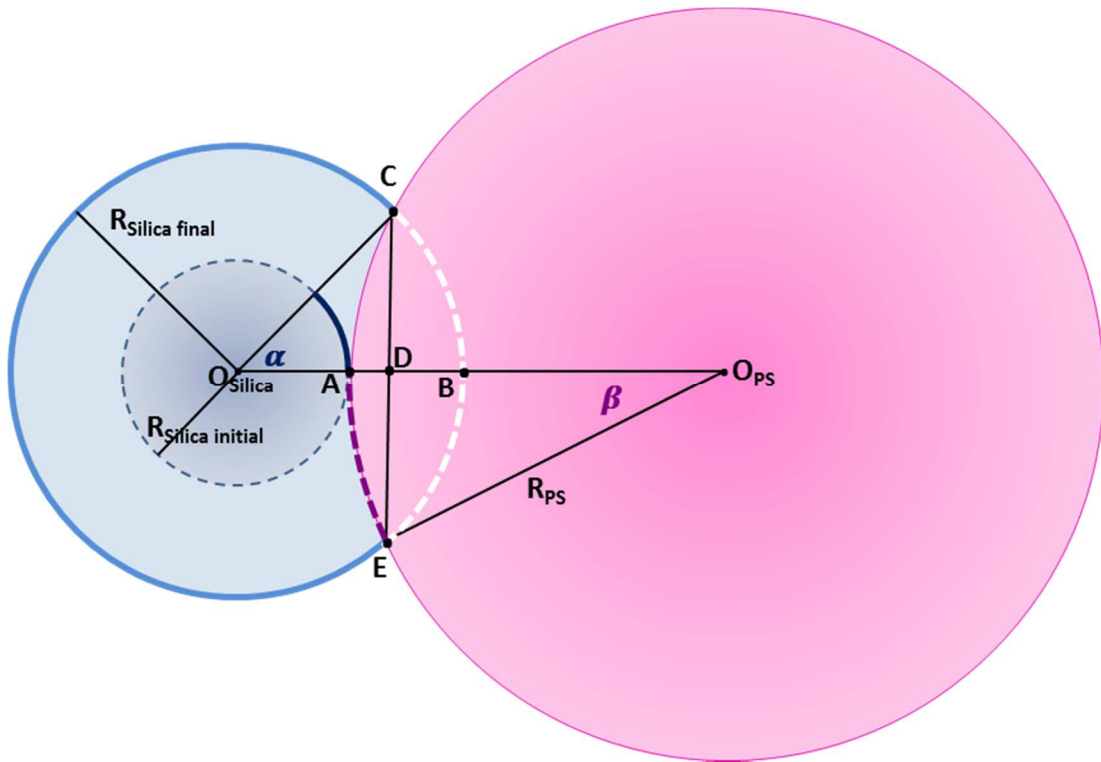
The samples were prepared as follow: A volume of 20 mL of the particle suspension in milliQ water was divided in two beakers. In the first, few drops of NaOH 1M were added into the sol to obtain high values of pH and samples of 4 mL were removed every 0.7 unity of pH. In the second, the same protocol was performed but this time by adding few drops of HCl 1 M to obtain low values of pH. The samples were injected in the cell of the zetameter at least 1 h after the sample preparation to ensure stabilization of pH. Finally, the pH of each sample was once again measured after analysis and this value was used to trace the curves.

2 Appendix: calculations used for protocol

2.1 Calculation of the TEOS volume required for silica regrowth

Scheme 27 represents a cross sectional view of a model cluster composed of one silica particle and one polystyrene particle.

Here, the point is to determine how much TEOS is needed to obtain a given silica size after regrowth. For that we need to calculate volume occupied by a PS nodule within the silica particle after silica regrowth. To do that and to simplify the calculation, the assumption is made that the PS and Silica surface are in tangential contact. In our system, the nominal amount of MMS function per nm² employed can provides some wettability. Indeed, the real contact angle value is rather around 160°.



Scheme 27: Section representing the geometrical configuration existing within the clusters during the silica growth.

For a given set of parameters noted $R_{Silica\ final}$: radius of the desired silica particle; $R_{Silica\ initial}$: radius of the initial silica beads; R_{PS} radius of the polystyrene nodules, the first task is to calculate the corresponding angle noted α and β by using **Eq. 16** and **Eq. 17**.

$$\alpha = \text{Acos} \frac{(R_{Silica\ final}^2 + (R_{Silica\ initial} + R_{PS})^2 - R_{PS}^2)}{2 \cdot (R_{Silica\ final} \cdot (R_{Silica\ initial} + R_{PS}))} \quad \text{Eq. 16}$$

The second part consists into the calculation of the lengths $[O_{PS}D]$ and $[O_{Silica}D]$ by using

$$\beta = \text{ACOS} \frac{(R_{PS}^2 + (R_{Silica\text{initial}} + R_{PS})^2 - R_{Silica\text{final}}^2)}{2 \cdot (R_{PS} \cdot (R_{Silica\text{initial}} + R_{PS}))} \quad \text{Eq. 17}$$

the previously determined value of α and β into the **Eq. 18** and **Eq. 19**.

$$[O_{PS}D] = \cos \beta \cdot R_{PS} \quad \text{Eq. 18}$$

$$[O_{Silica}D] = \cos \alpha \cdot R_{Silica\text{final}} \quad \text{Eq. 19}$$

The volume occupied by one nodule within the silica particle after growth can be seen as the sum of the two volumes noted V_{CBED} and V_{CAED} and can be calculated by using the **Eq. 20**.

$$V_{\text{occupied by one nodule}} = V_{CBED} + V_{CAED}$$

$$V_{CBED} + V_{CAED} = \left(\frac{4\pi R_{PS}^3}{3} - \pi \int_{-R_{PS}}^{O_{PS}D} (R_{PS}^2 - h^2) dh \right) + \left(\frac{4\pi R_{Silica\text{final}}^3}{3} - \pi \int_{-R_{Silica\text{final}}}^{O_{Silica}D} (R_{Silica\text{final}}^2 - h^2) dh \right) \quad \text{Eq. 20}$$

Considering one cluster, the volume of silica added corresponds to the volume of one sphere at the final size minus the volume of the initial silica bead and minus the volume occupied by all the polystyrene nodules within the silica as shown in **Eq. 21**.

$$V_{\text{Silica added per cluster}} = \left(\frac{4\pi R_{Silica\text{final}}^3}{3} \right) - \left(\frac{4\pi R_{Silica\text{initial}}^3}{3} + (N_{\text{nodules per cluster}} \cdot V_{\text{occupied by one nodules}}) \right) \quad \text{Eq. 21}$$

The amount of silica added per batch is calculated knowing the number of clusters in the considered volume of the polymerization solution and the volume of silica added per cluster (**Eq. 21**), as calculated in (**Eq. 22**) then the volume of TEOS required is calculated using **Eq. 23**.

$$V_{\text{Silica added per batch}} = V_{\text{Silica added per cluster}} \times N_{\text{Part Silica polym sol}} \quad \text{Eq. 22}$$

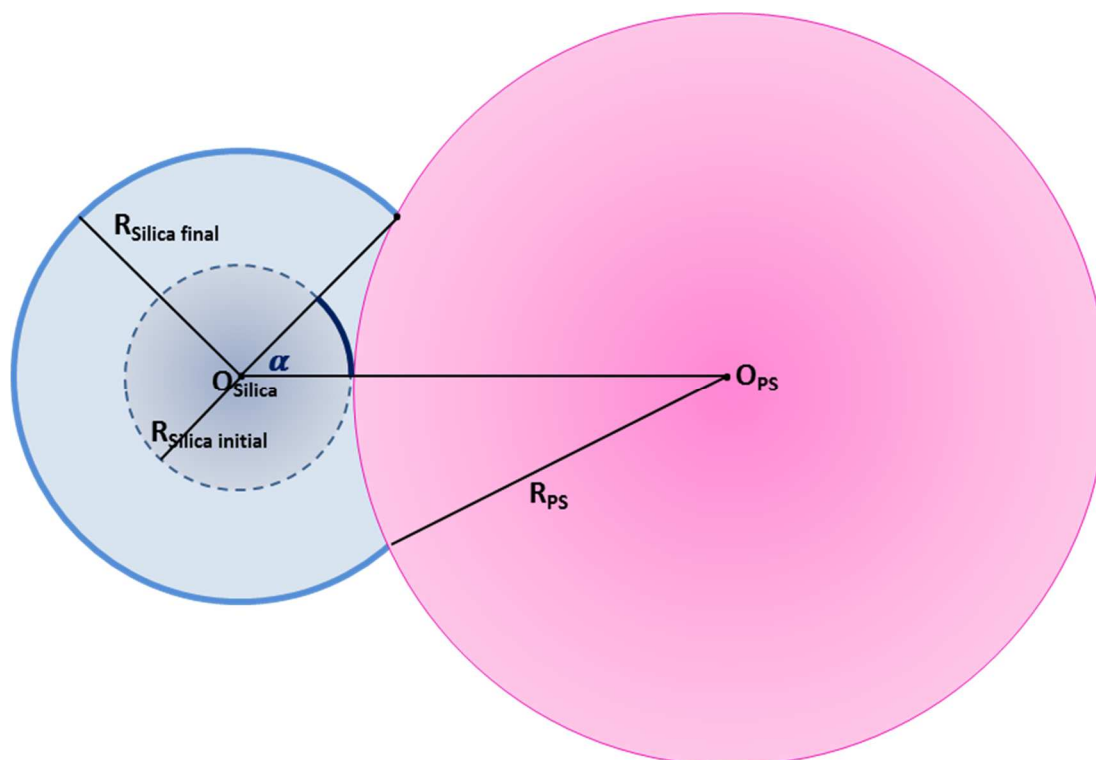
$$\frac{V_{\text{Silica added per batch}} \cdot M_{TEOS} \cdot \rho_{Silica} \cdot 1000 \cdot 1000}{M_{silica} \cdot \rho_{TEOS}} = V_{TEOS} \text{ in } \mu\text{L} \quad \text{Eq. 23}$$

The mass of one dimpled silica particle can be calculated knowing: the volume of silica added per cluster (**Eq. 21**) and the volume of initial silica core.

$$M_{\text{dimpled silica particle}} = (V_{\text{Silica added per cluster}} + \left(\frac{4}{3} \pi \cdot R_{Silica\text{initial}}^3 \right) \cdot \rho_{Silica}) \quad \text{Eq. 24}$$

2.2 Calculation of the inter-patch surface areas and the amount of coupling agent required for a given surface modification

Scheme 28 shows how to represent and determine the surface masked by one nodule. Once the α angle is determined –as previously described above- and so the solid angle can be calculated. In a second step, the surface of the silica masked by the nodules noted $S_{\text{solid angle}}$ is also calculated.



Scheme 28: Cross section representing the geometrical arrangement of the silica core and the PS before and after growth.

Eq. 25 is used to calculate the surface of the solid angle define at the surface of the regrowth silica particle. **Eq. 26** is used to calculate the functionalizable surface area per particle considering the numbers of polystyrene nodules and the radius of the silica particle after growth which is noted $R_{\text{growth Silica}}$. **Eq. 27** is used to determine the required amount of surface modification agent.

$$S_{\text{solid angle}} = R_{\text{growth Silica}}^2 \cdot 2\pi (1 - \cos \alpha) \quad \text{Eq. 25}$$

$$S_{\text{available}} = 4\pi R_{\text{growth Silica}}^2 - (N_{\text{PS}} \cdot S_{\text{solid angle}}) \quad \text{Eq. 26}$$

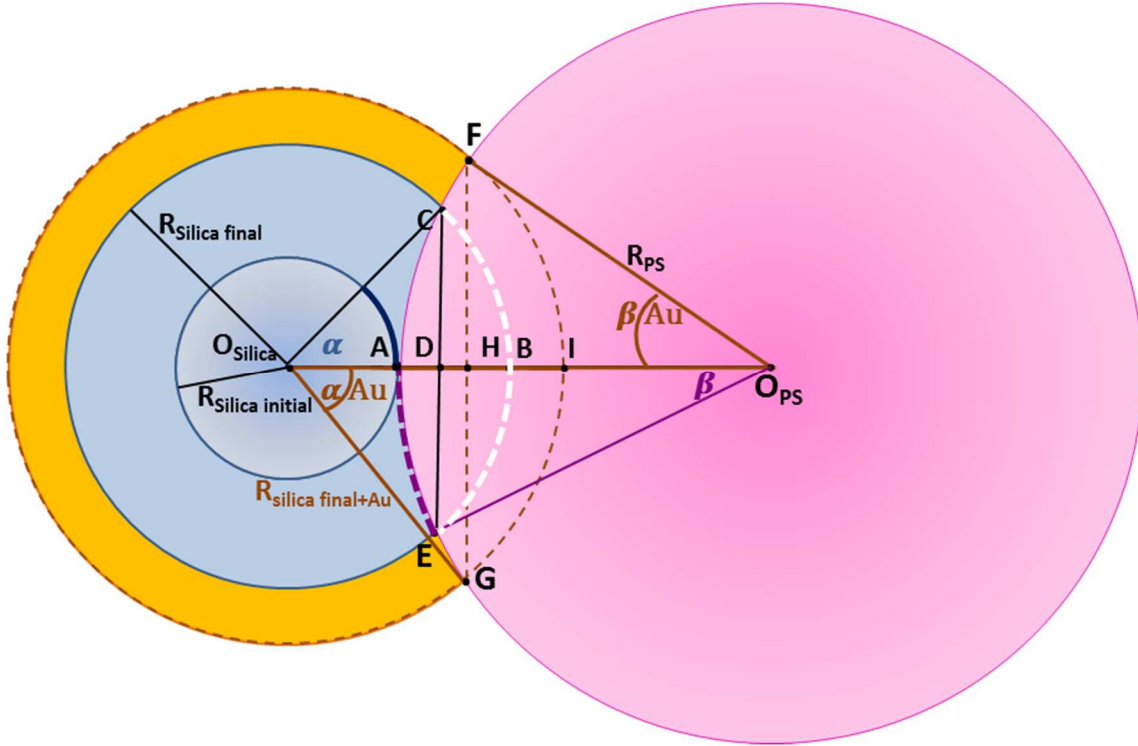
$$\text{Volume of modification agent} = \frac{(S_{\text{available}} \cdot N_{\text{Silica}})}{N_A} \cdot \frac{M_{(\text{modification agent})}}{\rho_{(\text{modification agent})}} \quad \text{Eq. 27}$$

M(APTES) = 221.37 g/mol ; ρ (APTES) = 0.946 g/mL (Sigma aldrich)

M (PTES) = 206.35 g/mol ; ρ (PTES) = 0.892 g/mL (Sigma aldrich)

2.3 Calculation of the amount of gold precursor required to grow a shell of a given thickness.

Scheme 29 is a representation in cross section of the arrangement of several part of the hybrid clusters: the initial silica part, the polystyrene nodules, the silica part after growth and the gold shell around. The approach was developed in the same spirit as the one for silica regrowth.



Scheme 29: Cross section representing the geometrical arrangement of the polystyrene nodule within the silica core after silica and gold growth.

$$\alpha_{Au} = \text{Acos} \frac{(R_{\text{Silica final+Au shell}}^2 + (R_{\text{Silica initial}} + R_{\text{PS}})^2 - R_{\text{PS}}^2)}{2 \cdot (R_{\text{Silica final+Au shell}} \cdot (R_{\text{Silica initial}} + R_{\text{PS}}))} \quad \text{Eq. 28}$$

$$\beta_{Au} = \text{Acos} \frac{(R_{\text{PS}}^2 + (R_{\text{Silica initial}} + R_{\text{PS}})^2 - R_{\text{Silica final+Au shell}}^2)}{2 \cdot (R_{\text{PS}} \cdot (R_{\text{Silica initial}} + R_{\text{PS}}))} \quad \text{Eq. 29}$$

The value $R_{\text{Silica final+Au shell}}$ corresponds to the radius of silica after silica growth and a desire shell thickness.

The value $R_{\text{Silica initial}}$ corresponds to the radius of the silica seeds and R_{PS} corresponds to the radius of the polystyrene nodules.

$$[O_{\text{PS}}H] = \cos \beta_{Au} \cdot R_{\text{PS}} \quad \text{Eq. 30}$$

$$[O_{\text{Silica}}H] = \cos \alpha_{Au} \cdot R_{\text{Silica final+Au shell}} \quad \text{Eq. 31}$$

$$V_{\text{occupied by one nodule}} = V_{\text{HFIG}} + V_{\text{GAFH}} \quad \text{Eq. 32}$$

$$V_{\text{Au not deposited per nodule}} = V_{\text{HFIG}} + V_{\text{GAFH}} - (V_{\text{ACDE}} + V_{\text{EDCB}}) \quad \text{Eq. 33}$$

$$\begin{aligned}
 V_{\text{Au not deposited per nodules}} &= \left(\frac{4\pi R_{\text{PS}}^3}{3} - \pi \int_{-R_{\text{PS}}}^{O_{\text{PS}}^{\text{H}}} (R_{\text{PS}}^2 - h^2) dh \right) \\
 &+ \left(\frac{4\pi R_{\text{Silica final+Au shell}}^3}{3} - \pi \int_{-R_{\text{Silica final+Au shell}}}^{O_{\text{Silica}}^{\text{H}}} (R_{\text{Silica final+Au shell}}^2 - h^2) dh \right) \\
 &- \left(\frac{4\pi R_{\text{PS}}^3}{3} - \pi \int_{-R_{\text{PS}}}^{O_{\text{PS}}^{\text{D}}} (R_{\text{PS}}^2 - h^2) dh \right) + \left(\frac{4\pi R_{\text{Silica final}}^3}{3} - \pi \int_{-R_{\text{Silica final}}}^{O_{\text{Silica}}^{\text{D}}} (R_{\text{Silica final}}^2 - h^2) dh \right)
 \end{aligned} \quad \text{Eq. 34}$$

$$V_{\text{Au added per cluster}} = \left(\frac{4\pi R_{\text{Silica final+Au shell}}^3}{3} \right) - \left(\frac{4\pi R_{\text{Silica final}}^3}{3} + (V_{\text{Au not deposited per nodule}} * N_{\text{nodules per cluster}}) \right) \quad \text{Eq. 35}$$

$$V_{\text{Au added per batch}} = V_{\text{Au added per cluster}} \times C_{\text{clusters with gold attached}} \quad \text{Eq. 36}$$

$$\frac{V_{\text{Au added per batch}} \cdot M_{\text{KAuCl}_4} \cdot \rho_{\text{Au}} \cdot 1000 \cdot 1000}{M_{\text{Au}}} = \text{mass of KAuCl}_4 \text{ in g} \quad \text{Eq. 37}$$

3 Appendix: synthesis of the chloromethylating agent

This reagent should obviously being inert regarding the silica surface from one side and active regarding the remaining polystyrene bumps on the other side. A good candidate for this work is the family of chloromethyl ether. Indeed, those compounds have a high reactivity. The synthesis of an alkyl chloromethyl ether typically involves reaction of an alkyl alcohol with paraformaldehyde and gaseous HCl. The reaction has to be performed at low temperature (5°C) in a chlorinated hydrocarbon solvent such as chloroform (**Figure 80**).^[1] In our work, for convenient reasons described in the previously mentioned paper, we chose to work with butan-1-ol. Indeed, the butan-1-ol is a primary alcohol and is made of chain long enough to not be volatile at ambient temperature making this reagent convenient to handle under lab conditions.

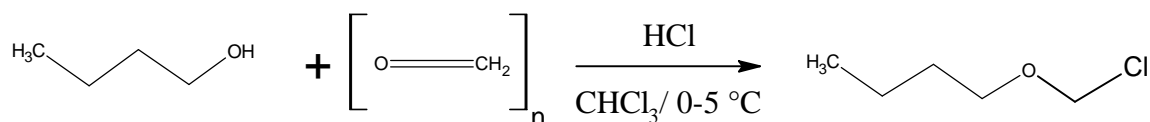


Figure 80: Scheme of the reaction involved in the synthesis of the chloromethylation agent.

Protocol 38: the synthesis of the chloromethylation agent.

This reaction is performed in a classical bubbling apparatus as shown on the **Figure 81**. Typically a large amount of CaCl_2 pellets are placed in a three-neck flask surmounted by a dropping funnel containing 37 % HCl in water. The flask is over a magnetic stirrer and a large magnetic stick is used to agitate the pellet. CaCl_2 ensured the dehydration of the aqueous HCl solution, in such a way that gaseous HCl is released, goes through the tube and bubbles into the solution of butan-1-ol and paraformaldehyde in chloroform. The amount of reactants are as following 1.05 equivalent of butan-1-ol for 1 equivalent of paraformaldehyde in term of monomer unit. The amount of solvent used is calculated in order to obtain a 3-M concentration of product in chloroform. The reaction is performed in a flask cooled down by an ice bath. The success of the reaction can be easily monitored by the disappearance of the paraformaldehyde crystal and the apparition of one equivalent of water forming an upper phase.

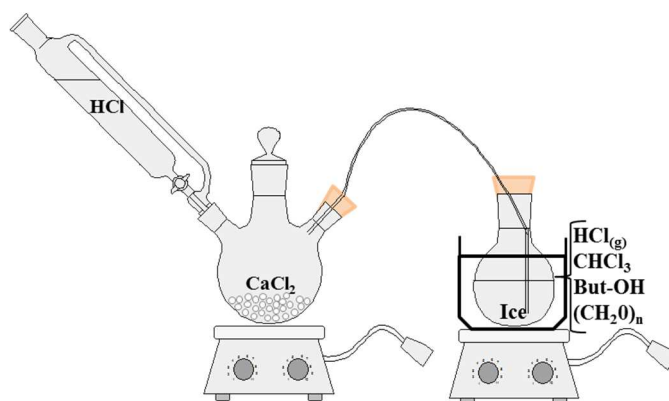


Figure 81: Scheme of the apparatus used for the synthesis of the chlorobutylether reagent.

4 Appendix: from gold nanoshells to nanocages

The improvements reported concerning the synthesis of a gold shell over the silica part of the silica/PS clusters led us to envision the production of more complex metallic nanostructures: gold nanocages exhibiting a controlled number of windows as well as rattle-type nanostructures. Such nano-objects present many opportunities for manipulating and controlling optical properties due to their strong SPR adjustable in the visible and the near infra-red part of the spectrum modifying the shell thickness and the presence of the hollow core. Through the sequential dissolution of the PS and the silica particles, gold nanocages with 4 windows could be, for example, produced. During my Ph.D thesis, two master students from the University of Bordeaux, Céline Hubert and Alexandra Madeira showed that gold nanocages with a higher number of windows could be produced as depicted in **Figure 82**.

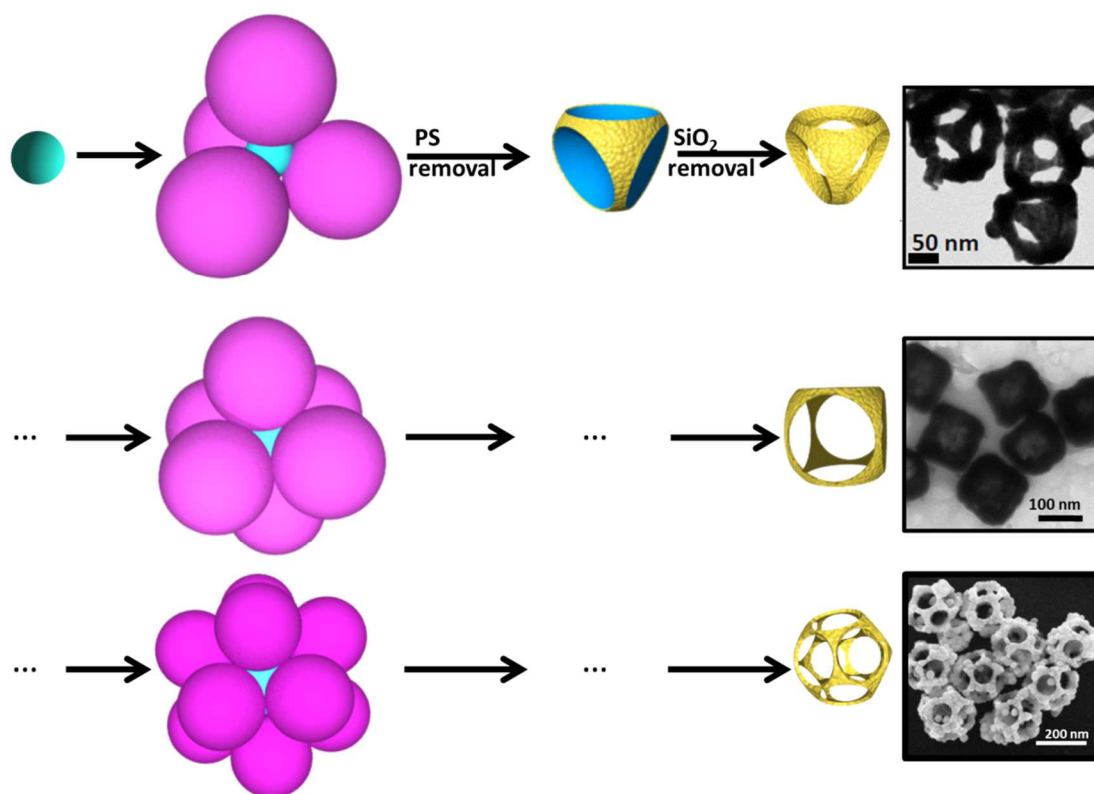


Figure 82: Scheme of the general strategies used to produce gold nanocages with a controlled number of windows and the corresponding TEM images.

Contrarily to the galvanic replacement approach which is mostly used in the literature to produce such metallic nanocages, the approach described here allows the fabrication of hollow particles with single metal shell with control of the windows. Both windows size and location could be accurately controlled via the control of the number and the mean diameter of the PS nodules which serve as temporary masks. This approach also offers the possibility to produce nanocages composed of noble as well as non-noble metallic system, even alloyed ones.

5 Appendix: dark-field spectroscopy

5.1 Geometrical construction used for the simulation

The simulations considering the batches of clusters presented on **Figure 67d** from chapter 3 were done for a structure built in the software considering the following features:

- Silica central core (0,0,0) radius 42.5
- Silica patchy structure (0,0,0) radius 100
- Silica satellite 1 (131,0,0) radius 67.5
- Silica satellite 2 (-131,0,0) radius 67.5
- Silica satellite 3 (0,131,0) radius 67.5
- Silica satellite 4 (0,-131,0) radius 67.5
- Silica satellite 5 (0,0,131) radius 67.5
- Silica satellite 6 (0,0,-131) radius 67.5
- Gold shell 1 (131,0,0) radius 90
- Gold shell 2 (-131,0,0) radius 90

- Gold shell 3 (0,131,0) radius 90
- Gold shell 4 (131,0,0) radius 90
- Gold shell 5 (0,0,131) radius 90
- Gold shell 6 (0,0,-131) radius 90

5.2 Series of TEM images used for the cluster targeting

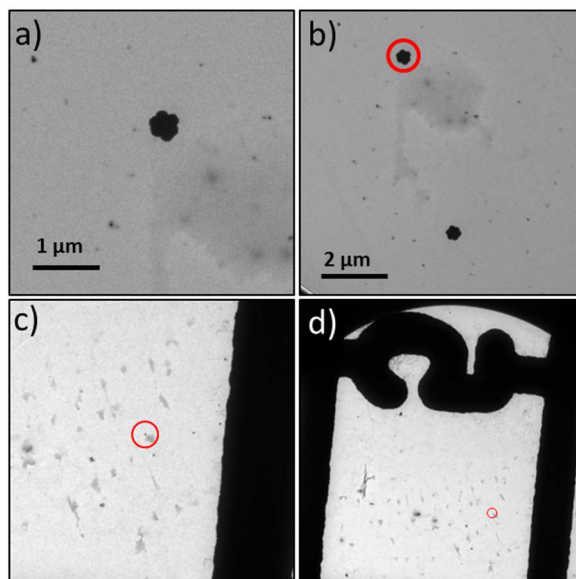


Figure 83: Series of TEM images of an octahedral cluster at various magnifications a), b), c), d) used for the targeting on labelled TEM grid. This cluster is tagged as 5_1.

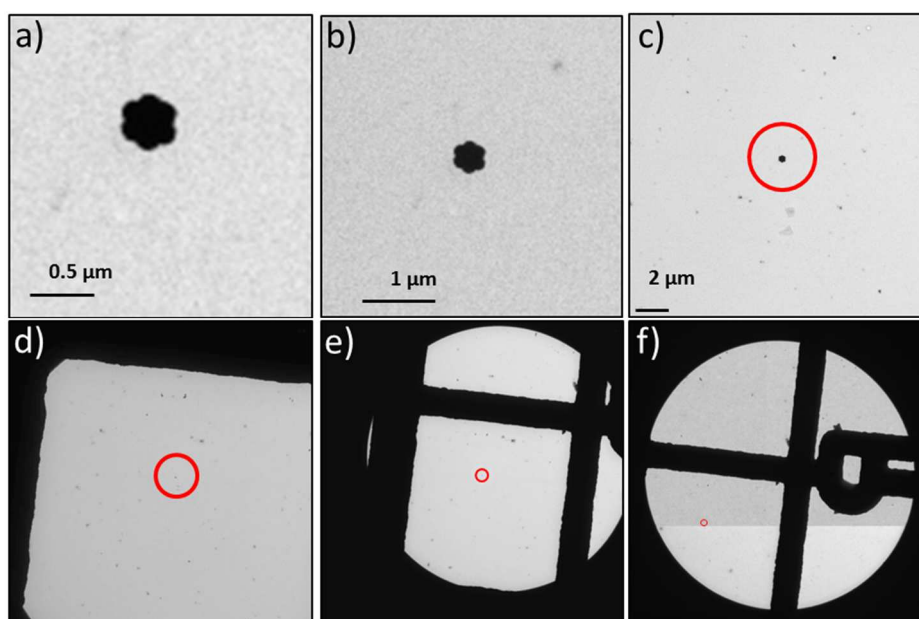


Figure 84: Series of TEM images of an octahedral cluster at various magnifications a), b), c), d) used for the targeting on labelled TEM grid. This cluster is tagged as P_U.

6 Appendix list of chemical

Name	Abbreviation	Chemical formula	Purity	Origin
Ascorbic acid		C ₆ H ₈ O ₆	99 %	Sigma-Aldrich
Aminopropyltriethoxysilane	APTES	C ₉ H ₂₃ NO ₃ Si	98 %	Sigma-Aldrich
Ammonia		NH ₄ OH	28-30 %	J.T.Baker
L-Arginine		C ₆ H ₁₄ N ₄ O ₂	99 %	Sigma-Aldrich
Butyl chloromethyl ether		C ₅ H ₁₁ Cl ₂	3 M in chloroform	Homemade
Cetyltrimethylammonium Bromide	CTAB	C ₁₉ H ₄₂ BrN	99 %	Sigma-Aldrich
Chloroauric acid		HAuCl ₄ (3 H ₂ O)	99.9 %	Sigma-Aldrich
Chloroform		CHCl ₃	99 %	Sigma-Aldrich
Dimethylformamide	DMF	C ₃ H ₇ NO	> 95 %	Sigma-Aldrich
Ethanol		C ₂ H ₆ O	99 %	Atlantic labo
Ethylchloroformate	ECF	C ₃ H ₅ ClO ₂	> 97 %	Sigma-Aldrich
Ethylene diamine		N ₂ H ₈ C ₂	99 %	Sigma-Aldrich
Ethylene glycol	EG	C ₂ H ₆ O	99 %	JT. Baker
Formaldehyde solution		CHOH	37 wt.% in water	Aldrich
Glycerol		C ₃ H ₈ O ₃ xH ₂ O	99 %	Sigma-Aldrich
Hydrochloric Acid		HCl	99 %	JT-Baker
Methacryloxymethyltriethoxysilane	MMS	C ₁₁ H ₂₂ O ₅ Si	98 %	ABCR
4-(4-Nitrobenzyl)pyridine	NBP	C ₁₂ H ₁₀ N ₂ O ₂	98 %	Sigma-Aldrich
Paraformaldehyde		OH(CH ₂ O) _n H _(n=8-100)	95 %	Sigma-Aldrich
Polyethylene glycol nonylphenyl ether	NP30	(C ₂ -H ₄ -O) ₃₀ -C ₁₅ -H ₂₄ -O		Sigma-Aldrich
Poly-vinyl-pyrrolidone	PVP	(C ₆ H ₉ NO) _n	98 %	Sigma-Aldrich
Potassium carbonate		K ₂ CO ₃ (1.5 H ₂ O)	95 %	Alpha aesar
Potassium chloroaurate		KAuCl ₄	98 %	Sigma-Aldrich
Propyltrimethoxysilane	PTMS	C ₆ H ₁₆ O ₃ Si	> 98 %	Sigma-Aldrich
Poly(diallyldimethylammoniumchloride)	PDDA	(C ₈ H ₁₆ NCl) _n $\overline{M}_w = 400-500\ 000\text{g/mol}^{-1}$	20 wt. % in water	Sigma-Aldrich
Sodium borohydride		NaBH ₄	96 %	Sigma-Aldrich
Sodium dodecyl sulfate	SDS	NaC ₁₂ H ₂₅ SO ₄	> 90 %	Sigma-Aldrich
Sodium Hydrogeno sulfide		NaSH	98 %	Alfa-Aesar
Sodium hydroxide		NaOH	98 %	Sigma-Aldrich
Sodium persulfate		Na ₂ S ₂ O ₈	99 %	Sigma-Aldrich
Styrene		C ₈ H ₈	99 %	Styrene
Succinic Anhydride		C ₄ H ₄ O ₃	> 99 %	Sigma-Aldrich
Tetraethoxysilane	TEOS	C ₈ H ₂₀ O ₄ Si	99 %	Sigma-Aldrich
Tetrahydrofuran	THF	C ₄ H ₈ O	> 90 %	Sigma-Aldrich
Tetrakis(hydroxymethyl)phosphonium chloride	THPC	(HOCH ₂) ₄ PCl	80 wt. % in water	Sigma-Aldrich
Tin tetrachloride		SnCl ₄	> 99 %	Sigma-Aldrich
Triethylamine	TEA	(C ₂ H ₅) ₃ N	99.5 %	Sigma-Aldrich
Trisodium citrate		Na ₃ C ₆ H ₅ O ₇	99 %	Sigma-Aldrich

7 Appendix list of protocols

Protocol 1: Synthesis of the silica “pre-seeds”.

One hundred mL of 6 mM L-Arginine (99 %, Sigma- Aldrich) aqueous solution are poured in a 150-mL double-walled vial and equipped with a reflux condenser **Figure 16b**). When the temperature is stabilized at 60°C, 10 mL of TEOS (99 %, Sigma-Aldrich) are added. The magnetic stirring is set to 150 rpm for a 3-cm cylindrical magnetic stirrer to generate a small and stable vortex and an interface between both phases of constant surface area. The reaction goes on until the TEOS (upper phase) fully disappears. Typically, two days are required to convert 10 mL of TEOS into pre-seeds.[2]

Protocol 2: Regrowth of the silica “pre-seeds”.

In a 1-L flask surmounted by a bubbler, 455 mL of ethanol (99 %), 35 mL of ammonia (28-30 %, J.T. Baker) corresponding to $[NH_3] = 1\text{ M}$ and 10 mL of pre-seed aqueous dispersion $[H_2O] = 3.6\text{ M}$ are mixed by magnetic stirring. The proper volume of TEOS as calculated from (Eq. 3) is added dropwise using a syringe pump at the rate of 0.5 mL/h.

Protocol 3: Functionalization of the silica seeds by MMS.

A known volume of the hydro-alcoholic dispersion of the silica seeds – as directly obtained from **Protocol 2** is introduced in a flask over a magnetic stirrer and surmounted by a condenser. The MMS amount calculated using **Eq. 4** is directly added to the reactor and let to react under stirring for 3 h at ambient temperature. The dispersion is then heated to 90°C for 1 h under reflux of ethanol. The dispersion is subsequently concentrated with a rotavap, let to cool down at room temperature and dialyzed against ultrapure water to remove ethanol and ammonia and replace them with water.

Protocol 4: Synthesis of multipod-like silica/PS clusters.

In a 250-mL three-neck flask, equipped with a stirring anchor and a condenser itself surmounted by a bubbler, are introduced 50 mL of an aqueous solution made of the proper amounts of MMS-functionalized silica seeds, NP30 and SDS. The third neck is closed with a septum, and a long needle is used to ensure nitrogen bubbling into the dispersion for 1 h, the stirring speed being set to 170 rpm. Then, 5 g of styrene (99 % Sigma-Aldrich) are added and the stirring speed is momentarily increased to 250 rpm for 15 min. The nitrogen flux is reduced in order to keep a low over-pressure. The temperature is raised to 70°C with a thermostated oil bath. Then, 1 mL of an aqueous solution previously degassed and containing 25 mg of sodium persulfate (99 %, Sigma-Aldrich) is added. The polymerization is performed for 6 h. Then, the monomer-to-polymer conversion is gravimetrically measured from two 1-mL extracts dried in an oven.

Protocol 5: Regrowth of the silica cores of the silica/PS clusters.

450 mL of ethanol (99 %) and 35 mL of ammonia (28-30 %, J.T. Baker) corresponding to $[NH_3] = 1\text{ M}$ are introduced in a 1 L flask equipped with a magnetic stirrer. A volume of 10 mL of the aqueous dispersion of silica/PS clusters as just-obtained at the end of the

polymerization stage is added leading to a total water concentration of 3.6 M. The flask is closed with a septum and the proper amount of ethanol solution of TEOS (10 vol.% concentrated) is dropwise added at a rate of 1 mL/h. The average size of the regrown silica cores is determined from the statistical analysis of the TEM images.

Protocol 6: Dissolution of the PS nodules.

Typically, the dispersion of PS-silica clusters into the ethanol/ammonia mixture as obtained after the regrowth stage (**Protocol 5**) is transferred into a flask. A volume of DMF corresponding to 10 % of the total volume is added. Subsequently the dispersion is heated at 70°C and partially evaporated under vacuum using a rotavap. Then, the temperature is increased to 90°C and the evaporation continued until the dispersion turns from white to almost transparent. The removal of the dissolved PS is performed by 3 cycles of centrifugation at 10 000 g during 20 min and redispersion in THF.

Protocol 7: Preparation of the PS sample for SEC characterization.

The first THF supernatant containing the dissolved PS chains is collected from the **Protocol 6**. Afterward, this organic dispersion is dried and the solid is weighted and dissolved in THF at a mass concentration of 1 mg/mL. Typically, 5 mL of this PS solution in THF are employed for a SEC experiment after addition of 0.2 vol. % of trichlorobenzene as standard. The UV-detector is tuned at 260 nm which is the maximal absorption for the phenyl groups of the PS chains.

Protocol 8: Preparation of control silica particles for TGA experiments.

Silica particles with a mean diameter of 86 nm used directly from their growth media (**Protocol 2**) and transferred into ultrapure water using the rotavap and centrifugation. Subsequently they are transferred into an emulsion polymerization of styrene and 5 g of styrene are polymerized according to the experimental conditions described in the **Protocol 4**. After completion of the polymerization, 10 mL of the mixture are added into a growth media and a silica regrowth is performed using 5 mL of TEOS in conditions similar to the **Protocol 5**. Those particles are treated according to the **Protocol 6** to wash out all the PS particles. Finally, the suspension is dried; the powder obtained is collected, then weighted for TGA experiments.

Protocol 9: Chloromethylation of the PS macromolecules on the silica patchy particles.

The dimpled silica particles obtained after the PS dissolution step (**Protocol 6**) are transferred into 40 mL of chloroform by using three cycles of centrifugation. 20 mL of this dispersion are introduced in a flask with 5 mL of butyl chloromethyl ether 3 M in chloroform (large excess) and 0.3 mL of SnCl₄. The temperature is set to 45°C and the mixture is aged overnight. Finally the solution is washed by three cycle of centrifugation/redispersion in HCl solution (4 wt.% in water) and three cycles of centrifugation/redispersion in water/EtOH (50/50 wt.%). Finally, the dimpled silica particles were redispersed in 20 mL of DMF. During each washing step, the particles are centrifuged at 12 000 g during 10 min.

Protocol 10: Colorimetric test highlighting the presence of chloromethyl groups.

1 mL of dimpled silica particles dispersion in DMF (corresponding to 10^{12} particles) is introduced in a 10-mL flask. 2 mL of 0.05 M NBP (Sigma Aldrich) and 15 μ L of TEA (Aldrich) are added. The temperature is increased to 90°C and the mixture is kept at that temperature under stirring for 30 min. Finally the dispersion is transferred into a falcon tube and centrifuged at 12 000 g for 10 min and observed with the eye.

Protocol 11: Amination of the chloromethylated PS macromolecules on the silica patchy particles.

Typically an amount of chloromethylated dimpled silica particles corresponding to 10^{13} particles dispersed in DMF is introduced in a flask equipped with a condenser and a magnetic stirrer. A volume of 3 mL of ethylene diamine which is assume to be a large excess is introduced then the temperature is set to 90°C overnight. Then, the particles are washed by two cycles of centrifugation/redispersion in ethanol and then washed 2 times in water, finally the solution is acidified using few drops of HCl then the particles are centrifuged and dispersed in milliQ water.

Protocol 12: Thiolation of the chloromethylated PS macromolecules on the silica patchy particles.

Typically, 10^{13} chloromethylated patchy particles are transferred into ethanol by centrifugation. Ten mL of ethanol containing 2-g of dissolved NaSH was added and let to react overnight under stirring. Finally, the particles are washed 5 times by centrifugation at 10 000 g during 15 min in ultrapure ethanol. The sample can be stored in ethanol. Before use, the particles are typically transferred into water then the potential disulfide bonding are reduced by the use of few drops of a dilute aqueous solution (1 M) of NaBH₄. Finally the solution is washed by centrifugation and stored in degassed water.

Protocol 13: Synthesis of citrate stabilized 12-nm gold nanoparticles.

A 1-L round bottom flask containing 700 mL of milliQ water was heated to 100°C under reflux and moderate agitation. Meanwhile, 314 mg of KAuCl₄ were diluted in 50 mL of milliQ water and then introduced in the round bottom flask. 1.53 g of trisodium citrate was diluted in 75 mL of milliQ water. When the solution temperature has reached 100°C, the citrate solution was added in one shot. The solution turned from yellow to colorless, black and then red. The dispersion was let to react during 15-20 min at 100°C.

Protocol 14: Decoration of aminated dimpled silica particles by citrate stabilized gold nanoparticles.

5 mL of the aminated patchy particles dispersion as obtained after **Protocol 11** are introduced into a 50-mL falcon tube. Few μ L of HCl are added in order to adjust the pH to \square 4. After homogenization using vortex device, 40 mL of citrate-stabilized gold nanoparticles as obtained after **Protocol 13** are added. The suspension is homogenized using vortex device and let overnight over the roller mixer. Afterward, the suspension is washed by 3 cycles of centrifugation/redispersion (4000 g; 15 min) with milliQ water.

Protocol 15: Decoration of thiolated dimpled silica particles by citrate stabilized gold nanoparticles.

In a 50-mL falcon tube, 45 mL of the citrate-stabilized gold nanoparticles in aqueous dispersion as prepared according to **Protocol 13** are centrifuged at 8 000 g during 30 min. The particles are re-dispersed into 1 mL of ultrapure water and 1 mL of the dispersion of thiolated patchy particles prepared according to **Protocol 12** is added in a gold-to-silica particle ratio of 400/1. After overnight incubation over stirring, the dispersion is washed by centrifugation using ultrapure water at 5 000 g for 10 min.

Protocol 16: Seeded-growth method inspired by the Rodriguez-Fernandez's work.

Typically, the thiolated patchy particles seeded by the citrate-stabilized gold nanoparticles are introduced into 250 mL of an aqueous solution containing CTAB (0.015 M), ascorbic acid (1 mM) and HAuCl_4 (0.5 mM). Typically, this solution is prepared from stock solutions of CTAB (0.1 M), ascorbic acid (0.1 M) and HAuCl_4 (25 mM). The volume of solution containing the seeded dimpled silica particles is calculated by using **Eq. 5** considering that the targeted particle diameter is from 12 to 60 nm.

Protocol 17: Seeded-growth method inspired by the Puntès' work.

A volume of thiolated patchy silica particles seeded by 12-nm citrate-stabilized gold nanoparticles calculated thanks to the **Eq. 5** is centrifuged and dispersed into 15 mL of sodium citrate solution (2.2 mM) and transferred into a 20 mL flask. This solution is heated to 90°C and 0.1 mL of HAuCl_4 (25 mM) is introduced, thirty min later the same volume of the same solution is added. The gold nanoparticles concentration is assumed to be around $3 \cdot 10^{12}$ part/ mL. After 30 min, 5.5 mL of the volume are removed from the flask and 5.3 mL of ultrapure water are added with 0.2 mL of citrate sodium solution (60 mM). After temperature stabilization (5 min), a growth cycle of the process is considered as completed. Finally, to stop the process, the solution is allowed to cool down to room temperature after completion of the last cycle.

Protocol 18: Seeded-growth method inspired by the Eychmüller's work.

In a three-neck round bottom flask, a typical volume of patchy particles seeded by citrate-stabilized gold nanoparticles is introduced. This volume is calculated knowing the concentration of patchy particles, the average number of patches and assuming one gold seed per patche. Taking those considerations into account, the volume of the suspension shall contain from 10^{10} - 10^{12} gold seeds.

The volume of gold precursor solution -concentrated at 5 mM- required to grow the seeds to a final diameter noted D_f is given by **Eq. 6** In a typical synthesis, this volume of gold precursor stock solution is extended to 10 mL and loaded in syringe A. A volume of ascorbic acid stock solution and sodium citrate stock solution corresponding to the volume ratio and concentration described in **Table 7** are mixed together, extended to 10 mL then loaded in syringe B. The two syringes are set on two syringe pumps which are adjusted to deliver their load in 45 min (13.3 mL/h).

Protocol 19: Synthesis of 1-3-nm gold nanoparticles according to the Duff's recipe.

In a 500-mL flask, 227.5 mL of milliQ water, 7.5 mL of an aqueous solution of NaOH (0.2 M) and 5 mL of THPC aqueous solution (120 μ L in 10 mL) are introduced. This solution is homogenized during 15 min. Subsequently, 10 mL of HAuCl₄ (25 mM) are quickly injected in the flask under stirring. The solution turns from pale yellow to brown in few seconds indicating the formation of gold nanoparticles.

Protocol 20: Adsorption of gold Duff seeds on the dimpled silica particles.

Typically an amount of dimpled silica particles corresponding to $2 \cdot 10^{13}$ particles in water have their medium acidified to pH 3-4 followed by centrifugation at 10 000 g during 15 min and redispersion into 20 mL of ultrapure water. Subsequently, 2 mL of this peptized silica nanoparticles dispersion are mixed with 50 mL of Duff gold seeds dispersion and are let to incubate for 6 h on the roller mixer. Finally, the dispersion is washed three times by centrifugation at 8 600 g during 15 min to eliminate the excess of gold seeds and redispersed in 40 mL of milliQ water. Basically, the minimal volume of Duff seeds required is calculated thanks to **Eq. 7** giving the number of Duff nanoparticles of diameter r required to completely cover the surface of a sphere of radius R . **Eq. 7** gives an estimation of the minimal volume of Duff solution required to seed the patches, where $N_{patches}$ corresponds to the number of patches per particle and C_{Duff} to the concentration of the Duff solution in part/L.

Protocol 21: Surface amination of the silica free surface of the silica/PS clusters.

Typically, 50 mL of the dispersion of silica/PS clusters (T-52) obtained after the silica regrowth in ammonia/ethanol medium (**Protocol 2**) are transferred into a 100-mL flask. A volume of APTES calculated as described in the section 2.2 from the appendix and corresponding to a surface coverage equivalent to 50 functions /nm² is introduced in one shot; the solution is let to be stirred overnight. Subsequently, the dispersion is heated 1 h at 50°C and washed 3 times by centrifugation at 4000 g during 20 min and redispersed into a solution of 1-mL of NP30 (150 g/L) and 39 mL of water. Finally, the dispersion is acidified by using few drops of HCl.

Protocol 22: Adsorption of gold NPs on the silica surface of the silica/PS particles.

In a 50-mL falcon tube, 30 mL of 1-3-nm gold nanoparticles dispersion as-prepared after **Protocol 20** is introduced and 10 mL of the solution of APTES-functionalized silica/PS clusters are added. The solution is incubated for at least 6 h. Finally, the as-obtained clusters are washed three times by centrifugation during 30 min at 2500 g and redispersed in 20 mL of milliQ water.

Protocol 23: Preparation of the GPS.[15]

First, 10 mL of a stock 25-mM solution of gold precursor is prepared from HAuCl₄ (99.9 % Sigma-Aldrich) and stored protected from light at 4°C. In a 100-mL flask, 8 mL of the gold stock solution and 300 mg of potassium carbonate K₂CO₃ (1.5 H₂O) are mixed and the flask is completed to 100 mL with milliQ water. The solution is stirred overnight at 4°C.

Protocol 24: Growth of the gold nanoshell on the silica surface of the silica/PS particles.

One mL of the solution of clusters after seeding with gold nuclei (**Protocol 19**) is introduced into a 50-mL falcon tube followed by the introduction of a given volume of the GPS calculated as described in the section 2.3 from appendix in order to obtain a targeted gold thickness. The mixture is homogenized and 10 mL of PVP solution (10 g/L; $\overline{M}_w = 29\,000$ g/mol) are introduced, the mixture is one more time homogenized and finally a volume of formaldehyde corresponding to 50 μL /mL of GPS is added in one shot. The solution is quickly homogenized by using vortex and let to react under stirring for 12 h. The solution turns from beige to blue/green depending on the thickness of the gold deposited.

Protocol 25: Seeded growth of the tiny seeds anchored to the aminated PS bumps by formaldehyde reduction method.

Typically, 1 mL of the dispersion of aminated patchy particles decorated by the gold seeds produced after **Protocol 19** is introduced in a falcon tube. Subsequently 10 mL of PVP solution (10 g/L; 29 000 g/mol) are added followed by the introduction of a volume of GPS (1 mM) produced according to the **Protocol 23**. After homogenization an amount of formaldehyde solution 37 % in water (Aldrich) corresponding to 50 μL per mL of GPS is introduced. The reaction is performed for at least 12 h over the roller mixer device, washed by three cycles of centrifugation at 3 000 g during 15 min and redispersion into 20 mL of milliQ water.

Protocol 26: “Passivation” of the inter-patch surface area using propyltrimethoxysilane (PTMS).

Typically the dispersion of the silica/PS clusters obtained after silica regrowth in their ethanol/ammonia medium are maintained in the growth flask and a volume of PTMS corresponding to 50 functions per nm^2 (section 2.2 from the appendix) is introduced in the flask in one shot. The reaction is let to be completed under stirring at ambient temperature for 12 h. Finally, the suspension is washed by three centrifugation/redispersion cycle in ethanol.

Protocol 27: Microwave treatment of the silica/gold clusters dispersion.

The plasmonic nanoclusters produced thanks to **Protocol 25** after gold growth using 8 mL of GPS are introduced into 20 mL of ultrapure water. This dispersion is transferred into the microwave sample container, set in the microwave oven and the treatment is performed for 45 min. The microwave oven is a MARS 5 from CEM, the reactor used is a XP-1500 used at fixed power of 400W at fixed temperature.

Protocol 28: Thermal treatment of the silica/gold clusters.

The dispersion of plasmonic nanoclusters produced thanks to the **Protocol 25** after two successive growth steps using 8 mL of GPS is transferred into 20 mL of ethylene glycol by centrifugation. Subsequently, the dispersion is heated at 190°C for 12 h then diluted into milliQ water and washed three times by using centrifugation (2500 g; 15 min). The treated clusters are finally used as seeds and a gold regrowth is performed after **Protocol 25**.

Protocol 29: Oxidative etching treatment of the silica/gold clusters.

Typically, 20 mL of the silica/gold clusters dispersion prepared by seeded-growth approach are centrifuged at 3 000 g for 15 min and redispersed into 20 mL of ethylene glycol (JT. Baker, Baker analyzed). 0.4 mL of PDDA ($\overline{M}_w = 400\,000 - 500\,000$ g/mol, Aldrich) solution in water (20 wt.%) is added, the dispersion is stirred during 15 min. A volume of gold etching solution ($\text{HAuCl}_4 \cdot 3\text{H}_2\text{O}$ Sigma-Aldrich 99.9 %) in water (0.5 M), corresponding to a fraction of the gold amount used to produce the sample is calculated thanks to **Eq. 10** and introduced into the dispersion. Afterward, the mixture is rapidly homogenized using vortex device, and the reaction is performed for 24 h at ambient temperature on the roller mixer. After reaction, the clusters are washed by centrifugation: typically the 20 mL of gold nanoclusters dispersion are diluted into 90 mL of milliQ water, and centrifuged into two 50-mL falcon tubes. The dispersion is centrifuged at 2500 g during 20 min and washed 3 times using milliQ water. At this point, the dispersion is either characterized or used in a new regrowth step.

Protocol 30: Amino modification of the silica particles surface.

Silica particles produced thanks to **Protocol 2** from Chapter 1 are typically used in their growth media (ethanol/ammonia). An amount of APTES (98 % Sigma Aldrich) corresponding to 20 functions per nm^2 of available silica surface is added the reactor. The dispersion is stirred for 12 h. A volume of glycerol (99 % Sigma Aldrich) corresponding to 10 % of the total volume of the dispersion is added. Ethanol and water are evaporated using rotary evaporator device set at 90°C . The dispersion, from now in glycerol, is heated by an oil bath set at 105°C for a subsequent 2 h thermal treatment conducted under the vacuum produced by a rotary vane pump. Finally the dispersion is washed by 4 cycles of centrifugation/redispersion in ethanol (12 000 g; 20 min).

Protocol 31: Functionalization of silica particles with carboxylic groups.

The aminated silica particles as obtained from **Protocol 30** are transferred into DMF by two centrifugation cycle at 12 000 g during 20 min. Subsequently an amount of triethylamine (TEA) corresponding to 50 functions per nm^2 of available silica surface is introduced into the dispersion which is centrifuged one more time at 12 000 g during 20 min and dispersed in DMF. The dispersion is transferred into a round bottom flask set in an oil bath at 60°C and dehydrated during 2 h under vacuum generated by a rotary vane pump. Subsequently an amount of succinic anhydride corresponding to 50 functions per nm^2 of available silica surface is introduced and let to react overnight at 60°C . The dispersion is washed 2 times by centrifugation in ethanol and 2 times in DMF, an amount of TEA corresponding to 50 functions per nm^2 is introduced and the dispersion is washed one more time at 12 000 g for 20 min and finally dispersed in DMF and dehydrated under vacuum using rotary vane pump (RV5 from Edwards).

Protocol 32: Assembly of the carboxylic-modified silica particles with aminated dimples.

A dispersion of aminated dimpled silica particles prepared according to **Protocol 30** is transferred in DMF by 2 centrifugation cycles at 12 000 g during 20 min. An amount of TEA corresponding to fifty functions per nm^2 of surface of a sphere of similar diameter is

introduced and the solution is washed one more time with DMF. Finally, the remaining water is removed from the dispersion, by heating at 50°C under stirring and vacuum generated by a rotary vane pump for 1 h. Meanwhile, 1 mL of the dispersion of carboxylic surface modified silica nanoparticles is introduced in an Eppendorf (55 nm in diameter 70 g/L). A volume of TEA (6.2 μ L) corresponding to 8 functions per nm^2 is introduced and the solution is homogenized using vortex device. The activation of the carboxylate groups into anhydride carbonate is performed by adding 2.4 μ L of ethyl chloroformate corresponding to 4 functions per nm^2 of available silica surface. The dispersion is mixed upon vortex device and homogenized on the roller mixer for 2 min. Finally 0.1 mL of the dehydrated dispersion of dimpled silica particles in DMF containing approximately 6×10^{11} dimpled silica particles is introduced in one shot into the Eppendorf containing the activated silica spheres. Then, the solution is homogenized and let to react over the roller mixer overnight. The dispersion is typically transferred in 40 mL of water and washed 3 times with 40 mL of water and 0.1 mL of TEA by using 3 cycles of centrifugation/redispersion at 500 g during 20 min.

Protocol 33: Seeding of the amino-modified silica particles by gold nuclei followed by conversion of the amino groups into carboxylic ones.

Typically, a volume of amino-modified silica particles as obtained after **Protocol 30** are transferred into water acidified by HCl (pH 4) by using two centrifugation/redispersion cycles (12 000 g; 15 min). A volume of gold nuclei prepared according to **Protocol 19** from chapter 2 is added. The solution is stirred overnight and finally washed from the free gold nuclei by three centrifugation/redispersion cycles (10 000 g during 20 min) in DMF. Then the **Protocol 31** is applied.

Protocol 34: Site specific decoration of the self-assembled silica/silica clusters with gold nuclei.

Typically, 20 mL of the dispersion of patchy particles assembled with the silica COO^- activated particles are washed in water and then deprotonated using TEA. The clusters are transferred into DMF by centrifugation and the COO^- groups are reactivated through the addition of an amount of ECF corresponding to 10 functions / nm^2 of the total silica satellite surface used for the assembly. After 5 min, an amount of ethylene diamine corresponding to 50 functions / nm^2 of the total silica satellite surface is added and the mixture is let to react overnight. Then, the dispersion is washed three times by centrifugation/redispersion in milliQ water, then acidified using few drops of HCl to protonate the amino group and washed one more time with milliQ water. This dispersion containing the assembly is mixed with gold dispersion as prepared from **Protocol 19** and let over roller mixer for at least 4 h. Finally, the dispersion corresponding to the assembly decorated by gold nuclei is washed three times by centrifugation/redispersion in milliQ water (2 000 g; 10 min).

Protocol 35: Growth of a gold layer over the silica satellites of the self-assembled silica silica clusters.

Typically, 0.5 mL of the dispersion containing the self-assembled silica-silica clusters decorated with Duff gold nuclei are introduced into a 50-mL falcon tube. A volume of PVP solution (10 g/L $\overline{M}_n = 29\,000$ g/mol) is added and mixed using the vortex and the adsorption

is completed to occur over the roller mixer for 5 min. Subsequently a volume of the gold plating solution prepared according to the **Protocol 23** is added and mixed with a volume of 50 μL of formaldehyde per mL of gold plating solution.

Protocol 36: Single object spectroscopy sample preparation.

10 μL of a dispersion of gold octahedral clusters as obtained after **Protocol 35** is introduced in an Eppendorf and 450 μL of ultrapure water are added. The dispersion is homogenized using vortex and ultrasonic bath. 3 μL of this suspension is deposited on a labelled Formvar TEM grid and let to dry. Afterwards, the sample is observed by TEM and isolated clusters are targeted. Their locations are identified thanks to the tag of the labelled grid. A series of TEM picture at several magnifications (from the highest to the lowest) are taken. Those pictures are subsequently used to track down the clusters when the sample is observed under optical microscope.

Protocol 37: Single object dark field spectroscopy measurement.

A targeted TEM sample as prepared according to **Protocol 36** is set on the sample stage of the dark field set up. The spectrometer is a LabRAM HR Horiba HR used with an Olympus optical microscope, the sample stage is disposed on a motorized stage. The light beam from the condenser is focused on the grid and the angle between the incoming light and the sample plane is measured. The sample is set at the focal plane of the 50X objective and clusters are tracked down thanks to the tag. The aperture size is set at 50 μm . The surface area on which the signal is collected can be imaged by activating the photodiode. The isolated targeted clusters have to be centered into this area. Sample measurements are performed for three polarization angles (*S*, *P* and 45°) then the same is done for background (typically an area of the Formvar film without any cluster deposited and also away from grid bar glare). A cross polarized series of measurements are collected and finally, a reference measurement is recorded using Spectralon® Diffuse Reflectance Standards from Labsphere. Depending on the wavelength range measured, two different detectors and their corresponding pairs of polarizers are used. One for the 650-1050 nm range (LPNIRE100-B from Thorlabs) and another one for the 1050-1700 nm range (LPIRE100-C from Thorlabs).

8 References

- [1] A. Warshawsky and A. Deshe, "Halomethyl Octyl Ethers: Convenient Halomethylation Reagents," *J. Polym. Sci. Polym. Chem. Ed.*, vol. 23, pp. 1839–1841, 1985.
- [2] A. Désert, "Thèse de l'Université Bordeaux 1: Colloïdes hybrides silice/polystyrène de morphologie contrôlée," 2011.

Titre : Design et fabrication de meta-atomes plasmoniques à partir de nanoparticules à patches.

Résumé : Les méta-matériaux sont une nouvelle classe de matériaux composites artificiels qui présentent des propriétés inédites. Ils sont typiquement sous divisés en unité appelées méta-atomes. Un design approprié de ces méta-atomes, architecturés à l'échelle nanométrique, permet d'induire des propriétés aussi extraordinaires qu'un indice de réfraction négatif. Dans ce contexte, nous avons développé des particules à patches, capable de développer des interactions selon des directions prédéterminées. Des clusters multipodiques fait de ces particules (diélectrique) entourées d'un nombre contrôlé de satellites plasmoniques (or) ont été développés. Nous nous sommes focalisés sur des clusters isotropes, dérivant de géométries tétraédriques, octaédriques et icosaédriques (trois des cinq solides de Platon). Pour cela, nous avons utilisé des clusters silice/polystyrène, obtenus par polymérisation ensemencée en émulsion, qui ont servi de préformes. Ils ont ainsi permis d'obtenir des particules dont les patches sont en fait des fossettes au fond desquelles subsiste un résidu de chaînes polystyrène greffées. En modifiant chimiquement ces chaînes, nous avons permis soit l'accrochage au fond de ces fossettes de colloïdes d'or puis leur croissance, soit l'accostage de satellites de silice sur lesquels nous avons ensuite fait croître une coquille d'or. La seconde voie à offert un meilleur contrôle de la morphologie des clusters et notamment de la distance entre les satellites d'or (quelques nanomètres) qui est primordiale pour assurer un couplage plasmonique optimal. Les propriétés des clusters obtenus ont été modélisées et mesurées.

Mots clés : particules à patches, résonance plasmon, nanoclusters, fossettes, or, métamatériaux, méta-atomes, auto-assemblage, croissance-ensemencée, silice, nanoparticules, spectroscopie en champ-sombre ;

Title: Design and synthesis of plasmonic meta-atoms from patchy particles.

Abstract: Metamaterials are a novel class of artificial composite materials, typically made of sub unit called meta-atoms and exhibiting unusual properties. Such meta-atoms, have to be architected at the nanometric level, to induce as extraordinary properties as a negative refractive index. In this context, we developed patchy particles, capable to create interactions along predetermined directions. Multipodic clusters made of those (dielectric) particles surrounded by a controlled number of plasmonic satellites (gold) were developed. We focused on isotropic clusters deriving from tetrahedral, octahedral and icosahedral geometry (three of the fifth Platonic solids). For that purpose, we used silica/polystyrene clusters, obtained from seeded emulsion polymerization, as template. By deriving those clusters, patchy particles bearing dimples containing grafted residual polystyrene chains were obtained. By chemically deriving those chains, we explored two synthetic pathways, the decoration of the dimples with gold colloids subsequently grown or the anchoring of silica satellites onto which gold shells were subsequently grown. The second one was prove to offer a better control over the cluster morphology as well as the inter-satellites gap (few nanometer) which is pivotal to ensure an optimal plasmonic coupling. Then, the optical properties of the as obtained clusters were simulated and measured.

Keywords: Patchy particles, plasmon resonance, nanoclusters, dimples, gold, metamaterials, meta-atoms, self-assembly, seeded-growth, silica, nanoparticles, dark-field spectroscopy;